Analysing Ground Deformation Data to Predict Characteristics of Smear Zone Induced by Vertical Drain Installation for Soft Soil Improvement

A thesis in fulfilment of the requirement
for the award of the degree

Doctor of Philosophy

from

University of Technology, Sydney

by

Ali Parsa-Pajouh, BSc Eng, Msc Eng

School of Civil and Environmental Engineering,
Faculty of Engineering and Information Technology

February 2014

CERTIFICATION

I, Ali Parsa-Pajouh, declare that this thesis, submitted in fulfilment of the requirements for the award of Doctor of Philosophy, in the Department of Civil and Environmental Engineering, University of Technology, Sydney, is wholly my own work unless otherwise referenced or acknowledged. The document has not been submitted for qualification at any other academic institution.

_____

Ali Parsa-Pajouh
February 2014

DEDICATION

This work is sincerely dedicated to the following special people:

To My Lovely Wife, Neda

For her endless encouragement and patience, without her love and support, I could have never completed this journey.

To My Father, Davoud

He was my role-model of hard work, persistence and personal sacrifices. He inspired me how to be strong, how to be honest.

To My Late Beloved Mother, Maryam

For all the sacrifices she has made to ensure that I obtain the best education possible, for her beautiful mind and unconditional love.

ABSTRACT

The use of prefabricated vertical drain (PVD) assisted preloading has been recognised over the last two decades as a very efficient method of ground improvement for sites with deposits of deep soft soil. One of the major parameters influencing the PVD assisted consolidation process, and consequently the required preloading time, is the formation of a smear zone around the vertical drains, and the corresponding soil properties. In this research a systematic procedure integrated with a developed numerical code is proposed to accurately back calculate the properties of the smear zone based on the consolidation data collected in the laboratory and in the field. Furthermore, an expanded back calculation method is developed to determine the minimum required degree of consolidation and corresponding time after the construction of the trial embankment that would result in accurately predicted smear zone characteristics. The explicit finite difference program FLAC 2D was used to develop the numerical code, simulate the laboratory testing and PVD assisted preloading case histories. Furthermore a comprehensive parametric study was conducted to investigate the effect of smear zone properties variations on the preloading process, and back calculated characteristics of the smear zone.

A large and fully instrumented Rowe cell apparatus was used to investigate the effect of the smear zone on the consolidation process and verify the developed numerical code. The Rowe cell was filled with the intact zone, smear zone, and vertical drain materials to evaluate the permeability and extent ratios of k_h/k_s=4 and r_s/r_m=3, respectively. The back calculation procedure was used to conduct the parametric study and predict the properties of the smear zone. According to the results, the predicted properties of the smear zone were similar to the properties of the applied soil, proving that the proposed back calculation procedure integrated with the developed numerical simulation can successfully predict these properties.

The developed numerical code was used to simulate five PVD assisted preloading case studies, including four trial embankments and a large scale consolidometer, while the back calculation procedure was used to conduct a parametric study to determine the extent and permeability of the smear zone. According to the results, integration of the back calculation procedure in the

numerical code can be used as a reliable tool to make an accurate prediction of the smear zone characteristics in PVD and vacuum assisted preloading projects.

The developed method in this research can be considered as a practical, accurate and cost effective tool, due to its capability in precise estimation of the extent and permeability of the smear zone in the early stages of constructing the trial embankment. In this study, the proposed systematic back calculation procedure was extended to determine the minimum degree of consolidation (i.e. the minimum waiting time after constructing the trial embankment), and accurately predict the properties of the smear zone. The numerical results of the simulated case studies were used to conduct the analyses. Accordingly, it is found that the extent and permeability of the smear zone can be predicted very well with the proposed calculation procedure when at least 33% of predicted final settlement has been reached (i.e. 33% of the degree of consolidation).

ACKNOWLEDGEMENT

Working as a PhD student at University of Technology, Sydney was a magnificent as well as challenging experience to me. In all these years, many people were involved directly or indirectly in shaping up my academic achievements. It was hardly possible for me to succeed in my doctoral work without the precious support of these kind personalities. Here is a small tribute to all those people.

First of all, I would like to express my deepest gratitude to my supervisor, Dr. Behzad Fatahi for his brilliant guidance, caring, patience, and providing me with an excellent atmosphere for doing research. It has been an honour to be his first PhD student. His numerous comments, criticisms and suggestions during the preparation of this thesis are gratefully acknowledged.

I would like to thank my co-supervisor, A/Prof. Hadi Khabbaz, who was abundantly helpful and offered invaluable assistance, support and guidance. His encouragement, support and critical review of the thesis, as well as his comprehensive suggestions at various stages of this study are greatly appreciated. I would also like to acknowledge Bill Clayton for his critical review of the thesis and helpful comments.

My appreciation is also extended to UTS laboratory and workshop staff Antonio Reyno and Laurence Stonard as well as the PhD students Babak Azari, and Thu Minh Le for their valuable assistance and contribution in running and conducting the laboratory test. I am also thankful to University of Technology, Sydeny and its staff for their financial, academic and technical support. The library and computer facilities of the University have been indispensable. I very much appreciate the Centre for Built Infrastructure Research (CBIR), particularly, Prof. Bijan Samali for their support and assistance since the start of my PhD study.

I gratefully acknowledge the funding sources that made my PhD work possible. This research was funded by Australian Research Council and supported by the Menard-Bachy Pty Ltd as the industry partner, which are so appreciated.

I would also like to acknowledge Road and Maritime Services (RMS) for providing the field measurements and site investigation results for Ballina Bypass and Cumbalam trial embankments.

I have been in charge of tutoring different subjects in last four years, which was a priceless experience for me. I would like to take this opportunity to express my special gratitude towards academic staff of the School of Civil and Environmental Engineering, Dr. Behzad Fatahi, A/Prof. Hadi Khabbaz, Dr. Shami Nejadi, Dr. Rezaul Karim, Anne Gardner, Chris Wilkinson and Dr. Rijun Shrestha, who supported me in this journey.

Gratitude is also expressed to my friends and fellow students at the University of Technology, Sydney, particularly, Amir Zad, Babak Azari, Behnam Fatahi, Binod Shresta, Hamid Tabatabaei, Thu minh Le and Yashar Maali for keeping the study atmosphere enjoyable and pleasant.

I would like to express heartfelt acknowledgement to my wife, Neda Khodadoust, for her constant love, sacrifices, support, encouragement, and patience. She was always there cheering me up and stood by me through the happy and hardships times. Without her guidance and support, I may never have come this far in my study.

Lastly, I would like to thank my parents, who raised me with a love of science and supported me in all my pursuits. Special thanks to my two elder sisters, and my younger brother, who were always supporting and encouraging me with their best wishes.

TABLE OF CONTENT

LIST OF FIGURES

LIST OF TABLES

LIST OF SYMBOLS

a_o	initial radius of cavity
B	equivalent plane-strain radius of the influence zone
BP	back Pressure
b_s	equivalent plane-strain radius of the smear zone
b_w	equivalent plane-strain radius of the drain
C_c	compression index
C_f	hydraulic conductivity ratio between the field and laboratory values
CP	cell Pressure
Cs	swelling index
c'	cohesion in drained condition
c_f	hydraulic conductivity ratio between field and laboratory values
c_h	coefficient of horizontal consolidation
c_k	permeability change index
c_v	vertical coefficient of consolidation
c_{vc}	coefficient of consolidation for the combined vacuum and surcharge preloading
D_{10}	effective particle size
D_{15}	grain diameter at 15% passing
D_{30}	grain diameter at 30% passing
D_{50}	grain diameter at 50% passing
D_{60}	grain diameter at 60% passing
D_{85}	grain diameter at 85% passing
DL	data logger
dc	diameter of unit cell
de	equivalent drain diameter
d_m	mandrel diameter
d_s	smear zone diameter
d_w	diameter of drain
E	Young's modulus
E_f	final cumulative error
$(E_f)_i$	cumulative error at step i

$(E_f)_s$	corresponding cumulative error to the extent ratio s
E_i	error between numerical predictions and field measurements at step i
$(E_{min})_s$	minimum error corresponding to step s
$(E_t)_n$	normalised cumulative error at time t and step number n
$(E_t)_n$	normalised cumulative error at time t and step number n
$(E_{U\%})_i$	corresponding error to U% at step i
$(E_{U\%})_{min}$	minimum error
$(E_{U\%})_s$	corresponding error to the extent ratio s
EPWP	excess pore water pressure
e	void ratio
e_{cs}	void ratio at the critical state
e_o	initial void ratio
F_k	field measurements
F_s	reduction factor
G	shear modulus
G_s	Specific garvity
g_i *or* g_k	gravity vector
H_d	vertical drainage length
I_r	normalised by the rigidity index
IVC	definite volume controller
K_w	water bulk modulus
k	coefficient of isotropic mobility
$(k_h/k_s)_i$	permeability ratio at step i
$(k_h/k_s)_{max}$	maximum permeability ratio
$(k_h/k_s)_{min}$	minimum permeability ratio
$(k_h/k_s)_o$	assumed initial permeability ratio
$(k_h/k_s)_{opt}$	predicted permeability ratio at $U\%_{min}$
$(k_h/k_s)_s$	permeability ratio corresponding to step s that gives the minimum error
$\hat{k}(s)$	relative permeability
k_1	ratio between the vacuum pressure at the top and bottom of the drain
$k_{e,ax}$	equivalent horizontal permeability for the axi-symmetric unit cell

$k_{e,pl}$	equivalent horizontal permeability for the plane-strain unit cell
k_{ep}	horizontal permeability coefficient in the equivalent zone of plane-strain unit
k_f	permeability of the filter
k_h	intact zone horizontal permeability
k_h/k_s	permeability ratio
k_{hp}	horizontal permeability of intact zone in plane-strain condition
k_{ij}	tensor of the coefficient of permeability
k_s	smear zone permeability
k_{sp}	horizontal permeability of smear zone in plane-strain condition
k_v	intact zone vertical permeability
k_{ve}	equivalent coefficient of vertical permeability
k_w	coefficient of permeability of PVD
LL	liquid limit
LVDT	linear vertical displacement Transducer
l	drainage length
l_m	the length of the vertical drain
$[\mathcal{M}]$	stiffness matrix
M_b	biot modulus
M	slope of the critical state line
MCC	modified cam clay
N	total number of observation points
n	porosity
$n = R/r_w$	ratio of the influence radius to the drain radius
$n = k_h/k_s$	permeability ratio
n_p	isotropic over consolidation ratio
O_{50}	opening size of the filter which is larger than 50% of the fabric pore
O_{95}	the apparent opening size of the filter
OCR	over consolidated ratio
P/V C	pressure/volume controller
PL	plastic limit
PVD	prefabricated vertical drain

PWPT	pore water Pressure Transducer
p'	mean effective stress
P'_1	reference pressure
P'_c	preconsolidation pressure
PI	plasticity index
P_k	numerical predictions
p_o	initial mean pressure
p'_o	initial effective mean pressure
P_{vo}	vacuum pressure applied at the top of the drain
p'_{y_o}	maximum isotropic preconsolidation stress
$\{Q\}$	nodal flow rate
q	deviator stress
q_i	specific discharge vector
q_{req}	required discharge capacity
q_v	intensity of the volumetric water source
q_w	discharge capacity of PVD
q_{wp}	equivalent plane-strain discharge capacity
R	radius of the influence zone
$(r_s/r_m)_i$	extent ratio at step i
$(r_s/r_m)_{max}$	maximum extent ratio
$(r_s/r_m)_{min}$	minimum extent ratio
$(r_s/r_m)_o$	assumed initial extent ratio
$(r_s/r_m)_{opt}$	predicted extent ratio at $U\%_{min}$
$(r_s/r_m)_s$	extent ratio corresponding to step s that gives the minimum error
r_1	instantaneous radius of an elliptical cavity
r_m	mandrel radius
r_o	initial radius (in the direction of the semi-major axis) of an elliptical cavity
r_p	radial distance of the plastic zone around the cavity
r_s	smear zone radius
r_s/r_m & r_s/r_w	extent ratio
r_{tr}	radius of transition zone

r_w	drain radius
S	drain spacing (centre to centre)
S_f	final primary consolidation settlement
S_{pr}	field settlement at the end of preloading time
S_t	field settlement at time t
S_{tp}	predicted settlement at time t
s	extent ratio (r_s/r_w) or (r_s/r_m)
T_{hp}	radial consolidation time factor
T_r or T_h	radial consolidation time factor
T_v	vertical consolidation time factor
T_{vc}	time factor for the combined vacuum and surcharge preloading
$t_{90\%}$	corresponding time at 90% degree of consolidation
t_{min}	corresponding consolidation time to the $U\%_{min}$
t_{pr}	preloading time
$\overline{U}$	total degree of consolidation in plane-strain condition
$U\%$	degree of consolidation at time t
$U\%_{min}$	minimum required degree of consolidation
$U\%_n$	degree of consolidation at step n
$\overline{U}_h$	average degree of radial consolidation in axi-symmetric condition
$\overline{U}_{hp}$	average degree of radial consolidation in plane-strain condition
$U_{pr}\%$	degree of consolidation at the end of preloading
$\overline{U}_v$	average degree of vertical consolidation
u_o	initial excess pore water pressure
V	total volume associated with the node
w	water Content
z	depth

Greek Letters

α	biot's coefficient
β	pore pressure coefficient
γ_q^p	plastic shear strain
γ_s	unit weight
ΔR	permeability ratio incremental rate

ΔS	extent ratio incremental rate
ΔV_{mech}	equivalent increase in the nodal volume arising from mechanical deformation of the grid
$\Delta\sigma_{oct}$	octahedral normal stress
$\Delta\tau_{oct}$	octahedral shear stress
ϵ	volumetric strain
ζ	ariation of water volume per unit volume of porous material
η	stress ratio
κ	slope of the specific volume versus ln(p') curve for swelling
Λ	plastic volumetric strain ratio
λ	slope of the specific volume versus ln(p') curve for compression
μ	Poisson's ratio
ν	specific volume
ν_λ	specific volume at the reference pressure
ρ_d	bulk density of the dry matrix
ρ_s	density of the solid phase
ρ_w	mass density of the water
σ_c	the lateral pressure
σ_o	initial cavity internal pressure
σ_r	total stress
σ_{rp}	total radial stress at the elastic-plastic boundary
φ'	friction angle in drained condition

CHAPTER ONE

1 INTRODUCTION

1.1 GENERAL

According to the Australian Bureau of Statistics (2008), the population of Australia would experience a growth of 60%, from 22 million to 35 million by 2056, and the population of Queensland and New South Wales would boom by about 110% and 50% by 2056, respectively. This rapid growth in population and development in urbanisation have increased the need to build and expand infrastructure such as highways, railways, and ports. In Australia, the major cities lie along coastlines that consist of deep soft clay deposits, especially in Northern Queensland and New South Wales. These deposits can be categorised as problematic soils due to their characteristic low bearing capacity and high compressibility.

Various ground improvement methods are available to improve the strength and stiffness of soft soil, shorten construction time, and reduce costs by considering the environmental aspects. To select the most appropriate method, various factors such as the significance of the structure, the loading and site conditions, the construction time limitation, and the type of soil, should be considered. Table 1.1 summarises the applicability of various ground improvement methods for different types of soils, and Figure 1.1 shows the procedure for selecting an appropriate ground improvement technique based on site conditions.

According to Table 1.1 and Figure 1.1, dewatering or preloading can be used efficiently to strengthen the soft clay deposits and reduces their compressibility.

Preloading is a successful technique for stabilising soft clays. In this method, a surcharge is applied onto the surface of the ground until most of the ground settlement, expected to occur due to future structural loads, is achieved. In soft and compressible soils that are relatively thick, consolidation takes a long time to complete due to the very low permeability of the soil. Hence, preloading is not an appropriate ground improvement method for projects with limited construction time.

Over the past decades, a system of prefabricated vertical drains has been used to accelerate the consolidation process.

Table 1.1 Applicability of ground improvement for different soil types (after Kamon and Bergado, 1992)

Improvement Mechanism	Reinforcement	Admixture or grouting	Compacting	Dewatering
Organic soil	✔	✔		✔
Volcanic clay soil	✔	✔		✔
Highly plastic clay	✔	✔		✔
Lowly plastic clay	✔	✔		✔
Silty soil	✔	✔	✔	✔
Sandy soil	✔		✔	
Gravel soil	✔		✔	
Improved state of soil	Interaction between soil and inclusion	Cementation	High density by decreasing void ratio	High density by decreasing void ratio

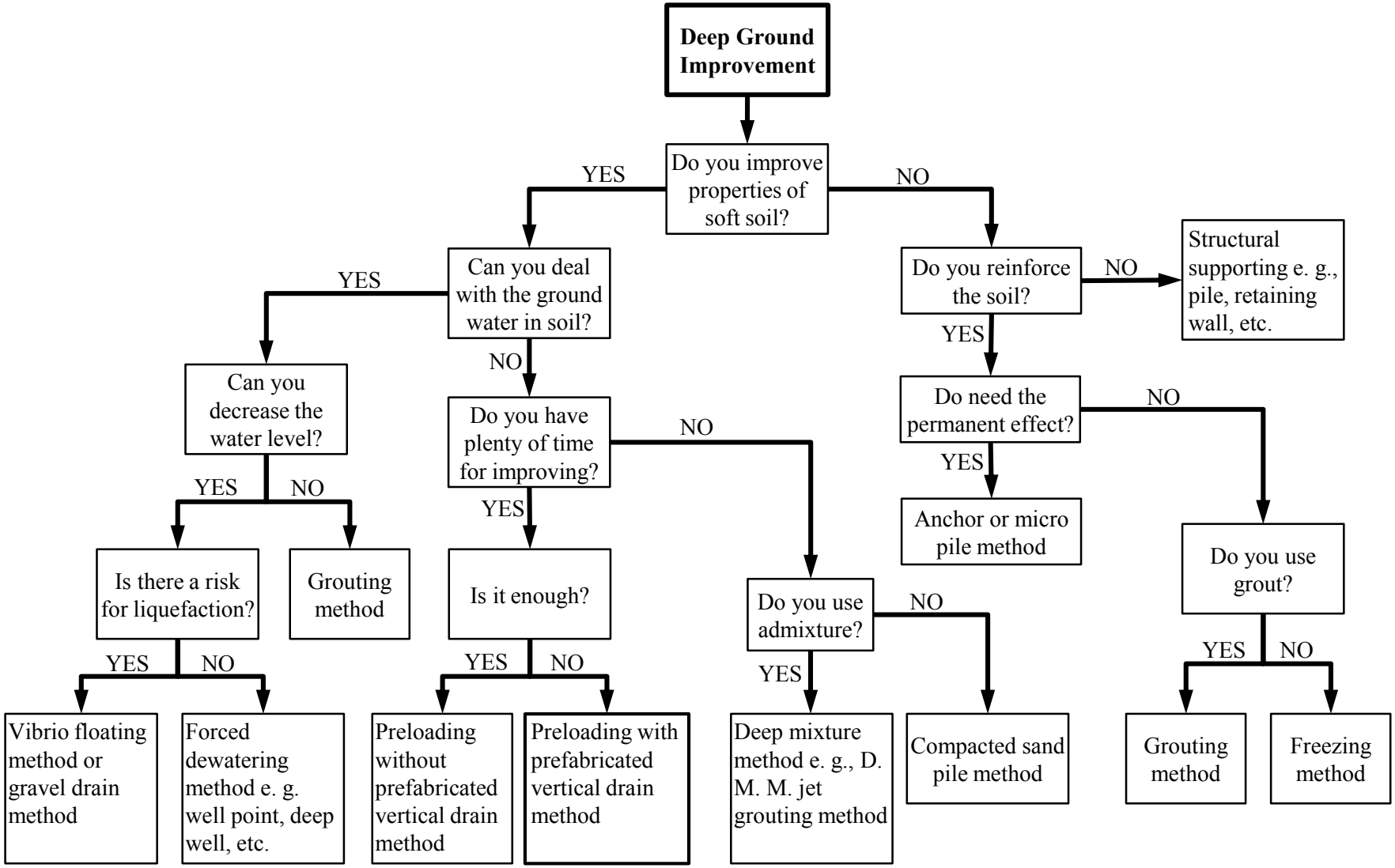

Figure 1.1 Procedure to select the appropriate technique for ground improvement

1.2 ACCELERATING THE CONSOLIDATION PROCESS

Soil may consist of two or three phases namely, solid, liquid, and gas. The voids between the solid particles are filled with water, air, or a combination of both. Soil deformation involves the reduction of voids under loads, compaction is the removal of air from the soil, and consolidation is removal of water from the soil by applying a surcharge. Figure 1.2 illustrates the settlement stages due to a reduction in the void ratio during consolidation; this process includes, (i) initial compression, (ii) primary consolidation, and (iii) secondary compression.

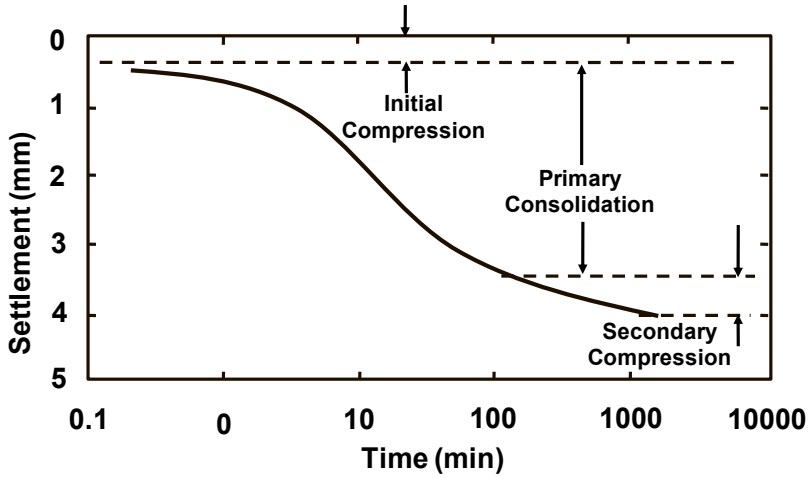

Figure 1.2 Typical consolidation settlement

Initial settlement in clayey soils occurs immediately after a load has been applied, with no change in void ratio, so that only the shape changes. In saturated soils (i.e. no free air in the voids), an increase in the stress induced by the external load is immediately taken by water, which can be reasonably assumed to be incompressible. The excess pore water pressure gradually dissipates as water seeps out of the soil through drainage boundaries, and the pressure is transferred to the soil skeleton; this is known as primary consolidation. Secondary compression might be determined as a continuation of the mechanism of a change in volume following primary consolidation (Mesri, 1973). This mechanism consists of the deformation of individual particles and their relative movements due to normal stresses or shear displacement where the particles contact each other, induced by shear stresses that exceed the shear resistance.

The average degree of radial consolidation at time t can be calculated by using the following equation (Hansbo 1981):

$$\bar{U}_h = 1 - exp\left(\frac{-8T_h}{F}\right) \tag{1.1}$$

$$T_h = \frac{c_h t}{R^2} \tag{1.2}$$

where, $\bar{U}_h$ is the average degree of radial consolidation, T_h is the radial drainage time factor, c_h is the radial consolidation coefficient, R is the radius of the influence zone, and F is a function related to factors such as the coefficient of permeability, the drain spacing, the smear effect, and the well resistance.

It is seen that the time needed to attain a certain degree of consolidation is governed by the permeability of the soil and the distance to the drainage boundaries. There a two approaches that can be used to accelerate the rate of natural settlement; (i) increasing the applied stress, or (ii) reducing the drainage length. Constructing a higher embankment can increase the applied stress and accelerate the rate of settlement, but in some cases, high embankments may cause stability problems. The installation of prefabricated vertical drains (PVDs) is highly recommended to accelerate the rate of radial drainage and consolidation by reducing the length of the drainage paths (Figure 1.3). The consolidation time is inversely proportional to the square of the length of the drainage path.

A prefabricated vertical drain (PVD) is a composite geosynthetic system consisting of a polymeric inner core with formed flow path grooves on both sides and an outer non-woven geotextile filter jacket (Figure 1.4). The main function of the filter in a vertical drain is to ensure that fine particles cannot pass through and clog the drainage channels in the core (Hansbo, 1981). Figure 1.5 shows how vertical drains can accelerate the rate of settlement. As observed, PVD assisted preloading reduces the time required to achieve a certain settlement compared to traditional preloading (excluding PVD).

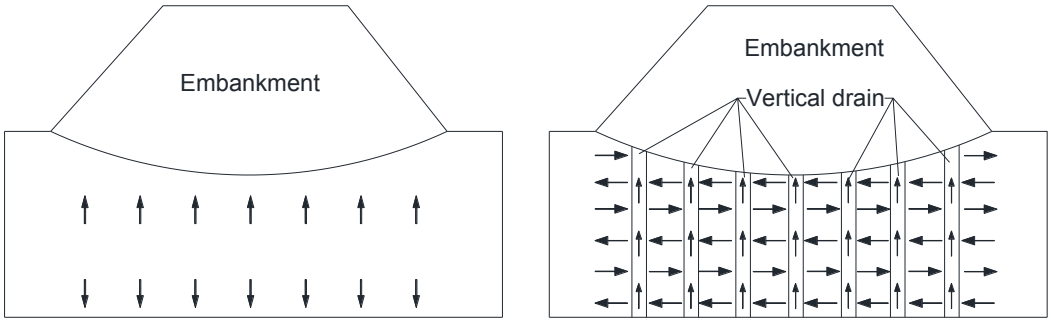

(a) (b)

Figure 1.3 Preloading method (a) without vertical drains, (b) with vertical drains

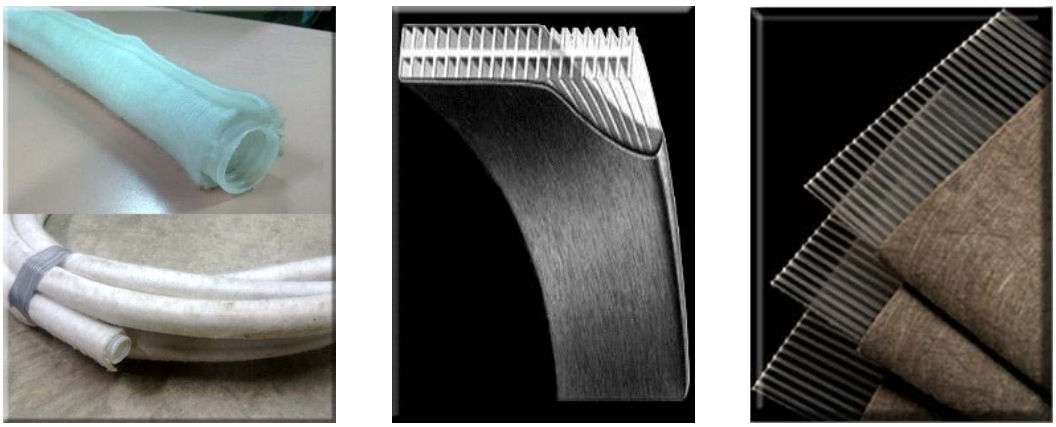

(a) (b) (c)

Figure 1.4 Prefabricated vertical drain, (a) Circular, (b) & (c) Band shape

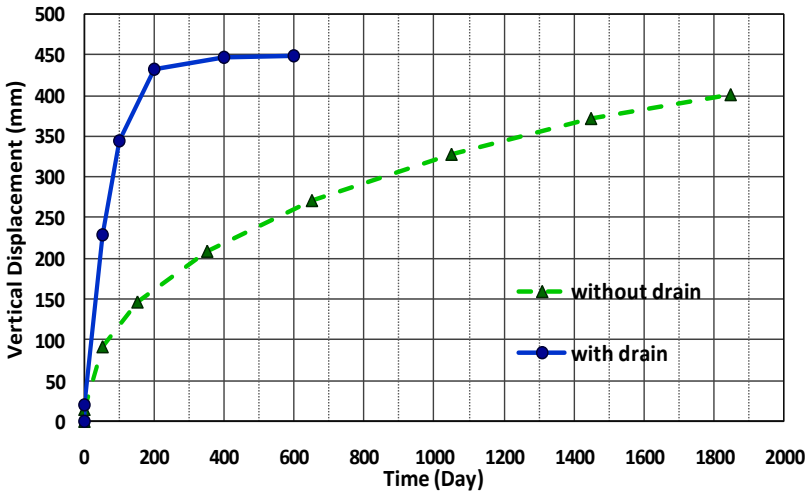

Figure 1.5 Typical effect of vertical drains on consolidation settlement rate of soft clay

A system of vertical drains combined with vacuum pressure and surcharge preloading can be used as an alternative method of ground improvement to increase the settlement rate and reduce construction time. This technique accelerates

consolidation by applying negative pore water pressures along the vertical drains and on the ground surface, which subsequently reduces the lateral pressure and increases the effective stress. This technique reduces the height of the surcharge embankment to prevent any instability and lateral movement in the soil.

1.3 INSTALLATION OF VERTICAL DRAINS AND SMEAR ZONE

Prefabricated vertical drains are installed by either vibratory or static crowd methods. In both cases, the drain is enclosed in a tubular steel mandrel with a small cross sectional area, and then a small steel anchor plate is attached to the drain at the bottom of the mandrel. The mandrel is then driven into the soil with a static crowd or vibratory rig. When the design depth is reached, the mandrel is extracted and the anchored plate holds the drain in the soil. Figure 1.6 shows the PVD installation process.

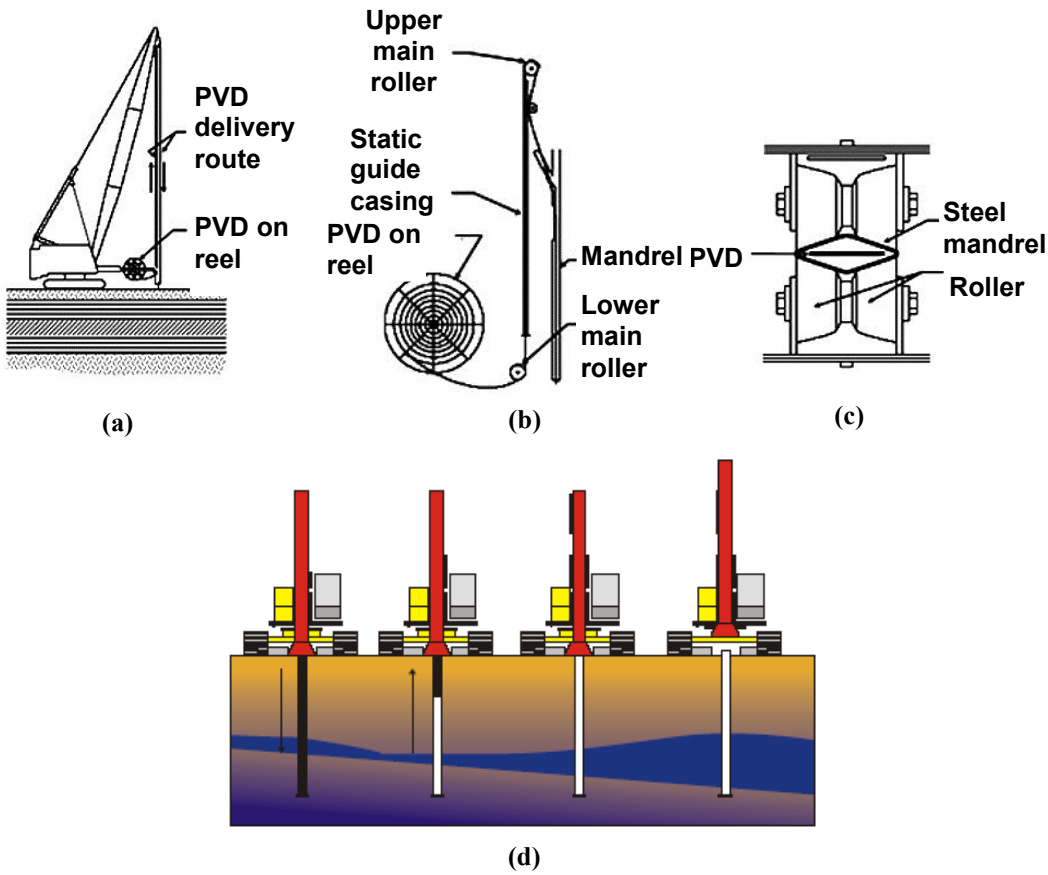

Figure 1.6 PVD installation (a) crane mounted installation rig, (b) drain delivery arrangement, (c) cross section of mandrel and drain (after Koerner, 1987), and (d) schematic installation process

Installing prefabricated vertical drains with a mandrel causes a significant disturbance of the subsoil, especially in the area immediately surrounding the mandrel. This disturbed zone is an area of reduced permeability that is called the smear zone (Figure 1.7). Typically, two parameters should be addressed to characterise this region, they include: (i) the permeability ratio, and (ii) the extent ratio. The permeability ratio is the ratio between the permeability of the intact zone and the permeability of the smear zone (k_h/k_s), and the extent ratio is equal to the radius of the smear zone over the radius of the drain or mandrel (r_s/r_w or r_s/r_m). The emerging smear zone and characteristics of the soil in this region can have a significant influence over the consolidation process. Therefore, an accurate estimation of the properties of the smear zone based on the type of soil and ground conditions is vital for ground improvement projects when using the prefabricated vertical drains assisted preloading method. Current literature indicates that further research is needed to quantify the properties of the smear zone based on the influencing factors, to help design engineers and clients optimise their designs and minimise construction costs, respectively.

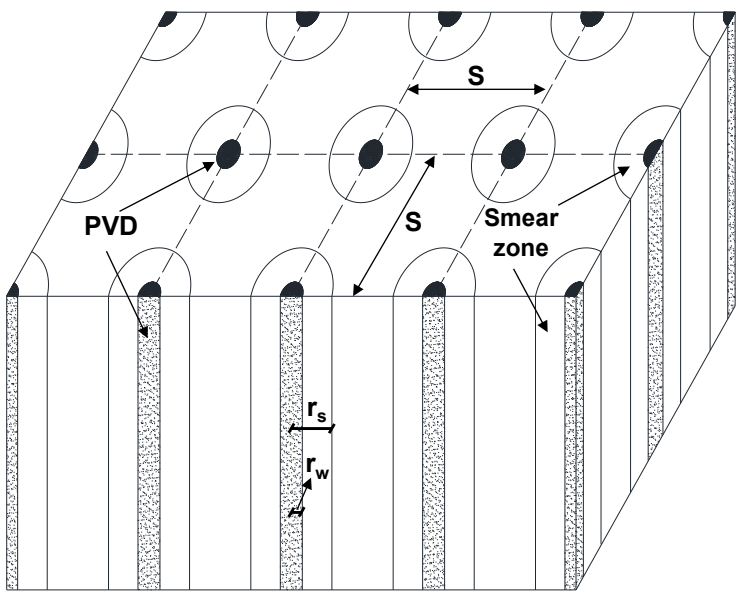

Figure 1.7 3D schematic diagram of the installation of vertical drains in a square patter

1.4 TRIAL EMBANKMENT MONITORING TO OBTAIN THE SMEAR ZONE PROPERTIES

Simulating the PVD assisted preloading process for complex ground conditions in a laboratory in order to estimate the characteristics of the smear zone is a challenging task due to the disturbed nature of the soil in the lab and simplifying the testing procedure. This means that a laboratory estimation of the properties of the smear zone may not be reliable for practical design purposes. Furthermore, most of the analytical solutions were developed on an assumption of a single axisymmetric drainage system and therefore cannot be used to directly analyse the behaviour of a soft soil deposit improved with multiple vertical drains. These limitations could well be magnified when the subsurface soil consists of a multi-layer soil profile. Assumed properties for the smear zone may result in inaccurate predictions of ground behaviour, and lead to an early removal of the surcharge in the construction process with subsequent excessive post construction settlements or construction time (required time to complete the construction project), and increasing the project cost. Field monitoring the actual preloading projects combined with a numerical analysis gives an opportunity to investigate the consolidation behaviour of the soft soil and back calculate the smear zone properties precisely.

The construction of a fully instrumented trial embankment has been used extensively as a reliable method to determine the feasibility of preloading with vertical drains, and to estimate the properties of the smear zone by applying a back calculation procedure. However, trial embankments take a long time to construct, which is the major challenge in using this method to estimate the extent and permeability of the smear zone, and in many cases may cause a considerable delay in the construction of the actual embankment and a significant increase in the project cost. Estimating the extent and permeability of the smear zone in the early stages of constructing a trial embankment can convert this method into a very practical, accurate, and cost effective approach, so in this study, it is investigated in depth.

1.5 OBJECTIVES AND SCOPE OF PRESENT STUDY

The ultimate goals of this study are to propose a systematic back calculation procedure to accurately estimate the properties of the smear zone and determine the

minimum degree of consolidation required, and consequently, the minimum time needed to wait after constructing a trial embankment, to obtain reliable smear zone properties. This research work consists of the following parts:

(i) Developing a numerical code and proposing a systematic back calculation procedure to obtain the properties of the smear zone,

(ii) Conducting laboratory testing to validate the designed back calculation procedure,

(iii) Simulating several case studies combined with parametric studies, and

(iv) Proposing an expanded back calculation procedure to determine the minimum required degree of consolidation that results in predictable smear zone properties.

FLAC software and its built-in programming language FISH have been used to develop a numerical code to be integrated into the proposed systematic back calculation procedure. A fully instrumented large Rowe cell has been used to conduct the laboratory test. The intact and smear zones have been simulated by filling the cell with clay that has a different permeability. A column of sand covered by geotextile filter has been placed at the centre of the cell to act as a vertical drain. The validity of the proposed back calculation procedure has been evaluated by comparing the numerical results with the laboratory measurements.

Then, the numerical code has been used to simulate the selected case histories and back calculate the smear zone properties using the proposed procedure. The numerical results of the simulated case studies have been used to determine the minimum degree of consolidation (after constructing a trial embankment) required, and the corresponding time that resulted in accurate smear zone properties by using an expanded back calculation procedure.

The specific objectives of this study are:

- Investigating the effects of the variability of smear zone characteristics on the PVD assisted consolidation process and preloading design,

- Investigating the variations of pore water pressure with vertical and radial distances from the drainage boundaries, and
- Evaluating how effectively the proposed equations are for converting the soil permeability from an axisymmetric condition to a plane-strain condition.

A systematic parametric study has been conducted on several case histories using the proposed back calculation procedure to investigate the variability of the smear zone properties on the preloading process. The laboratory test process has been simulated numerically in the axisymmetric condition, as well as the plane-strain condition, by adopting the proposed axisymmetric to plane-strain conversion equations. The numerical results for plane-strain and axisymmetric conditions have been compared to evaluate the accuracy of the conversion methods now available.

Finally, a minimum preloading time has been proposed for practicing engineers to predict the smear zone properties, which converts the construction of a trial embankment into a very efficient and practical method.

1.6 ORGANISATION OF THE THESIS

In Chapter 1, a brief introduction is presented where the aim and scope of the present research are highlighted. Chapter 2 presents a comprehensive survey of the literature review associated with the present work. The history of vertical drains and factors that affect the efficacy of consolidation by vertical drains are reviewed, with the focus directed towards existing experimental, analytical, and numerical approaches to estimate smear zone properties.

Chapter 3 presents the developed numerical code and the systematic back calculation procedure adopted in this research. FLAC software (v6.0.287) and its built-in programing language FISH are introduced for the development of numerical code, and the governing equations and adopted soil constitutive model are described.

In Chapter 4, the procedure for a laboratory consolidation test is described and the numerical code and back calculation procedure developed in Chapter 3 is verified using the experimental results. Furthermore, an evaluation of the available axisymmetric to plane-strain conversion equations is presented. A large Rowe cell with a diameter of 250 mm and a height of 200 mm was used to conduct the PVD assisted consolidation test procedure. The cell was fully instrumented and included a

vertical displacement gauge at the surface level and nine pore water pressure transducers on the sides and at the base of the cell.

In Chapter 5, five case studies are numerically simulated, including four trial embankments stabilised with vertical drains and one large consolidometer test. The systematic back calculation procedure was used to predict the characteristics of the smear zone. Chapter 6 presents the results of a parametric study where the simulated case studies in Chapter 5 were used to investigate the effect of changes in the property of the smear zone on the preloading process. Furthermore, the extended back calculation procedure was used to determine the minimum waiting time required after the construction of a trial embankment to reliably predict and report the smear zone properties to be used by practicing geotechnical engineers.

Chapter 7 draws conclusions from the current research and provides recommendations for future work. Following Chapter 7 are the list of references and the appendices.

CHAPTER TWO

2 LITERATURE REVIEW

2.1 HISTORY AND DEVELOPMENT OF VERTICAL DRAIN ASSISTED PRELOADING

To improve soft ground, different types of vertical drainage systems (e.g. sand compaction piles and prefabricated vertical drains) have been used extensively over the past few decades. According to Johnson (1970), the application of a vertical drainage system was first proposed around the 1920's and was patented in 1926 by Daniel J. Moran, an American engineer. Moran suggested the first practical application of sand drains to stabilise the mud soil beneath the roadway approach to the San Francisco Oakland Bay Bridge.

This solution led to comprehensive laboratory and field-testing by the California Division of Highways in 1933 on the effectiveness of sand drains on the rate of consolidation, and in 1936 Porter described some successful trials and contributed to further studies and developments. Since World War Two, the application of sand drains has undergone enormous development, largely due to better methods of installation and greater knowledge of the principles controlling their performance in different types of soft clays (Jamiolkowski et al., 1983). In Japan, during the 1940's, the behaviour of vertical sand drains was not understood very well because although the bearing capacity of the foundation was considered to be sufficient for a full load immediately after installation, frequent failures of foundations had been reported (Aboshi, 1992).

Walter Kjellman installed the first prefabricated drain system in a field test in 1937 using tubes made from a wood/fibre material, but after realising this material was inappropriate and too expensive, Kjellman invented and patented a band shaped cardboard drain in 1939, and a method for driving it into the ground. This cardboard drain consisted of two cardboard sheets glued together with an external cross section that was 100 mm wide by 3 mm thick, with ten 3-mm wide by 1-mm thick longitudinal internal channels. The efficiency of cardboard wicks was first

investigated at Lilla Mellosa in Sweden, in a full-scale test, after which several types of prefabricated band drains such as Geodrain (Sweden), Alidrain (England), and Mebradrain (Netherlands), were developed. Basically, prefabricated vertical drains (PVDs) have a rectangular cross section consisting of a filter fabric sleeve or jacket surrounding a plastic core. The sleeve acts as a physical barrier separating the core and the surrounding soil but permits pore water to enter the drain. It is made from non-woven polyester geotextiles, polypropylene geotextiles, or synthetic papers. The plastic core has grooved channels, which act as flow paths and supports for the filter sleeve (Bergado et al., 1996).

In the last 20 years, the PVD assisted preloading has been widely used as an efficient ground improvement technique. A selected number of successful PVD assisted projects are summarised in Table 2.1.

Table 2.1 PVD assisted preloading projects

Project	Location	Reference
Ningbo international airport	China	Zhu et al. (1993)
Coal & iron ore stack yard	India	Bhosle and Vaishampayan (2009)
Changi east reclamation project	Singapore	Bo et al. (2007)
Sunshine motorway	Australia	Sathananthan et al. (2008)
Chittagong airport	Bangladesh	Dhar et al. (2011)
Sarapui trial embankmnet	Brazil	Almeida et al. (2005)
Barra da Tijuca embankmnet	Brazil	Almeida et al. (2005)
Cumbulum trial embankment	Australia	Kelly (2008)
Muar test embankments	Malaysia	Balasubramaniam et al. (2007)
Haarajoki trial embankment	Finland	Yildiz and Karstunen (2009)

2.2 VACUUM PRELOADING AIDED PREFABRICATED VERTICAL DRAINS

Sometimes it is not feasible to build a high embankment over soft soil, as it might be extremely weak so that even a common 1.5m high embankment might cause a stability problem. Hence, it can be suitable to use vacuum preloading, because it will rectify the stability problems due to the reduced embankment height. A prefabricated

vertical drain combined with vacuum pressure is used to further enhance the rate of consolidation and shorten the construction periods (Chu et al., 2000; Chai et al., 2005; Liu and Chu, 2009; Liu et al., 2009). It can be noted that the prefabricated vertical drains used in vacuum preloading commonly have a circular cross section that facilitates the transfer of vacuum pressure to deeper soil layers with greater efficiency.

2.2.1 History and Developments of Vacuum Preloading

The concept of a vacuum preloading method (VPM) was first proposed by W. Kjellman of the Swedish Geotechnical Institute in 1952 (Kjellman, 1952). Since then, the vacuum preloading method has evolved into a mature and efficient technique for treating soft clays. This method has been successfully used for soil improvement or land reclamation projects in a number of countries (Bergado et al., 1990; Chu et al., 2000; Cao et al., 2001; Indraratna et al., 2007a). With the merging of new materials and new technologies, this method has been further improved in recent years. In adopting this technique, sand drains and recently prefabricated vertical drains have often been used to distribute the vacuum pressure and discharge pore water. A nominal vacuum load of 80 kPa is normally used in design, although a higher vacuum pressure of up to 90 kPa may be achieved. When a surcharge load higher than 80 kPa is required, a combined vacuum and fill surcharge can be applied. For the treatment of very soft ground, the vacuum preloading method is faster than the fill surcharge method, because an 80-kPa vacuum pressure can be applied almost instantly, without causing stability problems.

In terms of cost, the vacuum preloading is a very competitive option when the required embankment fill is high requiring large berms or heavy reinforcement. However, according to a comparison made by TPEI (1995), the cost of soil improvement using vacuum preloading is only two-thirds of that by fill surcharge. The vacuum preloading method has also been incorporated in the land reclamation process when clay slurry dredged from the seabed is used as fill material for land reclamation. As the dredged clay slurry is too soft to withstand the fill surcharge placed on top, the vacuum preloading method can be ideally used to consolidate the clay slurry. Table 2.2 shows a selected number of vacuum preloading projects successfully completed in different countries.

Table 2.2 Vacuum preloading projects

Project	Location	Reference
Tianjin Port	China	Yan & Chu (2005)
Survarnabhumi Airport	Thailand	Saowapakpiboon et al. (2009)
Port of Brisbane	Australia	Indraratna et al. (2011)
Ballina Bypass Highway	Australia	Kelly and Wong (2009)
Yaoqiang Airport	China	Tang and Sang (2000)
Kimhae Port Airport Highway	South Korea	Masse et al. (2002)
Second Bangkok International Airport	Thailand	Indraratna et al. (2004a)
Sewage Disposal Plant	Jang-U, Korea	Songa and Kim (2004)
Huanghua Port	China	Gao (2004)
Roadway embankment	France	Spaulding and Porbaha (2004)
Saga Road Construction	Japan	Chai et al. (2006)
Reclaimed land	Japan	Chai et al. (2008)
Maizuru Wakasa Expressway	Japan	Kawaida et al. (2012)
Nakorn Sri Thammarat Airport	Thailand	Teparaksa and Ngo (2012)

The Vacuum pressure technique has several advantages over the embankment loading, and they are summarised below:

(i) Less fill material needs to be used,

(ii) Construction period is generally shorter,

(iii) No need for heavy machinery for heavy preloading,

(iv) No need to add any chemical admixtures into the ground, and

(v) Environmentally friendly ground improvement method.

Indraratna et al. (2010) reported that the carbon emissions from vacuum technology with PVDs are much lower than the pile foundations because the production of concrete and steel requires significant levels of energy. Two different methods are proposed to conduct the vacuum preloading process; (i) Vacuum preloading using membrane, and (ii) Membrane free technique.

2.2.2 Vacuum Preloading Using Membrane

In this method, vacuum consolidation consists of a system of vertical drains and a drainage sand blanket on top sealed from the atmosphere by an impervious membrane on top. Horizontal drains are installed in the drainage layer and are connected to a vacuum pump. To maintain air tightness, the ends of the membrane are placed at the bottom of a peripheral trench filled with bentonite. Negative pressure is created in the drainage layer by the vacuum pump. The negative pressure generates negative pore water pressures, resulting in an increase in the effective stresses in the soil, which in turn leads to an accelerated consolidation process (Qian et al, 2003). This system is illustrated in Figure 2.1.

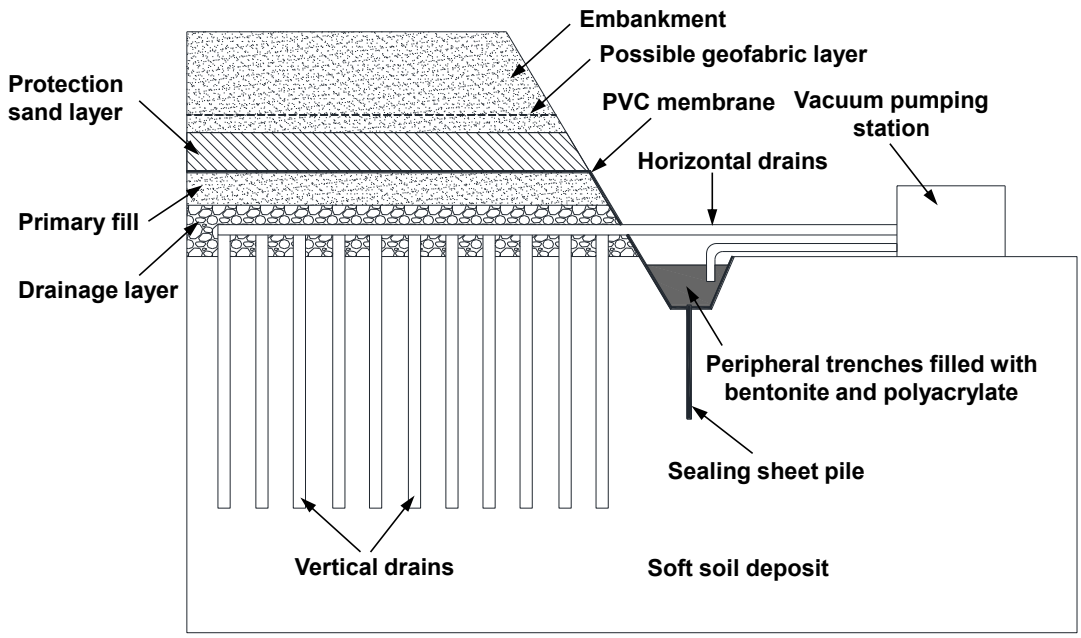

Figure 2.1Vacuum preloading system

In recent years, new materials have been developed for horizontal drain pipes to improve the vacuum preloading process (Figure 2.2). The drain panels can be used instead of pipes to ensure the drainage channels will still function correctly under a high surcharge pressure, as in the case of combined fill and vacuum preloading. The drainage panels also provide better channels for distributing vacuum pressure and water discharging. Some drainage panels also have slots for a direct connection with PVDs, which also improves the efficiency of the system.

(a) **(b)** **(c)**

Figure 2.2 Horizontal pipe used for vacuum preloading (a) corrugate flexible pipes, (b) and (c) other types of geo-composites (after Chu et al. 2008)

2.2.3 Vacuum Preloading: Membrane Free Techniques

When the total area must be sub-divided into a number of sections to facilitate the installation of the membrane, vacuum preloading can only be carried out in one section at a time. This may not be efficient when vacuum preloading is used for land reclamation over a large area. A common method to overcome this problem is to connect the vacuum channel directly to each individual drain using a tubing system, as shown in Figure 2.3a. In this way, the channel from the top of the PVD to the vacuum line is sealed. Hence, a sand blanket and membranes are not required (Figure 2.3b). This system was used for constructing the new Bangkok International Airport (Seah, 2006). However, as such a system does not provide an airtight condition for the entire area, its efficiency can be low, and the vacuum pressure applied may only be 50 kPa or lower (Seah, 2006). This method only works when the layer of soil to be improved is predominantly clay with a very low permeability.

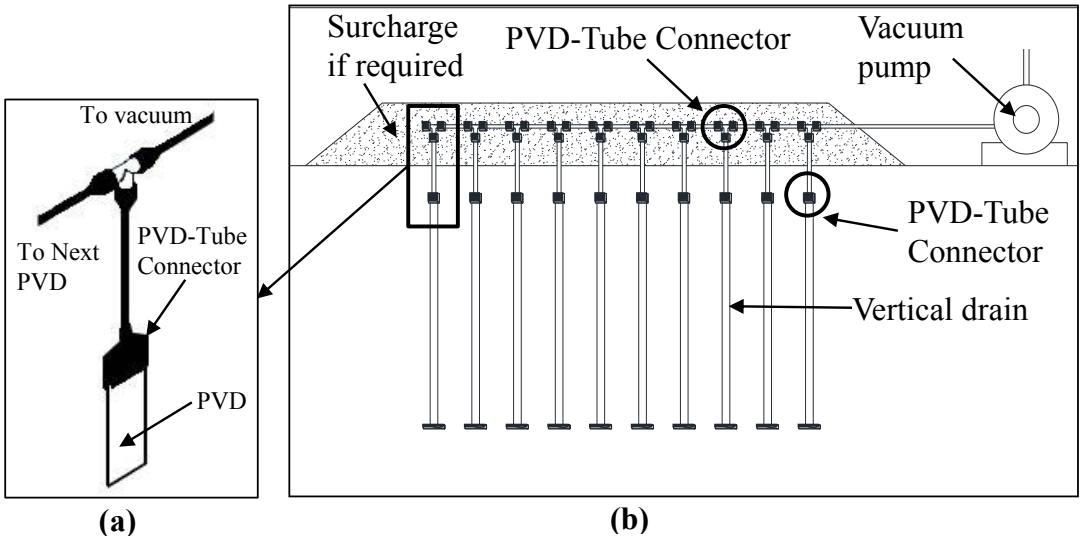

Figure 2.3 Vacuum preloading-membrane free technique (a) PVD and tubing for vacuum preloading, and (b) cross section of vacuum-PVDs method

Another method to exclude the membrane is to use the so-called low level vacuum preloading method (Yan and Cao, 2005). This method is schematically illustrated in Figure 2.4. When clay slurry is used as fill for land reclamation, the vacuum pipes can be installed at the seabed or a few metres below the ground surface, and the clay slurry fill can be placed on top of the vacuum pipes. As clay has a low permeability, the fill material will provide a good sealing cap and membranes will not be required. However, this method is not free of problems. Tension cracks will develop in the top layer when dried under the sunlight (Chu et al., 2008). The vacuum pressure may not be distributed properly unless a drainage blanket is used at the level where the drainage pipes are installed, or where the individual drains are directly connected to the vacuum pipes. It is also difficult to install drainage pipes or panels underwater. Nevertheless, this method does not require the construction of inner dikes for a sub-division and thus cuts down the project costs substantially (Chu et al., 2008).

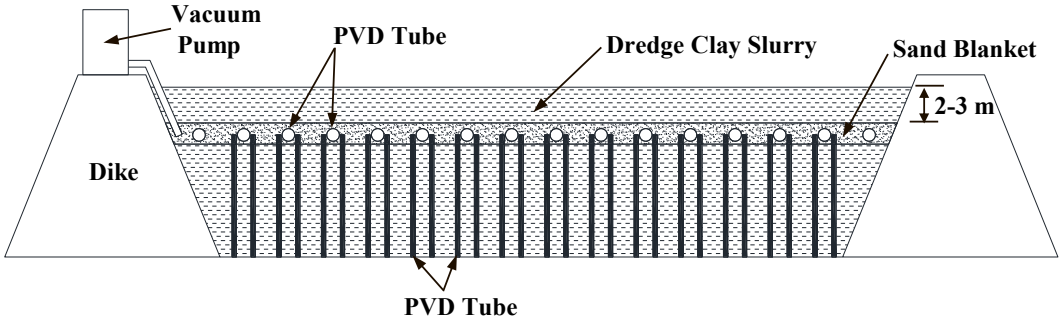

Figure 2.4 Low level vacuum preloading with no membrane (after Chu et al. 2008)

2.3 FACTORS AFFECTING CONSOLIDATION OF CLAY WITH PVDS

The design of prefabricated vertical drains varies according to the specific application. The key parameters and factors influencing the PVD assisted preloading design are the equivalent diameter, the filter and apparent opening size, the tensile strength, the discharge capacity and well resistance, smear zone, soil macro fibre, mandrel size and shape, installation procedure, and the drain spacing and influence zone, all of which are explained in detail in the following section.

2.3.1 Equivalent Diameter

In the equivalent two dimensional design, it is necessary to convert the band shaped drain into an equivalent circular diameter called the "equivalent diameter," as shown in Figure 2.5. This dimension dictates the size of the inflow surface.

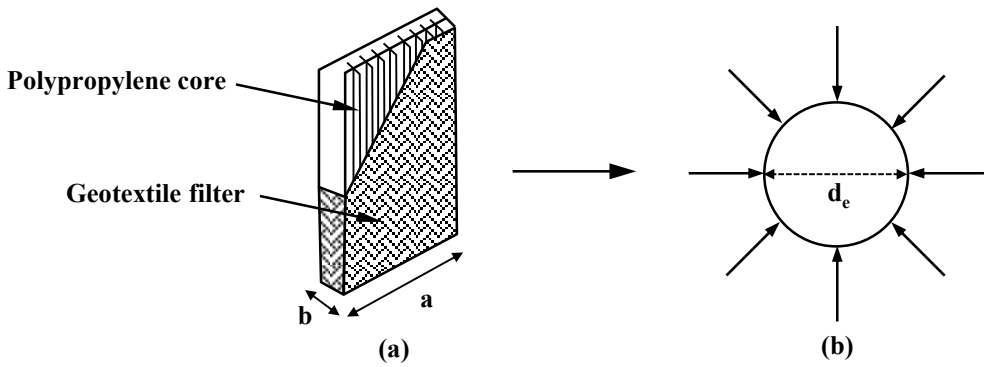

Figure 2.5 Equivalent diameter, (a) vertical band shaped drain, and (b) PVD equivalent diameter

Different equations for the equivalent drain diameter (d_e) of band shaped PVD have been proposed and are presented in Table 2.3. The dimensions a=100 mm and b=4 mm are considered to compare the results of different equations.

Table 2.3 Suggested equations for equivalent diameter of PVD

References	Suggested equation	Equivalent diameter of drain (mm) (PVD 100×4 mm)
Hansbo (1979)	$d_e=\frac{2\times(a+b)}{\pi}$	66.2
Atkinson and Eldred (1981)	$d_e=\frac{a+b}{2}$	52.0
Fellenius and Castonguay (1985)	$d_e=\left(\frac{4ab}{\pi}\right)^{0.5}$	22.6
Pradhan et al. (1993)	$d_e=d_e-2\sqrt{(\bar{s}^2)}+b$ $\bar{s}^2=\frac{1}{4}d_e^{\ 2}+\frac{1}{12}a^2-\frac{2a}{\pi^2}d_e$	44.1
Long and Covo (1994)	$d_e=0.5a+0.7b$	52.8
Abuel-Naga and Bouazza (2009)	$d_e=0.4546a$ $0.0333\leq b/a\leq 0.0875$	45.4

Ideally, it is proper to adopt Hansbo's method (1979, 1981), wherein the d_e value is the diameter of an annulus having the equivalent circumference of a PVD. This method gives rise to the largest value (6.62 cm) among the listed values, which is exclusively used in practice. Holtz et al. (1991) reported that Hansbo's method is reasonable. However, the other methods present reduced values compared to the above value, possibly due to the effectiveness of the size of the PVD.

A numerical study was performed by Abuel-Naga and Bouazza (2009) to establish the equivalent diameter of a PVD well by considering the equal flow condition. According to this research, for a rectangular section ($0.0333 \leq b/a \leq 0.0875$), the equivalent diameter is only a function of the width of the PVD. The equivalent diameter equation presented in this study is close to the equations proposed by Atkinson and Eldred (1981), Pradhan et al. (1993), and Long and Covo (1994), and is in agreement with the experimental results reported in literature. It is

therefore suggested that the proposed equation, together with Long and Covo's (1994) equation, can be used to evaluate the PVD equivalent PVD diameter. Figure 2.6 shows a schematic comparison of d_e derived from three different equations.

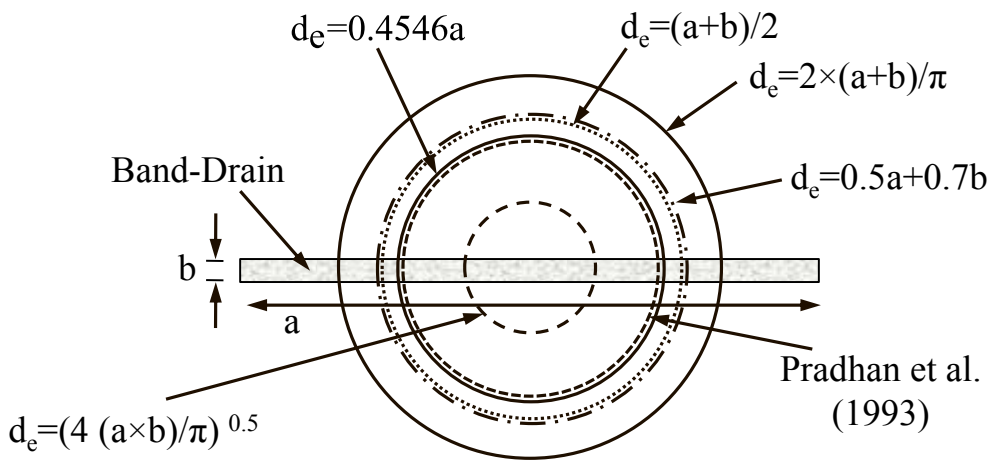

Figure 2.6 Schematic comparison of different PVD equivalent diameter calculation approach

Welker and Herdin (2003) conducted five experiments with both an injection and an extraction component to evaluate four of the most commonly used equivalent diameter formulations for PVDs. The injection and extraction tests were performed applying constant head and constant vacuum pressure, respectively. Based on the results, there is little difference between the Hansbo (1979), Long and Covo (1994), and Atkinson and Eldred's (1981) formulations based on their corresponding injection flow rates. All three of those equations had injection and extraction rates that were similar to those obtained for the PVD both with and without considering the effects of the smear zone. The Fellenius and Castonguay (1985) formulation held the least correlation to the PVD under injection conditions.

2.3.2 Filter and Apparent Opening Size (AOS)

As explained by Indratana et al. (2002), the drain material (sand drain) and the filter jacket of PVD have two basic but contrasting roles, which are: (i) retaining the soil particles, and (ii) at the same time allowing the pore water to pass through. The characteristics of the filter that affect the functionality of the vertical drain are reported as follows:

(i) Permeability of the filter jacket,

(ii) Filtration (effective filtration can minimise movement of soil particles through the filter),

(iii) Retention ability of the filter, and

(iv) Filter clogging (filter material may be clogged when the soil particles are trapped within the filter fabric)

To cover the PVD functions, the apparent opening size (AOS) should satisfy the proposed requirements given in Table 2.4. The parameter O_{95} indicates the approximate largest particle that would effectively pass through the filter.

Table 2.4 Apparatus opening size requirements of PVD

Function	Requirement	Reference
Drainage	$k_f > 2k_{soil}$	Bo et al. (2003)
Filtration	$\frac{O_{95}}{D_{85}} \leq 2\text{-}3$	Caroll (1983)
Retention ability	$\frac{O_{50}}{D_{50}} \leq 10\text{-}12$	Caroll (1983)
Clog preventing	$\frac{O_{95}}{D_{15}} \geq 3$	Christopher and Holtz, 1985

Note: k_f is the permeability of the filter and k_{soil} is the permeability of the soil, O_{95} is the AOS of the filter, O_{50} is the size which is larger than 50% of the fabric pore, D_{85} is the size for 85% of passing of the soil particles, D_{50} is the size for 50% of passing of the soil particles, and D_{15} is the size for 15% of passing the soil particles.

Bo et al. (2003) reported that the permeability of the filter is normally required to be at least one order of magnitude higher than the soil. Considering the clogging effect, a much higher permeability should be required for the filter. Nevertheless, even more stringent requirements on the permeability of the filter can be met easily because most of the PVDs have a filter permeability that is higher than 10^{-4} m/s, which is far more than what is required. The thickness of the filter is another consideration. Normally, the thicker the filter, the better it becomes, while keeping the other conditions the same. Based on Wang and Chen (1996), the mass to area ratio should be generally larger than 90 g/m^2.

2.3.3 Tensile Strengths

Prefabricated vertical drains should be strong enough to sustain the tensile stresses subjected to it during installation, and therefore the strength of the core, the filter,

and the strength of the entire drain and the spliced drain should be specified in both wet and dry conditions (Bo et al., 2003). Kremer et al. (1983) reported that a drain should be able to withstand at least 0.5 kN of tensile force without exceeding 10% of elongation. It is common nowadays to specify the tensile strength of the entire drain at wet and dry conditions to be larger than 1 kN at a tensile strain of 10% (Bo et al., 2003). A spliced vertical drain should also be required to have a tensile strength comparable to an unspliced drain.

2.3.4 Discharge Capacity and Well Resistance

Prefabricated vertical drains are used to dissipate excess pore water pressure in the soil and discharge water, and therefore the higher their discharge capacity the better they perform. The discharge capacity of a band drain, denoted as q_w, is defined as the rate of flow through the drain at a hydraulic gradient of unity. Bergado et al. (1996) reported that the discharge capacity can be expressed as the product of the longitudinal permeability of the drain and its cross sectional area. The discharge capacity of vertical drains can be affected by factors such as the consolidation stress, deformation of the drain, time, clogging, and the hydraulic gradient and temperature.

When the discharge capacity of a vertical drain is smaller than the amount of water that needs to be discharged, well resistance will occur. Ideally, the discharge capacity of the drain should be large enough to ignore the well resistance in the design because the well resistance increases as the length of the drain increases, and reduces the rate of consolidation. Well resistance retards the dissipation of pore pressure, which means that settlement is retarded. According to Bamunawita (2004), the three main factors that increase the well resistance are as follows:

(i) Deterioration of the drain filter (reduction of the cross section of the drain),

(ii) Passing of fine soil particles through the filter (reduction of the cross section of the drain), and

(iii) The drain folds due to large settlement or lateral movement.

Xie (1987) and Wang and Chen (1996) reported that the following condition must be met in order to maintain the well resistance at an insignificant level:

$$\frac{\pi}{4}\frac{k_h}{q_w}{l_m}^2 < 0.1 \quad (2.1)$$

where, k_h is the horizontal hydraulic conductivity of soil (m/s) and l_m is the length of the vertical drain (m).

To satisfy Equation (2.1), the discharge factor (D_F) must be held by the following equation:

$$D_F = \frac{q_w}{k_h {l_m}^2} \geq 7.85 \quad (2.2)$$

The required discharge capacity after applying a reduction factor to consider all the factors influencing the discharge capacity is reduced to:

$$q_{req} \geq 7.85 F_s k_h {l_m}^2 \quad (2.3)$$

where, q_{req} is the required discharge capacity (m^3/s) and F_s is the reduction factor with a value between 4 and 6.

Bo et al. (2003) states that it is unnecessary to use an excessively high reduction factor for the discharge capacity because, although the discharge capacity reduces with the deformation of the vertical drain and time, the permeability of the soil reduces with consolidation, so the amount of water discharged also reduces over time. Different studies have been carried out to determine the value of q_w, and they are summarised in Table 2.5.

It can be observed that the discharge capacity is affected by the lateral confining pressure. According to Indraratna and Bamunawita (2002), in the absence of laboratory test data, the discharge capacity can be conservatively assumed to be 100 m^3/year. The results of the back analysis showed that the discharge capacity can fall below this desired value due to the drain kinking and clogging (e.g. 25-100 m^3/year) (Indraratna and Bamunawita, 2002). Clearly, the 'clogged' drains are associated with q_w values approaching zero.

Table 2.5 Suggested values for discharge capacity of PVD

References	Discharge capacity	Remarks
Den Hoedt (1981)	95	Lab. Test (σ_c=50-300 kPa)
Kremer *et al*. (1982)	160	Lab. Test (σ_c=100 kPa)
Jamiolkowski *et al*. (1983)	10~15	Lab. Test (σ_c=300-500 kPa)
Oostveen (1986)	150	Back analysis
Rixner *et al*. (1986)	100	Lab. test
Hansbo (1987)	50~100	Lab. test
Koda *et al*. (1984)	100	Lab. test
Holtz *et al*. (1991)	100~150	Lab. Test (σ_c=300-500 kPa)
Mesri and Lo (1991)	2~80	Back analysis
Koerner & Ko (1992)	50~150	Back analysis
Indraratna (2002)	100	Back analysis
Bo (2004)	27~405	Back analysis
Kamon and Suwa (2006)	48~125	Lab. Test (σ_c= 300 kPa)

Note: σ_c is the lateral pressure

A new type of PVD, the so called integrated PVD where the core and filter adhered together due to heat melting, was introduced by Liu and Chu (2009). The integrated PVD offers a number of advantages over the separable PVD. Both the tensile strength and the discharge capacity of the integrated PVD were higher than the separable one made from the same material.

2.3.5 Smear Zone

Installing vertical drains with a mandrel causes a significant disturbance of the sub-soil, especially near the mandrel. This disturbed zone is called the smear zone. According to Sharma and Xiao (2000), the permeability of the soil around the drain can be decreased significantly by smearing and retarding the rate of consolidation. Two parameters are needed to characterise the smear effects, namely the smear zone radius (r_s), and the permeability of the smear zone. The smearing effect is comprehensively discussed in Section 2.4.

2.3.6 Soil Macro Fibre

For soils with pronounced macro fabrics, the ratio of horizontal permeability to vertical permeability (k_h/k_v) can be very high, whereas the k_h/k_v ratio becomes unity within the disturbed (smear) zone. Vertical drains are very efficient where the layers of clay contain many micro layers of horizontal sand or silt lenses. However, if these micro layers are continuous in a horizontal direction, installing vertical drains may be ineffective because rapid drainage of the pore water out of the layers of soil may occur irrespective of whether drains are installed or not (Sharma and Xiao 2000).

2.3.7 Mandrel Size and Shape

Prefabricated vertical drains are installed by pushing a steel mandrel, approximately 5 inches (127 mm) by 2 inches (51 mm) in section, vertically into the ground. The material of the PVDs is protected inside the mandrel and is affixed to an anchor plate or bar at the base of the mandrel. Generally, any disturbance increases with the total cross sectional area of the mandrel, which means the size of the mandrel should be as close as possible to the drain to minimise the smearing effect. The common types of mandrel cross sections are shown in Figure 2.7.

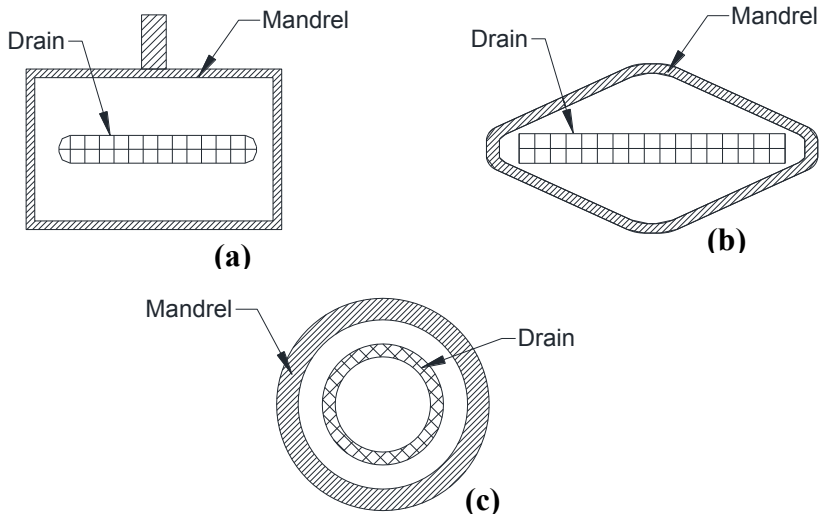

Figure 2.7 Examples of mandrel shapes, (a) rectangular, (b) rhombic and (c) circular

The effect of the shape of the mandrel was investigated analytically by Basu et. al (2010) using four different size mandrels: 125 mm × 50 mm, 150 mm × 50 mm, 120

mm × 120 mm, and 150 mm × 150 mm. The results clearly showed that the rate of consolidation decreased as the size of the mandrel increased. Furthermore, square mandrels disturb a much larger area than rectangular mandrels, which means that PVDs installed with square mandrels are less effective.

2.3.8 Installation Procedure

Prefabricated vertical drains should be installed using approved equipment which can insert the material into the ground with the minimum possible disturbance to the soils while keeping the mandrel vertical during installation. The PVD is forced into the soil with the hollow mandrel, and once a firm layer is encountered or the target depth is reached, the mandrel is retracted and the PVD, which is held in the ground by the anchor, stays in place. Once the bottom of the mandrel reaches the surface, the PVD is cut and the anchor for the next drain is attached. The mandrel is part of a mast assembly, which is supported and powered by a hydraulic excavator or crane, and it is then removed leaving the PVD in place. Figure 2.8 illustrates the installation rig.

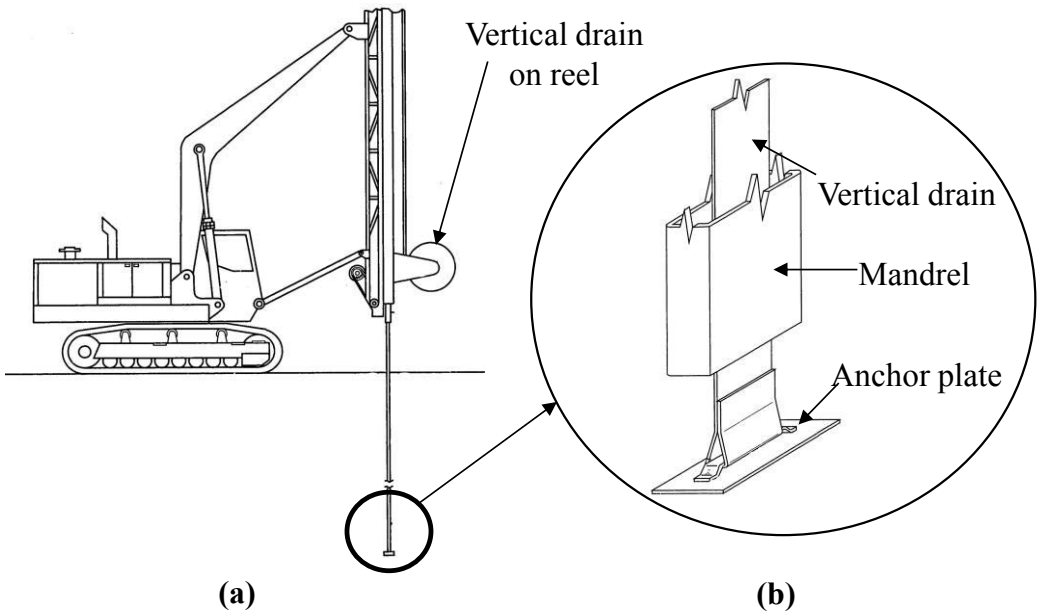

Figure 2.8 PVD installation equipment, (a) crane and drain delivery arrangement, and (b) vertical drain surrounded by hollow mandrel and attached to the anchor plate at bottom

2.3.9 Drain Spacing and Influence Zone

Vertical drains may be installed at regular intervals in a square, rectangular, or triangular pattern (Bergado et al. 1996), with centre to centre distance (S) varying from about 1.0 to 3.5 m (Holtz 1987). As illustrated in Figure 2.9, the radius of the influence zone (R) is a controlled variable because it is a function of the drain spacing (S). The zone of influence can be determined using following equations:

$$R=0.546S \text{ (square pattern)} \tag{2.4}$$

$$R=0.525S \text{ (triangular pattern)} \tag{2.5}$$

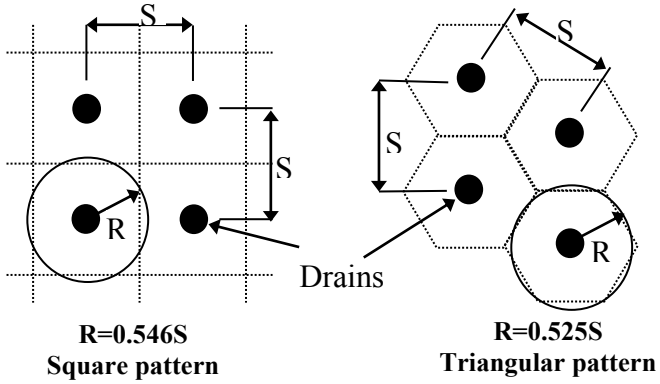

Figure 2.9 Influence zone of PVD, (a) square patter and (b) triangular pattern

A square pattern of drains is often easier to lay out during field installation, although a triangular pattern is usually preferred because it provides more uniform consolidation between the drains (Indraratna and Bamunawita, 2002). Drain spacing can be determined based on the required degree of consolidation and work timeframe by adopting analytical solutions. According to the practical recommendations the drain spacing should usually be more than 0.8 m.

2.4 SMEARING EFFECT

According to Sharma and Xiao (2000), the installation of prefabricated vertical drains (PVDs) using a mandrel disturbs the soil around the drain, which results in a smear zone of reduced permeability that adversely affects the consolidation process. Predicting the behaviour of soil surrounding the drain requires an accurate estimation

of the smear zone properties. Generally, two major parameters are proposed to characterise the smear zone, the permeability (k_s), and the extent (r_s) of the smear zone.

Factors affecting the properties of the smear zone are explained by Bergado et al. (1991) as follows:

(i) PVD installation procedure,

(ii) Specifications of the mandrel the type of anchor at the bottom of the PVD, and

(iii) Type of soil.

Hird and Moseley (2000) mentioned that the surface roughness of the mandrel and the inward movement of the soil when the mandrel sheath is removed are the key parameters affecting the characteristics of the smear zone. According to their study, the smearing effects increase in severity as the thickness of the clay layer or the driving rate is reduced. It was indicated that the angle of the tip of the mandrel does not necessarily influence the severity of smearing in layered soils.

According to the experimental results reported by Hird and Sangtian (2002), the smearing effects can be reduced substantially by changing the cross section of the driving mandrel from a circular shape to a slim rectangular one.

2.4.1 Smear Zone Generation

Generally, two main reasons and theories have been proposed to explain the generation of the smear zone: (i) the concept of soil remoulding, and (ii) the reconsolidation theory.

2.4.1.1 Soil Remoulding Concept

When drain wells are installed by driving cased holes, which are back filled as the casing is withdrawn, driving and pulling the casing would distort and remould the adjacent soil (e.g. Barron 1948). According to the remoulding concept restated by several other researchers (Barron 1948; Hansbo 1981; Indraratna and Redana 1997), for PVD assisted preloading design, the soil surrounding the drain is divided into two sections: (i) the disturbed region near the drain, and (ii) the intact or undisturbed zone

beyond the undisturbed zone. Figure 2.10 shows the smear zone near a vertical drain based on the remoulding concept.

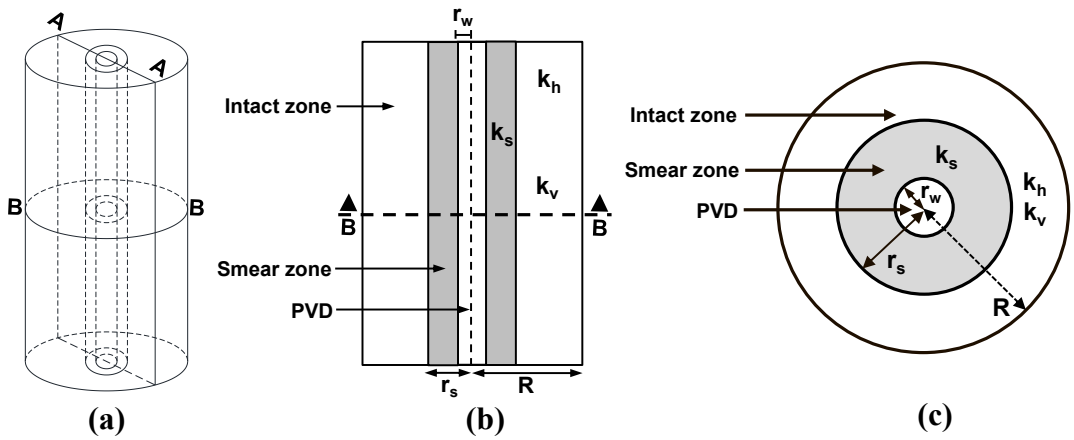

Figure 2.10 PVD surrounding by smear zone (remoulding theory), (a) installed drain, (b) profile A-A, and (c) cross section B-B

Note: r_s is the radius of the smear zone, r_w is the radius of the vertical drain, k_h is the horizontal permeability of the intact zone, k_v is the vertical permeability of the intact zone, k_s is the permeability of the smear zone, and R is radius of drain influence zone.

2.4.1.2 The Reconsolidation Theory

Sharma and Xiao (2000) reported that the change in the properties of the clay layer due to mandrel insertion is brought about by a combination of reconsolidation due to the dissipation of excess pore pressure and remoulding of the clay layer due to the shear stresses applied by the outer surface of the mandrel. According to the above mentioned study, the process of reconsolidation has a much greater influence on the properties of the clay layer than the process of remoulding, even for sensitive, structured clays. The so-called smear zone around the vertical drains may be further divided into two zones: (a) a remoulded zone of rather limited extent located close to the drain, and (b) a reconsolidated zone of much wider extent located between the remoulded zone and the intact clay (Figure 2.11).

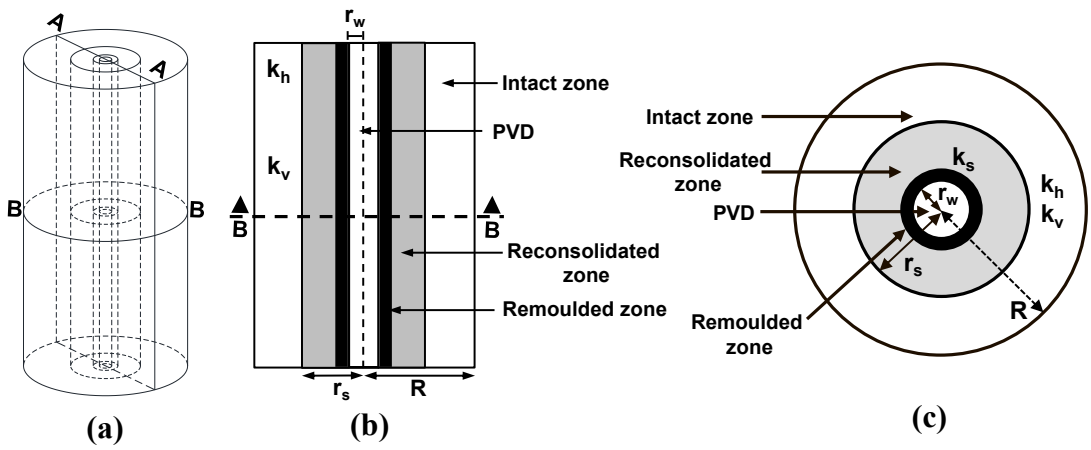

Figure 2.11 PVD surrounding by disturbed soil (reconsolidation theory), (a) installed drain, (b) profile A-A, and (c) cross section B-B

In recent years, a few researchers have used the cavity expansion theory to analyse the reconsolidation of soil associated with the installation of mandrel driven prefabricated vertical drains with a mandrel (e.g. Sathananthan et al. 2008; Ghandeharioon et al. 2010). Furthermore, Shin et al. (2009) used a micro-cone and an electrical resistance probe to investigate the smearing effect before and after reconsolidation.

2.4.2 Smear Zone Extent & Permeability Variation

The combined effects of permeability and compressibility within the smear zone result in a different smeared soil behaviour compared to undisturbed soil. Predicting the behaviour of soil surrounding the drain requires an accurate estimation of the properties of the smear zone (Sathananthan, 2005).

There are two main schools of thought to determine the characteristics of the soil surrounding the drain:

(a) Two zones hypothesis, which divides the surrounding soil into the smear zone and undisturbed (intact) zone.

(b) Three zones hypothesis which considers three zones; the smear zone (inner smear zone) in the immediate vicinity of the drain, the transition zone (outer smear zone), and the undisturbed (intact) zone.

In the two zone hypothesis, two major parameters are proposed to characterise the smear zone; the extent ratio (s) and the permeability ratio (n):

$$s = \frac{r_s}{r_m} \; or \; \frac{r_s}{r_w} \tag{2.6}$$

$$n = \frac{k_h}{k_s} \tag{2.7}$$

where, r_s is the radius of the smear zone, r_m is the radius of the mandrel, r_w is the radius of the vertical drain, k_h is the horizontal permeability of the intact zone, and k_s is the permeability of the smear zone. It should be noted that it is usually assumed that the vertical and horizontal permeability values in the smear zone are the same (Indraratna and Redana, 1998).

Figure 2.12 illustrates the cross section of the ground near a vertical drain for both hypotheses.

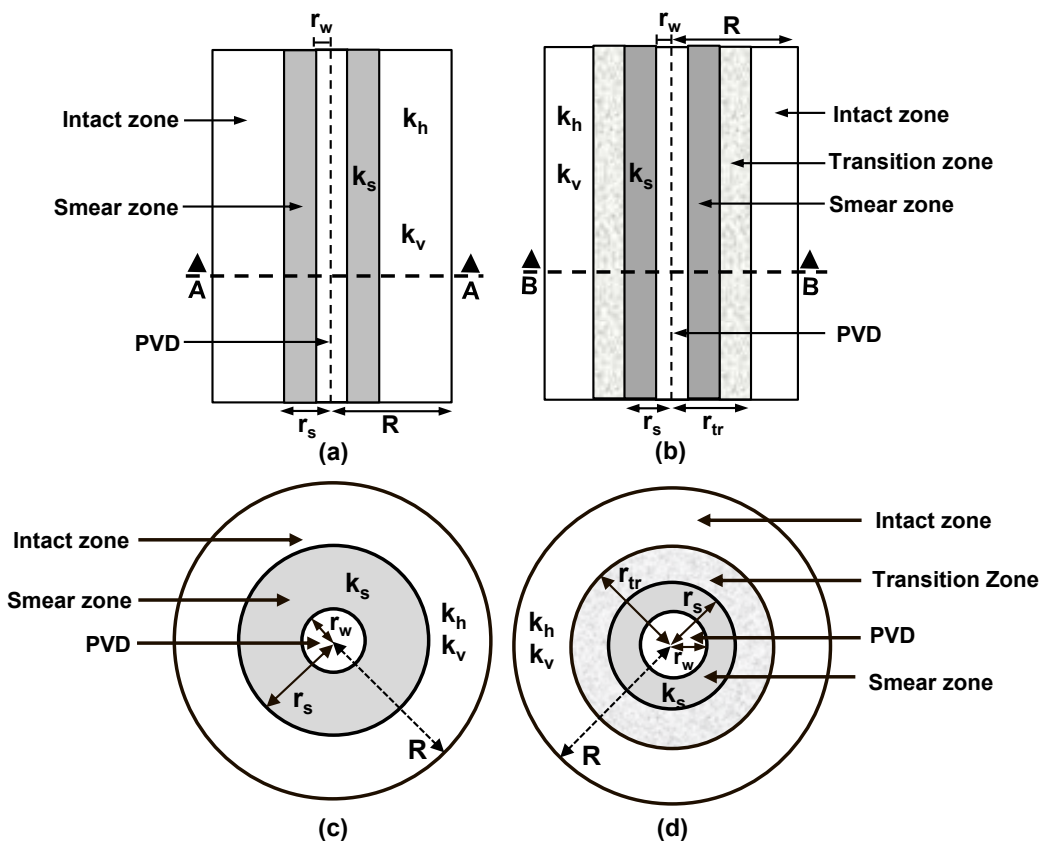

Figure 2.12 PVD surrounded by smear zone, (a) for two zones hypothesis profile, (b) for three zones hypothesis profile, (c) cross section A-A for two zones hypothesis, and (d) cross section B-B for three zones hypothesis

According to the literature (e.g. Barron, 1948; Hansbo, 1981; Jamiolkowski et al., 1983; Onoue et al., 1991; Madhav et al., 1993; Chai and Miura, 1999; Hawlader et al., 2002; Walker and Indraratna, 2006; Basu et al., 2006; Rujikiatkamjorn and

Indraratna, 2009) different patterns are proposed for the permeability variation in the disturbed zone (Figures 2.13a and 2.13b).

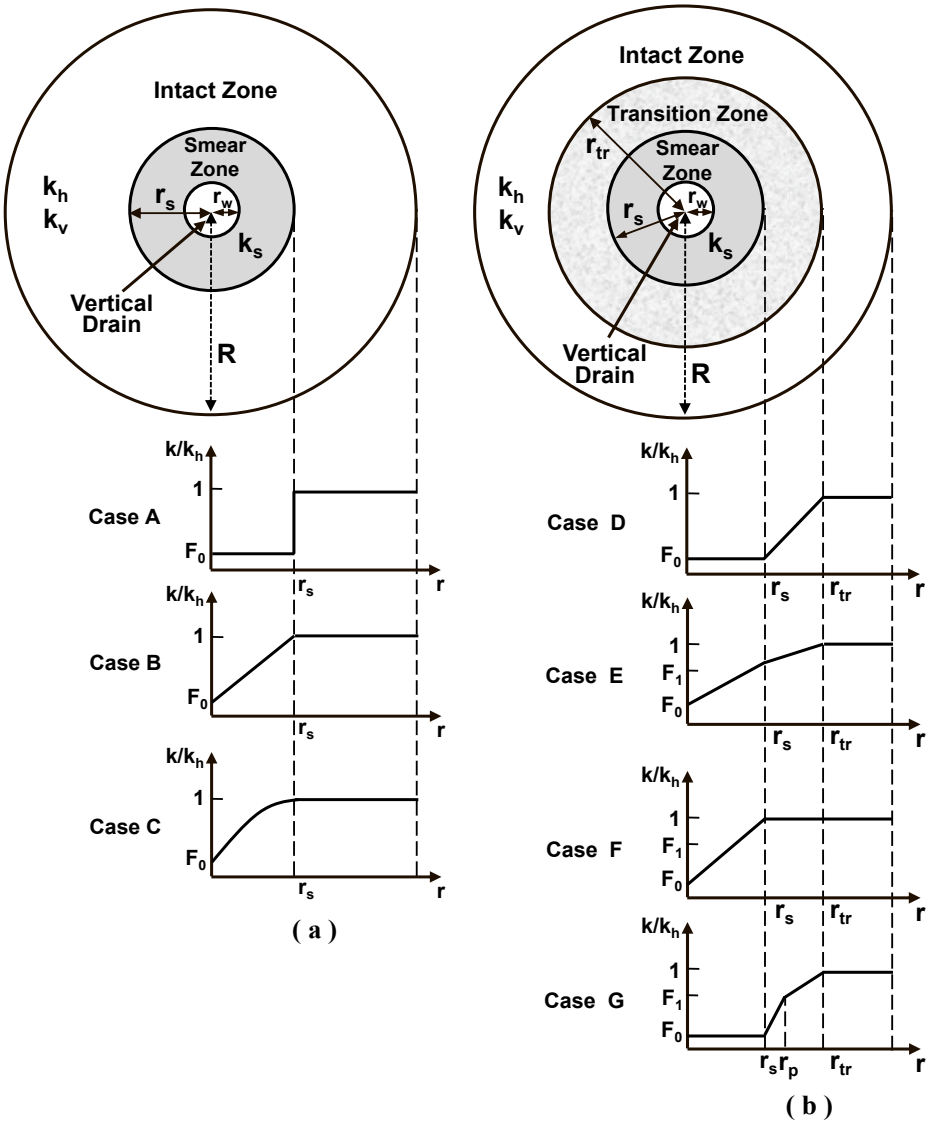

Figure 2.13 Variation of permeability in the disturbed zone, (a) two zones hypothesis and (b) three zones hypothesis

Following the two zones hypothesis, a number of researchers (e.g. Barron 1948; Holtz and Holm 1973; Hansbo 1981; Jamiolkowski et al. 1983; Chai and Miura 1999) have proposed a constant smear zone permeability (Figure 2.13a, Case A). Rujikiatkamjorn and Indraratna (2009) considered a linear variation for the permeability of the smear zone with the radial distance (Figure 2.13a, Case B), whereas Walker and Indraratna (2006) assumed a parabolic distribution for permeability in the smear zone (Figure 2.13a, Case C).

Following the three zones hypothesis, Madhav et al. (1993) suggested that soil has a constant permeability (k_s) in the smear zone, while in the transition zone surrounding the smear zone, the permeability linearly decreases from a value equal to k_s at the smear zone boundary to the initial in situ value k_h at the boundary of the transition zone (Figure 2.13b, Case D). Onoue et al. (1991) proposed two equations for the variation of the permeability coefficients in the smear zone and transition zone (Figure 2.13b, Case E). Hawlader et al. (2002) proposed a linear variation of permeability within the smear zone changing from k_s to k_h and a constant permeability of k_h for the transition zone (Figure 2.13b, Case F). It was indicated that the overall progress of consolidation is mainly controlled by the smear zone surrounding the drains, while the transition zone has almost no influence. In addition, Basu et al. (2006) reported that permeability remains constant at the value of k_s within the smear zone and increases in the transition zone following a bi-linear curve with an initial slope from k_s at the smear zone boundary to k_p at an intermediate point (at $r=r_p$), and a secondary slope from k_p (at $r=r_p$) to k_h at the transition zone boundary (Figure 2.13b, Case G).

2.4.3 Estimation of the Smear Zone Properties

2.4.3.1 Experimental Methods

Estimating the radius and permeability of the smear zone has been the subject of intense discussion in the geotechnical engineering industry and research. In many classical theories the influence of the smear zone is described based on the two zone hypotheses, i.e., an undisturbed zone with natural permeability and a smear zone with reduced permeability. The accuracy of the predictions using classical theories depends on a correct assessment of the horizontal permeability and extent of the smear zone. Typically, the properties of a constant smear zone were assumed or back calculated by geotechnical experts (e.g. Baron 1948; Casagrande and Poulos 1969; Holtz and Holm 1973; Akagi 1976; Hanso 1981; Jamiolkowski et al. 1983; and Bergado et al. 1991) to be used in practical designs, and no laboratory tests to evaluate the characteristics of the smear zone were conducted until 1991.

Since 1991, comprehensive experimental studies have been conducted to determine the extent and permeability of the smear zone (Bergado 1991; Onoue et al.

1991; Madhav et al. 1993; Indraratna and Redana 1998; Hird 2000; Sharma and Xiao 2000; Sathanantan and Indraratna 2006; Shin et al. 2009; Ghandeharioon 2009).

Indraratna and Redana (1998) investigated the effect of smearing due to the installation of a vertical sand compaction pile in the laboratory, using a large scale consolidometer, which is illustrated in Figure 2.14.

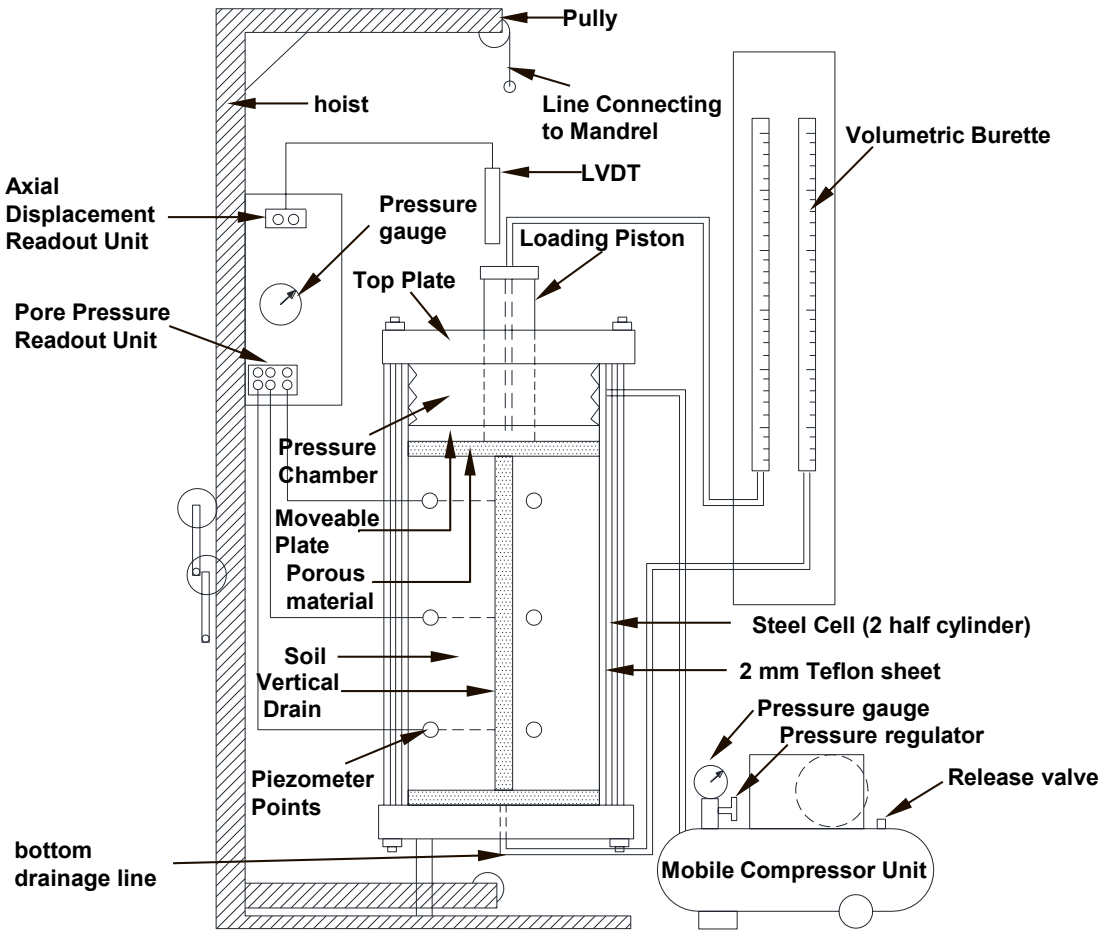

Figure 2.14 Large-scale consolidation apparatus (after Indraratna and Redana 1998)

The clay was thoroughly mixed with water before placing into the large cylinder, and then the soil was placed inside and compacted in layers. A vertical drain was installed using a purpose designed "pipe" mandrel and hoist (pulley system). The mandrel was 50 mm in diameter by 2mm thick. After the sand was poured into the pipe, it was gradually withdrawn with the hoist while the pipe was lightly vibrated and the sand was compacted with an external rod.

After installing the sand compaction pile into the large cell, small specimens were collected from different locations within the cell at known radial distances,

using a specially designed tube sampler. The samples were subjected to one-dimensional consolidation using conventional oedometers in order to study the variation in the properties of the soil close to and away from the central drain. It was observed that the compressibility and permeability of the smear zone near the sand drain would be quite different from the clay unaffected by the installation of the sand compaction pile. The radius of the smear zone (r_s) was estimated to be a factor of 4 to 5 times the radius of the mandrel (r_m).

A large scale test apparatus was developed by Sharma and Xiao (2000) to examine the extent and characteristics of the smear zone surrounding the prefabricated vertical drains. The apparatus consists of three main components: a consolidation tank, a motorised drain installation machine, and instrumentation. A schematic diagram of the test apparatus is illustrated in Figure 2.15.

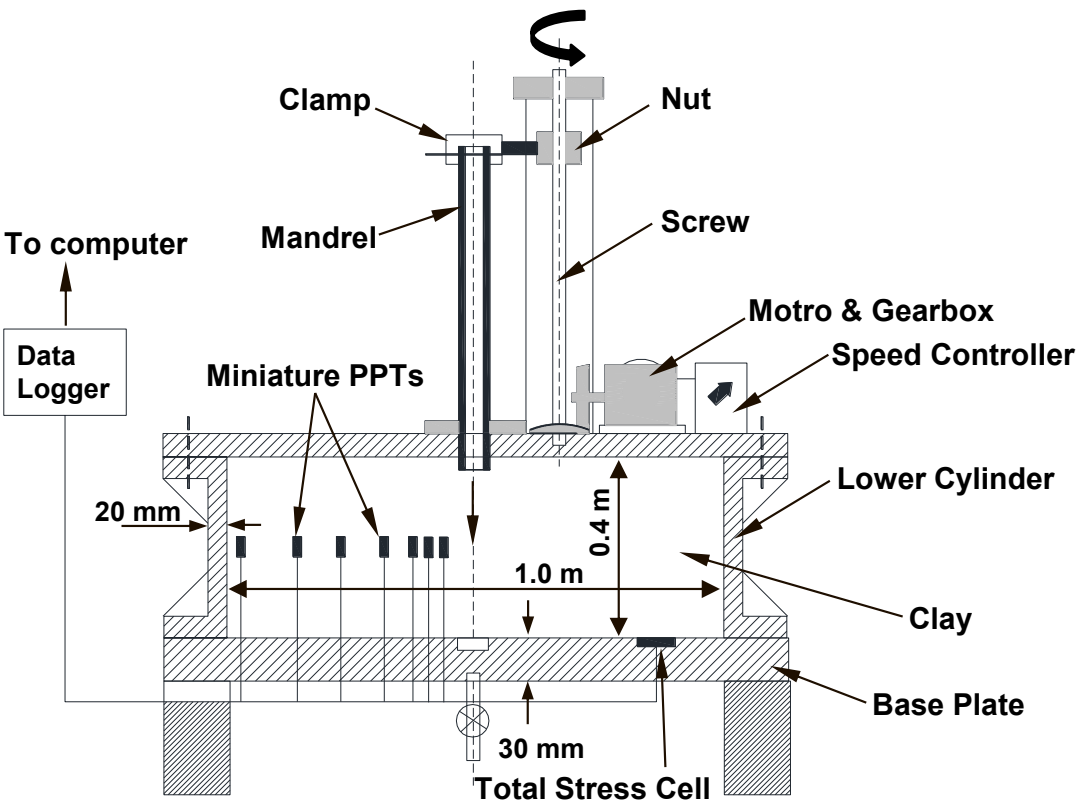

Figure 2.15 Large scale consolidation apparatus (after Sharma and Xiao 2000)

A motorised drain installation machine was developed to install the PVD by pushing or pulling the mandrel at speeds ranging from 0.1 to 4 m/min. The miniature PPTs were inserted from the base plate through the cable adapters and fixed at predetermined radial and vertical distances using 5 mm diameter bronze rods.

A typical test was carried out in three stages: preparation of the clay deposit, installation of the drain, and collection of the oedometer and moisture content samples. After the excess pore water pressures induced by installing the PVD were dissipated, the test was stopped and the entire clay deposit was removed from the lower cylinder. Undisturbed vertical and horizontal samples were taken from the middle section of the clay deposit at seven different locations, as shown in Figure 2.16. Oedometer tests were performed on these samples to evaluate the permeability and compressibility of the clay deposit.

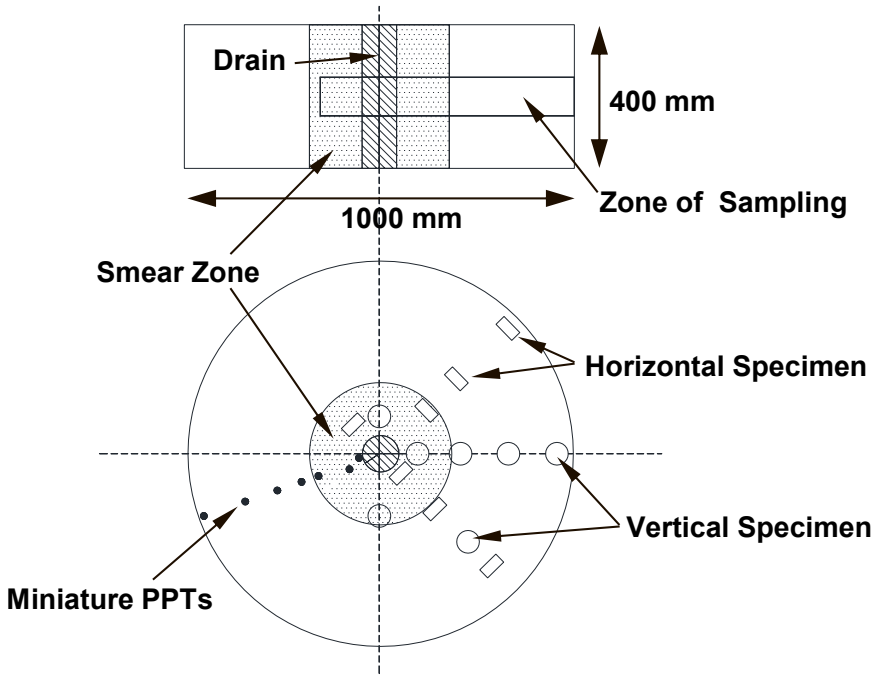

Figure 2.16 Schematic diagram of sampling locations for the Oedometer test specimen (after Sharma and Xiao 2000)

The test results indicated that the radial extent of the smear zone was 4 times greater than the vertical drain radius. The average permeability of the clay in the smear zone was 1.3 times smaller than in the intact zone.

Shin et al. (2009) conducted a series of radial penetration tests, including a micro-cone penetrometer (MCP) and an electrical resistance probe (ERP), into the specimen of reconstituted clay prepared in a large scale consolidometer to evaluate the extent of the smear zone induced by the installation of a prefabricated vertical drain with a rectangular mandrel and an anchor shoe. The schematics of large scale consolidometer and micro-cone penetrometer are shown in Figure 2.17.

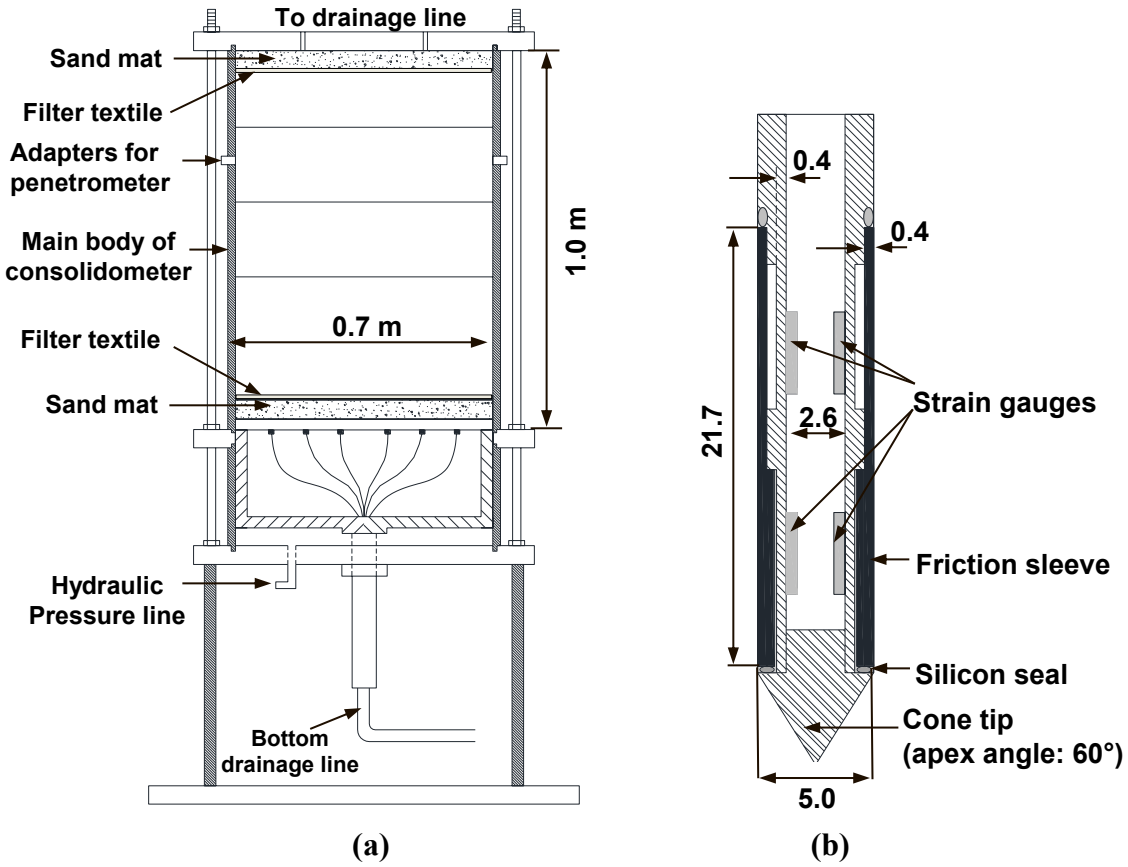

Figure 2.17 Radial penetration test, (a) Large-scale consolidometer, and (b) Micro-cone penetrometer (after Shine et al. 2009)

The main test procedure consisted of six stages; (i) preparing the clay specimen, (ii) horizontal penetration tests of the micro-cone and ERP to obtain the reference profiles of the resistance of the cone tip, and the electrical resistivity, (iii) installation of the PVD, (iv) horizontal penetration tests of the micro-cone and ERP to detect the smear zone, (v) a 7 day consolidation with PVD, and (vi) horizontal penetration tests of the micro-cone and ERP to observe any changes in the smear zone. Both penetration tests were conducted at 0.3 m below the top of the specimen. Each penetration test was conducted at a rate of 1 mm/s to 300-340 mm from the chamber wall. Figure 2.18 shows a plan view indicating the directions of each horizontal penetration test.

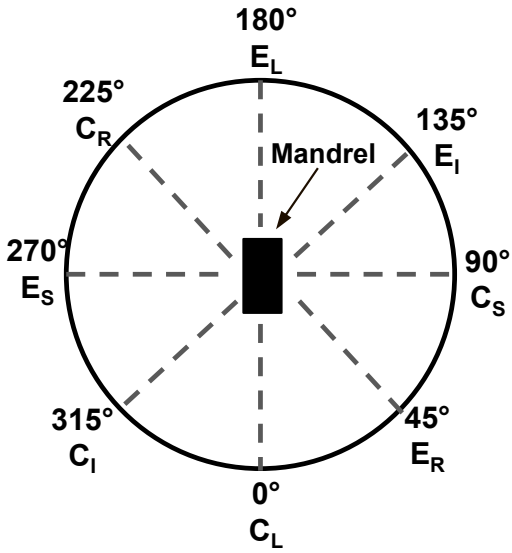

	Micro-cone Penetrometer (MCP)	Electrical Resistance Probe (ERP)
Reference	C_I	E_I
After PVD installation	C_L C_S	E_L E_S
After re-consolidation with PVD	C_R	E_R

Figure 2.18 Directions of MCPs and ERPs horizontal penetration (after Sine et al. 2009)

As reported by Shine et al. (2009) after 32 days of consolidation under 200 kPa pressure, horizontal penetration tests of the micro-cone and ERP were performed in 315° and 135° directions to obtain the reference profiles of the resistance of the cone tip and the electrical resistivity (C_I and E_I, respectively). As there was no disturbed zone in the specimen before the installation of PVD these profiles were expected to be referred to when a comparison was made with those following the installation of PVD. A modified double core PVD was driven into the soil specimen prepared in the consolidometer with a rectangular steel mandrel. A rectangular shaped shoe was attached to the end of the PVD and the mandrel was inserted to a depth of 0.6 m at a constant penetration rate of 20 mm/s. Immediately after the PVD was installed, micro-cone penetration tests were performed in 0° and 90° directions to determine the extent of the smear zone (C_L and C_S, respectively).

While the PVD was being installed, an undrained condition was maintained and excess pore water pressure built up in the smear zone (Onoue et al. 1991; Hird

and Moseley 2000; Sharma and Xiao 2000). It was therefore expected that the void ratio or the electrical resistivity was the same throughout the specimen if the ERP tests were carried out immediately after the installation of PVD. The ERP penetration tests were performed in 180° and 270° directions (E_L and E_S, respectively) about 6 h after the micro-cone penetration tests. After the clay specimen was re-consolidated with the PVD for 7 days and the applied pressure of 200 kPa was maintained, both penetration tests were performed in 225° and 45° directions (C_R and E_R, respectively).

According to the continuous profiles of cone resistance and electrical resistivity obtained from the penetrations of the micro-cone and ERP (Shin et al., 2009), in the intact zone where the specimen was not affected by the installation of PVD, both measurements reached constant values once the boundary effect of the cylinder wall had disappeared. The resistance of the cone tip and electrical resistivity started to deviate from constant values at certain locations, suspected to be the outer boundary of the smear zone, and the magnitudes of the deviation continued to increase towards the area where the PVD was installed. After allowing 7 days of consolidation with the PVD, the resistance of the cone tip within the smear zone increased significantly, while a slight increase in the electrical resistivity occurred throughout the whole specimen. It was found that the size of the smear zone was approximately 3.2~3.4 times the half-length and 5.3~5.4 times the half-width of the mandrel. This implied that the shape of the smear zone was elliptical. In other words the smear zone was about 4.0~4.2 times that of the equivalent radius in the longer axis of the mandrel and 3.3~3.4 times that of the equivalent radius in the shorter axis of the mandrel.

The installation of mandrel driven prefabricated vertical drains was simulated in large scale laboratory conditions by Ghandeharioon et al. (2012) (Figure 2.19). The laboratory experiments were carried out with a consolidometer specifically designed for that purpose, and a machine capable of driving mandrels at realistic rates. The variations of pore water pressure at different locations during the installation of the mandrel driven PVD, and while the mandrel was being withdrawn, were also investigated.

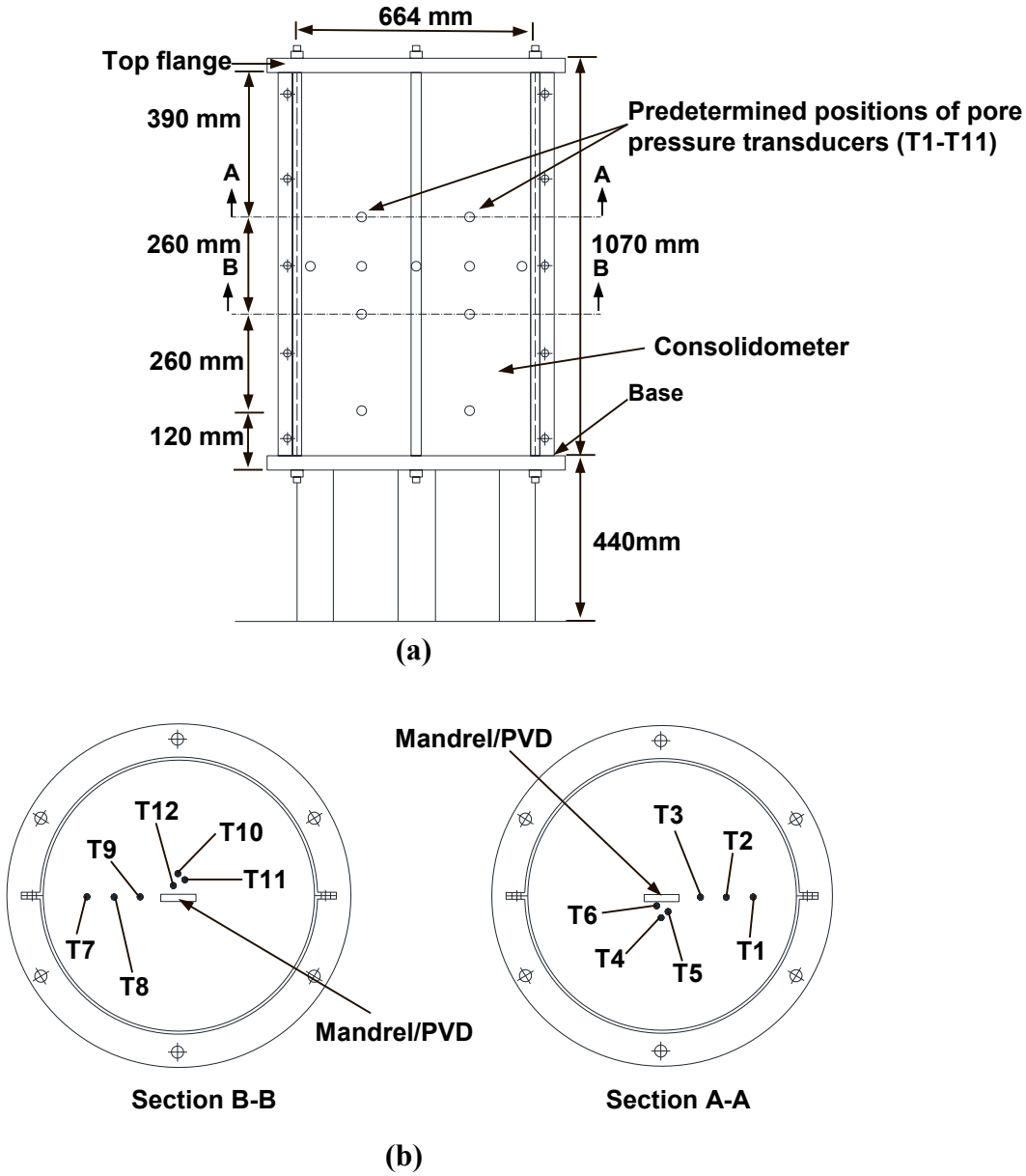

Figure 2.19 Schematic design, (a) Large consolidometer, and (b) radial positions (plannar view) of fast response pore pressure transducers (Ts) relative to the centre of the cell at levels identified in (a) (after Ghandeharioon et al., 2012)

The extent of the smear zone in the large-scale consolidometer was determined using the results from moisture content tests on samples, which in relation to the installed PVD, were cored from various locations along different polar axes. The results verified the concept of an elliptical smear zone around drains driven by rectangular mandrels, and showed that for a given type of soft soil subjected to a particular rate of installation, the size of the smear zone around the mandrel decreased as the in situ effective stresses increased. On the basis of these results, the average radius of the

smear zone around each PVD was predicted to be about 3.5 times the equivalent radius of the mandrel.

According to the current literature, the proposed experimental values for the smear zone permeability ratio (k_h/k_s) and extent ratio (r_s/r_m or r_s/r_w) are between 1.34 to 3 and 1.6 to 7, respectively. The properties of the smear zone obtained from experimental studies and laboratory measurements were compiled and are summarised in Figure 2.23 in section 2.4.3.4.

2.4.3.2 Cavity Expansion Theory

It can be observed that a wide range is proposed for the characteristics of the smear zone based on laboratory investigations and no comprehensive method is recommended to precisely predict their properties.

In recent years a few researchers have used the cavity expansion theory (CET) to analyse the reconsolidation of soil associated with mandrel driven prefabricated vertical drain installation (Sathananthan et al. 2008 and Ghandeharioon et al. 2010). Using this theory, the installation process is modelled as the expansion of a cavity with a final radius equal to that of the mandrel (r_m). The shape of the mandrel can be rectangular, circular, or rhombic; hence, an equivalent mandrel radius is evaluated by equating the area between the assumed circular cross section and the actual shape of the mandrel.

The analytical cavity expansion solutions capturing the critical state theories were developed by Collins and Yu (1996), and comprehensively described by Yu (2000). The expansion of a cavity is illustrated in Figure 2.20. This figure shows a cavity with an initial radius a_0 and an internal pressure σ_0. The cavity expands to a radius of a when the internal pressure increases from σ_0 to σ_a, whereas an element initially at a radial distance r_0 from the centre of the cavity moves to a new radial position r from the centre. The soil on the cavity wall will yield when the pressure in the cavity is large enough, whereas further increases in this pressure will lead to the formation of a plastic zone around the cavity. The radial distance of the plastic zone around the cavity is denoted by r_p, whereas the soil beyond this would remain in a state of elastic equilibrium.

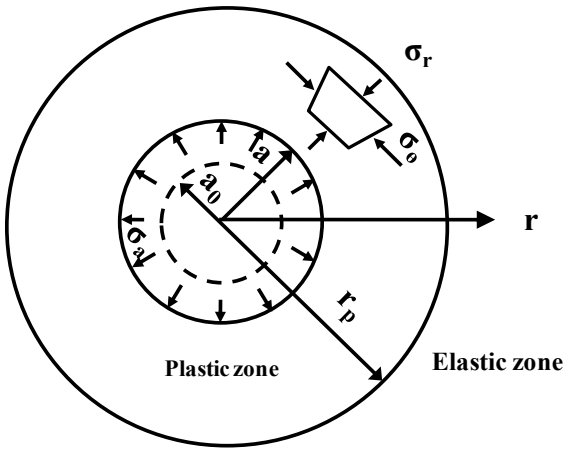

Figure 2.20 Expansion of a cavity (after Yu 2000)

Developing an analytical framework to analyse cavity expansion can be based on the assumption that soil obeys Hooke's elasticity until the onset of yielding (elastic zone), and the yielding of soil (plastic zone) is described by the MCC model (Sathananthan et al., 2008).

According to Sathananthan et al. (2008), the stress ratio, $\eta = q/p'$, and the radial distance from the centre of cavity (r) can be related by:

$$ln\left(1-\frac{r_m{}^2}{r^2}\right) = -\frac{2(1+\mu)}{3\sqrt{3}(1-2\mu)}\frac{\kappa}{v}\eta 2\sqrt{3}\frac{\kappa\Lambda}{\upsilon M}f(M,\eta,R_1) \tag{2.8}$$

where

$$f(M,\eta,R_1) = \frac{1}{2}ln\left[\frac{(M+\eta)(1-\sqrt{R_1-1})}{(M-\eta)(1+\sqrt{R_1-1})}\right] - tan^{-1}\left(\frac{\eta}{M}\right) + tan^{-1}\left(\sqrt{R_1-1}\right)$$

where, v=specific volume; μ=Poisson's ratio; p'=effective mean pressure; q=deviator stress; $\Lambda = 1-\kappa/\lambda$=plastic volumetric strain ratio; λ=gradient of the virgin compression line on $\upsilon - lnp'$ space; κ=slope of swelling line on $\upsilon - lnp'$ space; M=slope of the critical state line; and the isotropic over-consolidation ratio (R_1) can be related to the conventional over consolidation ratio (OCR) as follows:

$$R_1 = \frac{3(45-12M+M^2)OCR}{(6-M)(6+M+2(6-M)OCR^{(3M/6+M)})} \tag{2.9}$$

The radius of the plastic zone (r_p) could be determined by substituting $\eta = M\sqrt{R-1}$ in Equation (2.8) and the stress ratio (η) and the effective mean pressure (p') in the plastic zone can be calculated by the Equation (2.10) (Sathananthan et al. 2008).

$$p' = p_0' \left[\frac{R}{1+\left(\frac{\eta}{M}\right)^2}\right]^{\Lambda} \tag{2.10}$$

where, p_0'=initial effective mean pressure.

A series representation of the effective mean pressure and the deviatoric stress with radius can be found using Equation (2.8) and (2.10). As proposed by Sathananthan et al. (2008), the variation of the pore water pressure (u) with radial distance can be obtained from the Equation (2.11), when the cavity radius becomes equal to the equivalent mandrel radius:

$$u = p_0 + \frac{Mp_0'}{\sqrt{3}}\sqrt{R-1} - \frac{q}{\sqrt{3}} + \frac{2}{\sqrt{3}}\int_r^{r_p}\frac{q}{r}dr - p' \tag{2.11}$$

where, p_0=initial mean pressure.

The cavity expansion theory (CET) was used by Sathananthan et al. (2008) by incorporating the Modified Cam-Clay model to predict the extent of the smear zone (r_m). It was assumed that within the smear zone the normalised pore pressure u/σ_{v0}, (i.e., pore pressure/initial overburden stress) exceeded unity, but according to the results, the size of the smear zone was at least 2.5 times the equivalent mandrel radius and the permeability of the smear zone varied from 61% to 92% (average of 75%) of the intact zone permeability. The predicted radius of the smear zone was verified using the large scale consolidometer. The test was conducted on the basis of the development of excess pore water pressure while the mandrel was being installed, the variation of normalised permeability (k_h /k_{hu}) (k_{hu} is the maximum undisturbed zone horizontal permeability), and a reduction of the normalised water content. The results of this verification indicated there was a good agreement between the analytical predictions and the laboratory measurements.

Ghandeharioon et al. (2010) used a new elliptical cavity expansion theory to characterise the disturbed zone around rectangular and rhomboidal mandrels, while incorporating a Modified Cam-Clay model for the soft soil. They assumed that the

installation rate of PVDs was more than 0.15 m/s so mandrel penetration was considered as undrained, which may not be applicable in every case. Moreover, the variation of shear strain and excess pore pressure were determined just after the mandrel was inserted and the extent of the smear zone was estimated based on these changes, even though in reality the properties of the smear zone should be defined after reconsolidation and complete dissipation of any excess pore pressure. In this elliptical solution, the changes in the ratio of the semi-major axis to the semi-minor axis were not considered and a constant ratio was assumed.

Ghandeharioon et al. (2010) determined the excess pore water pressure at a certain radial distance from the centre as follows:

$$\Delta u = \Delta p - \Delta p' \tag{2.12}$$

Equations (2.13)-(2.15) were used by Ghandeharioon et al. (2010) to calculate the total stress (σ_r), effective stress (p') and the deviator stress (q) at any soil element inside the plastic region:

$$\sigma_r = \sigma_{r_p} - \frac{2}{\sqrt{3}} \int_{r_p}^{r} q \frac{dr}{r} \tag{2.13}$$

$$ln\left(1 - \frac{r_1^2 - r_0^2}{r^2}\right) = \frac{q}{\sqrt{3}G} - 2\sqrt{3}\frac{\kappa\Lambda}{\nu M}\left[\zeta - tan^{-1}\left(\frac{\eta}{M}\right) + tan^{-1}\sqrt{n_p - 1}\right] \tag{2.14}$$

$$q = Mp'\sqrt{n_p\left(\frac{p'}{p_0'}\right)^{-1/\Lambda} - 1} \tag{2.15}$$

where, $\zeta = \frac{1}{2} ln \frac{(\eta+M)(\sqrt{n_p-1}-1)}{(\eta+M)(\sqrt{n_p-1}+1)}$ and $\eta = \frac{q}{p'}$.

In the above equations, r_p is the initial radius of the plastic zone measured from the centre of the cavity, r_0 is the initial radius (in the direction of the semi-major axis) of an elliptical cavity, r_1 is the instantaneous radius of an elliptical cavity, $n_p = p'_{y_0}/p'_0$ is the isotropic over consolidation ratio (p'_{y_0} is the maximum isotropic preconsolidation stress), σ_{r_p} is the total radial stress at the elastic-plastic boundary (kPa), $\Lambda = 1 - (\kappa/\lambda)$ is the plastic volumetric strain ratio, λ is the slope of the normal compression line in the $\nu - lnp'$ space, κ is slope of the elastic swelling

line in the $v - lnp'$ space, v is the soil specific volume (1+e), M is the slope of the critical state line in the $p' - q$ plane, r is the instantaneous position of a soil element measured from the centre of the cavity, and p'_0 is the initial effective mean stress.

According to the results reported by Ghandeharioon et al. (2010), the proposed relationship for determining the excess pore water pressure (Equation 2.12) based on elliptical CET captures the actual position of the soil elements (polar coordinates) and therefore provides a better match for the actual disturbance.

The plastic shear strain (γ_q^p) normalised by the rigidity index (I_r) may also be used to characterise the disturbed soil surrounding the mandrel (Figure 2.21). Ghandeharioon et al. (2010) reported that γ_q^p/I_r is as large as 0.86–1.05% at the boundary of the failed soil (Figure 2.21). The smear zone propagates outward where the normalised plastic shear strain within the smear zone is from 0.10 to 0.17%. At the boundary of the marginally disturbed zone γ_q^p/I_r is about 0.01– 0.05%. The region in which γ_q^p is greater than zero constitutes the plastic zone, while the outer elastic zone (zero plastic shear strain) is not affected by any change in the pore water pressure before or after driving the mandrel.

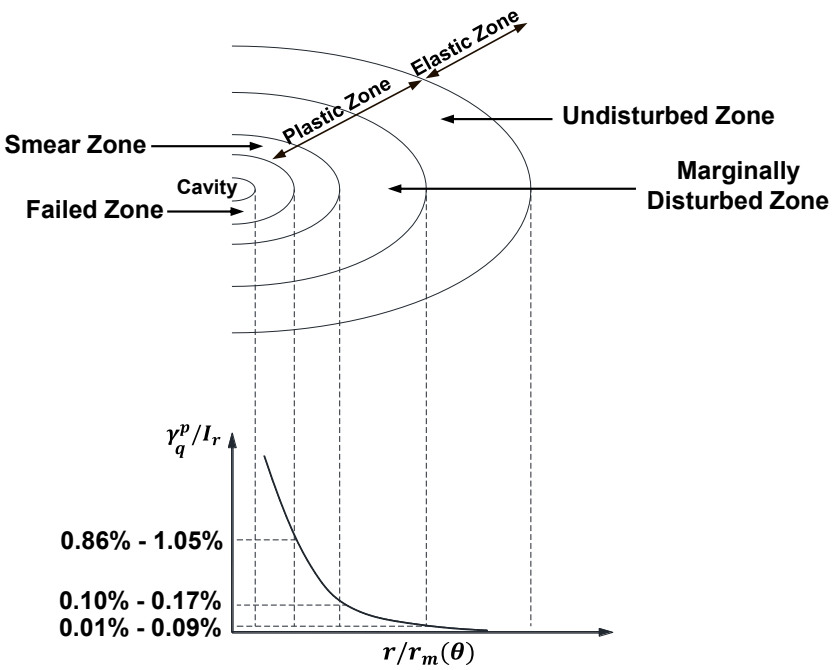

Figure 2.21 Distribution pattern for the ratio of the plastic shear strain to the rigidity index in relation to the radial distance normalized by the equivalent elliptical radius of the mandrel characterising the disturbed soil surrounding a PVD (after Ghandeharioon et al. 2010)

The proposed analytical solution by Ghandeharioon et al. (2010) was successfully verified by using a case history from the Muar clay region in Malaysia. According to the results of this verification, the radius of the smear zone was about 3.1 times the equivalent radius of the mandrel, a value that is close to the radius suggested by previous studies.

2.4.3.3 Finite Element Methods

The advancements in finite element codes have assisted geotechnical researchers to simulate mandrel insertion numerically and investigate the load deformation during installation of the mandrel by incorporating a large strain condition. This method is typically used to simulate the installation of piles (Sheng et al. 2005; Walker and Yu, 2006).

Small et al. (1976) stated that the behaviour of saturated clays under rapid loading occurred under fully undrained conditions and therefore the study of mandrel penetration in saturated clays is essentially an undrained analysis. During installation, excess pore water pressure can be induced as a result of a change in the octahedral normal stress ($\Delta\sigma_{oct}$) and the octahedral shear stress ($\Delta\tau_{oct}$) (Burns and Maynes, 1998). While the volumetric strain remains constant during undrained conditions, as does the octahedral normal stress, variations in the shear strain adjacent to the side of the mandrel alters the octahedral shear stress. This zone of disturbance depends on the size and shape of the mandrel, the properties of the soil, the speed of installation, and the geometry of the cone (Kim et al. 2007).

Rujikiatkamjorn et al. (2009) used the ABAQUS finite element code for a numerical simulation of mandrel penetration in normally consolidated soils. The geometry, mesh, and boundary condition of the simulated large scale laboratory model is illustrated in Figure 2.22. The Axisymmetric 4-node bi-linear displacement and pore pressure elements (CAX4P), and the axisymmetric 4-node bi-linear displacement elements (CAX4), were used to simulate the soil and the mandrel respectively. A coupled analysis with large strain frictional contact was used to simulate the soil-mandrel interface during mandrel penetration. The modified Cam Clay model was used to represent the soft soil. The numerical predictions were then compared with the excess pore pressures obtained from the large scale laboratory

tests to predict the extent of the smear zone. According to this research, the smear zone was approximately 2.5 times the diameter of the mandrel.

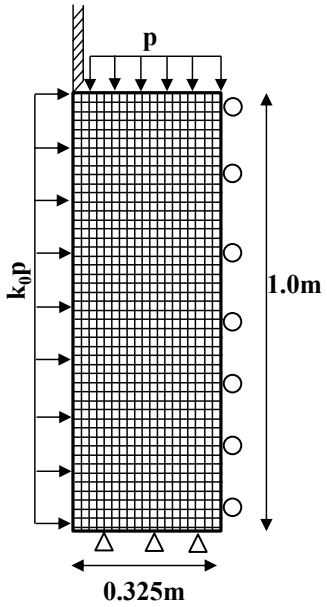

Figure 2.22 Mesh and boundary conditions for the large-scale test (after Rujikiatkamjorn et al. 2009)

In addition, ABAQUS software package was used by Ghandeharioon et al. (2012) to numerically model the installation of mandrel driven prefabricated vertical drains. It was assumed that the mandrel would be installed into a homogeneous soil. The behaviour of saturated clays under rapid installation was analysed in undrained conditions. It was also assumed that the elastic behaviour of saturated soft clays could be described by Hook's law of elasticity, and the Modified Cam-Clay model would be suitable for studying the plastic behaviour of cohesive soils. The master-slave concept was used to simulate driving a mandrel into soft clay, where the periphery of the mandrel was specified as the master surface, and the top and lateral surfaces of the soil (in an axisymmetric configuration) were identified as the slave surfaces. This technique allowed the mandrel to develop a cavity and accommodate its volume in the soil by displacing the soil during installation.

The numerical model showed how a smooth corner at the bottom of the drain shoe, and the penalty parameter, affected the deformation, stresses, and the constraints of physical contact within the soil. The variations of excess pore water pressure at different locations during the installation of a mandrel driven PVD, and while the mandrel was removed, were also investigated. According to the outcomes

of this verification, there was a good agreement between the pore pressures measured in the laboratory and the finite element predictions.

According to Ghandeharioon et al. (2012), the laboratory observations indicated that the soil near the mandrel moves radially and downward as the mandrel is installed. The magnitude of displacement experienced by the soil surrounding the mandrel justifies the large-strain formulation used for the frictional contact between the mandrel and the soft clay. The extent of the smear zone in the large scale consolidometer was determined using the results from the moisture content tests on samples, which in relation to the installed PVDs, were cored from various locations along different polar axes.

The results obtained by Ghandeharioon et al. (2012) verified the concept of an elliptical smear zone around drains driven by rectangular mandrels, and showed that for a given type of soft soil subjected to a particular rate of installation, the size of the smear zone around the mandrel decreased as the effective in situ stresses increased. Furthermore, the normalised plastic shear strain associated with the boundary of the smear zone was almost constant for a given type of soil, regardless of the effective in situ stresses under a specified rate of mandrel driving. The numerical model of mandrel installation was applied to a case history from the Second Bangkok International Airport. On the basis of these results, the average radius of the smear zone around each PVD was predicted to be about 3.5 times the equivalent radius of the mandrel, a value that is in agreement with the size suggested in previous studies. It was shown that the smear zone expands when the over consolidation ratio of the soil decreased.

2.4.3.4 Back Calculation Methods

The measurements obtained from the large scale consolidation tests and the construction of trial embankments have been widely used to back calculate the required parameters for the design of PVD assisted preloading, including the characteristics of the smear zone. The back calculation procedure can be conducted through a parametric study by applying numerical or analytical approaches. Different values for the properties of the smear zone may be used to carry out the parametric study, including the characteristics of the smear zone, which result in the best

agreement between the field measurements and numerical/analytical predictions, and can be reported as reasonable values for design purposes.

Bergado et al. (1991) used the back calculation method based on the observed time-settlement relationship of the large scale laboratory consolidation test to determine the extent and permeability of the smear zone. According to the results of the back analysis the diameter of the smear zone was 2 times the equivalent diameter of the mandrel, and the permeability of the smear zone (k_s) was approximated to be equal to the vertical permeability coefficient of the soil in the intact zone (k_v).

Bergado et al. (1993) used the computer program VERDRN, which was written in FORTRAN 77, to conduct numerical simulations of a large scale consolidation test and a full scale test embankment, and then to back calculate the properties of the smear zone. The laboratory settlement measurements were compared with the finite element predictions, which indicated that adopting k_h/k_s=2 and r_s/r_m=2 resulted in the most accurate predictions. According to the numerical results obtained for the full-scale test embankment, the performance of the vertical drains was predicted quite well when the permeability and extent ratios were considered as k_h/k_s=10 and r_s/r_m=2, respectively. In addition, the effect of the k_h/k_s ratio on the settlement rate was more than the r_s/r_m ratio.

The trial embankment in Saga Airport (Japan) was simulated by Chai and Miura (1999) using the finite element program CRISP (Britto and Gunn 1987) to conduct a back analysis process and predict the characteristics of the smear zone. Two different approaches were proposed to carry out the parametric study; (i) considering the k_h/k_s and r_s/r_m as the constant values and back calculate q_w (discharge capacity), (ii) considering the r_s/r_m and q_w as the constant values and back calculate k_h/k_s. The results of the back calculation procedure conducted by Chai and Miura (1999) are summarised in Table 2.6.

Table 2.6 Back calculated smear zone properties (after Chai and Miura, 1999)

Case	k_h/k_s	r_s/r_m	q_w (m^3/yr)	Description
1	10	3	85	Fix k_h/k_s and r_s/r_m, and then back calculate q_w
2	11	3	150	Fix r_s/r_m and q_w, and then back calculate k_h/k_s

Saowapakpiboon et al. (2010) conducted a large scale consolidometer test with reconstituted specimens installed with prefabricated vertical drains with and without vacuum preloading. Additionally, field measurements were collected from the Second Bangkok International Airport site improved by PVD, with and without vacuum pressures. The Hansbo (1979) method was applied to conduct the analytical analyses for both cases and predict the consolidation settlement by adopting different smear zone permeability coefficients. Also, the finite element software called PVDCON was used by Saowapakpiboon et al. (2010) for numerical simulation of PVD improved soft clay with and without vacuum preloading to back calculate the smear zone permeability. Table 2.7 indicates the back calculated k_h/k_s ratios.

Table 2.7 Back calculated k_h/k_s ratio (reported by Saowapakpiboon et al., 2010)

Method of simulation	Measurements	k_h/k_s PVD only	k_h/k_s PVD-vacuum	r_s/r_m Constant
Analytical (Hansbo, 1979)	Large-scale consolidometer	2.7	2.5	2
	Trial embankment	7.2	6.6	2
Finite element (PVDCON)	Trial embankment OCR=1.2	4-6	4-8	2

In the current literature, the properties of the smear zone were back calculated by comparing the field measurements and numerical results for at least 90% of consolidation. In many cases, a long period of time is required to obtain 90% of consolidation after constructing a trial embankment, which may increase the cost of the project quite considerably. Determining the minimum degree of consolidation that results in predicable smear zone properties can convert the construction of a trial embankment to a very practical and cost effective method in design of PVD assisted preloading projects.

Researchers have used different methods to investigate the characteristics of the smear zone and very diverse values have been reported regarding the extent and permeability of the smear zone. A summary of the proposed values for the k_h/k_s and r_s/r_m ratios are illustrated in Figure 2.23.

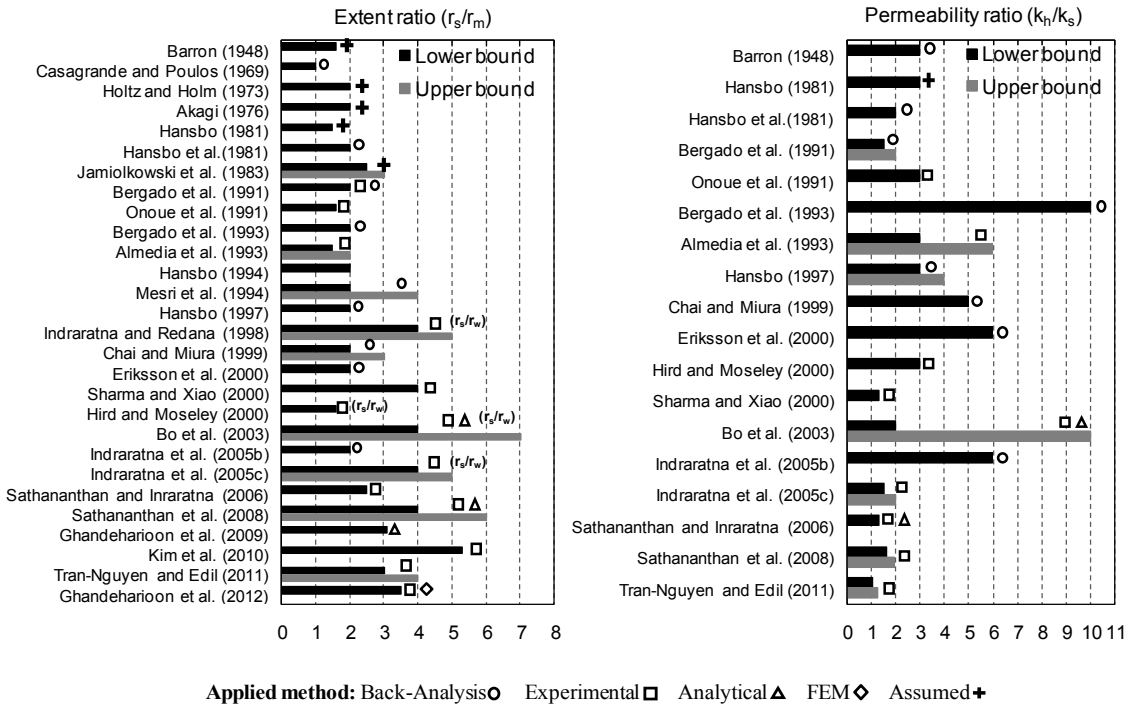

Figure 2.23 Proposed values for smear zone characteristics

Figure 2.23 indicates that the extent ratio (r_s/r_m) or (r_s/r_w) is generally assumed as 2 (Holtz and Holm, 1973; Akagi, 1976; Bergado *et al.*, 1991; Mersi et al. 1994; Hansbo 1997). According to some recent experimental results the smear zone radius (r_s) may be 4 times the radius of the mandrel (Sharma and Xiao, 2000; Sathananthan et al. 2008). The proposed range shows that the extent of the smear zone (r_s) may vary from 1.6 to 7 times the radius of the drain (r_w) or 1 to 6 times the equivalent diameter of the mandrel (r_m). The maximum values for r_s/r_w and r_s/r_m were proposed by Bo et al. (2003) and Sathananthan (2008), respectively. The results reported in Figure 2.23 indicate that the proposed range for the permeability ratio (k_h/k_s) is 1.03 to 10. The minimum and maximum values for k_h/k_s were reported by Tran-Nguyen and Edil (2011) and Bo et al. (2003), respectively.

According to Figure 2.23, wide ranges were proposed for k_h/k_s and r_s/r_m and there is no specific recommended method that practising engineers can use to predict these parameters precisely. This can lead to an early removal of the surcharge in the construction process and result in excessive post construction settlement or excessive construction time, which would increase the project cost.

2.4.4 Relationship between Experimental and Practical Results for Smear Zone Properties

There are many uncertainties regarding the k_h/k_s value. As Chai and Miura (1999) and Shen et al. (2005) mentioned, the experimental results for the permeability of the smear zone are underestimated values and a coefficient is required to convert these values for practical design purposes. Chai and Miura (1999) suggested the following equation as the relationship between the experimental and practical results for k_h/k_s:

$$\frac{k_h}{k_s} = \left(\frac{k_h}{k_s}\right)_l . C_f \qquad (2.16)$$

where, the subscript *l* represents the value determined in the laboratory, and C_f *is the* hydraulic conductivity ratio between the field and laboratory values. In some cases $(k_h/k_s) = (k_h/k_v)$, which means that the horizontal permeability in the smear zone is equal to the vertical permeability in the intact zone. One way to estimate the value of field hydraulic conductivity is to back analyse the local case histories, such as the measured embankment settlement, or to measure hydraulic conductivity in the field using a self-boring permeameter, if this sophisticated piece of equipment is available (Tavenas et al. 1986). According Chai and Miura (1999), the most important factors affecting the value of C_f are considered to be the deposit stratifications. For a homogeneous deposit the C_f value can be close to 1.0, but for stratified deposits, even those with thin layers of sand and seams of sand that cannot be clearly identified from the borehole record, the C_f value can be much larger than 1.0. The C_f values of a few clay deposits are listed in Table 2.8.

Table 2.8 Proposed values for C_f (after Chai and Miura, 1999)

Deposit	C_f Value	Method for evaluating field value of hydraulic conductivity	Remarks
Bangkok clay at Asian Institute of Technology campus	25	Back analysis	Chai et al. (1995)
Bangkok clay at Nong Ngu Hao	4	Back analysis	Chai et al. (1996)
Malaysia Muar clay deposit	2	Back analysis	Chai and Bergado (1993)
Ariake clay (close to sea)	4	Back analysis	Chai and Miura (1999)
Louiseville (Canada)	Around 1*	Self-boring permeameter	Tavenas et al. (1986)
St-Alban (Canada)	Around 3*	Self-boring permeameter	Tavenas et al. (1986)

*The laboratory value was determined by direct measurements. For other cases, laboratory values were deducted from the coefficient of consolidation, C_v.)

2.5 DEVELOPMENT OF CONSOLIDATION THEORY

2.5.1 Vertical Consolidation

The basic theory for vertical consolidation was proposed by Terzaghi (1925). This theory is based on the following assumptions:

(i) Soil is homogeneous and fully saturated,

(ii) Pore water flow is solely in the vertical direction,

(iii) Pore water flow is governed by Darcy's law,

(iv) Relationship between the void ratio and effective stress is linear,

(v) The permeability coefficient of the soil is constant during consolidation,

(vi) No creep occurs during soil settlement, and

(vii) The effect of geometric changes caused by the soil compressing is insignificant (i. e. small strain theory)

Terzaghi (1925) presented the average degree of consolidation ($\overline{U}_v$) as a function of dimensionless time factor T_v:

$$\bar{U}_v = 1 - \sum_{m=0}^{m=\infty} \frac{2}{M^2}\, exp\,(M^2 T_v) \tag{2.17}$$

where

$$M = \left(\frac{\pi}{2}\right)(2m+1) \tag{2.18}$$

$$T_v = \frac{c_v t}{H_d^2} \tag{2.19}$$

where, c_v is the vertical coefficient of consolidation, and H_d is the vertical drainage distance. The average degree of consolidation versus the time factor curves are plotted in Figure 2.24 based on Equation (2.17) for different distributions of pore water pressure while considering one way and two-way drainage boundary conditions.

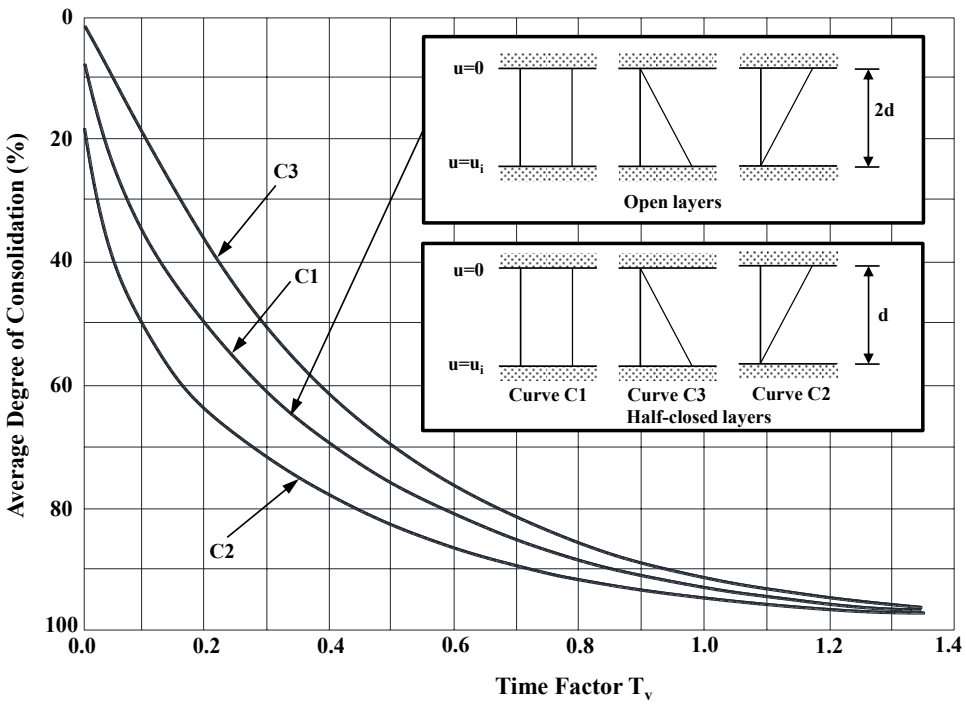

Figure 2.24 Average degree of consolidation versus time factor based on Equation 2.9 (after Das, 2008)

According to Figure 2.24, the distribution of pore water pressure is constant in curve C1, while the curves C2 and C3 represent the linear variation of pore water pressure. In curve C2 the pore water pressure changes from zero at the top of the drainage boundary to the maximum value at the bottom of the clay layer, while the condition

is vice versa in curve C3. Among the closed form approximations of Eq. (2.17), the following equation provides almost the same results as Equation (2.17) for $0 \leq U_v \leq 0.997$, or $0 \leq T_v \leq 6$, as reported by Sivaram and Swamee (1977).

$$\bar{U}_v = \frac{\left(4T_v/\pi\right)^{0.5}}{\left[1+\left(4T_v/\pi\right)^{2.8}\right]^{0.179}} \tag{2.20}$$

According to the literature, a number of solutions have been developed, relaxing some of the assumptions in Terzaghi's theory (1925). Morris (2005) assumed a finite strain to develop analytical solutions for one dimensional consolidation. Finite difference techniques with a piecewise linear formulation for large strain consolidation were used by Fox and Berles (1997). Fox and Qui (2004) applied the finite difference method to include compressible pore fluid. Xie and Leo (2004) considered one dimensional large strain consolidation with variable compressibility and permeability. According to Xie and Leo (2004), predicting small strain settlement is more difficult than predicting large strains. Small strain pore pressure and settlement evolution is slower than large strain evolution. Zhu and Yin (1998) considered the consolidation of soil under depth dependant ramp load. Furthermore, the consolidation of unsaturated ground was investigated by Vaziri and Christian (1994).

2.5.2 Radial (or Horizontal) Consolidation Considering Smear Zone Characteristics

Barron (1948) introduced the first classical solutions (rigorous and approximate) to estimate the radial consolidation based on the Terzaghi (1925) consolidation theory. This rigorous solution was developed based on 'free strain hypothesis,' and the approximate solution was established based on 'equal strain hypothesis.' The difference between free and equal strain cases was found to be negligible so an equal strain case was used. Barron (1948) also included the effect of the smear zone properties. The constant smear zone properties were considered following the two zone hypothesis (Figure 2.9a, Case A). The solutions involved Bessel functions and were time consuming to perform, so the effects of smear and well resistance were often ignored to simplify the calculation (e.g. Hansbo, 1981).

A number of solutions were developed to improve the Barron (1948) theory for radial consolidation (Scott, 1963; Hansbo, 1981; Onoue, 1988; and Lo 1991). The solutions proposed for radial consolidation are summarised in Table 2.9. The equations proposed in Table 2.9 indicate that all the solutions can be expressed in a general form as shown below:

$$\bar{U}_h = 1 - exp\left(\frac{-8T_h}{F}\right) \tag{2.21}$$

where, $T_h = c_h t/S^2$ is the radial drainage time factor, and F is a function related to factors such as drain spacing, the smear effect, and well resistance.

A rigorous approach was used in a number of studies to develop an analytical solution for axisymmetric radial drainage that considers both the smear effect and well resistance (Barron, 1948; Onoue, 1988; Zeng and Xie, 1989; Lo, 1991). As mentioned earlier, Hansbo (1981) developed an approximate equation for horizontal drainage based on "equal strain hypothesis" to take both the smear zone with a reduced permeability and the well resistance effect into consideration. Function F in Hansbo's (1981) equation that only considers the smear effect (ignoring well resistance) is then reduced to:

$$F = \ln(\frac{n}{s}) + \frac{k_h}{k_s}\ln(n) - \frac{3}{4} \tag{2.22}$$

In the case of a perfect drain (neglecting the effects of both smear and well resistance), the function F is as follows:

$$F = \ln(n) - \frac{3}{4} \tag{2.23}$$

Scott (1963) proposed an approximate solution for radial consolidation by considering the smear effect and ignoring the well resistance factor. In the proposed equation by Yoshikuni and Nakanodo (1974), only the well resistance factor was considered. According to Table 2.9, Indraratna and Redanna (1997) developed an equation to determine the average degree of horizontal consolidation for the plane-strain condition by converting the radius of the smear zone and its permeability (axisymmetric) into equivalent plane-strain parameters.

Table 2.9 Proposed solutions for radial consolidation considering constant smear zone properties

Reference	Suggested theoretical solution for radial consolidation
Barron (1948)	$\bar{U}_h=1-\exp(\frac{-8T_r}{F_{(n+s)}})$, $F_{(n+S)}=\frac{n^2}{n^2-1}\ln\left(\frac{n}{s}\right)-\frac{3n^2-s^2}{4n^2}+\frac{k_h}{k_s}\times\frac{3n^2-s^2}{n^2}\ln(s)\approx\ln\left(\frac{n}{s}\right)-\frac{3}{4}+\frac{k_h}{k_s}\ln(s)$ $\bar{U}_h=\frac{1}{2H_d}\int_0^{2H_d}(1-\exp(\frac{-8T_r}{F_{(n+s)}}\times f(z)dz))$, $F_{(z)}=\frac{\exp[b(z-2H_d)]+\exp(-bz)}{1+\exp(-2bH_d)}$, $b=\left[\frac{2k_h}{k_w}\times\frac{(n^2-s^2)}{R^2.F_{(n+s)}}\right]^2$, $R=\frac{d_e}{2}$
Scott (1963)	$\bar{U}_h=1-\exp(\frac{-8T_r}{F_{(n+s)}})$, $F_{(n+S)}=\frac{n^2}{n^2-1}\ln(n)-\frac{3n^2-1}{4n^2}+\frac{k_h}{r_wk_w}\times\frac{n^2-1}{n^2}\ln(s)=\frac{n^2}{n^2-1}\ln(n)-\frac{3n^2-1}{4n^2}+\frac{(s-1)k_h}{k_s}\times\frac{n^2-1}{n^2}$
Yoshikuni & Nakanodo (1974)	$\bar{U}_h=1-\exp(\frac{-8T_r}{F_{(n)}+0.8\times L})=1-\exp(\frac{-8T_r}{F_{(n)}+2.6G})$, $F_{(n)}=\frac{n^2}{n^2-1}\ln(n)-\frac{3n^2-1}{4n^2}\approx\frac{k_h}{k_s}\times\frac{3n^2-s^2}{n^2}\ln(s)\approx\ln(n)-\frac{3}{4}$, $L=\frac{32}{\pi^2}\times\frac{k_h}{k_w}\left(\frac{l}{d_w}\right)^2$, $G=\frac{k_h}{k_w}(\frac{1}{d_w})^2$
Hansbo (1981)	$\bar{U}_h=1-\exp(\frac{-8T_r}{F})$ $F=\frac{n^2}{n^2-1}\ln(\frac{n}{s}+\frac{k_h}{k_s}\ln(s)-\frac{3}{4})+\frac{s^2}{n^2-1}(1-\frac{s^2}{4n^2})+$ $\frac{k_h}{k_s}.\frac{1}{n^2-1}(\frac{s^4-1}{4n^2}-s^2+1)+\pi z(2l-z)\frac{k_h}{q_w}(1-\frac{1}{n^2})\approx\ln(\frac{n}{s})+\frac{k_h}{k_s}\ln(n)-\frac{3}{4}+\pi z(2l-z)\frac{k_h}{q_w}$
Rixner et al. (1986)	$\bar{U}_h=1-\exp(\frac{-8T_r}{F})$ $F=\frac{n^2}{n^2-1}\ln(\frac{n}{s}+\frac{k_h}{k_s}\ln(s)-\frac{3}{4})+\frac{s^2}{n^2-1}(1-\frac{s^2}{4n^2})+\frac{k_h}{k_s}.\frac{1}{n^2-1}(\frac{s^4-1}{4n^2}-s^2+1)+$ $\frac{2}{3}\pi\frac{k_h.l^2}{q_w}(1-\frac{1}{n^2})$
Onoue (1988)	$\bar{U}_h=1-\exp(\frac{-8T_r}{F_{n'}+0.8\times L^*})$, $F_{n'}=\frac{(n')^2}{(n')^2-1}\times\ln(n')-\frac{3(n')^2-1}{4(n')^2}$, $n'=n.\,s^{\eta-1}$, $\eta=\frac{k_h}{k_s}$, $L^*=\times\frac{32}{\pi^2}\times\frac{k_h}{k_w}(\frac{1}{d_w})$
Xie (1987) Zeng & Xie (1989)	$\bar{U}_h=1-\sum_{m=0}^{\infty}\frac{2}{M^2}\exp\left(\frac{-8T_r}{F_{(n+s)}+d_e}\right)=1-\exp\left(\frac{-8T_r}{F_{(n+s)}+\pi G}\right)$, $F_{(n+S)}=\ln\left(\frac{n}{s}\right)+\frac{k_h}{k_s}-\frac{3}{4}$ and $G=\frac{k_h}{k_w}(\frac{1}{d_w})^2$
Lo (1991)	$\bar{U}_h=1-\exp(\frac{-8T_r}{F_{(n+s)}+2.5G})$, $F_{(n+S)}=\frac{n^2}{n^2-1}\ln(\frac{n}{s}+\frac{k_h}{k_s}\ln(s)-\frac{3}{4})+\frac{s^2}{n^2-1}(1-\frac{s^2}{4n^2})+\frac{k_h}{k_s}.\frac{1}{n^2-1}(\frac{s^4-1}{4n^2}-s^2+1)$
Indraratna & Redana (1997)	$\bar{U}_{hp}=1-\exp(\frac{-8T_{hp}}{\mu_p})$, $\mu_p=\left[\alpha+(\beta)\frac{k_{hp}}{k'_{hp}}+(\theta)(2lz-z^2)\right]$, $\alpha=\frac{2}{3}-\frac{2b_s}{B}\left(1-\frac{b_s}{B}+\frac{2b_s{}^2}{3B^2}\right)$, $\beta=\frac{1}{B^2}(b_s-b_w)^2+\frac{b_s{}^2}{3B^3}(3b_w{}^2-b_s{}^2)$, $\theta=\frac{2k_{hp}{}^2}{k'_{hp}q_{wp}B}\left(1-\frac{b_w}{B}\right)$, $q_z=\frac{2}{\pi B}q_w$

Note: $\bar{U}_h$ and $\bar{U}_{hp}$ are the average degree of radial consolidation in axisymmetric and plane-strain condition respectively; T_r is the radial consolidation time factor; H_d is the vertical drainage distance; n is the ratio of the influence radius to the drain radius (R/r_w); s is the extent ratio (r_s/r_w); k_w is the coefficient of permeability of PVD; q_w is the discharge capacity of PVD; z is depth; l is drainage length; k_{hp} and k'_{hp} are horizontal permeability of intact zone and smear zone in plane-strain condition, respectively; b_w and b_s are the equivalent plane-strain radius of the drain and smear zone, respectively; B is the equivalent plane-strain radius of the influence zone; and q_{wp} is the equivalent plane-strain discharge capacity.

Walker and Indraratna (2006) proposed a vertical drain radial consolidation equation based on the parabolic reduction of permeability in the smear zone towards the vertical drain, thus modifying Hansbo's (1981) well-known radial consolidation

equations (where a constant coefficient of consolidation is assumed), without increasing the number of variables (Figure 2.9 case C). The validity of this method was examined by comparing it with settlement data using a large scale consolidometer.

Basu et al. (2006) developed analytical solutions to estimate the average degree of consolidation for the cases based on the two & three zone hypotheses (Figure 2.13b cases D, E, F, and G) that are shown in Table 2.10.

Table 2.10 Proposed solutions for radial consolidation considering variable smear zone properties

Case	Permeability variation pattern	Analytical solution for radial consolidation (Basu et al. 2006)
C	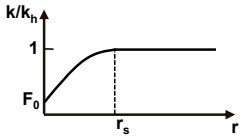	$\bar{U}_h = 1 - \exp\left(\frac{-8T_r}{F}\right), F = \ln\left(\frac{n}{s}\right) - \frac{3}{4} + \frac{\kappa(s-1)^2}{(s^2 - 2\kappa s + \kappa)} \ln\left(\frac{s}{\sqrt{\kappa}}\right) - \frac{s(s-1)\sqrt{\kappa(k-1)}}{2(s^2 - 2\kappa s + \kappa)} ln\left(\frac{\sqrt{\kappa} + \sqrt{\kappa - 1}}{\sqrt{\kappa} - \sqrt{\kappa - 1}}\right) + \frac{k}{q_w} \pi z(2l - z)$
D	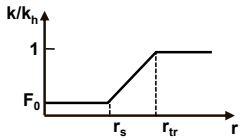	$\bar{U}_h = 1 - \exp\left(\frac{-8T_r}{F}\right), F = \ln\left(\frac{n}{q}\right) + \frac{1}{\beta}\ln(s) + \frac{(q-s)}{(\beta q - s)} ln\left(\frac{\beta q}{s}\right) - \frac{3}{4}$
E	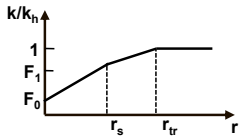	$\bar{U}_h = 1 - \exp\left(\frac{-8T_r}{F}\right), F = \ln\left(\frac{n}{q}\right) + \frac{(s-1)}{(\beta s - \beta_t)} \ln\left(\frac{\beta s}{\beta_t}\right) + \frac{(q-s)}{(\beta_t q - s)} ln\left(\frac{\beta_t q}{s}\right) - \frac{3}{4}$
F	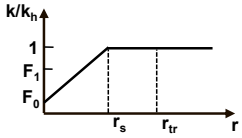	$\bar{U}_h = 1 - exp(\frac{-8T_r}{F}), F = ln(\frac{n}{q}) + \frac{(q-1)}{(\beta q - 1)} ln(\beta q) - \frac{3}{4}$
G	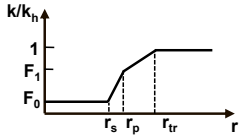	$\bar{U}_h = 1 - \exp\left(\frac{-8T_r}{F}\right), F = \ln\left(\frac{n}{q}\right) + \frac{1}{\beta}\ln(s) + \frac{(p-s)}{(\beta p - \beta_p s)} ln\left(\frac{\beta p}{\beta_p s}\right) + \frac{(q-p)}{(\beta_p q - p)} ln\left(\frac{\beta_p q}{p}\right) - \frac{3}{4}$
$\kappa = \frac{k_h}{k_s}, \beta = \frac{k_s}{k_h}, \beta_t = \frac{k_t}{k_h}, \beta_p = \frac{k_p}{k_h}, q = \frac{r_{tr}}{r_w}, n = \frac{R}{r_w}, s = \frac{r_s}{r_w}, p = \frac{r_p}{r_w}$		

Note: $\bar{U}_h$ is the average degree of radial consolidation; T_r is the radial consolidation time factor; R is the influence radius; r_w is the drain radius; r_s is the smear zone radius; r_p is the distance from the centre of the PVD to any intermediate point within the transition zone; r_{tr} is the radius of the transition zone; k_s is the permeability at the drain boundary; k_t is the permeability at the smear zone boundary; k_p is the permeability at any intermediate point within the transition zone; k_h is the permeability at the transition zone boundary or intact zone permeability; *l* is the length of the drainage path; *z* is depth of horizontal plane, and q_w is the discharge capacity of the drain.

According to Basu et al. (2006), the transition zone has a definite impact in slowing the consolidation process down. Moreover, the rate of consolidation depends a great deal on the variations in hydraulic conductivity within the transition zone. According to their study, an accurate definition of the most likely hydraulic conductivity profile cannot be reached due to the limited amount of experimental data, so all possible hydraulic conductivity profiles, as outlined in Figure 2.13, should be considered before final design decisions are made.

A simple but practical procedure for designing prefabricated vertical drains was proposed by Bellezza and Fentini (2008) which included the effects of smear and well resistance. Based on Hansbo's well-known solution, a simplified design equation was obtained that can be effectively used for design purposes by considering the drain spacing ratio (*n*) as an explicit function of the drain size, the degree of consolidation required, the time available, the geotechnical properties of the compressible layer, and the smear and well resistance parameters. According to the procedure proposed by Bellezza and Fentini (2008), the drain spacing can be designed using the following equations:

$$\lambda = \frac{T_w}{ln[(1-\bar{U}_v)/(1-\bar{U})]} \tag{2.24}$$

$$n = \left(\frac{\lambda}{A}\right)^B \tag{2.25}$$

$$A = \frac{exp(-3.45g_c)}{2g_c} \tag{2.26}$$

$$B = (2 + g_c)^{-1} \tag{2.27}$$

$$g_c = (F_S + F_R + 2.7)^{-1} \tag{2.28}$$

where, $T_w = \frac{C_h t}{r_w^2}$ is the time factor in terms of the equivalent radius of the vertical drain (r_w), $\bar{U}_v$ is the average degree of vertical consolidation, $\bar{U}$ is the overall degree of consolidation due to a combination of drainage in the horizontal and vertical directions; $n=R/r_w$ is the drain spacing ratio, $F_S = \left(\frac{k_h}{k_s} - 1\right) ln\ s$ and $F_R = \frac{2\pi k_{hL^2}}{3q_w}$ are dimensionless parameters.

The first stage of the above procedure is to calculate the parameter λ using Equation (2.24). Then, Equations (2.25) to (2.28) can be used to determine the drain spacing ratio ($n=R/r_w$) and subsequently, the radius of the influence zone (R) can be obtained for a given r_w. The drain spacing can be determined as the final stage by considering the installation pattern to be applied (i.e. square or triangular).

Chung et al. (2009) developed a method to predict the performance of prefabricated vertical drains based on the Baron's solution and the hyperbolic settlement-time relationship. The method proposed by Chung et al. (2009) was validated using three case studies. According to the analytical analyses, the hyperbolic method developed is suitable when the degrees of consolidation are between 60 and 90%.

Kianfar et al. (2013) proposed a non-linear relationship between the flow velocity and the hydraulic gradient for the entire consolidation process, including the smear effect. The proposed relationship was developed based on the laboratory measurements and by conducting radial consolidation tests that were subjected to vacuum and surcharge loading using a modified Rowe cell. Kianfar et al. (2013) summarised the advantages of the developed flow relationship as follows: (i) it provides more realistic flow behaviour during consolidation, and (ii) in contrast to the relationship proposed by Hansbo (1960), the threshold hydraulic gradient was not required to differentiate between the linear and non-linear flow relationships.

2.5.2.1 Conversion of Axisymmetric to Plane-Strain Condition

The axisymmetric classical solutions proposed by Barron (1948) and Hansbo (1981) can be applied to analyse the performance of a vertical drain under a conventional embankment (along the centreline of the embankment). Although single drain analysis is often enough to model the behaviour of soil along the embankment centreline, multi-drain analysis is needed to incorporate the effect of changing the gravity load along the embankment to accurately predict settlement and lateral displacement (Indraratna and Redana, 2000). Due to the rapid development of computer technology in recent years, it is possible to conduct a numerical simulation of the multiple vertical drains system under an embankment and analyse the consolidation of the now stabilised soft soil using developed numerical programs. For this purpose, a 3D full scale numerical model of the ground improved by PVD

should be simulated with a lot of cubic elements. Yildiz (2009) reported that a full scale 3D analysis of an embankment on PVD improved soft clays is very time consuming and not practical for engineers. The 2D model can be applied instead of the 3D one to facilitate and accelerate the numerical simulation of the multiple vertical drains or complex tree root system adopting the equivalent plane-strain permeability for the intact region and the smear zone (Indraratna et al., 2005a; Fatahi et al, 2009 and 2010).

Hird (1992) proposed three procedures based on Hansbo's (1981) solution to match the average degree of consolidation, at any time and depth, in the axisymmetric and plane-strain unit cells, including; (i) geometric mapping – the drain spacing is matched while maintaining the same permeability coefficient; (ii) permeability mapping – the coefficient of permeability is matched while keeping the same drain spacing; and (iii) a combination of (i) and (ii), with the plane-strain permeability calculated for a convenient drain spacing. Yildiz et al. (2006) showed that three proposed matching procedures by Hird et al. (1992) resulted in similar settlement predictions. According to the combined procedure proposed by Hird et al. (1992), the equivalent plane-strain permeability (k_{hp}) can be determined as follows:

$$\frac{k_{hp}}{k_h} = \frac{2B^2}{3R^2\left[ln\left(\frac{R}{r_s}\right)+\left(\frac{k_h}{k_s}\right)ln(s)-\frac{3}{4}\right]} \tag{2.29}$$

where, B is the half-width of the unit cell, k_h and k_{hp} are the axisymmetric and plane-strain horizontal permeability values of the intact zone respectively, and k_s is the axisymmetric coefficient of permeability in the smear zone.

Equation (2.30) indicates the reduced form of Equation (2.29) by ignoring the effects of smear and well resistance.

$$\frac{k_{hp}}{k_h} = \frac{0.67}{[ln(n)-0.75]} \tag{2.30}$$

Indraratna and Redana (1997) proposed a solution to estimate the degree of radial consolidation for the plane-strain condition by considering the effects of smear and well resistance. For this purpose, an analytical solution was developed to calculate the equivalent plane-strain permeability for both the smear zone and undisturbed soils. The relationship between the coefficient of permeability in the intact zone (k_{hp})

and the smear zone (k_{sp}) for the equivalent plane-strain condition can be determined with Equation (2.31) by considering both the smear effect and well resistance.

$$\frac{k_{hp}}{k_h} = \frac{\left[\alpha+\beta\frac{k_{hp}}{k_{sp}}+\theta\left(2lz-z^2\right)\right]}{\left[ln\left(\frac{n}{s}\right)+\left(\frac{k_h}{k_s}\right)ln(s)-0.75\pi(2lz-z^2)\frac{k_h}{q_w}\right]} \tag{2.31}$$

Equation (2.31) can be simplified to Equation (2.30) by ignoring the smear effect and the well resistance factor. If the effect of well resistance is ignored, the final terms in Equation (2.31) can be neglected and the equation would be reduced to:

$$\frac{k_{sp}}{k_{hp}} = \frac{\beta}{\frac{k_{hp}}{k_h}\left[ln\left(\frac{n}{s}\right)+\left(\frac{k_h}{k_s}\right)ln(s)-0.75\right]-\alpha} \tag{2.32}$$

where

$$\alpha = \frac{2}{3} - \frac{2b_s}{B}\left(1 - \frac{b_s}{B} + \frac{b_s^2}{3B^2}\right) \tag{2.33}$$

$$\beta = \frac{1}{B^2}(b_s - b_w)^2 + \frac{b_s}{3B^3}(3b_w^2 - b_s^2) \tag{2.34}$$

$$\theta = \frac{2}{k_{sp}}\frac{k_{hp}^2}{Bq_{wp}}\left(1 - \frac{b_w}{B}\right) \tag{2.35}$$

where, k_{sp} is the plane-strain permeability coefficient of the smear zone, α, β, and θ are geometric coefficients, n is the spacing ratio equal to $R/r_w=B/b_w$, $s=r_s/r_w$, q_{wp} is the equivalent plane-strain discharge capacity of the drain, z is the depth of the drain, B, b_s and b_w are the drain dimensions (Figure 2.25). For plane-strain analysis, B, b_s, and b_w are assumed to be equal to R (radius of the influence zone), r_s (radius of the smear zone), and r_w (radius of the drain well), respectively. The value of k_h needs to be determined first (laboratory or field), then k_{hp} can be calculated using Equation (2.30). When k_{hp} is known, k_{sp} can be obtained from Equations (2.32). Figure 2.25 shows the axisymmetric and plane-strain profiles of the PVD and the surrounding ground.

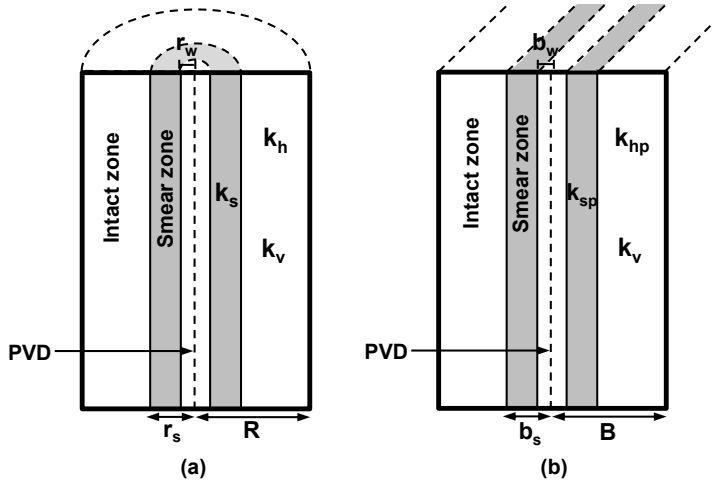

Figure 2.25 Profile of prefabricated vertical drain and smear zone, (a) axisymmetric, (b) plane-strain

Lin et al. (2000) developed analytical solutions by proposing equivalent horizontal permeability coefficients for both axisymmetric and plane-strain unit cells to consider the smear effect, which can then be adopted in finite element analyses. The equivalent horizontal permeability for the axisymmetric unit cell ($k_{e,ax}$) can be determined by the following equation:

$$k_{e,ax} = \frac{k_h ln(n)}{ln(n)+\left(\frac{k_h}{k_s}\right)ln(s)} \tag{2.36}$$

The equivalent horizontal permeability for the plane-strain unit cell ($k_{e,pl}$) can be calculated by Equation 2.37:

$$k_{e,pl} = \frac{k_h \pi}{6\left[ln\left(\frac{n}{s}\right)+\left(\frac{k_h}{k_s}\right)ln(s)-\frac{3}{4}\right]} \tag{2.37}$$

According to Chai et al. (2001), the installation of PVDs increases the mass permeability of the improved subsoil in a vertical direction and an equivalent vertical permeability can be established that represents the effect of both vertical drainage of the natural subsoil and the radial flow due to the installation of vertical drains. The proposed equivalent value of the vertical coefficient of permeability (k_{ve}) was derived based on the equal average degree of consolidation under the 1D condition proposed by Carrillo (1942), which can be expressed as:

$$k_{\mathrm{ve}} = \left(1 + \frac{2.5l^2}{\delta}\frac{k_h}{{d_c}^2}\right)k_h \tag{2.38}$$

where, k_{v} is the vertical coefficient of permeability in the undisturbed soil, l is the length of the drainage, and d_c is the diameter of unit cell. The value of δ can be expressed as

$$\delta = ln\frac{n}{s} + \frac{k_h}{k_s}\ln(s) - \frac{3}{4} + \pi\frac{2l^2k_h}{3q_w} \tag{2.39}$$

This method is more practical than the other methods since both the vertical drain and the associated smear zone do not need to be represented in the equivalent plane-strain analyses (Yildiz, 2009).

Indraratna et al. (2005a) derived permeability and vacuum pressure relationships between the axisymmetric and equivalent plane-strain conditions by extending the theory developed by Indraratna and Redana (1997), and assuming that the average excess pore pressures for both axisymmetric and plane-strain conditions are equal. According to Indraratna et al. (2005a), the equivalent permeability under plane-strain condition can be determined using the following equations:

$$\frac{k_{hp}}{k_h} = \frac{\left[\alpha + \beta\frac{k_{hp}}{k_{sp}} + \theta\right]}{\left[ln\left(\frac{n}{s}\right) + \left(\frac{k_h}{k_s}\right)ln(s) - 0.75\pi(2lz - z^2)\frac{k_h}{q_w}\right]} \tag{2.40}$$

$$\alpha = \frac{2}{3}\frac{(n-s)^3}{n^2(n-1)} \tag{2.41}$$

$$\beta = \frac{2(s-1)}{n^2(n-1)}\left[n(n-s-1) + \frac{1}{3}(s^2 + s + 1)\right] \tag{2.42}$$

$$\theta = \frac{4k_{hp}}{3Bq_{wp}}\left(1 - \frac{1}{n}\right)l^2 \tag{2.43}$$

where, l is the length of the drain, and q_w and q_{wp} are the axisymmetric and plane-strain discharge capacities, respectively.

Equation (2.44) shows the ratio of equivalent plane-strain permeability to axisymmetric permeability in the intact zone by neglecting the effects of smear and well resistance (Indraratna et al., 2005a).

$$\frac{k_{hp}}{k_h} = \frac{\frac{2(n-1)^2}{3 \quad n^2}}{[ln(n)-0.75]} \tag{2.44}$$

Equation (2.32) can be used the effect of well resistance is neglected.

Tran and Mitachi (2008) proposed a method to convert the axisymmetric unit cell to an equivalent plane-strain unit cell under vacuum-surcharge preloading, which can be expressed as:

$$k_{ep} = \frac{2B^2}{3R^2} \frac{k_h}{ln\frac{n}{s} - \frac{3}{4} + \frac{k_h}{k_s} lns} \tag{2.45}$$

$$q_{wp} = \frac{2B}{\pi R^2} q_w \tag{2.46}$$

where, k_{ep} is the horizontal permeability coefficient in the equivalent zone of plane-strain unit, and $n=R/r_w$. The proposed equivalent plane-strain models by Indraratna et al. (1997), and Tran and Mitachi (2008) are compared in Figure 2.26.

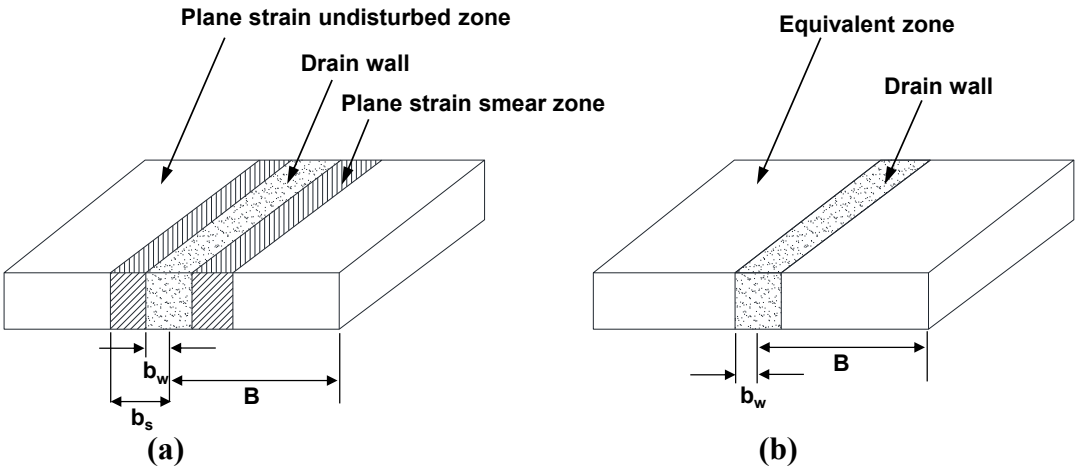

Figure 2.26 Proposed equivalent plane-strain unit cells, (a) Indraratna et al. (1997), and (b) Tran and Mitachi (2008)

2.5.3 Combined Vertical and Radial Consolidation Theory

2.5.3.1 Single Layer Consolidation (Rigorous Solutions)

In vertical drain consolidation problems, the radial component of flow is often much larger than the vertical component. Thus, consolidation due to vertical flow in the

soil is ignored in many cases, especially for long drains. Obviously, when vertical drainage does become significant, it must be included in the analysis.

Yoshikuni and Nakanodo (1974) reported a solution to free strain consolidation by combined vertical and radial drainage, including the effects of well resistance. Zhu and Yin (2001) proposed design charts on the same problem under ramp loading by ignoring well resistance. Both solutions are lengthy and involve double summation series solutions. By using the separation of variables, the radial drainage is solved with Bessel functions, while the vertical drainage is solved with Fourier sine series. The coupled problem is simplified quite significantly if flow in the vertical direction is assumed to occur due to the average hydraulic gradient across a radial cross section. This approach was taken by Tang and Onitsuka (2000), who produced a solution with a single Fourier series. Leo (2004) determined that a closed form solution could be found to the equal strain problem by using modified Bessel functions for both instantaneous and ramp loadings. The advantage of the proposed closed form solution (similar to Terzaghi's one dimensional consolidation solution) is that each term in the series summation is a simple expression rather than the zeros of a transcendental equation, as is the case for Yoshikuni and Nakanodo (1974) and Zhu and Yin (2001).

2.5.3.2 Single Layer Consolidation (Approximate Solutions)

Researchers developed a number of approximate solutions due to the difficulty of implementing rigorous solutions. The simplest approximate equation was proposed by Carillo (1942), which relates the total degree of consolidation to the separately considered radial and vertical degrees of consolidation as follows:

$$1 - \overline{U} = (1 - \overline{U}_v)(1 - \overline{U}_r) \tag{2.47}$$

where, $\overline{U}$ is the average degree of consolidation of PVD improved subsoil, $\overline{U}_r$ is the average degree of consolidation due to radial drainage, and $\overline{U}_v$ is the average degree of consolidation due to vertical drainage. It should be noted that the above relationship is only valid for homogeneous soil conditions.

Tang and Onitsuka (2000) proposed a solution for consolidation by vertical drains with well resistance under a time dependent loading. It was indicated that Carillo's solution was not strictly applicable for ramped loading, even though the

discrepancy was small. Chai et al. (2001) developed a simple approximate method to analyse soft soil improved by PVD in the same way as the unimproved case, by proposing an equivalent vertical hydraulic conductivity which represents the effect of both vertical and radial hydraulic conductivity, coefficients (Equations 2.33 and 2.34). According to Chai et al. (2001), the proposed method can be used for 1D, 2D, and 3D analyses.

2.5.3.3 Multi-Layered Consolidation

As explained earlier, many analytical solutions have been developed for consolidating homogeneous single layered soils with vertical drains. Usually, the ground consists of several layers that must be considered in PVD consolidation analyses to obtain more realistic results. A number of solutions were proposed to predict the consolidation behaviour of layered soils. Chai et al. (2001) proposed a simple approximate method for analysing PVD improved multi-layered subsoils by considering an equivalent vertical hydraulic conductivity k_{ve} for the PVD improved subsoil.

Tang and Onitsuka (2001) developed an analytical solution for the consolidation of double-layered ground with vertical drains by considering the effects of well resistance and smear. It was assumed that the layer of soil consisted of two parts. The upper part of the layer with the vertical drains was considered to be homogenous ground with both vertical and horizontal flow, while the lower part was considered to be single layered ground with only vertical flow. In other words, in the model proposed by Tang and Onitsuka (2001), horizontal flow in the lower part of the soil was neglected.

An analytical solution for calculating the overall degree of consolidation for partially penetrating vertical drains was developed after Tang and Onitsuka's (2001) work, by Wang and Jiao (2004) using a one dimensional double porosity model (DPM). The partially penetrating drain was approximated by a fully penetrating drain and two segments were considered; (i) the upper with a real drain, and (ii) the lower one with an imaginary drain, with the same radius as the upper one and the same properties as the undisturbed soil (Figure 2.27). In the study conducted by Wang and Jiao (2004), horizontal flow in the lower part and the vertical compressibility of the drain (neglected by Tang and Onitsuka, 2001) were considered.

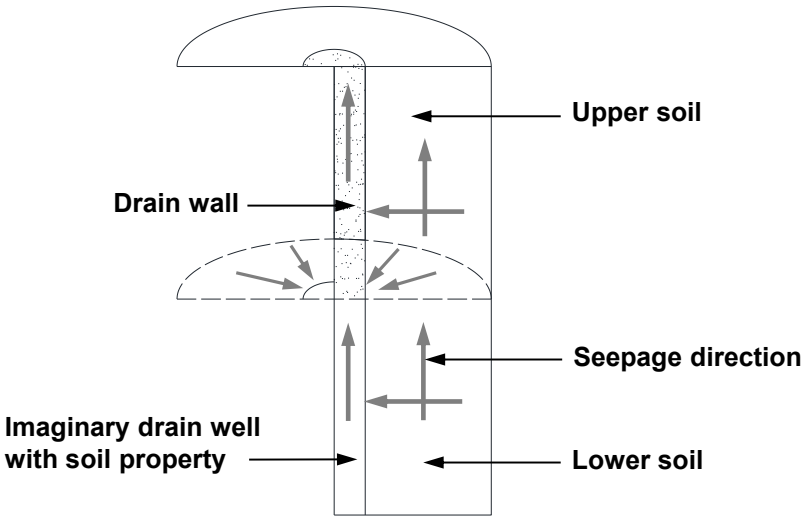

Figure 2.27 Partially penetrating drain based on DPM model (after Wang and Jiao, 2004)

Zhu and Yin (2005) developed design charts for vertical drainage with two layers. Xie et al. (1999) solved the same problem with partially drained boundaries, while Xie et al. (2002) incorporated small strain theory and non-linear soil properties where the decrease in permeability was assumed to be proportional to the decrease in compressibility (i.e. the coefficient of consolidation was assumed to be constant).

Walker et al. (2009) developed a solution to the consolidation of multi-layered soils based on the spectral method by considering combined vertical and radial drainage under instantaneous or single ramp loading, and by ignoring well resistance. The most important advantage of the spectral methods is its ease of implementation as the profile of excess pore water pressure across all the layers of soil is conveniently described by a single expression, whereas existing solutions to multi-layered consolidation problems have a separate equation for each layer. Calculating the average excess pore pressures within or across any number of layers would be far easier with a single expression. This solution includes the smear effect by basing flow in a vertical direction on the average hydraulic gradient at a particular depth.

Rujikiatkamjorn and Indraratna (2010) reported that the consolidation of multi-layer deposits of soil depends on the characteristics of the smear zone, the permeability ratio between the upper and lower layers of soil, the depth of penetration, and the

drain spacing. When the horizontal permeability in the upper layer is less than the underlying layer, the duration of consolidation of the underlying layer can be retarded depending on the depth of penetration of the upper layer of soil. On the other hand, the consolidation process can be accelerated further when the down dragged upper layer of soil has a higher permeability. The down drag effect due to mandrel installation in layered soil is illustrated in Figure 2.28.

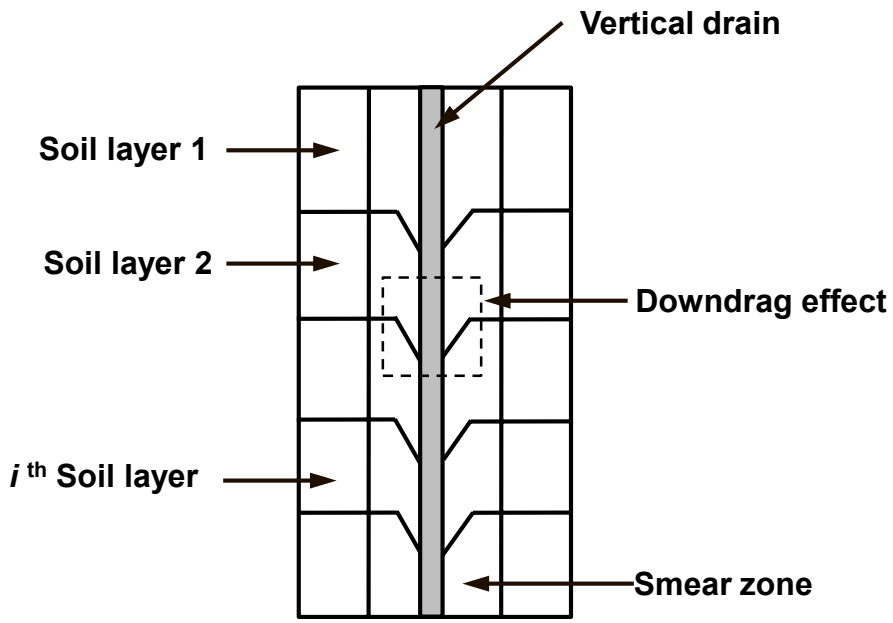

Figure 2.28 Down drag effects due to mandrel installation in layered soil (after Rujikiatkamjorn and Indraratna 2010)

In the study conducted by Rujikiatkamjorn and Indraratna (2010), a radial consolidation model using a piecewise technique was proposed to investigate the smear effect in layered soils. It was reported that the intrusion of the upper layer of soil into the underlying layer of soil creates an additional zone where the remoulded permeability can be increased or decreased depending on the initial permeability of the upper layer. In the intrusion zone located in the lower layer of soil the variations in permeability can be divided into three zones, including (i) a smear zone due to the down drag of the upper layer of soil, (ii) a smear zone due to a remoulding of the underlying soil, and (iii) the undisturbed lower layer of soil.

2.5.4 Theoretical Solutions for Vacuum Consolidation

A combined vacuum and surcharge one dimensional consolidation model was proposed by Mohamedelhassan and Shang (2002) based on Terzaghi's consolidation theory. The mechanism of a combined vacuum and surcharge loading may be determined by the law of superposition as a combination of surcharge preloading and vacuum preloading (Figure 2.29).

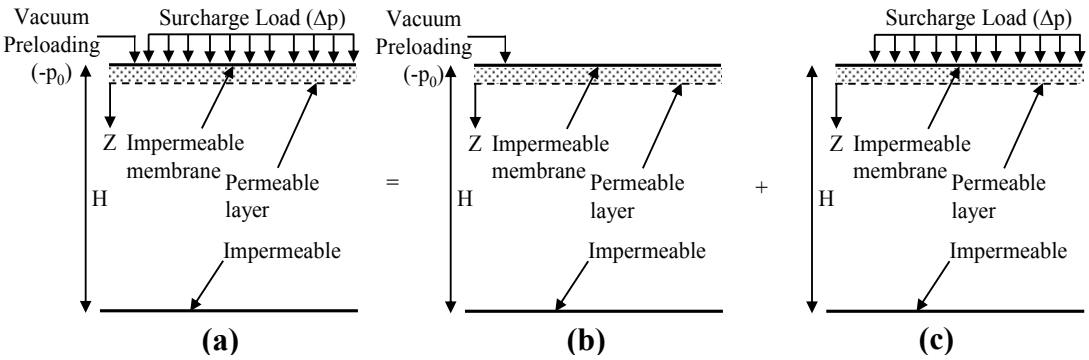

Figure 2.29 A schematic diagram of a vacuum preloading system: (a) vacuum and surcharge combining load, (b) vacuum preloading, and (c) surcharge preloading (after Mohamedelhassan and Shang 2002)

According to Mohamedelhassan and Shang (2002), the average degree of consolidation for combined vacuum and surcharge preloading can be expressed by:

$$U_v = 1 - \sum_{m=0}^{m=\infty} \frac{2}{M}\, exp\,(-M^2 T_{vc}) \tag{2.48}$$

$$T_v = c_{vc} t / H_d^2 \tag{2.49}$$

where, T_{vc} is a time factor for the combined vacuum and surcharge preloading, and c_{vc} is the coefficient of consolidation for the combined vacuum and surcharge preloading.

According to Indraratna et al. (2004b), when a vacuum pressure is applied in the field through PVDs, the suction head along the length of the drain may decrease with depth, thereby reducing its efficiency. Laboratory measurements taken at a few points along PVDs installed in a large scale consolidometer clearly indicated that the vacuum pressure propagates immediately, but a slight reduction in suction pressure might be found down the length of the drain. The rate at which a vacuum

pressure develops within the drain may depend on the length and type of PVDs (core and filter properties), but some field studies suggest that the vacuum pressure develops rapidly even if the PVDs are up to 30 m long (Bo et al., 2003; Indraratna et al., 2005a; Basu et al., 2007; Tran and Mitachi, 2008; Walker and Indraratna, 2007 and 2009; Walker et al., 2009b).

Based on laboratory observations, Indraratna et al. (2005a) developed a modified radial consolidation theory to include different patterns of vacuum pressure distribution (Figure 2.30). The results indicate that the efficiency of vertical drains depends on both the magnitude of the vacuum pressure and its distribution. In order to study the effect of the loss of vacuum, a trapezoidal distribution of vacuum pressure may be assumed.

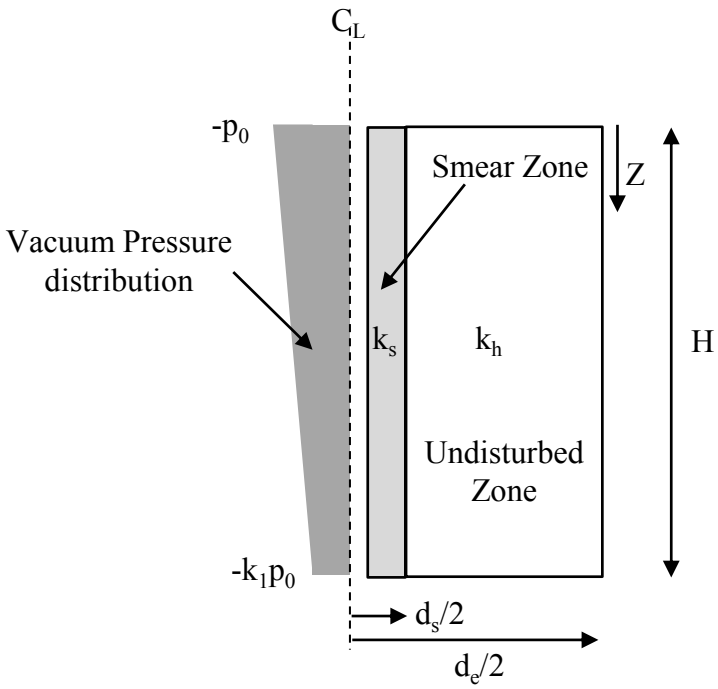

Figure 2.30 The distribution patterns of vacuum pressure in the horizontal and vertical directions (after Indraratna et al. 2005a)

Indraratna et al. (2005b) assumed that the average excess pore pressure ratio ($R_u = \Delta p/\bar{u}_0$) of the soil cylinder for radial drainage incorporating vacuum preloading can be given by:

$$R_u = \left(1 + \frac{p_{v0}}{\bar{u}_0}\frac{(1+k_1)}{2}\right)\exp\left(-\frac{8T_h}{\mu}\right) - \frac{p_{v0}}{\bar{u}_0}\frac{(1+k_1)}{2} \quad (2.50)$$

$$\mu = \ln\left(\frac{n}{s}\right) + \left(\frac{k_h}{k_s}\right)\ln(s) - 0.75 + \frac{\pi z(2l-z)k_h}{q_w}\left\{1 - \frac{\frac{k_h}{k_s}-1}{\left(\frac{k_h}{k_s}\right)\left(\frac{n}{s}\right)^2}\right\} \quad (2.51)$$

where, p_{v0} is the vacuum pressure applied at the top of the drain, k_1 is the ratio between the vacuum pressure at the top and bottom of the drain, u_0 is the initial excess pore water pressure, k_h is the horizontal coefficient of permeability of soil in the intact zone, k_s is the horizontal coefficient of permeability of soil in the smear zone, T_h is time factor, n is ratio R/r_w (R is the radius of the equivalent soil cylinder), s is the ratio r_s/r_w , z is the depth, l is the equivalent length of the drain, and q_w is the discharge capacity of the well.

Geng et al. (2012) developed analytical solutions for vertical drains with vacuum preloading for membrane and membrane-less systems under time-dependent surcharge preloading by considering both vertical and horizontal drainage. The properties of the constant smear zone (permeability and extent) and well resistance were also considered in both models. According to the Laboratory results and field measurements, the solution proposed by Geng et al. (2012) for the membrane-less system includes a loss of vacuum along the length of the drain. The Laplace transform technique was applied to derive the general solutions for pore water pressure, settlement, and the degree of consolidation. Time dependent surcharge preloading was considered by using the Laplace transform to simulate the history of the embankment construction and the changes in vacuum pressure over time.

2.6 NUMERICAL SIMULATION OF PVD ASSISTED PRELOADING

Different methods of numerical analysis have been widely used by geotechnical engineers to rectify the limitations of analytical approaches in simulating complex PVD assisted preloading projects to predict the ground behaviour, as well as conduct parametric studies and back calculate the properties of the smear zone. Different numerical programs such as CRISP, PLAXIS, ABAQUS, and FLAC have been used by researchers to conduct numerical analyses. A number of numerical investigations already performed are summarised in Table 2.11.

Indraratna and Redana (2000) used the finite element code CRISP92 (Britto and Gunn 1987) to simulate PVD improved ground under the load of an embankment by

adopting the equivalent coefficient of permeability for the undisturbed soil and the smear zone, and by incorporating Equations (2.32) and (2.33). The Modified Cam-Clay model was applied as the soil constitutive model to conduct the numerical analysis. The equivalent plane-strain width of the drain and smear zone were taken to be similar to the axisymmetric radius. The discretised finite element mesh was generated by linear strain quadrilateral elements with pore pressure nodes at the corners. The embankment surcharge was modelled by applying incremental vertical loads to the upper boundary. The smear zone was assumed to be three to four times the radius of the mandrel while assuming a linearly decreasing permeability within the smear zone. The numerical simulation conducted by Indraratna and Redana (2000) indicated that including the smearing effects can significantly increase the accuracy of the predicted settlements.

Arulrajah et al. (2005) used the PLAXIS 2D V.8 program to finite element model vertical drains that simulated the unit cell and the full scale embankment. The equivalent coefficients of horizontal permeability for the unit cells (axisymmetric to plane-strain) were adopted to conduct the numerical simulations with the conversion method proposed by Lin et al. (2000). The equivalent horizontal permeability of the surrounding soil was taken as twice that of the equivalent vertical permeability. According to Arulrajah et al. (2005), a good agreement was achieved between the numerical results and the field measurements. Settlement predictions obtained from the axisymmetric unit cell and the full scale analysis of vertical drains were found to be in a good agreement with each other, as well as with the actual field measurements.

Table 2.11 Summary of conducted numerical studies to simulate PVD assisted preloading process

Reference	Objective of the Numerical Study	Simulated Case Study	Applied Numerical Program
Indraratna & Redana (2000)	To evaluate the performance of soft clay foundation beneath embankments stabilised with vertical drains considering smear effects	Muar clay embankment Malaysia	CRISP92 2D
Indraratna et al. (2004a)	To investigate the effect of unsaturation at a drain boundary on the behaviour of a single PVD subjected to vacuum preloading applying 2D plane-strain model	Large-scale consolidometer test	ABAQUS 2D
Indraratna et al. (2005a)	To study the performance of a full-scale test embankment constructed on PVD improved soft clay incorporating vacuum preloading	Second Bangkok international airport	ABAQUS 2D
Indraratna et al. (2005b)	To model a single vertical drain incorporating the effects of vacuum preloading and compare the results with proposed analytical solutions	-	ABAQUS 2D
Arulrajah et al. (2005)	To investigate the deformation behaviour of marine clay under reclamation fills conducting full-scale analysis of PVDs and compare the results with the axisymmetric approach	Singapore marine clay at Changi	PLAXIS 2D
Chai et al. (2006)	To determine the optimum penetration depth of PVDs in combined vacuum-surcharge loading	Vacuum consolidation Saga, Japan	CRISP-AIT 2D
Rujikiatkamjor et al. (2008)	To conduct 2D and 3D numerical modelling of combined surcharge and vacuum preloading with vertical drains	storage yard at Tianjin Port, China	ABAQUS 2D & 3D
Indraratna et al. (2008)	To evaluate the consolidation behaviour of PVD improved soft soil beneath a circular embankment	Skå-Edeby Sweden	ABAQUS 2D
Tran & Mitachi (2008)	To evaluate the efficiency of a proposed conversion method converting from an axisymmetric unit cell to an equivalent plane-strain unit cell under embankment loading combined with vacuum preloading	-	CRISP 2D

Table 2.12 (cont.)

Yildiz and Karstunen (2009)	To study the performance of the matching procedures proposed by Hird et al. (1991 & 1995) when complex elasto-plastic models are used in the plane-strain analyses of vertical drains	Haarajoki embankment Finland	PLAXIS 3D
Yildiz (2009)	To evaluate the accuracy of three different matching methods for conversion of axisymmetric to plane-strain conditions by comparing results of 2D and 3D analyses	Haarajoki embankment Finland	PLAXIS 3D
Lin and Chang (2009)	To investigate the drainage behaviour of the PVD unit cell and the full-scale PVD improved ground conducting 3D numerical simulation	Second Bangkok international airport	FLAC 3D

A number of researchers applied the numerical approach to analyse the combined vacuum-surcharge preloading process by considering the smearing effects (Indraratna et al., 2005a; Chai et al., 2006; Rujikiatkamjorn et al. 2008). 2D and 3D multi-drain finite element analyses were conducted by Rujikiatkamjorn et al. (2008) using ABAQUS software coupled with Biot consolidation theory to predict the behaviour of PVD improved soft soil under combined vacuum and surcharge (embankment) loading. The Modified Cam-Clay theory was adopted as the soil constitutive model in these numerical analyses. The finite element mesh was generated by C3D8RP solid elements (eight node tri-linear displacement and pore pressure). The negative pore pressure was specified along the length of the PVD to simulate the vacuum pressure. The equivalent coefficients of permeability in the smear zone and undisturbed region were determined using the 2D conversion method proposed by Indraratna et al. (2005a), and the extent of the smear zone extent was considered to be twice the equivalent radius of the mandrel. The numerical study conducted by Rujikiatkamjorn et al. (2008) indicated that the results of 2D and 3D analyses were in good agreement, in terms of settlements, excess pore pressures, and lateral displacements. Rujikiatkamjorn et al. (2008) reported that the application of the equivalent plane-strain approach can result in accurate 2D numerical predictions for multi-drain systems in large projects. According to Rujikiatkamjorn et al. (2008), the height of the surcharge fill can be reduced by a vacuum preloading to achieve the same desired rate of consolidation.

Yildiz (2009) conducted 2D and 3D finite element simulations to model PVD improved soft soil under the embankment loading by adopting a recently developed elasto-plastic S-CLAY1S constitutive model to represent the soft soil. The three different conversion methods proposed by Hird et al. (1992), Indraratna and Redana (1997), and Chai et al. (2001) were used to convert the 3D behaviour of the PVDs into the equivalent plane-strain condition. A comparison between 3D and 2D analyses showed that all the conversion methods applied resulted in acceptable predictions, however, the method proposed by Indraratna and Redana (1997) produced the best agreement with the 3D results, with a maximum difference of 3% in the predicted settlements.

2.7 SUMMARY

As elaborated in this Chapter, the PVD assisted preloading system has been widely used as a soft soil ground improvement technique to accelerate consolidation and improve the strength of the soil, including the bearing capacity and the shear strength. The installation of vertical drains disturbs the soil near the drains, reduces the permeability of the smear zone, and retards the rate of consolidation quite significantly.

Being able to accurately predict the characteristics of the smear zone is essential in any analysis of the soil surrounding the drain, and to carry out reliable practical designs. Two major parameters were proposed to characterise the smear zone; , including the extent ratio ($s= r_s/r_m$) and the permeability ratio ($n= k_h/k_s$). Determining the radius and permeability of the smear zone has been a subject of intense discussion in literature. Different approaches have been proposed to evaluate the extent and permeability of the smear zone, including analytical solutions, laboratory tests, finite element methods, and back calculation techniques.

According to the available literature, r_s/r_m may vary from 1.6 to 7, while the permeability ratio (k_h/k_s) changes from 1 to 10. It can be noted that wide ranges are proposed for k_h/k_s and r_s/r_m and there is no meticulous method for being able to predict these parameters precisely that can be used by practising engineers. The assumed properties of the smear zone can lead to an early removal of the surcharge during construction, which would result in excessive post-construction settlement or excessive construction time and a subsequent increase in the project cost.

In this Chapter, the development of a consolidation theory (for vertical and radial conditions) was explained by focusing on the solutions proposed for radial consolidation and by considering the constant and variable properties of the smear zone. Furthermore, the solutions proposed for the combined vertical and radial consolidation theory in a single layer and multi-layered soil profiles were discussed.

Generally, 2D analysis with plane-strain permeability was used for the numerical simulation of real PVD assisted case studies. The approaches available to convert permeability from axisymmetric to plane-strain conditions were described in this Chapter. Moreover, the application of numerical programs in simulating PVD assisted preloading was discussed by presenting a summary of numerical studies previously conducted in this area.

Construction of a trial embankment on the top of ground improved by PVD is one of the most reliable techniques for accurately estimating the characteristics of the smear zone in conjunction with the back analysis method. In many cases, a long period of time is required to complete the consolidation process or to obtain 90% of consolidation after constructing the trial embankment, which may delay the project quite considerably, and also increase the costs significantly. Although back calculation is used in practice, there is no indication of the minimum monitoring time required. Determining the minimum degree of consolidation required resulting in predicable properties of the smear zone can convert the construction of the trial embankment into a very practical and cost effective method in the design of PVD assisted preloading projects.

In this research, a numerical based attempt has been made to estimate the minimum required degree of consolidation and consequently the minimum required preloading time that would result in a reliable prediction of the extent and permeability of the smear zone. In addition, an experimental program has been conducted to validate the proposed back calculation procedure to obtain the smear zone properties.

CHAPTER THREE

3 PVD ASSISTED PRELOADING SIMULATION AND BACK CALCULATION PROCEDURE USING FLAC

3.1 GENERAL

Numerical analysis methods have been widely used by geotechnical engineers to rectify the limitations that analytical approaches have in simulating complex prefabricated vertical drain (PVD) assisted preloading projects to predict ground behaviour, conduct parametric studies, and back calculate the properties of the smear zone. Bergado et al. (1993) applied the numerical program VERDRN, developed in FORTRAN 77, to model and back calculate the characteristics of the smear zone in a single vertical drain. The finite element program CRISP (Britto and Gunn, 1987) was used by Chai et al. (1999) to simulate a trial embankment at Saga Airport in Japan by adopting a one-dimensional finite element model. The smear zone properties were simulated by Indraratna et al. (2005b) through a back calculation process simulating the Suvarnabhumi Airport in Bangkok using ABAQUS software. Lin and Chang (2009) applied *FLAC 3D* to investigate the consolidation of a full scale PVD improved ground by simulating the Second Bangkok International Airport case history. Lin and Chang (2009) multiplied the permeability ratio obtained in the laboratory ($(k_h/k_s)_{\text{laboratory}}$) by the modification coefficient of 4 (C_f =4) to determine the permeability ratio in field conditions ($(k_h/k_s)_{\text{field}}$). The horizontal permeability of the undisturbed soil was then measured and the permeability ratio ($(k_h/k_s)_{\text{field}}$) was used to determine the permeability of the smear zone. Lin and Chang (2009) applied the equation proposed by Bergado and Long (1993) to determine the equivalent horizontal permeability by taking the smearing effect into consideration.

Literature shows that CRISP, ABAQUS, and PLAXIS are the most commonly used software packages by researchers conducting numerical simulations (e.g. Indraratna and Redana, 2000; Saowapakpiboon et al., 2011; Sathananthan et al., 2008; Stapelfeldt et al., 2008).

The main purpose of this chapter is to back calculate the properties of the smear zone using the available consolidation data, which needs a coded numerical program with the capability of conducting an efficient parametric study. Therefore, a systematic back calculation procedure was proposed to obtain accurate smear zone properties. The finite difference program *FLAC 2D*, was introduced and selected as the appropriate numerical code to conduct consolidation analyses for PVD assisted preloading case histories with complex geometries, and by adopting the proposed procedure for back analysis.

3.2 NUMERICAL MODELLING

3.2.1 Adopted Numerical Simulation Software

In this study the capabilities of different numerical programs (e.g. PLAXIS, FLAC, ABAQUS, and CRISP) were investigated to select suitable software embracing the requirements of this research.

PLAXIS and CRISP are finite element packages that are intended for a two dimensional analysis of deformation and stability in geotechnical engineering. The convenient CAD-style drawing option and automatic generation process of unstructured 2D finite element meshes converted these codes into practical tools which are being used for geotechnical analysis by geotechnical engineers who are not necessarily numerical specialists. However, the lack of a built-in programming language and the automatic mesh generation can be addressed as the limitations of these two programs in conducting parametric studies and sensitive analysis for research purposes. It should be noted that the manual process in CRISP to generate meshes, is time consuming and tedious.

For example, when simulating PVD assisted preloading to investigate the characteristics of the smear zone on consolidation, the geometry of the model should be changed manually every time. There are new values for the extent and permeability of the smear zone, to be implemented in the program, which is a tedious and time consuming process and may increase the risk of having faults and errors. Furthermore, the size of meshes cannot be defined manually in an appropriate way to suit the specific needs. Another limitation, associated with PLAXIS to model the preloading projects, is lack of a procedure to assign and fix certain values, such as

the pore water pressure at the vertical drain boundaries, to properly model the vertical drain and vacuum pressure. Therefore, numerical software with more advanced features is needed to conduct geotechnical research studies, especially when simulating prefabricated vertical drain preloading projects.

ABAQUS 2D is a general finite element code, which is also an appropriate numerical code for simulating mandrel driven PVD performance. This software suite incorporated many civil and structural features, but not developed exclusively for geotechnical engineering design purposes. *FLAC 2D* is specifically designed for 2D geotechnical analyses, which is more popular in the geotechnical industry than ABAQUS. However, limited researchers have used *FLAC 2D* to model PVD performance and verify its accuracy for potential users. Therefore, *FLAC 2D* software was selected for numerical simulation in this study because of its ability to conduct systematic parametric studies and back calculation procedures.

FLAC 2D v6.0 was used to model the PVD assisted preloading process that focuses on the variability of the smear zone. *FLAC 2D* is a two-dimensional explicit finite difference program for engineering mechanics computation. In comparison to the common commercial finite element numerical modelling software, the mixed discretisation scheme developed by Marti and Cundall (1982) was used to model plastic deformation and flow accurately because it was believed to be physically more justifiable than the reduced integration scheme that is commonly used with finite element analysis. In addition, the explicit solution scheme used in *FLAC 2D,* unlike the common implicit methods, can compute any material non-linear behaviour in almost the same computation time as a linear law, whereas an implicit solution can take significantly longer to solve non-linear problems such as fully coupled time dependent stress-deformation analysis capturing soil consolidation. In addition, large strain simulation (e.g. deformation of deep soft layers of clay due to preloading) in *FLAC 2D* is hardly more time consuming than a small strain case.

3.2.2 Explicit Finite Difference Method and Lagrangian Analysis

FLAC 2D is an explicit, finite difference program that performs a Lagrangian analysis. The finite difference method is a numerical technique, which solves sets of differential equations, and given initial values and/or boundary values (Atkinson and Han, 2005). In the finite difference method every derivative in the set of

governing equations is replaced directly by an algebraic expression, written in terms of the field variables (e.g., stress or displacement) at discrete points in space, which are undefined within the elements. In contrast, the finite element method has a central requirement that the field quantities (stress, displacement) vary in each element in a prescribed fashion, using specific functions. It can be noted that finite element programs often combine the matrices of the element into a large global stiffness matrix (Logan, 2007), whereas this is not normally conducted in the finite difference approach because it is relatively efficient to regenerate the finite difference equations at each step. *FLAC 2D* uses an explicit, time-marching method to solve the algebraic equations.

The general calculation sequence embodied in *FLAC 2D* is illustrated in Figure 3.1. This procedure first invokes the equations of motion to derive new velocities and displacements from stresses and forces, and the strain rates are derived from velocities and new stresses are derived from the strain rates. One time-step is taken for every cycle around the loop. It should be remembered that each box in Figure 3.1 updates all of its grid variables from known values that remain fixed while control is within the box. The selected time-step is so small that information cannot physically pass from one element to another in that interval, and since one loop of the cycle occupies one time-step, an assumption of "frozen" velocities (i.e., the newly calculated stresses do not affect the velocities) is justified (neighboring elements really cannot affect one another during the period of calculation) (Itasca, 2008).

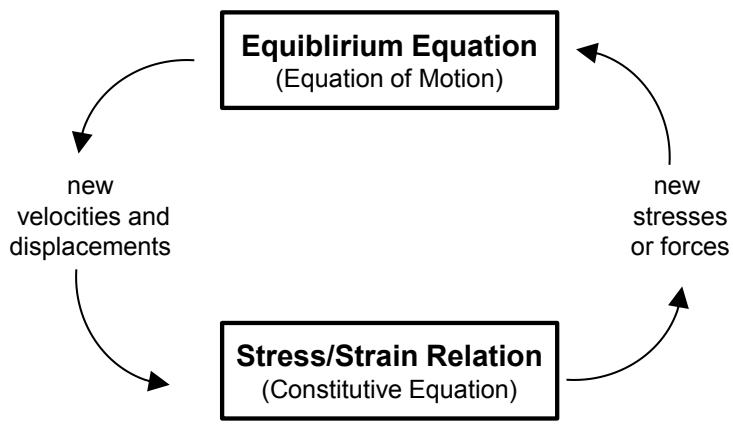

Figure 3.1 Basic explicit calculation cycle (after Itasca, 2008)

The central mathematical concept of the explicit method is that the calculated "wave speed" always keeps ahead of the physical wave speed, so that the equations always operate on known values that are fixed for the duration of the calculation. The most important advantage of this concept is that no iteration process is required while the stresses are being computed from strains in an element, even if the constitutive law is significantly non-linear. In an implicit method (which is commonly used in finite element programs), every element communicates with every other element during one solution step, thus, several cycles of iteration are necessary before compatibility and equilibrium are obtained. Table 3.1 compares the explicit and implicit methods. The key disadvantage of the explicit method is that small time-steps should be used which means that a large number of steps must be taken. Overall, the explicit methods are best for ill-behaved systems (e.g., non-linear, large strain, and physical instability).

Table 3.1 Comparison of explicit and implicit solution methods (after Itasca, 2008)

Explicit	**Implicit**
Time-step must be smaller than a critical value for stability	Time-step can be arbitrarily large, with unconditionally stable schemes
Small amount of computational effort per time-step	Large amount of computational effort per time-step
No significant numerical damping introduced for dynamic solution	Numerical damping dependent on time-step present with unconditionally stable schemes
No iterations necessary to follow nonlinear constitutive law	Iterative procedure necessary to follow nonlinear constitutive law
Provided that the time-step criterion is always satisfied, nonlinear laws are always followed in a valid physical way	Always necessary to demonstrate that the above- mentioned procedure is: (a) stable; and (b) follows the physically correct path (for path-sensitive problems)
Matrices are never formed. Memory requirements are always at a minimum. No bandwidth limitations	Stiffness matrices must be stored. Ways must be found to overcome associated problems such as bandwidth. Memory requirements tend to be large
Since matrices are never formed, large displacements and strains are accommodated without additional computing effort	Additional computing effort needed to follow large displacements and strains

Since there is no need to form a global stiffness matrix, it is a small matter to update coordinates at each time-step in the large-strain mode. These incremental

displacements are added to the coordinates so that the grid moves and deforms with the material it represents. This is termed a "Lagrangian" formulation, in contrast to an "Eulerian" formulation where the material moves and deforms relative to a fixed grid. The constitutive formulation at each step is a small-strain one, but is equivalent to a large-strain formulation over many steps.

FEM codes usually represent steady plastic flow by a series of static equilibrium solutions (Zienkiewicz et al., 2005). The quality of the solution for increasing applied displacements depends on the nature of the algorithm used to return stresses to the yield surface, following an initial estimate using linear stiffness matrices. The best FEM codes will give a limit load (for a perfectly plastic material) that remains constant with an increasing applied displacement. The solution provided by these codes will be similar to that provided by *FLAC 2D*. However, FLAC's formulation is simpler because no algorithm is needed to bring the stress of each element to the yield surface, and therefore the plasticity equations are solved exactly in one step. Therefore, *FLAC 2D* may be more efficient than some FEM codes for modelling steady plastic flow. Moreover, *FLAC 2D* is robust in a sense that it can handle any constitutive model with no adjustment to the solution algorithm, while many FEM codes need different solution techniques for different constitutive models.

3.2.3 The Grid and Mixed-Discretization Zoning Technique

In this study a solid body is divided into a finite difference mesh consisting of quadrilateral elements in order to carry out numerical modelling. Internally, *FLAC 2D* sub-divides each element into two overlaid sets of constant-strain triangular elements, as shown in Figure 3.2.

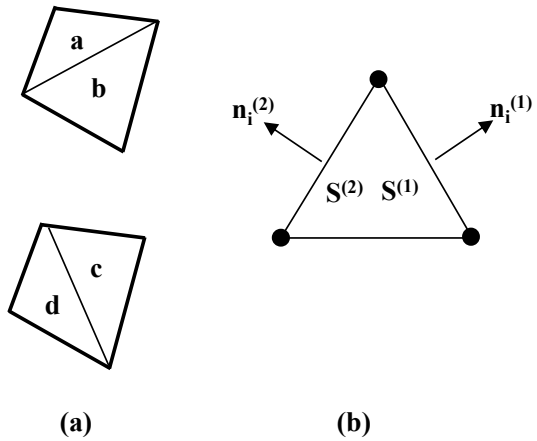

Figure 3.2 Finite difference mesh, (a) FLAC 2D zone composed of overlaid triangular elements and (b) typical triangular element

The four triangular sub-elements are called *a*, *b*, *c* and *d* (see Figure 3.2). The deviatoric stress components of each triangle are maintained independently, requiring sixteen stress components to be stored for each quadrilateral ($4 \times \sigma_{xx}, \sigma_{yy}, \sigma_{zz}, \sigma_{xy}$). The force vector exerted on each node is taken to be the mean of the two force vectors exerted by the two overlaid quadrilaterals so that the response of the composite element is symmetrical for a symmetric loading. If one pair of triangles becomes significantly distorted (e.g., if the area of one triangle becomes much smaller than the area of its companion), then the corresponding quadrilateral is not used, and only nodal forces from other (more reasonably shaped) quadrilaterals are used. It can be noted that if both overlaid sets of triangles are badly distorted, *FLAC 2D* complains with an error message.

The use of triangular elements eliminates the problem of hourglass deformation, which may occur with constant-strain finite difference quadrilaterals. The term "hourglassing" comes from the shape of the deformation pattern of elements within a mesh. A common problem, which occurs when modelling materials that will undergo yielding, is the incompressibility of plastic flow (volume change is zero). The use of plane-strain or axisymmetric geometries introduces a kinematic restraint in the out-of-plane direction which often gives rise to an over prediction of the collapse load. This condition is sometimes referred to as "mesh-locking" or "excessively stiff" elements, and is discussed in detail by Nagtegaal et al. (1974). The problem arises as a condition of local mesh incompressibility which must be satisfied during flow, and which results in over constrained elements. To

overcome this problem the isotropic stress and strain components are taken to be constant over the whole quadrilateral element, while the deviatoric components are treated separately for each triangular sub-element. This procedure, referred to as mixed discretisation, was described by Marti and Cundall (1982). The term mixed discretisation arises from the different discretisations for the isotropic and deviatoric parts of the stress and stain tensors.

3.2.4 Continuum Expression of the Governing Equations

Applying a surcharge on top of the ground will result in a sudden change in the pore water pressure along the saturated soil profile (e.g. Terzaghi and Frohlich, 1936; Jacob, 1940; Skempton, 1954). This change in the pore water pressure is often known as the excess pore water pressure, and the difference between the applied total stress and the pore water pressure is referred to as the effective stress (Terzaghi, 1925). Since soil is a compressible porous medium with interconnected pores linked to drainage boundaries, the excess pore water pressure dissipates gradually over time and causes a time dependent deformation of the soil body, called "consolidation" (Terzaghi, 1925). First, changes in the pore water pressure induce changes in the effective stress, which affects the response of the solid (for example, a reduction in the effective stress may cause plastic yield). Second, a change in the pore water pressure alters the volume of soil in a zone.

In this study, a coupled fluid-mechanical approach was used to simulate consolidation by adopting a basic fluid flow model with the following characteristics:

i. The fluid flow law corresponds to both isotropic and anisotropic permeability,

ii. Different zones may have different fluid-flow properties,

iii. Fluid pressure, flux, and impermeable boundary conditions may be prescribed,

iv. Fluid sources (wells) may be inserted into the material as either point sources (interior discharge) or volume source (interior well), and

v. Any of the mechanical models may be used with the fluid flow models.

The fluid and mechanical loops are implemented alternately to conduct a coupled fluid-mechanical modelling. Saturated transient fluid flow through the soil is modelled in the fluid loops to simulate the generation and dissipation of excess pore water pressure, while the stress-displacement development processes are modelled in the mechanical loops. The Biot theory of consolidation (Biot, 1941) was used in *FLAC 2D* to formulate coupled fluid-deformation mechanisms. Biot (1941) developed four differential equations as general equations governing consolidation in a three-dimensional environment. They are satisfied by four unknowns, including the components of displacement in x, y, and z directions (denoted by u, ϑ, and *w*, respectively) and the increment of water pressure (σ). The equations proposed by Biot (1941) are shown as follows:

$$G\nabla^2 u + \frac{G}{1-2\mu}\frac{\partial \epsilon}{\partial x} - \alpha\frac{\partial \sigma}{\partial x} = 0 \tag{3.1}$$

$$G\nabla^2 \vartheta + \frac{G}{1-2\mu}\frac{\partial \epsilon}{\partial y} - \alpha\frac{\partial \sigma}{\partial y} = 0 \tag{3.2}$$

$$G\nabla^2 w + \frac{G}{1-2\mu}\frac{\partial \epsilon}{\partial z} - \alpha\frac{\partial \sigma}{\partial z} = 0 \tag{3.3}$$

$$k\nabla^2 \sigma = \alpha\frac{\partial \epsilon}{\partial t} + \frac{1}{Q}\frac{\partial \sigma}{\partial t} \tag{3.4}$$

where,

$$\nabla^2 = \frac{\partial^2}{\partial x^2} + \frac{\partial^2}{\partial y^2} + \frac{\partial^2}{\partial z^2} \tag{3.5}$$

$$\alpha = \frac{2(1+\mu)}{3(1-2\mu)}\frac{G}{H} \tag{3.6}$$

$$\frac{1}{Q} = \frac{1}{R} - \frac{\alpha}{H} \tag{3.7}$$

$$\zeta = -\frac{\sigma}{R} \tag{3.8}$$

$$\epsilon = -\frac{\sigma}{H} \tag{3.9}$$

where, G is the shear modulus, μ is Poisson's ratio, ϵ is the volumetric strain, α is Biot's coefficient, ζ denotes the variation of water content (variation of water volume per unit volume of porous material), k is the coefficient of permeability, *1/H* is a measure of the compressibility of the soil due to a change in water pressure, *1/R* is a measure of the change in water content due to a given change in water pressure, and *1/Q* is a measure of the amount of water, which can be forced into the soil under pressure while the volume of the soil is kept constant.

Biot (1941) reported that the constants α and Q are dependent on the degree of saturation and incompressibility of the system, respectively, and can be taken as 1 and ∞ ($\alpha = 1$ and $Q = \infty$) by assuming that water is an incompressible material (with no air bubbles), and by considering the soil to be a fully saturated material. Furthermore, the change in volume of the saturated soil is equal to the amount of water squeezed out. Based on these assumptions, the fundamental equations governing the consolidation of completely saturated clay were proposed by Biot (1941) in the following forms:

$$G\nabla^2 u + \frac{G}{1-2\mu}\frac{\partial \epsilon}{\partial x} - \frac{\partial \sigma}{\partial x} = 0 \tag{3.10}$$

$$G\nabla^2 \vartheta + \frac{G}{1-2\mu}\frac{\partial \epsilon}{\partial y} - \frac{\partial \sigma}{\partial y} = 0 \tag{3.11}$$

$$G\nabla^2 w + \frac{G}{1-2\mu}\frac{\partial \epsilon}{\partial z} - \frac{\partial \sigma}{\partial z} = 0 \tag{3.12}$$

$$k\nabla^2 \sigma = \frac{\partial \epsilon}{\partial t} \tag{3.13}$$

where

$$H = R = \frac{2G(1+\mu)}{3(1-2\mu)} \tag{3.14}$$

$$\zeta = \epsilon \tag{3.15}$$

The coupled calculation process starts with a fluid loop that evaluates pore water pressure and specific discharge using the transport law (Darcy's law), the fluid balance laws, and the compatibility law. Then the change of pore water pressure is

passed to the mechanical loop to update the effective stress, which is used to check against failure and calculate the volumetric strain based on the selected constitutive model. The calculated volumetric strain is passed back to the fluid loop to account for the pore water pressure and specific discharge in the new fluid loop on the basis of the linear quasi-static Biot's theory (Biot, 1941), which was formulated in an incremental format. Because these two loops were implemented alternately, pore water pressures and volumetric strains are kept exchanging and updating. Modelling this process may require thousands of cycles, which is terminated when a specific criterion (such as the maximum unbalanced force, the flow time, the stress ratio and so on) is reached.

The governing differential equations corresponding to FLAC numerical implementation are discussed below.

3.2.4.1 Water Flow Equation

Darcy's law was used in *FLAC 2D* to describe the water flow as follows:

$$q_i = -k_{ij}\hat{k}(s)\frac{\partial}{\partial x_i}(P - \rho_w g_k x_k) \tag{3.16}$$

where, q_i is the specific discharge vector (i.e. volumetric flux or the filtration velocity per unit volume), k_{ij} is the tensor of the coefficient of permeability (FLAC permeability tensor), $\hat{k}(s)$ is the relative permeability (when soil is fully saturated $\hat{k}(s) = 1$), P is the water pressure, ρ_w is the mass density of the water, and g_k is the gravity vector (0,0,g). For saturated/unsaturated flow in *FLAC 2D*, the air pressure is assumed to be constant and equal to zero.

3.2.4.2 Balance Laws

Biot (1941) applied Darcy's law to derive the water mass balance equation based on the fact that the rate of the water content of an element of soil must be equal to the volume of water entering per unit time through the surface of the element, assuming the water to be incompressible. The equation proposed by Biot (1941) was used in *FLAC 2D* for the water mass balance as follows:

$$\frac{\partial \zeta}{\partial t} = -\frac{\partial q_i}{\partial x_i} + q_v \tag{3.17}$$

where, q_v is the intensity of the volumetric water source. According to Bear (1972), the balance of momentum has the following form:

$$\frac{\partial \sigma_{ij}}{\partial x_i} + \rho g_i = \rho \frac{d\dot{u}_i}{dt} \tag{3.18}$$

where, σ_{ij} is the effective stress, $\rho = (1-n)\rho_s + n\rho_w$ is the solid bulk density, ρ_s and ρ_w are the densities of the solid and water phases, respectively, and n is porosity. Note that $(1-n)\rho_s$ corresponds to the bulk density of the dry matrix (ρ_d) (i.e., $\rho = \rho_d + n\rho_w$).

3.2.4.3 Constitutive Laws

In order to have a complete set of differential equations for the transient phenomenon of consolidation (i.e., those equations governing the distribution of stress, water content, and settlement as a function of time in a soil under given loads), Dracy's law was used by Biot (1941) to develop an extra equation which relates the variations of water pressure (P), water content (ζ), and volume changes (ϵ) over time to each other (Equation (3.4)). This relationship is called the response equation for the pore water and depends on the degree of saturation. In *FLAC 2D*, the following form of the response equation is used:

$$\frac{\partial P}{\partial t} = M_b \left(\frac{\partial \zeta}{\partial t} - \alpha \frac{\partial \epsilon}{\partial t}\right) \tag{3.19}$$

where, M_b is the Biot modulus, α is the Biot coefficient and ϵ is the volumetric strain. The Biot modulus is related to the drained bulk modulus of the porous medium (K) and the water bulk modulus, (K_W), via n and α, as follows:

$$M_b = \frac{K_W}{n + (\alpha - n)(1-\alpha)\frac{K_W}{K}} \tag{3.20}$$

For saturated clay when the compressibility of grains is negligible compared to the drained bulk material ($\alpha = 1$), the Equation (3.20) is converted to:

$$M_b = \frac{K_w}{n} \tag{3.21}$$

The small-strain constitutive response for the porous solid is described by:

$$\frac{d}{dt}\left(\sigma_{ij} + \alpha P \delta_{ij}\right) = H\left(\sigma_{ij}, \dot{\epsilon}_{ij}, \kappa\right) \tag{3.22}$$

where, H is the functional form of the constitutive law (e.g. modified Cam-clay, Mohr-Coulomb, Hoek-Brown, strain-hardening/softening) and κ is a history parameter. In particular, the elastic relationships that relate effective stresses to strains have the following form:

$$\sigma_{ij} - \sigma_{ij}^{o} + \alpha(P - P^{o})\delta_{ij} = 2G\dot{\epsilon}_{ij} + (K - \frac{2}{3}G)\dot{\epsilon}_{kk}\delta_{ij} \tag{3.23}$$

where, the superscript " o " refers to the initial state and $\dot{\epsilon}_{kk}$ is the volumetric strain increment.

3.2.4.4 Compatibility Equation

In numerical analysis approaches, the equations of equilibrium satisfying the strain compatibility equations can be solved by using a certain constitutive law under prescribed boundary conditions. In *FLAC 2D*, Equation (3.24) was used as the strain compatibility equation because it relates the strain rate to the velocity gradient.

$$\dot{\epsilon}_{ij} = \frac{1}{2}\left[\frac{\partial \dot{u}_i}{\partial x_j} + \frac{\partial \dot{u}_j}{\partial x_i}\right] \tag{3.24}$$

3.2.5 Numerical Fluid Flow Formulation

3.2.5.1 Basic Scheme

The basic fluid flow scheme can be applied for fully saturated transient or steady state fluid flow, run independently or coupled to a mechanical calculation. Substituting Equation (3.17) into Equation (3.19) yields expressions for the fluid continuity equations, which are then solved in *FLAC 2D* using a finite-difference approach based on a discretisation of the medium into zones composed of two overlays of triangles. The pore water pressure varies linearly in a triangle,

assuming a uniform specific discharge in the triangle. Figure 3.2 should be consulted whenever reference is made to the triangles that make up FLAC's quadrilateral elements. In the related equations, pressures and saturation values are assumed to be located at grid points (or "nodes"). Zone pressures are derived from the surrounding nodal values by simple averaging.

Commencing from a state of mechanical equilibrium, a coupled hydro-mechanical static simulation using the basic scheme in *FLAC 2D* involves a series of steps (Itasca, 2008). Each step includes one or more flow steps (flow loop), followed by enough mechanical steps (mechanical loop) to maintain a quasi-static equilibrium. The increment of the pore water pressure due to water flow was evaluated in the flow loop, while the contribution from volumetric strain was evaluated in the mechanical loop as a zone value, which is then distributed to the nodes. The total stress correction due to the change in pore water pressure arising from the mechanical volume strain is performed in the mechanical loop, and that arising from the flow of water in the flow loop. The total value of the pore water pressure was used to evaluate effective stresses and detect failure in plastic materials (Itasca, 2008).

3.2.5.2 Constitutive Law: Derivation of Element "Stiffness Matrix"

Neglecting gravity for the moment (it will be incorporated later), Darcy's Equation for an anisotropic porous medium is reduced to the following equation:

$$q_i = -k_{ij}\frac{\partial P}{\partial x_i} \tag{3.25}$$

Each quadrilateral element is divided into triangles in two different ways (see Figure 3.2(a)). The pore water pressure was assumed to vary linearly in a triangle, and the vector q_i was derived for a generic triangle of area A by applying the Gauss divergence theorem (Itasca, 2008). For a triangular sub-element, Equation (3.25) has the following finite difference form:

$$q_i \cong \frac{k_{ij}}{A}\sum Pn_j s \tag{3.26}$$

where, $\sum$ is the summation over the three sides of the triangle, n_i is the unit normal to the side i, and s is the length of the side. The two components of the specific discharge capacity (q) are:

$$q_1 = \frac{1}{A}[k_{11}\sum Pn_1 s + k_{12}\sum Pn_2 s] \tag{3.27}$$

$$q_2 = \frac{1}{A}[k_{21}\sum Pn_1 s + k_{22}\sum Pn_2 s] \tag{3.28}$$

where, q_1 is the specific discharge capacity vector for triangle side 1, q_2 is the specific discharge capacity vector for triangle side 2 (Figure 3.2).

Considering, for example, the contribution of side *(ab)* of the triangle (Figure 3.2) to the summations:

$$q_1^{(ab)} = \frac{1}{2A}\left[-k_{11}\left(P^{(b)}+P^{(a)}\right)\left(x_2^{(b)}-x_2^{(a)}\right)+k_{12}\left(P^{(b)}+P^{(a)}\right)\left(x_1^{(b)}-x_1^{(a)}\right)\right] \tag{3.29}$$

$$q_2^{(ab)} = \frac{1}{2A}\left[-k_{21}\left(P^{(b)}+P^{(a)}\right)\left(x_2^{(b)}-x_2^{(a)}\right)+k_{22}\left(P^{(b)}+P^{(a)}\right)\left(x_1^{(b)}-x_1^{(a)}\right)\right] \tag{3.30}$$

The two other sides, *(bc)* and *(ca)* (Figure 3.2), provide similar contributions to q_i. This specific discharge vector contribution was then converted to scalar volumetric flow rates at the nodes by making dot products with the normals to the three sides of the triangle. The general expression is:

$$Q = q_i n_i s \tag{3.31}$$

For example the flow rate into node *(a)* is:

$$Q^{(a)} = \left\{-q_1\left(x_2^{(b)} - x_2^{(c)}\right) + q_2\left(x_1^{(b)} - x_1^{(c)}\right)\right\}/2 \tag{3.32}$$

The factor of 2 accounts for the fact that the node only captures half the flow crossing a neighboring edge (since the other half goes to the other node of the edge). Similar expressions apply to nodes *(b)* and *(c)*. Nodal flow rates are added from the three triangles meeting at the node and are divided by 2 since the flow sum comes from two overlaid grids. The "stiffness" matrix $[\mathcal{M}]$ of the whole quadrilateral element is

defined in terms of the relationship between the pressures at the four nodes and the four nodal flow rates, as derived above:

$$\{Q\} = [\mathcal{M}]\{P\} \tag{3.33}$$

For the special case of a square zone, aligned with the coordinate axes, the stiffness matrix has the following form:

$$[\mathcal{M}] = -\frac{k}{2}\begin{bmatrix} 2 & -1 & 0 & -1 \\ -1 & 2 & -1 & 0 \\ 0 & -1 & 2 & -1 \\ -1 & 0 & -1 & 2 \end{bmatrix} \tag{3.34}$$

where, k is the coefficient of isotropic mobility, which is the coefficient of pore pressure term in Darcy's law that can be defined as the ratio of intrinsic permeability to fluid dynamic viscosity. This matrix is identical to the one that would be obtained in a classical finite difference method.

By including gravity, when the grid point pressures around a zone conform to the gradient $\frac{\partial \mathrm{P}}{\partial \mathrm{x_i}} = \mathrm{g_i}\rho_\mathrm{w}$, where $\mathrm{g_i}$ is the vector of gravitational acceleration, then the nodal flow rates *{Q}* should be zero. Hence, Equation (3.33) is modified as follows:

$$\{Q\} = [\mathcal{M}]\{P - (x_i - x_i^{(1)})\mathrm{g}_i\rho_w\} \tag{3.35}$$

where, $x_i^{(1)}$ is the x-coordinate of one of the corners.

3.2.5.3 Continuity Equation

The flow imbalance ($\sum Q$) at a node causes a change in the pore water pressure at a saturated node as follows:

$$\frac{\partial P}{\partial t} = -\frac{M_b}{V}\left(\sum Q + \alpha\frac{\partial V}{\partial t}\right) \tag{3.36}$$

where, V is the total volume associated with the node. The term $\sum Q$ includes contributions from the four surrounding zones and any sources that are specified by

the user (e.g. outflow from a well). Equation (3.36) has the following finite difference form:

$$P_{i+1} = P_i - \frac{M_b(\sum Q\Delta t + \alpha \Delta V_{mech})}{V} \quad (3.37)$$

where, ΔV_{mech} is the equivalent increase in the nodal volume arising from mechanical deformation of the grid. The term V was computed as the sum of the contributions from all triangular subzones connected to the node. Each triangle contributes a third of its volume, and the resulting sum is divided by two, to account for the double overlay scheme in *FLAC 2D*.

3.2.5.4 Numerical Stability: Fluid Time-step

There are two aspects of numerical stability associated with the pore-fluid scheme. First, an explicit solution of the fluid flow equations requires that the time-step be less than a critical value. Second, as the bulk modulus of the water increases the mechanical stiffness of a saturated zone, the effect of increased mechanical stiffness is incorporated into quasi-static analysis in the density-scaling scheme in *FLAC 2D*. The apparent mechanical bulk modulus of a zone is modified by the presence of water as follows:

$$K_{i+1} = K_i + \alpha^2 M_b \quad (3.38)$$

where, α is the Biot coefficient and M_b is the Biot modulus, which are explained in previous sections.

The explicit fluid time-step can be derived by imagining that one node at the centre of four zones is given a pressure of P_0. The resulting nodal flow is then given by Equation (3.35) as $Q = P_0 \sum M_{kk}$, where, $\sum M_{kk}$ is the sum over the four zones of the diagonal terms corresponding to the selected node. The excess nodal flow gives rise to an increment in ΔP, according to Equation (3.37).

$$\Delta P = -\frac{M_b Q \Delta t}{V} \quad (3.39)$$

The new pressure at the node P_1 is then

$$P_1 = P_0 + \Delta P = P_0 \left(1 - \frac{M_b \sum \mathcal{M}_{kk} \Delta t}{V}\right) \tag{3.40}$$

where, $[\mathcal{M}]$ is the stiffness matrix relating the pore water pressure to the flow rate, as defined by Equation (3.33). Equation (3.40) is stable and monotonic if the following equation is satisfied:

$$\Delta t < \frac{V}{M_b \sum \mathcal{M}_{kk}} \tag{3.41}$$

The value of Δt used in *FLAC 2D* is that given by Equation (3.41) multiplied by a safety factor of 0.8.

3.2.6 Optimisation of the Mechanical and Fluid Time steps

The fluid flow solution is controlled by the "SET" and "SOLVE" commands in *FLAC 2D*. The "SET" command allows certain options to be switched on or off, and certain solution parameters to be specified. The keywords "flow" and "mech" are used to define the method of analysis. For example, the "flow" and "mech" keywords should be switched on using the "SET" command to conduct coupled fluid and mechanical analysis.

In practice the mechanical effects occur instantaneously compared to the diffusion effects, where no time is associated with any of the mechanical sub-steps taken in association with fluid-flow steps in order to satisfy quasi-static equilibrium. Each fluid step corresponds to a real period of time. By default, *FLAC 2D* alternates the mechanical steps and fluid steps in the basic fluid flow scheme, by one mechanical step and then by one fluid step.

At the beginning of the solution of a coupled problem, even one fluid step may put the system a long way out of equilibrium (i.e., there will be large unbalanced forces). Hence, many mechanical steps should be taken for each fluid step. As consolidation continues, the changes in fluid pressure will become small, so the system will remain in equilibrium. At this stage, several fluid time steps may be taken for each mechanical step (the reverse of the previous strategy). Two methods were proposed by Itasca (2008) to obtain the optimum combination of fluid and mechanical time steps that would result in an acceptable accuracy, and they are explained below.

3.2.6.1 Manual Method

In this method the number of fluid and mechanical steps is controlled manually. The "SET nmech" and "SET ngw" commands are used to set the number of mechanical and fluid steps for each cycle, as denoted by the "STEP" command, respectively. The unbalanced force ratio (or unbalanced force), which is generally assumed to be 0.001 or 0.01, should be monitored during this process. The unbalanced force ratio can be defined using "SET sratio" command. It should be noted that adopting large fluid and mechanical steps may increase the required time for numerical analyses significantly.

The optimum combination of fluid and mechanical steps can be selected when two criteria are satisfied; (i) the unbalanced force ratio (sratio) falls below the defined value (0.001 or 0.01), and (ii) a numerical analyses is being conducted in a minimum period of time. In this study a parametric study was carried out to determine the optimum combination of fluid and mechanical steps which indicated that adopting "nmech" and "ngw" in the range of 5 to 10 can result in accurate outcomes and acceptable time for numerical calculations.

3.2.6.2 Automatic Method

In this approach the number of fluid and mechanical sub-cycles is adjusted automatically to keep the maximum unbalanced force ratio (or unbalanced force) below a present value. This algorithm is activated by the "auto on" keyword in the "SOLVE" command; the total groundwater time (consolidation time) to be modelled is specified by the "age" keyword in the "SOLVE" command (SOLVE auto on age =consolidation time), keeping the computation until the time given by the "age" parameter is reached. Also, parameters "step" and "clock" should also be set, to prevent premature truncation of the run due to limits on step number and elapsed time, respectively, from being reached.

According to the investigations carried out in this study, applying the automatic approach results in acceptable numerical predictions, and therefore the number of fluid and mechanical sub-cycles was adjusted automatically to conduct the coupled fluid-mechanical analyses.

3.2.7 Modified Cam-Clay Model

In this study the modified Cam-Clay (MCC) model was adopted in the developed numerical code to investigate the consolidation of soft soil. The MCC model was introduced by Roscoe & Burland (1968) to model the behaviour of clay soil. The details of this model and its numerical implementation can be found in a number of references such as Wood (1990), and Gens and Potts (1988). The MCC model is an incremental hardening/softening elasto-plastic model. Its features include a particular form of non-linear elasticity (semi logarithmic), and a hardening/softening behaviour governed by volumetric plastic strain. The failure envelopes are similar in shape, and correspond to ellipsoids of rotation about the mean stress axis in the principal stress space. The shear flow rule is associated and no resistance to tensile mean stress is offered in this model. The MCC model has been discussed extensively by Roscoe & Burland (1968).

The MCC model is expressed in terms of three variables; the mean effective pressure (p'); the deviator stress (q); and the specific volume (v). The generalised stress components p' and q may be expressed in terms of principal stresses, as follows:

$$p' = -\frac{1}{3}(\sigma_1 + \sigma_2 + \sigma_3 +) \tag{3.42}$$

$$q = -\frac{1}{\sqrt{2}}\sqrt{(\sigma_1 - \sigma_2)^2 + (\sigma_2 - \sigma_3)^2 + (\sigma_1 - \sigma_3)^2} \tag{3.43}$$

3.2.7.1 Virgin Consolidation Line and Swelling Lines

In the MCC model the assumption is that when a sample of soft soil is slowly compressed under isotropic stress and under perfectly drained conditions, the relationship between specific volume (v) and $\ln p'$ consists of a straight virgin consolidation line (also known as the normal compression line) and a set of straight swelling lines (Figure 3.3). Swelling lines are also called unloading-reloading lines.

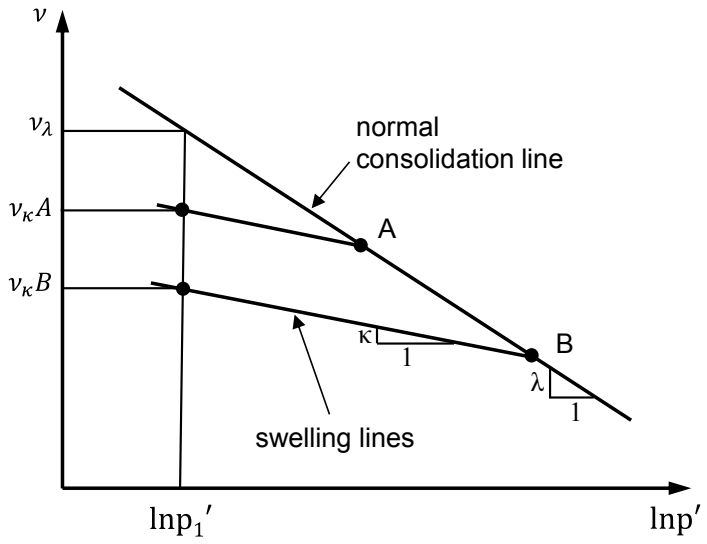

Figure 3.3 Normal consolidation line swelling lines for an isotropic compression test

The normal consolidation line (loading line) and swelling line (reloading line) are defined by the Equations (3.44) and (3.45), respectively.

$$v = v_\lambda - \lambda ln \frac{p'}{p_1'} \tag{3.44}$$

$$v = v_\kappa - \kappa ln \frac{p'}{p_1'} \tag{3.45}$$

where, $\lambda, \kappa,\ and\ v_\lambda$ are the constant properties of the soil. The parameter λ represents the slope of the normal compression (virgin consolidation) line, or critical state line in $v - lnp'$ space, κ is the slope of the swelling line in $v - lnp'$ space, p_1' is the reference pressure, and v_λ is the value of the specific volume at the reference pressure. The value of v_κ for a particular line depends on the location of the point on the normal consolidation line from which unloading is performed.

3.2.7.2 Yield and Potential Functions

Under increasing triaxial shear loading (q), MCC soil behaves elastically until a yield value of q is attained (Roscoe and Borland, 1968; Wood, 1990). Coordinates at the yielding point (p', q) are determined from the following function:

$$f = q^2 + M^2 p(p - p_c) \tag{3.46}$$

where, $p_c{}'$ is preconsolidation pressure and M is the slope of the critical state line (CSL) in $p' - q$ space. The yield condition f=0 is represented by an ellipse with horizontal axis, $p_c{}'$, and vertical axis, $Mp_c{}'$, in the $p' - q$ space. Figure 3.4 indicates the yield function for the MCC model.

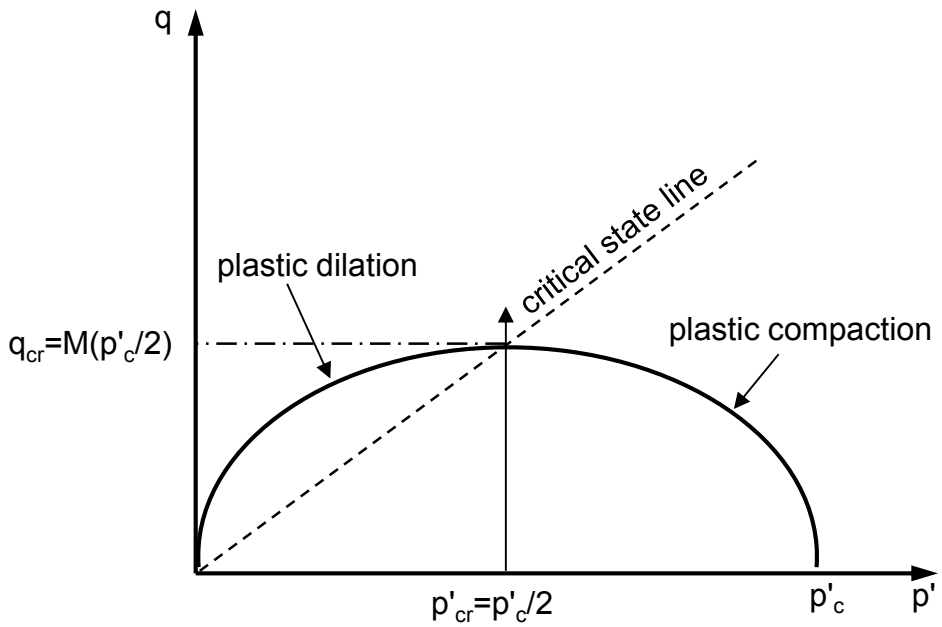

Figure 3.4 Yield surface of the Modified Cam-Clay model in p´-q plane (after Roscoe and Borland, 1968)

3.2.7.3 Determination of the Input Parameters

The slope M of the CSL in $p' - q$ space can be calculated from the friction angle φ'(Huang et al., 2006) of the Mohr-Coulomb yield criterion through the following equation:

$$M = \frac{6sin\varphi'}{3-sin\varphi'} \tag{3.47}$$

The slopes λ and κ of the normal compression and swelling lines in $v - lnp'$space are related to the compression index C_c, and the swelling index C_s, and can be determined through the following equations, respectively (Huang et al., 2006):

$$\lambda = \frac{C_c}{\ln 10} \tag{3.48}$$

$$\kappa = \frac{C_s}{\ln 10} \tag{3.49}$$

Often κ is chosen to be in the range of 0.1λ to 0.3 λ (Graham, 2010; Budhu, 2010; Liu and Evett, 2013).

3.3 NUMERICAL CODE DEVELOPMENT

3.3.1 General

In the present study, a comprehensive numerical code was developed using the *FLAC 2D* program to simulate the process of PVD assisted preloading. The developed code can simulate the laboratory consolidation test and fully instrumented trial embankment by using the axisymmetric and plane-strain models. A systematic back calculation procedure was embedded in the numerical code to conduct the parametric study and back calculate the properties of the smear zone for a given set of consolidation results obtained from laboratory or field measurements.

The Modified Cam-Clay (MCC) model was used to simulate the behaviour of soft clay during the process of PVD assisted preloading. The smear zone was simulated by applying the mechanical properties of undisturbed soil with a reduced coefficient of permeability. The sub-routines were written using the built-in programming language *FISH* (*FLACish*) to tailor the analyses to suit the specific needs of the parametric study and by giving the following unique advantages to the developed codes for this study:

(i) Automatic mesh generation by entering the parameters needed to modify the grid pattern inside and outside the smear zone,
(ii) Considering variations in permeability with the void ratio during consolidation,
(iii) Ability to change different parameters such as the dimensions of the model, the properties of the vertical drain, the profile of the subsoil, characteristics of the smear zone, and the preloading conditions,
(iv) Integrated permeability axisymmetric to equivalent plane-strain permeability conversion,
(v) The option to define the exact location of the desired points to generate and plot any future history graphs,
(vi) Automatic solving process based on the modified input data, and

(vii) The option to adjust the number of mechanical and flow steps to optimise the analyses and minimise the numerical calculation issues.

The solid body is divided into a finite difference mesh composed of quadrilateral elements as described in Figure 3.2. A sample of the generated numerical mesh pattern using the developed code is illustrated in Figure 3.5.

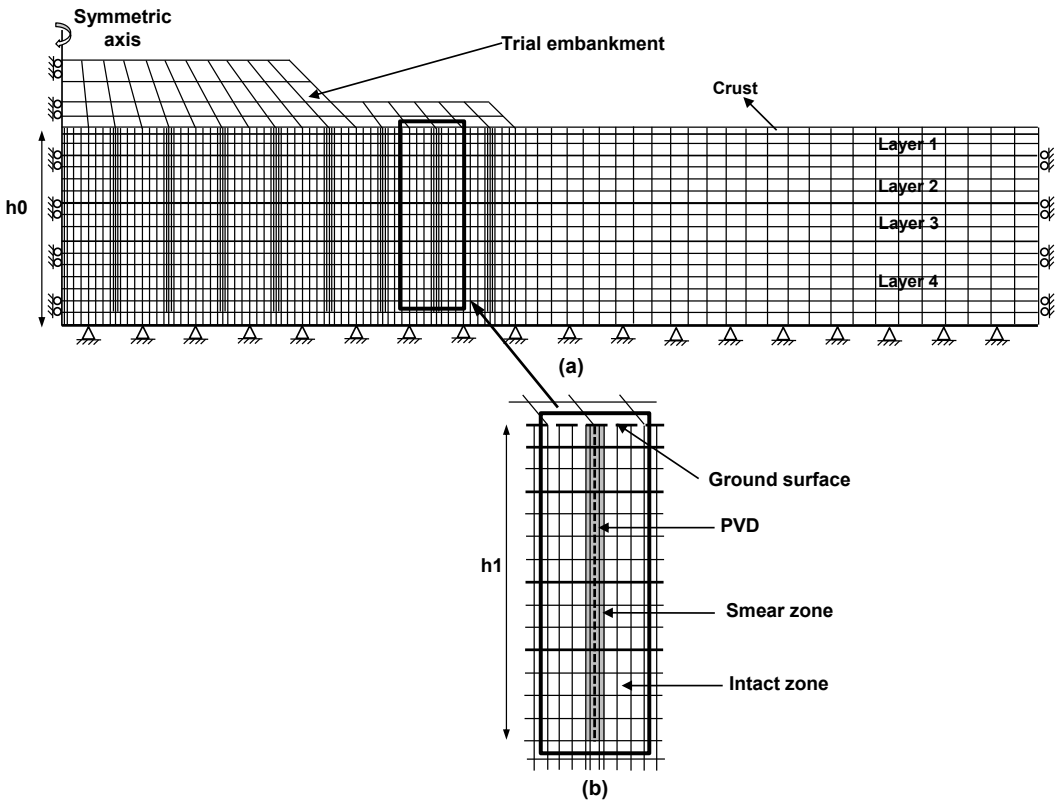

Figure 3.5 Generated FLAC mesh, (a) sample of discretised finite-difference mesh of trial embankment, and (b) the pattern of meshes in the smear zone and undisturbed region

3.3.2 Numerical Code Structure

The structure of the developed numerical code is explained in this section. It was implemented into the back calculation procedure to predict reliable smear zone properties. A schematic diagram of the code's structure is illustrated in Figure 3.6.

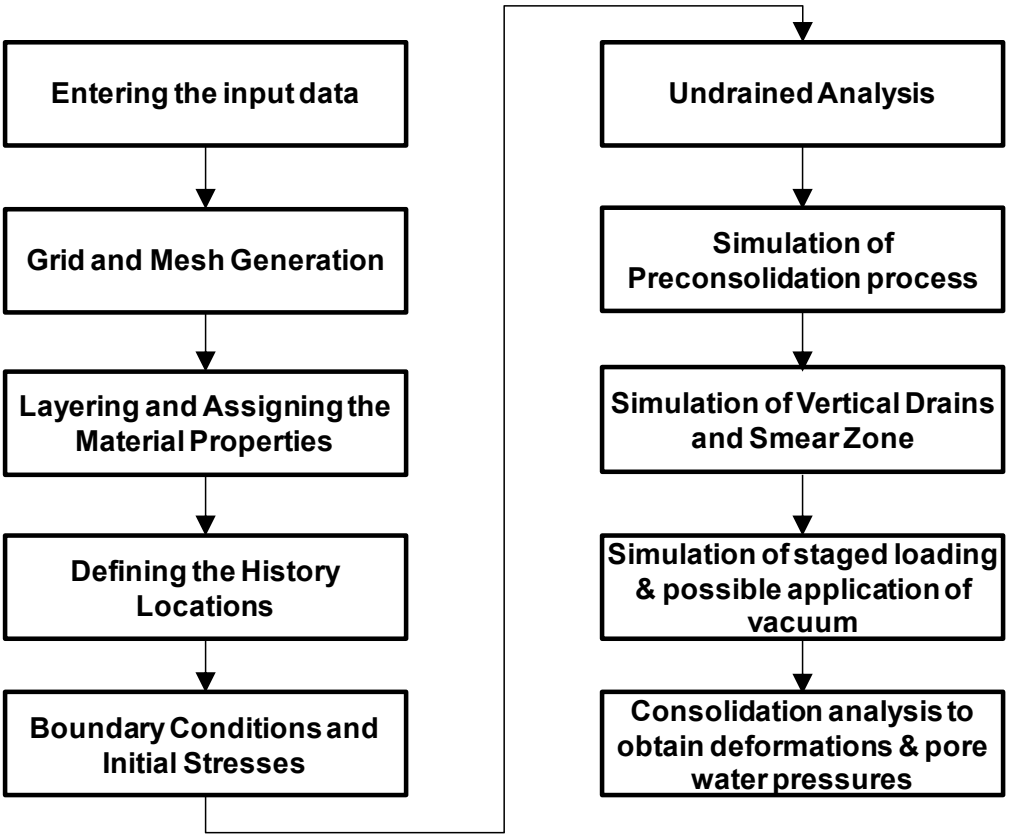

Figure 3.6 Structure of the developed numerical code

3.3.2.1 Input data: Geometry and properties of the Materials

The first section of the code was developed to enter the parameters needed for numerical modelling, such as the model geometry, PVD properties, and mesh generation parameters. A *FISH* sub-routine was embedded in the developed code to automatically convert the coefficient of permeability from axisymmetric to plane-strain condition using the conversion equations proposed by Indraratna et al. (2005a).

FLAC code can adopt the strain-dependent permeability using the "per_table" keyword (Itasca, 2008). A table can be created to provide permeability values as a function of accumulated volume strain. It should be noted that sufficient scope must be provided in the table so that all possible volume excursions are anticipated. Since changes in the permeability affect the critical timestep and element matrices, a recalculation of these quantities is done if the table is active, but only at every tenth step. Recalculating the quantities of groundwater increases the solution

time. The parameters applied in the numerical code are illustrated in Figure 3.7. A sample of the developed code for this part is indicated in Appendix A (Section A-1).

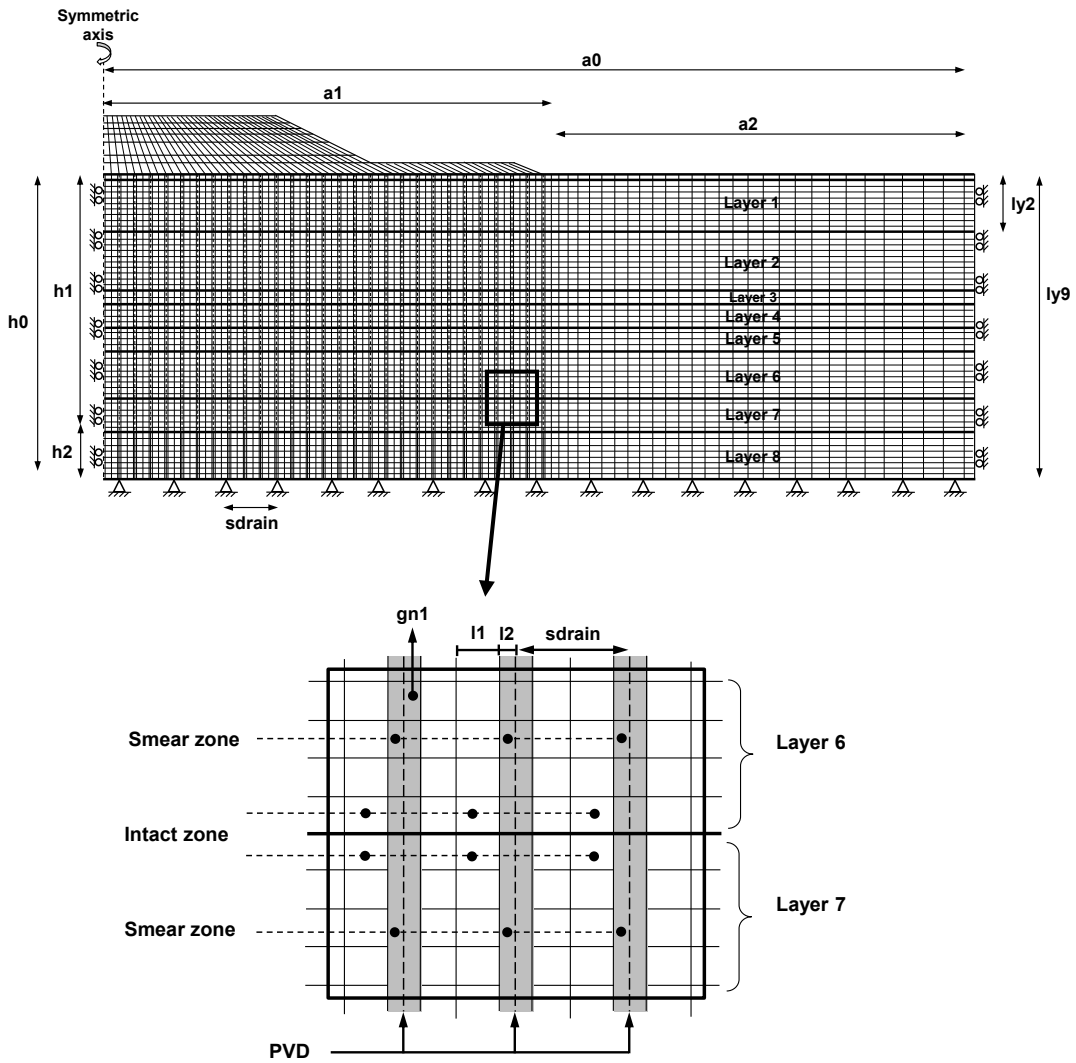

Figure 3.7 Typical input parameters for numerical simulation

It should be mentioned that a specific spreadsheet was designed to calculate the reference pressure and corresponding specific volume by considering the pre-consolidation pressures at each depth and the initial void ratios. The loading and reloading curves in Figure 3.3 were referred to when conducting the calculations.

3.3.2.2 Grid and Mesh Generation

This section of the code was developed to conduct the automatic process of generating the grid and mesh for the numerical model by considering the dimensions of the model, length of the PVD, radius of the mandrel, the extent ratio (r_s/r_m), the number of mesh zones inside the smear zone, the length ratio (l_1/l_2), the length of the vertical zones, and the drain spacing. For this purpose, the following stages were followed:

- Calculation of the number of zones needed in the horizontal direction
- Calculation of the number of zones needed in the vertical direction
- Grid and mesh generation of the soil profile
- Grid and mesh generation of the trial embankment

A sample of the generated mesh is illustrated in Figure 3.6 and the developed code for this section is presented in Appendix A (Section A-2).

3.3.2.3 Layering and Assigning Material Properties

In this part the layers of soil and the stages of constructing a trial embankment were categorised in different groups and input soil properties were assigned to each of them (Figure 3.8). The trial embankment stages were deactivated to generate the initial stress condition in the soils. The corresponding developed code for this purpose is presented in Appendix A (Section A-3).

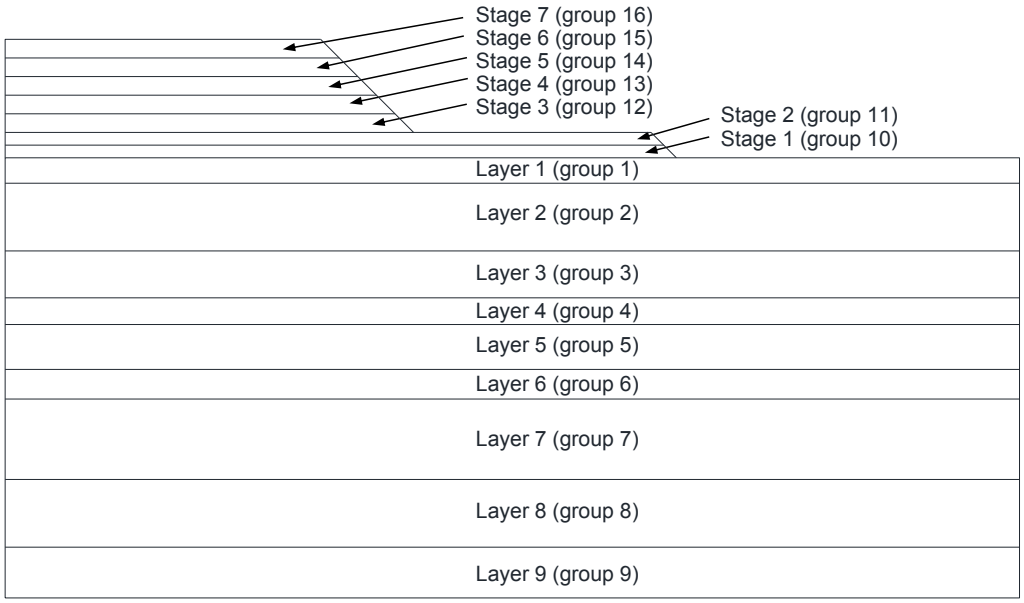

Figure 3.8 Input parameters in terms of different groups for numerical simulation

3.3.2.4 Defining the location of instrumentations and transducers

The developed code has an option to predefine any grid point or zone to record changes in the required variables such as vertical displacement and pore water pressure as time-stepping proceeds. A summary of the requested histories may be plotted at any time. Variables can be plotted versus step number or versus other histories. An example of the developed code is reported in Appendix A (Section A-4), where some grid points were defined to record the changes in vertical displacement and pore water pressure during consolidation.

3.3.2.5 Boundary Conditions, Initial Stresses, and Undrained Analysis

A sub-routine was developed to define the boundary conditions, generate the initial stresses in the soil profile, and conduct the undrained analysis to obtain the initial equilibrium stress condition. The boundary conditions are shown in Figure 3.9.

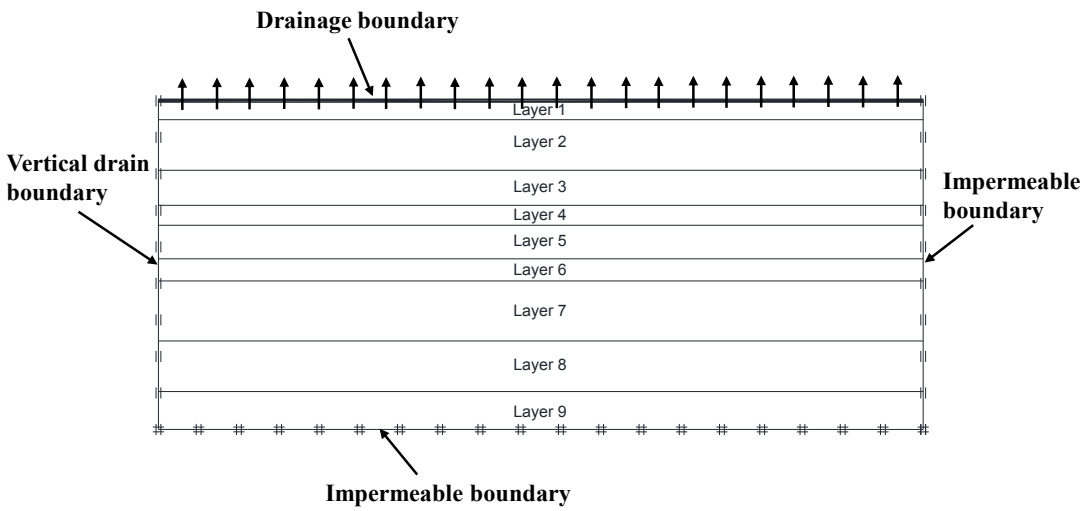

Figure 3.9 Boundary conditions of the numerical model

The displacement of soil at the bottom boundary was fixed in all directions and the side boundaries are vertical rollers, which allowed for vertical displacement. The drainage boundary is at the ground surface and the bottom and side boundaries are impermeable. A specific *FISH* function (ininv.fis) was used to automatically compute the initial condition for the horizontally layered soil profile by using the depth of the ground water table and lateral pressure coefficients as the input data. Finally, an undrained analysis was conducted to obtain the initial state of equilibrium. The code developed for this section is reported in Appendix A (Section A-5).

3.3.2.6 Simulation of Preconsolidation Stage

This section of the code was designed to conduct the preconsolidation process by activating the mesh of the trial embankment platform (drainage blanket) and assigning the Mohr-Coulomb model and corresponding soil properties. Figure 3.10 shows the schematic numerical model of this stage. The corresponding code developed for this purpose is presented in Appendix A (Section A-6).

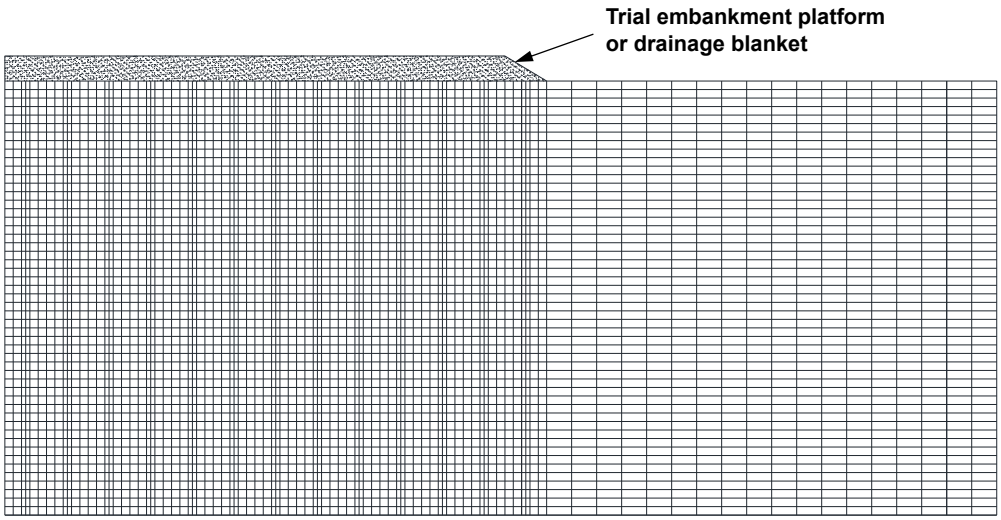

Figure 3.10 Schematic model for the preconsolidation stage

3.3.2.7 Vertical Drains and Smear Zone

Specific functions were implemented in the developed code to automatically model the vertical drains and smear zones. To simulate the vertical drains, the pore water pressure was fixed to hydrostatic pressure at every node along the grids of the vertical drain (i.e. zero excess pore water pressure). The smear zones were modelled by assigning reduced permeability values to them. Figure 3.11 shows a sample of the numerically simulated vertical drain and adjacent disturbed area. An example of the developed code is reported in Appendix A (Section A-7).

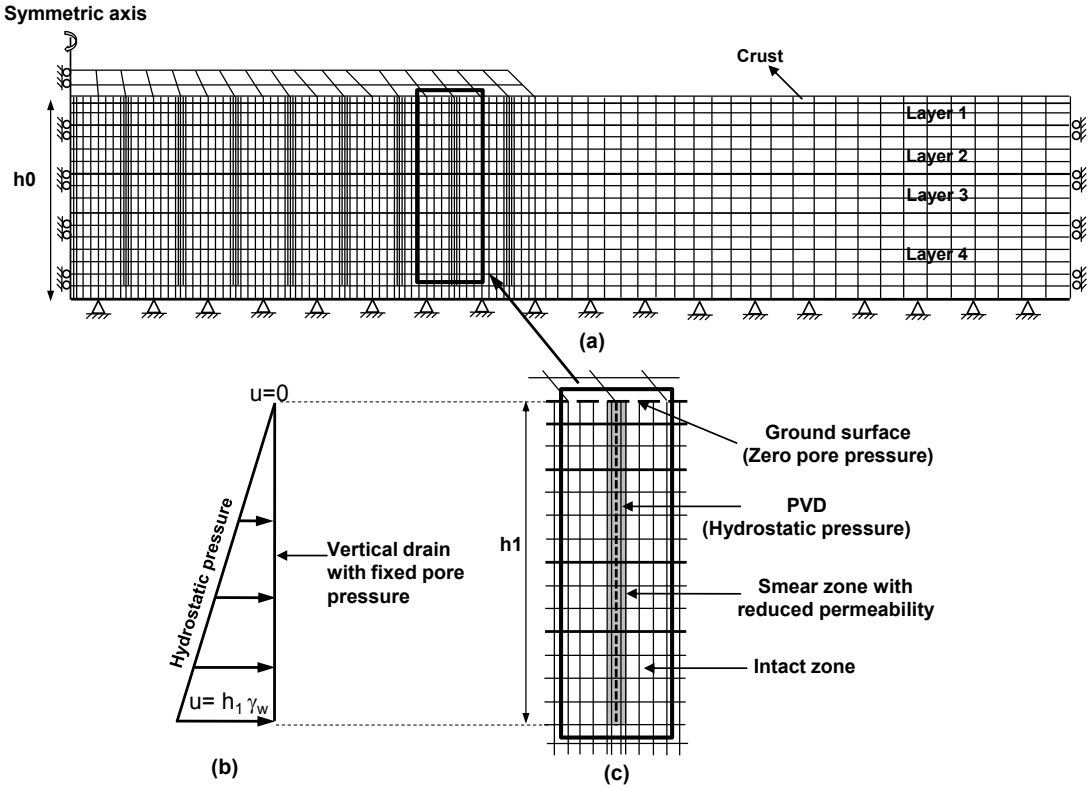

Figure 3.11 Sample of the simulated vertical drain and adjacent disturbed area, (a) Discretised finite-difference mesh of the trial embankment, (b) Variation of the hydrostatic pressure along the vertical drain and (c) the pattern of meshes in the smear zone and undisturbed region elements

3.3.2.8 Vacuum Pressure

In *FLAC 2D*, the vacuum pressure can be simulated by applying and fixing a negative pore water pressure along the vertical drain. The simulation of vacuum pressure is indicated in Figure 3.12. For this purpose a *FISH* function was developed, which is presented in Appendix A (Section A-8).

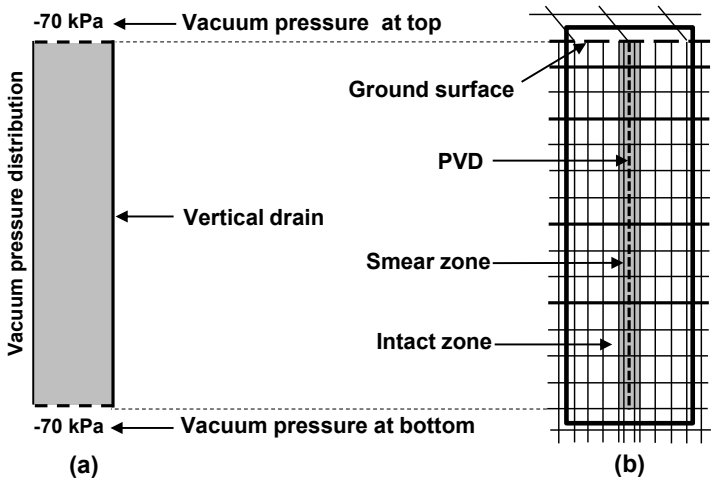

Figure 3.12 Simulation of vacuum pressure, (a) variation of vacuum pressure along the vertical drain and (b) the pattern of meshes in the smear zone and undisturbed region elements

3.3.2.9 Construction of Trial Embankment and Consolidation Process

The final section of the numerical code was developed to simulate the time history of constructing a trial embankment and conducting a consolidation analysis. The changes in the required variables can be plotted against the consolidation time at predefined gridpoints and zones after completing the numerical analyses. The developed code for this section is presented in Appendix A (Section A-9).

3.4 SYSTEMATIC BACK CALCULATION PROCEDURE

In this study, the construction of a trial embankment was introduced as a practical and reliable solution to predict the properties of the smear zone using the back calculation approach. For this purpose, a systematic back calculation procedure was designed and integrated with the developed numerical code to define the properties of the smear zone using the field measurements. Figure 3.13 presents a detailed flowchart, including the back calculation procedure used to find the characteristics of the smear zone that resulted in the best fit with the field measurements.

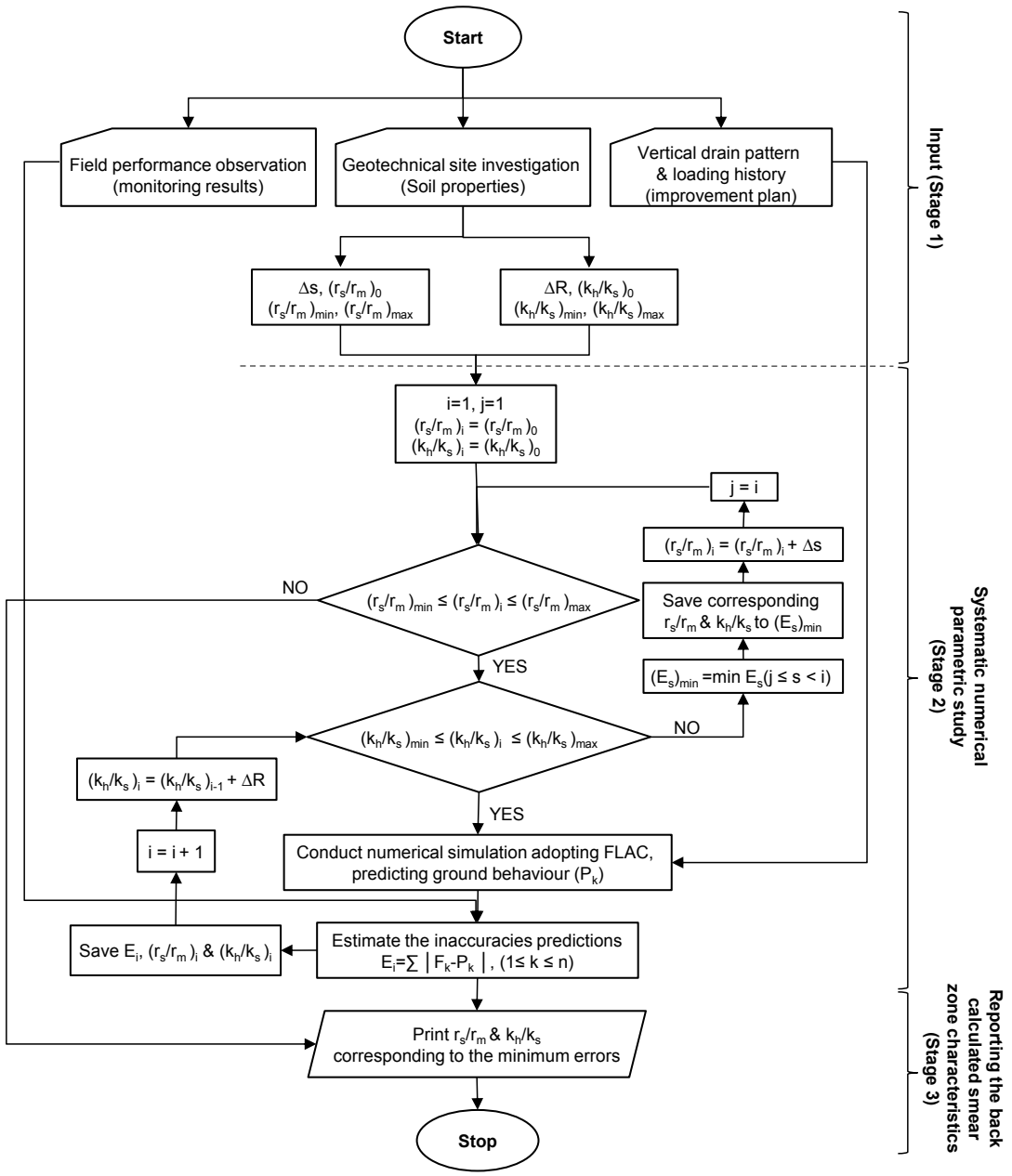

Figure 3.13 Back calculation flowchart for smear zone characteristics and the minimum required monitoring time for trial embankment

$(r_s/r_m)_0$	assumed initial extent ratio	ΔR	permeability ratio increment depending on the required accuracy
$(k_h/k_s)_0$	assumed initial permeability ratio	ΔS	extent ratio increment depending on the required accuracy
$(r_s/r_m)_{min}$	minimum extent ratio	E_i	error between numerical predictions and field measurements at step i
$(r_s/r_m)_{max}$	maximum extent ratio	$(E_{min})_s$	minimum error corresponding to step s
$(k_h/k_s)_{min}$	minimum permeability ratio	$(r_s/r_m)_s$	extent ratio corresponding to step s that gives the minimum error
$(k_h/k_s)_{max}$	maximum permeability ratio	$(k_h/k_s)_s$	permeability ratio corresponding to step s that gives the minimum error
$(r_s/r_m)_i$	extent ratio at step i	F_k	Field measurements
$(k_h/k_s)_i$	permeability ratio at step i	P_k	Numerical predictions

The proposed back calculation procedure had three stages as follows:

(i) Stage 1: Entering the input data, including the ground conditions, soil properties, details of installing the PVD, and the upper and lower bound values for the properties of the smear zone (r_s/r_m and k_h/k_s).

(ii) Stage 2: Conducting a numerical analysis varying r_s/r_m and k_h/k_s in the given range to predict the ground behaviour, determine the corresponding settlement curves, and calculate the error that accumulated between the numerical results and field measurements at every degree of consolidation.

(iii) Stage 3: Analysing the outcomes of the second stage to define the optimum combination of r_s/r_m and k_h/k_s that gave the best predicted settlement curve, and which is in best agreement with the field measurements.

As illustrated in the flowchart of Figure 3.13, the approach began with collecting the input data, including the soil properties, the PVD assisted preloading specifications (PVD pattern and loading history), and field monitoring results (settlement and excess pore water pressure variations). The first stage was completed by defining the initial values, the minimum and maximum values, and the incremental rates for the extent and permeability ratios. In the second stage, a systematic parametric study was designed to back calculate and predict the properties of the smear zone as follows:

- Defining an external loop to vary the extent ratio (r_s/r_m),

- Defining an internal loop for each step of the external loop to change the permeability ratio (k_h/k_s),

- Implementing the developed *FLAC* code in each step of the internal loop to conduct a numerical simulation using the properties of the smear zone and input data,

- Completing each step of the internal loop by calculating the computational error, and comparing the numerical predictions and field monitoring results,

- Stopping the internal loop once the permeability ratio (k_h/k_s) was out of range, and saving the extent and permeability of the smear zone that corresponded to the minimum error, and

- Continuing the procedure in Stage 2 as long as the extent ratio (r_s/r_m) was in the defined range.

Stage two stopped as soon as the extent ratio was out of the input range. The last stage of the flowchart shown in Figure 3.13 was to report the back calculated pairs of the extent and permeability of the smear zone that corresponded to the minimum errors. It should be mentioned that in Stages 2 and 3, the *FLAC* output was linked to a visual basic code to calculate the error and report the results.

The normalised error between the numerical prediction and field measurement in every step of the consolidation process was calculated using the following equation:

$$(E_i)_n = \frac{(S_t)_i - (S_{tp})_i}{S_f} \tag{3.50}$$

where, $(E_i)_n$ is the normalised error at time t and step number n, S_t is the field settlement at time t, S_{tp} is the predicted settlement at time t, and S_f is the final primary consolidation settlement.

The predicted errors in stage 3 were used to calculate cumulative error for each case at every step of the consolidation process using the following equation:

$$(E_t)_n = \sum_{i=1}^{n} \frac{(S_t)_i - (S_{tp})_i}{N \times S_f} \tag{3.51}$$

where, $(E_t)_n$ is the normalised cumulative error at time t and step number n, and N is the total number of steps. The most accurate smear zone properties belong to the case with the minimum amount of cumulative error.

3.5 SUMMARY

In this chapter, a systematic procedure was proposed to back calculate the properties of the smear zone using the consolidation data measured in the laboratory and the field. A numerical approach was employed to simulate layered soft clay improved by PVD, using the proposed back calculation procedure. The explicit finite difference program *FLAC 2D* was used to develop the numerical code. The explicit scheme could incorporate the large deformations that soft soil may experience. The built-in programming language *FISH* (*FLACish*) was used to write the sub-routines and tailor the analyses to suit specific needs. The governing differential equations corresponding to FLAC's numerical implementation and the numerical formulation of the coupled fluid-deformation mechanisms in *FLAC 2D* (which is based on the Biot theory of consolidation) was also discussed.

The methods existing in *FLAC 2D* for optimising the mechanical and fluid time steps was described in order to keep the system in an equilibrium condition. Two criteria were used to determine the optimum combination of fluid and mechanical steps, (i) the unbalanced force ratio (sratio) falls below the defined values (0.001 or 0.01), and (ii) the numerical analyses was conducted in a minimum period of time.

The Modified Cam-Clay (MCC) theory, developed based on an incremental hardening/softening elasto-plastic model, was used as the soil constitutive model in the numerical simulations. The MCC model relates the specific volume (v) to $\ln p'$ with a straight virgin consolidation line as the soft soil sample was slowly compressed under the isotropic stress and perfectly drained conditions.

The structure of the developed code was explained and included, (i) the data entering process, (ii) generation of the grid and mesh, (iii) layering and assigning material properties, (iv) applying the boundary conditions and initial stresses, (v) simulation of the pre-consolidation process, (vi) simulation of the vertical drain,

smear zone, and vacuum pressure and (vii) construction of a trial embankment and the process of consolidation.

Finally, a diagram of the systematic back calculation procedure was described (Figure 3.13). It was combined with the *FLAC* code, developed to reliably predict the properties of the smear zone. A parametric study scheme was implemented into the procedure proposed in Figure 3.13, using different combinations of smear zone properties to predict the total cumulative error between the numerical results and field measurements for each case. The extent and permeability of the smear zone for the case with the minimum total cumulative error can be reported as the optimum combination, which could be used by practicing engineers.

CHAPTER FOUR

4 LABORATORY STUDY TO INVESTIGATE THE SMEARING EFFECT ON THE PERFORMANCE OF PVD ASSISTED PRELOADING

4.1 GENERAL

In recent years a number of experimental studies were carried out to investigate the formation of a disturbed zone near the vertical drains resulting from installing a mandrel (e.g. Bergado et al., 1991; Indraratna and Redana, 1998; Sharma and Xiao, 2000; Sathanantha and Indraratna, 2006; Shin et al., 2009; Ghandeharioon et al., 2012). However, because the parameters of the smear zone vary due to mandrel insertion, using the experimental results to evaluate the accuracy of the analytical and numerical solutions is very difficult.

In this study an array of laboratory tests were conducted using a large, fully instrumented Rowe cell apparatus (250mm diameter by 200mm high) to investigate how the reduced permeability surrounding the drain affects consolidation, and verify the numerical procedure developed to back calculate the properties of the smear zone. The disturbed/smear soil near the vertical drain was simulated using clay with a reduced permeability and a compacted sand pile covered with flexible porous geotextile that was installed in the centre to act as a vertical drain. The dissipation of pore pressure was captured during consolidation using transducers installed at various distances away from the vertical drain. At the same time the surface settlement was measured using a vertical settlement transducer connected to a data logger. Finally, the laboratory test results were used to verify the numerical procedure developed to back calculate the permeability of the smear zone, and the formulations available for converting the axisymmetric condition to a plane-strain condition were evaluated by comparing the numerical results with the experimental measurements.

4.2 TESTING APPARATUS AND EXPERIMENTAL PROCEDURE

4.2.1 Apparatus

The large scale Rowe cell used in this study consists of the body, the base, and the top. The internal diameter is 250 mm and the height is 200 mm (Figure 4.1a). The base and the cover are bolted to flanges on the body in nine locations. An 'O' ring seals the base, and a rubber loading jack and another 'O' ring seal the top part.

A uniform load was applied to the sample by water pressure acting on a convoluted rubber jack made from rubber. Vertical settlement was measured at the centre of the sample where it connected to a spindle that is attached to the jack and passes through the cover of the cell using an LVDT (Linear Variable Differential Transformer). The spindle is sealed through the centre of the rubber diaphragm on the jack by two washers to eliminate any error in the settlement readings due to the rubber diaphragm compressing under pressure. Nine pore water pressure transducers (PWPTs) were installed in various distances and depths to capture the changes in pore water pressure during consolidation (Figure 4.1a and 4.1b). All the transducers are connected to a PC based data logger to continuously measure and record the test data.

The Rowe cell was designed to have a single drainage system from the top through a perforated brass disc situated between the sample and the jacket. The drainage outlet is via the centre of the settlement spindle and a short flexible tube leading to a Klinger valve at the edge and on top of the cell (Figure 4.1a).

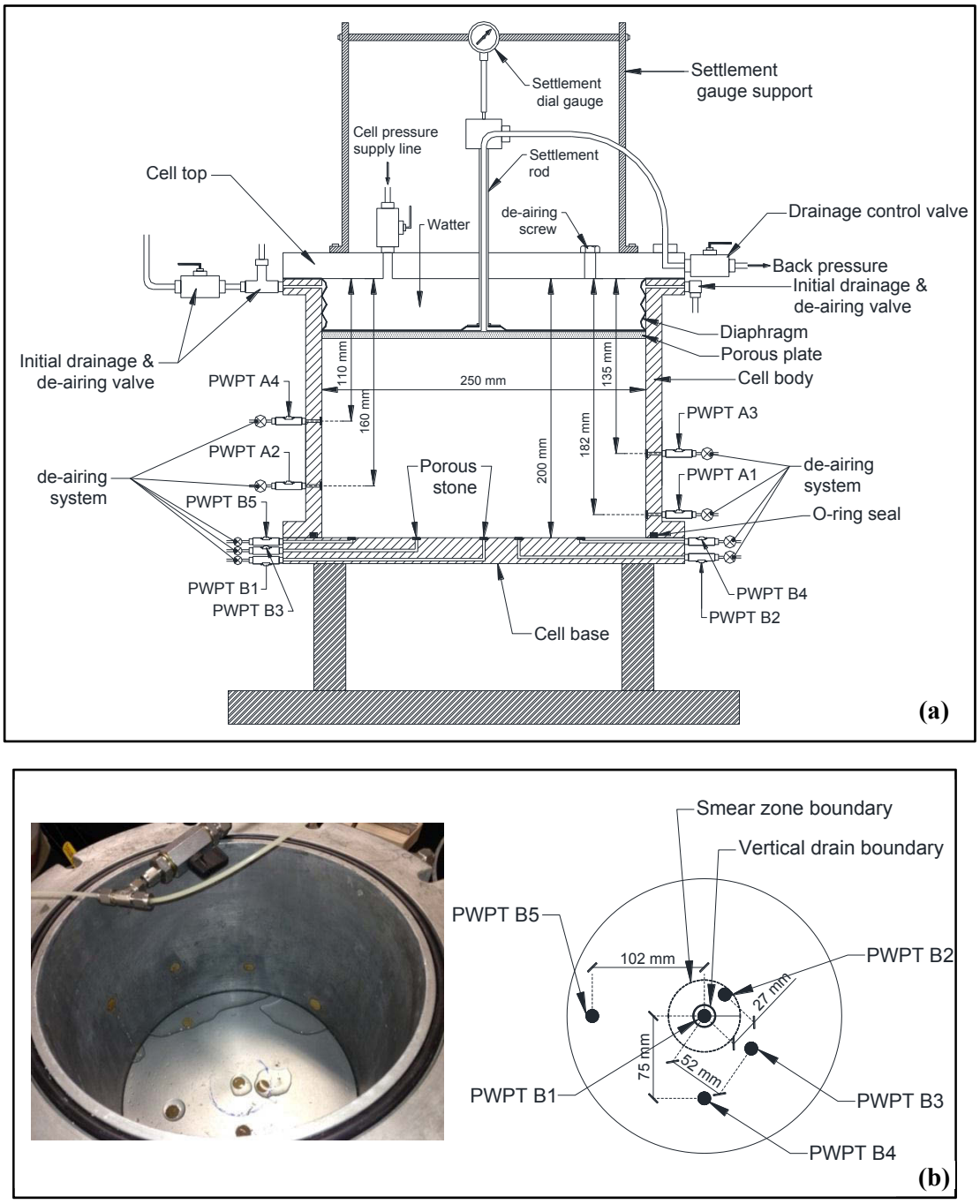

Figure 4.1 Large scale Rowe cell apparatus (a) schematic diagram of the cell and (b) locations of the pore pressure transducers at the base of the cell

Pressure is applied to the cell, and back pressure to the jacket from a series of pressure lines connected to the enterprise level pressure/volume controllers (ELDPC) that are filled with de-aired water. The de-aired water in the ELDPC cylinder is pressurised and displaced by a piston moving in the cylinder. The piston is actuated

by a ball screw that rotates in a ball nut held by an electric motor and gearbox that move rectilinearly on a ball slide. The ELDPC instrument and its operational schematic are illustrated in Figures 4.2a and 4.2b. The applied ELDPC had a volumetric capacity (nominal) of 200cc for a pressure range of 1MPa. The resolution of the measurements for pressure and volume were 1kPa and 1 mm^3, respectively. The pressure and volume measurements were accurate to 0.25% of the full range and 0.4% of the measured value with +/- 500mm^3 back lash, respectively.

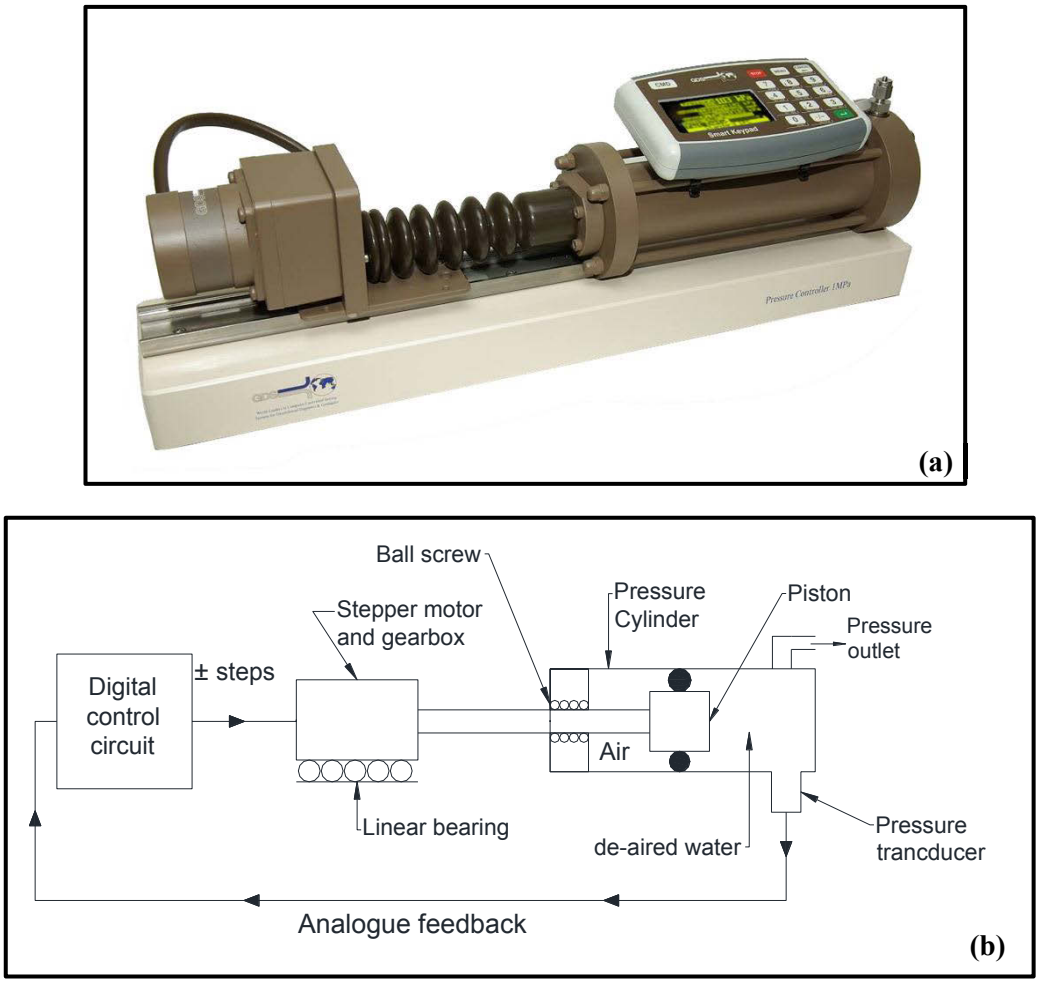

Figure 4.2 Pressure/volume controller device, (a) a photographic view of the GDS controller and (b) an operational schematic diagram of the instrument (http://gdsinstruments.com)

The pressure was measured by an integral solid state transducer. Control algorithms were built into the on-board micro-controller to enable the controller to seek a target pressure or step to a target volume change. The change in volume was measured by

counting the steps of the incremental motor. The instrument was controlled via PC based software.

When a single pressure/volume controller is used, , it will need to manually fill or empty the controller once the volumetric capacity of the barrel has reached either 100% full or 100% empty. To fix this problem in this study, 2 parallel pressure/volume controllers (primary and secondary) connected to an infinite volume controller (IVC) device (Figure 4.3) were used for each pressure line. The IVC was designed to remove constraints from the volume such that in a test, fluid can flow continuously under pressure control or volume control. The IVC system automatically switches between the two controllers when one runs out of volume.

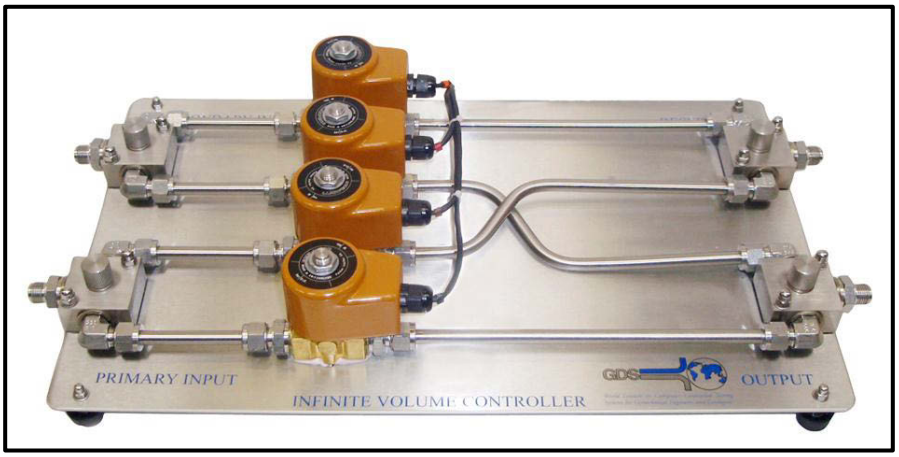

Figure 4.3 Infinite volume controller instrument (http://gdsinstruments.com)

One controller was called the primary controller and it was used to provide a pressure source, while the other was called the 'master' controller and it acted as the pressure source (is this correct?). At the same time the secondary 'slave' controller can refill and centre itself and become ready for switching when the master controller exceeds its volumetric limit. When this happens the secondary controller takes over by providing the pressure and thus becomes the master. The primary controller becomes the slave and hence can refill/empty and centralise itself. When this is complete, the primary controller resumes pressure control and becomes the master again and the secondary controller centralises itself.

The secondary pressure controller is only temporarily used as the master (to provide pressure or a change in volume) when the primary controller exceeds

its volume capacity and thus needs to refill/empty and centralise itself. The IVC valve panel comes complete with 4 channel IVC control boxes that are connect the IVC valve panel to the computer. GDS software controls the system and collects the data from data loggers in every stage of loading. The de-aired water needed, is provided through an elevated water reservoir. A schematic diagram of the experimental set up is shown in Figure 4.4. Figure 4.5 shows the set up established in the laboratory.

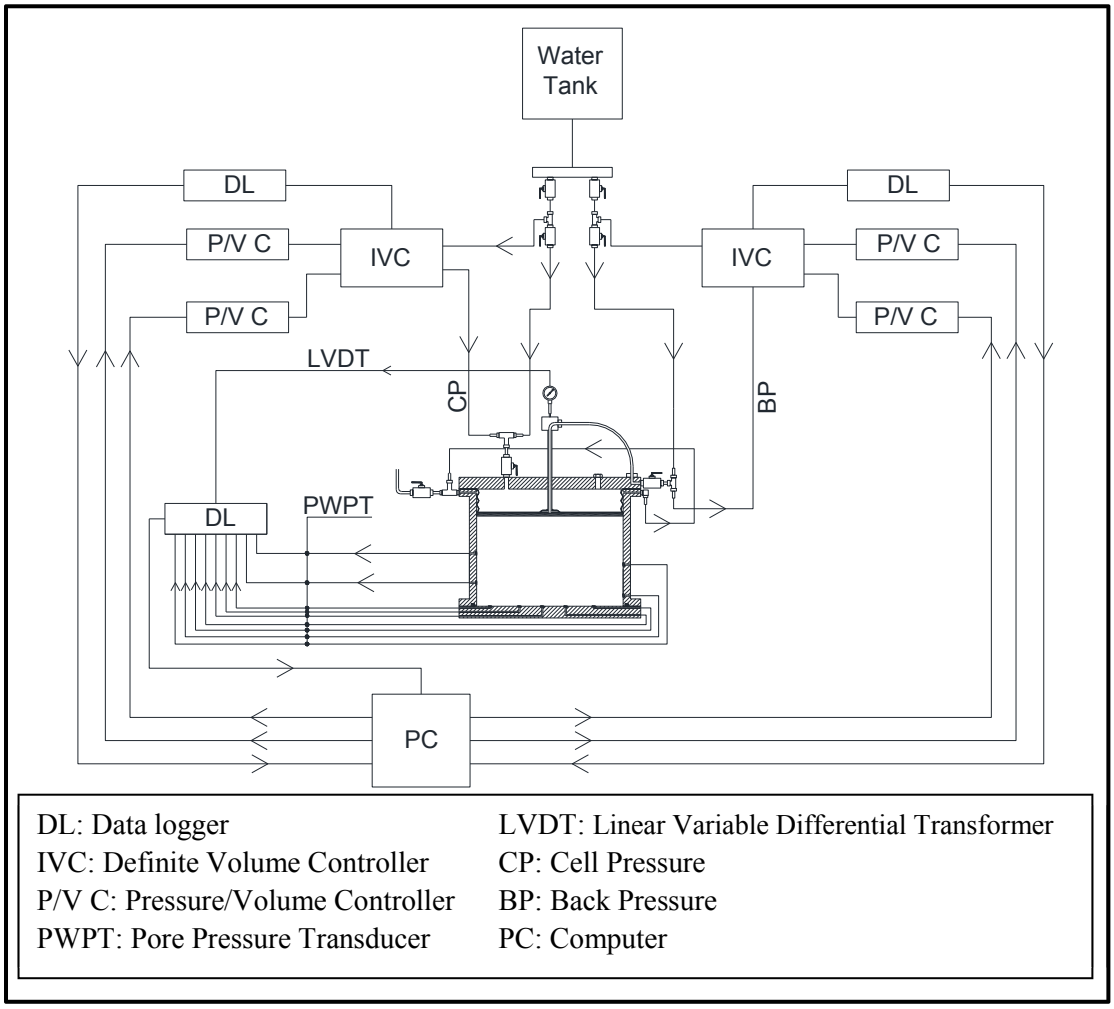

Figure 4.4 Schematic diagram of Rowe cell set-up

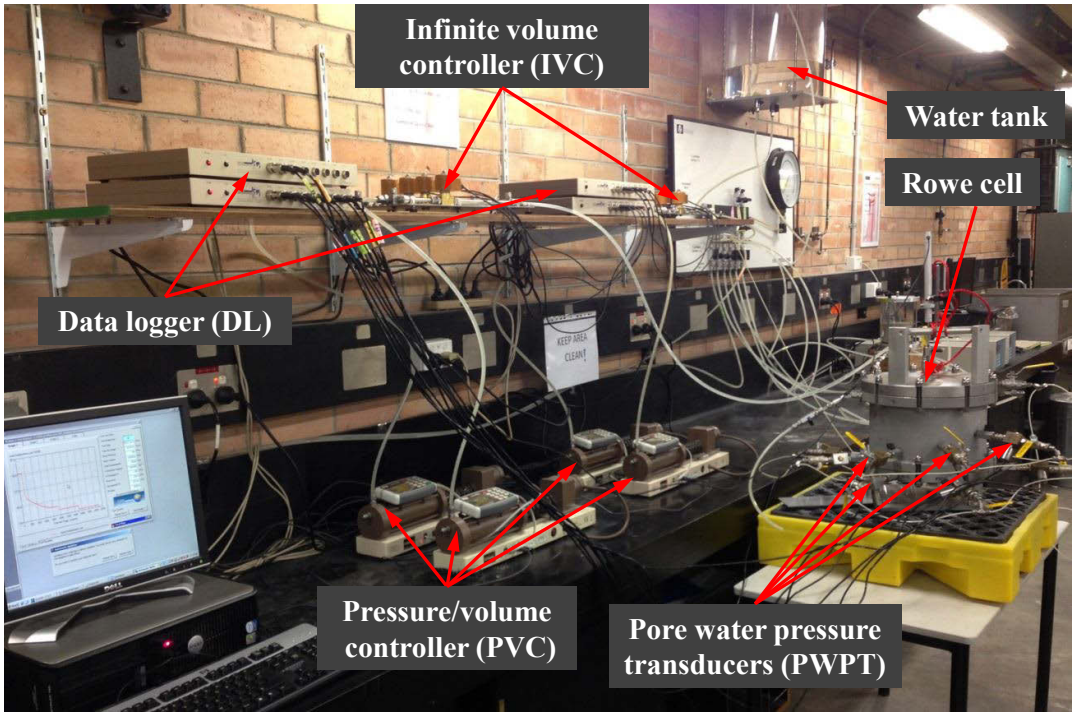

Figure 4.5 Established setup in the laboratory

4.2.2 Material Properties

4.2.2.1 Soil samples

To select soils for the Rowe cell test with a reduced horizontal permeability for the smear zone and the undisturbed region, a number of reconstituted clay samples were prepared by mixing the following materials:

- Q38 kaolinite
- ActiveBond23 bentonite
- Fine sand

Kaolinite and bentonite were selected because they are common artificial clays with significantly different properties. The kaolinite samples had an average liquid limit of 50% compared to 340% for the bentonite samples. The kaolinite and bentonite samples indicated 9% and 35%, respectively as their shrinkage limits, when

measured according to AS 1289.3.4.1. Table 4.1 summarises the properties of the clay samples used in this study.

Table 4.1 Properties of the adopted soil samples in this study

Soil Type	Liquid Limit (%)	Plastic Limit (%)	Linear Shrinkage (%)	USCS
Q38 kaolinite	49.5	27.5	9	CL
ActiveBond23 Bentonite	340	50	35	CH

According to Nelson and Miller's (1997) sorting, the kaolinite and bentonite clays have had medium and very high expansion/shrinkage potentials, respectively. ActiveBond 23 is a pure form of bentonite which is plastic and impermeable, and has a high absorbing and swelling capacity, as well as being highly viscous when suspended in water. Common uses of bentonite include constructing the diaphragm wall, piling, tunnelling, and sealing the dam and containing waste. The high swelling properties of bentonite on exposure to water facilitate sealing porous soils and leaking dams. Q38 kaolinite clay is a dry milled creamy white kaolin China clay. Kaolinite is one of the most abundant minerals in soil, and as such is often encountered in on-site conditions. Kaolinite is formed by the breakdown of feldspar, which is induced by water and carbon dioxide, and is often formed by the alteration of aluminium silicate minerals in a warm and humid environment (Craig, 2000; Murray, 1999). Uniformly graded sand (SP) was used for two purposes: (i) to achieve the target permeability of the soil mixture, and (ii) represent the drain material. The grain size distribution curve of the applied sand is illustrated in Figure 4.6, and some important sizes are shown in Table 4.2.

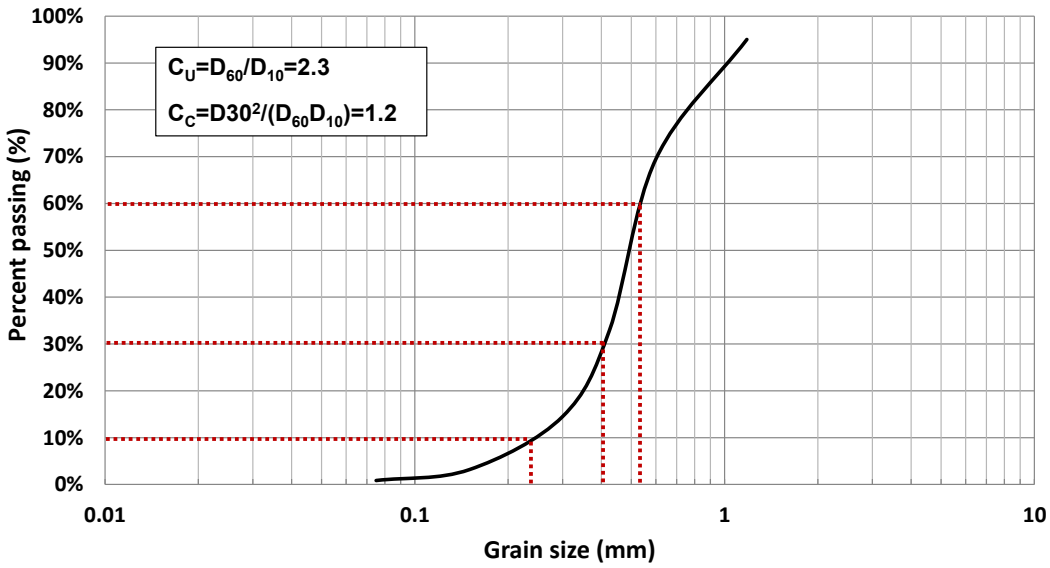

Figure 4.6 Grain size distribution curve for vertical drain sand

Table 4.2 Important sizes

Symbol	Grain size (mm)
D_{10}	0.24
D_{30}	0.4
D_{60}	0.55

Note: D_{10} is the effective particle size (the grain diameter at 10% passing), D_{30} is the grain diameter at 30% passing, and D_{60} is the grain diameter at 60% passing

Table 4.3 shows the mixed design of the samples. The Australian Standard (AS 1289.3.5.2) was used to determine the plastic limit (PL) and liquid limit (LL) of the mixtures, which are illustrated in Table 4.4. The specimens were thoroughly mixed with a water content that was 1.4-1.8 times the liquid limit (LL) and kept in a closed container for couple of days to ensure full saturation and homogeneity. The properties of the reconstituted clay samples are shown in Table 4.4.

Table 4.3 Mix design for the reconstituted samples

Soil Reference Number	Q38 Kaolinite (%)	ActiveBond 23 Bentonite (%)	Fine sand (%)
S1	70	15	15
S2	68	17	15
S3	65	20	15

Table 4.4 Properties of the reconstituted samples

Soil Reference Number	S1	S2	S3
Water Content, w (%)	120	120	120
Liquid Limit, LL (%)	67	70	87
Plastic Limit, PL (%)	27	29	34
Plasticity Index, PI	40	41	43

4.2.2.2 Consolidation test on reconstituted samples

Materials for the disturbed/smear zone and the intact area have been selected from the reconstituted samples after a number of oedometer tests were conducted. Samples were subjected to a pre-consolidation pressure of 20 kPa before the consolidation test was carried out. For this purpose, three cylinders were filled with the reconstituted samples (Table 4.3) and submerged in buckets of water to maintain their saturation condition. The pre-consolidation process is shown in Figure 4.7. Once pre-consolidation was completed, samples were taken from the soils using the oedometer ring (Figure 4.8).

(a) **(b)**

Figure 4.7 Pre-consolidation process prior to the oedometer test; (a) cylinder contacting reconstituted sample and (b) samples under pre-consolidation pressure

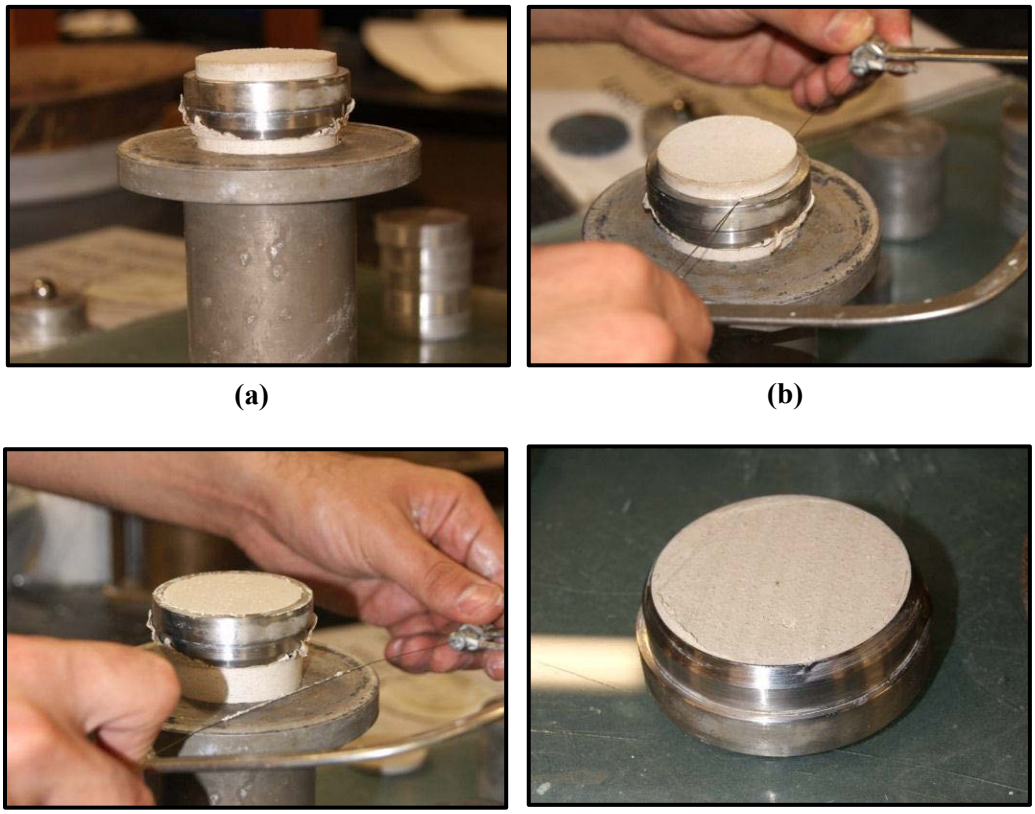

(a) **(b)**

(c) **(d)**

Figure 4.8 Preparing the samples for the oedometer test, (a) placing the oedometer ring, (b) cutting the extra top part, (c) cutting the extra bottom part, and (d) the final sample

A conventional oedometer test was conducted based on the Australian Standard (AS 1289.6.6.1) to determine the coefficient of permeability for each sample by applying five stages of loading, including: 12.5 kPa, 25 kPa, 50 kPa, 100 kPa, and 200 kPa (Figure 4.9). The soil samples were 20 mm thick by 50 mm in diameter, respectively.

The settlement and pore water pressure data were collected continuously for 24 hours for each load increment using a data logger.

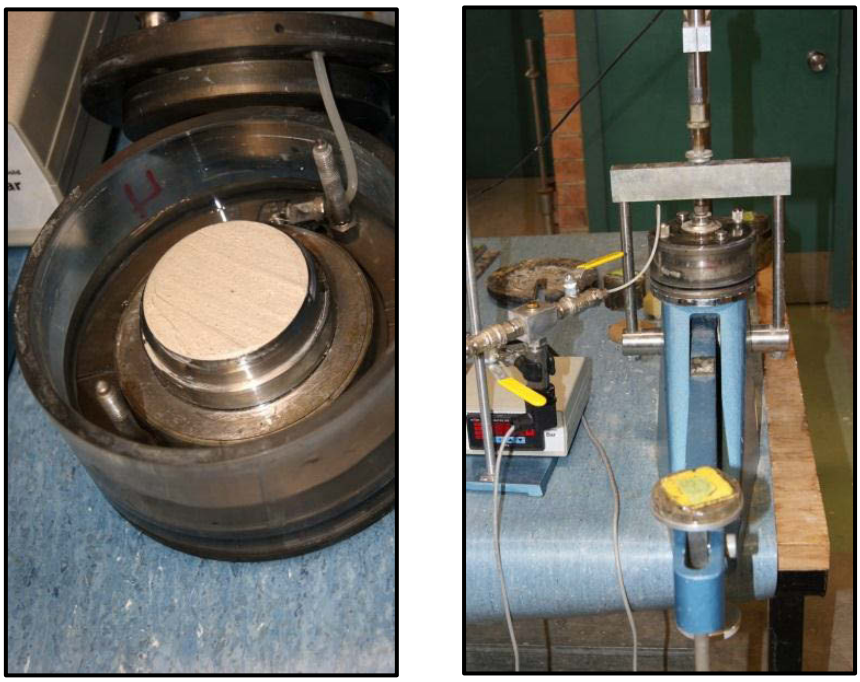

(a) **(b)**

Figure 4.9 Consolidation test, (a) placing the prepared sample and (b) oedometer apparatus connected to the data logger

The data collected from the oedometer tests were analysed to obtain the consolidation parameters of the reconstituted samples. According to Taylor (1948), the variation of permeability (k) with void ratio (e) for the clays can be determined using the following equation:

$$\log k = \log k_0 - \frac{e_0 - e}{c_k} \tag{4.1}$$

where, c_k is the permeability change index, k_0 and e_0 are the initial coefficient of permeability and the void ratio, respectively. The consolidation results indicated that the permeability change indices (c_k) for the reconstituted samples S1 and S3 were 0.3 and 0.72, respectively. The variations of permeability against the void ratio, for both samples, are shown in Figures 4.10 and 4.11. Table 4.5 shows the permeability of the samples under a surcharge of 20 kPa, which is simulating 1m of working platform installed before ground improvement.

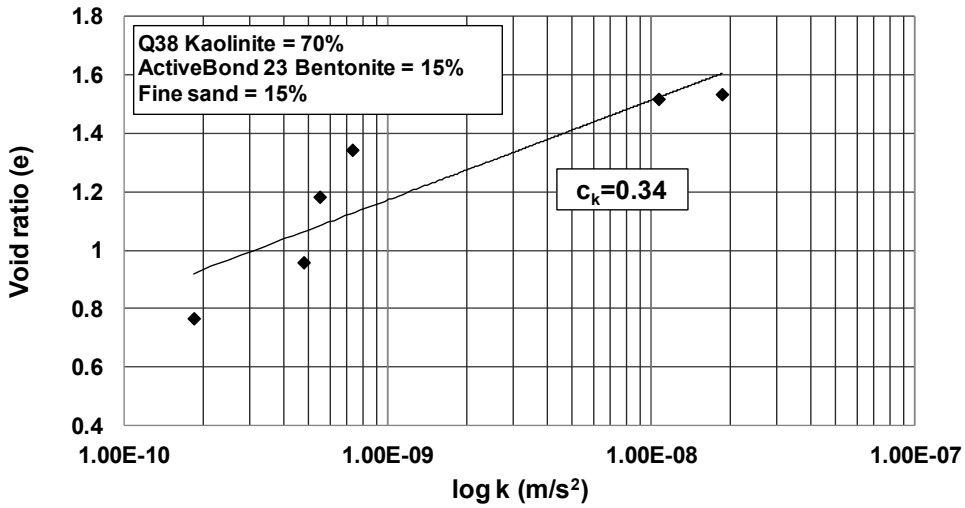

Figure 4.10 Variation of permeability against void ratio (sample S1)

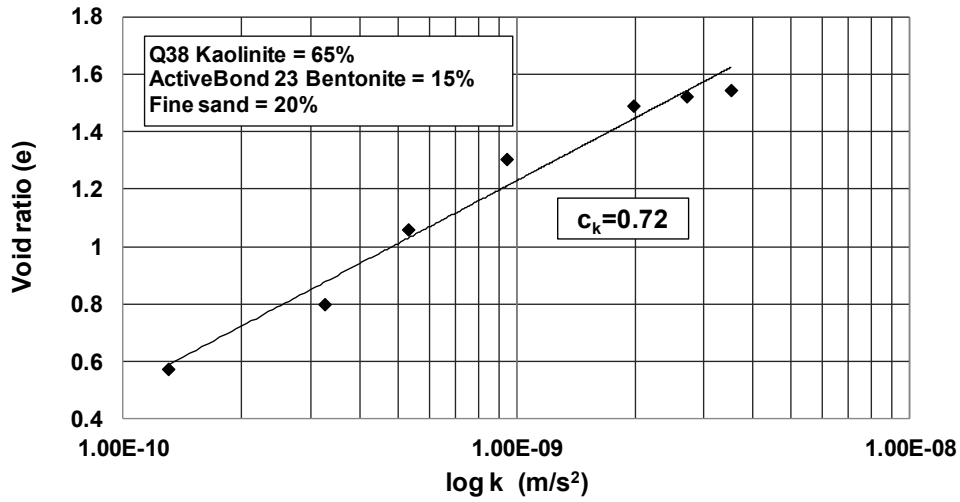

Figure 4.11 Variation of permeability against void ratio (sample S3)

Table 4.5 Permeability of mixtures (Surcharge = 20 kPa)

Soil reference number	S1	S2	S3
Permeability (m/s^2)	$1.060E10^{-8}$	$7.446E10^{-9}$	$2.710E10^{-9}$

In this research the permeability ratio (k_h/k_s) of 4 and an extent ratio (r_s/r_w) of 3 were used to conduct the consolidation test assisted with a vertical drain. Samples S1 and S3 were chosen as the soils for the intact and smear zones, respectively, to meet the permeability ratio criteria. The variations of void ratio versus effective stress for samples S1 and S3 are plotted in Figures 4.12 and 4.13, respectively.

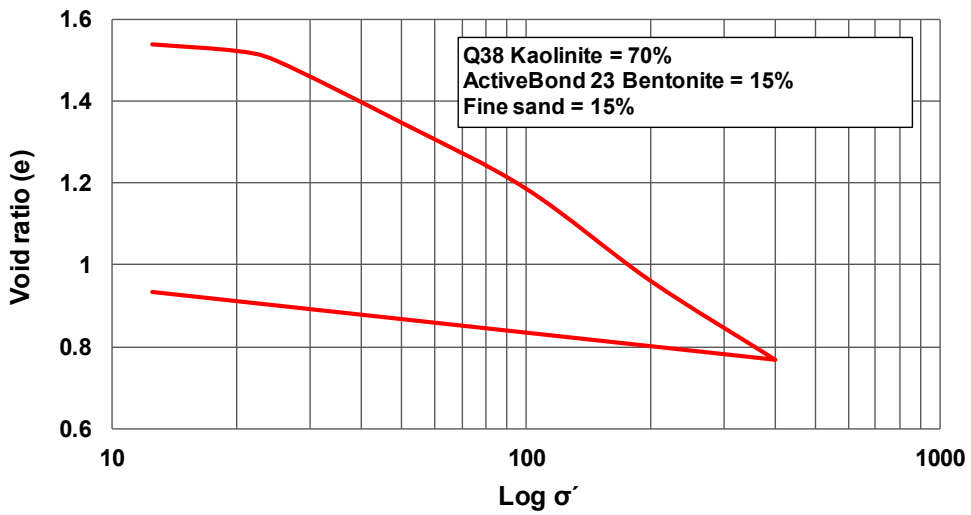

Figure 4.12 Variation of void ratio versus effective stress (sample S1)

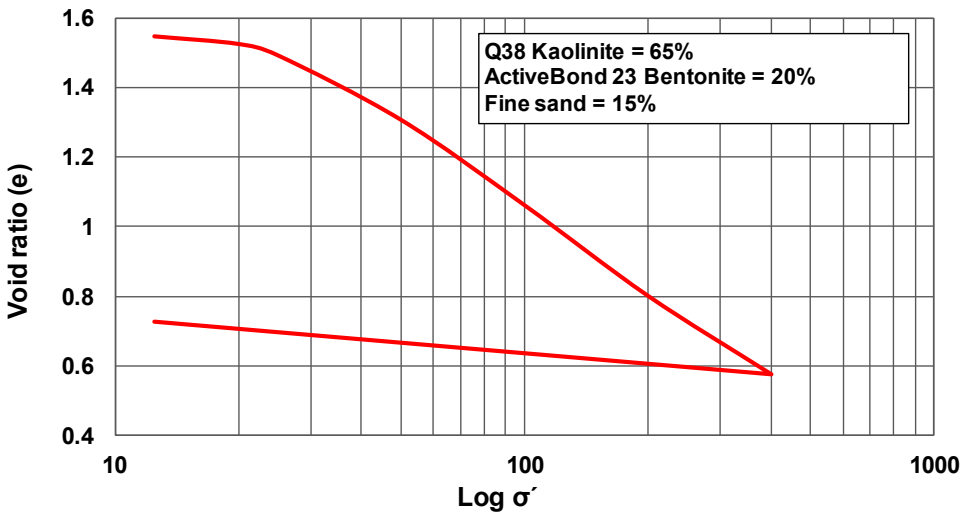

Figure 4.13 Variation of void ratio versus effective stress (sample S3)

Table 4.6 indicates the properties (permeability and extent) of the undisturbed/intact zone, the disturbed/smear zone, and the vertical drain. The soil properties used to conduct the numerical analysis are summarised in Table 4.7.

Table 4.6 Properties of the intact zone, the smear zone, and drain

Area	Intact zone	Smear zone	Vertical drain
Permeability(m/s^2) (σ_z'=20 kPa)	$1.060E10^{-8}$	$2.710E10^{-9}$	$4.50E10^{-3}$
Radius (mm)	125	33	11
Selected Soil	S1	S3	Uniformly graded sand (SP)

Table 4.7 Adopted properties for the numerical simulation

Sample	Soil type	M	λ	κ	μ	$e_\circ$	γ_{dry} (kN/m^3)	k (10^{-9} m/s)	k_h/ k_v
S1	Intact zone	1.1	0.37	0.049	0.3	1.57	10.4	18	1
S3	Smear zone	1.15	0.34	0.054	0.3	1.55	10.6	4.5	1

Note: *M* is the slope of the critical state line; λ and κ are slopes of the specific volume versus *ln(p′)* curves for compression and swelling, respectively, where *p′* is the mean effective stress; μ is the Poisson's ratio; $e_\circ$ is the initial void ratio; and *k* is the permeability in the axisymmetric condition.

4.2.3 Preparation of Rowe cell and initial sample

The following steps were carried out to prepare the Rowe cell apparatus for the consolidation test:

- Applying a vacuum pressure to the water tank for the de-airing process,
- Connecting the pore pressure transducers, pressure lines, drainage and de-airing pipes, and data transfer cables according to the illustrated diagram in Figure 4.4,
- Running the software to check the functionality of pressure controllers, infinite volume controllers, and data loggers,
- De-airing process of the pore pressure transducers, and
- Levelling the main body of the Rowe cell.

After the initial preparation of the Rowe cell, two thin PVC and brass pipes with diameters of 66 mm and 22 mm (r_s/r_w=3) respectively, were placed at the centre of the cell at the base to act as the smear zone and vertical drain boundaries, respectively. The pipe for the vertical drain was covered with a filter paper to prevent the smear zone material from mixing with the sand used in the vertical drain. The pipes and a cross sectional view of the cell are shown in Figures 4.14a to 4.14c.

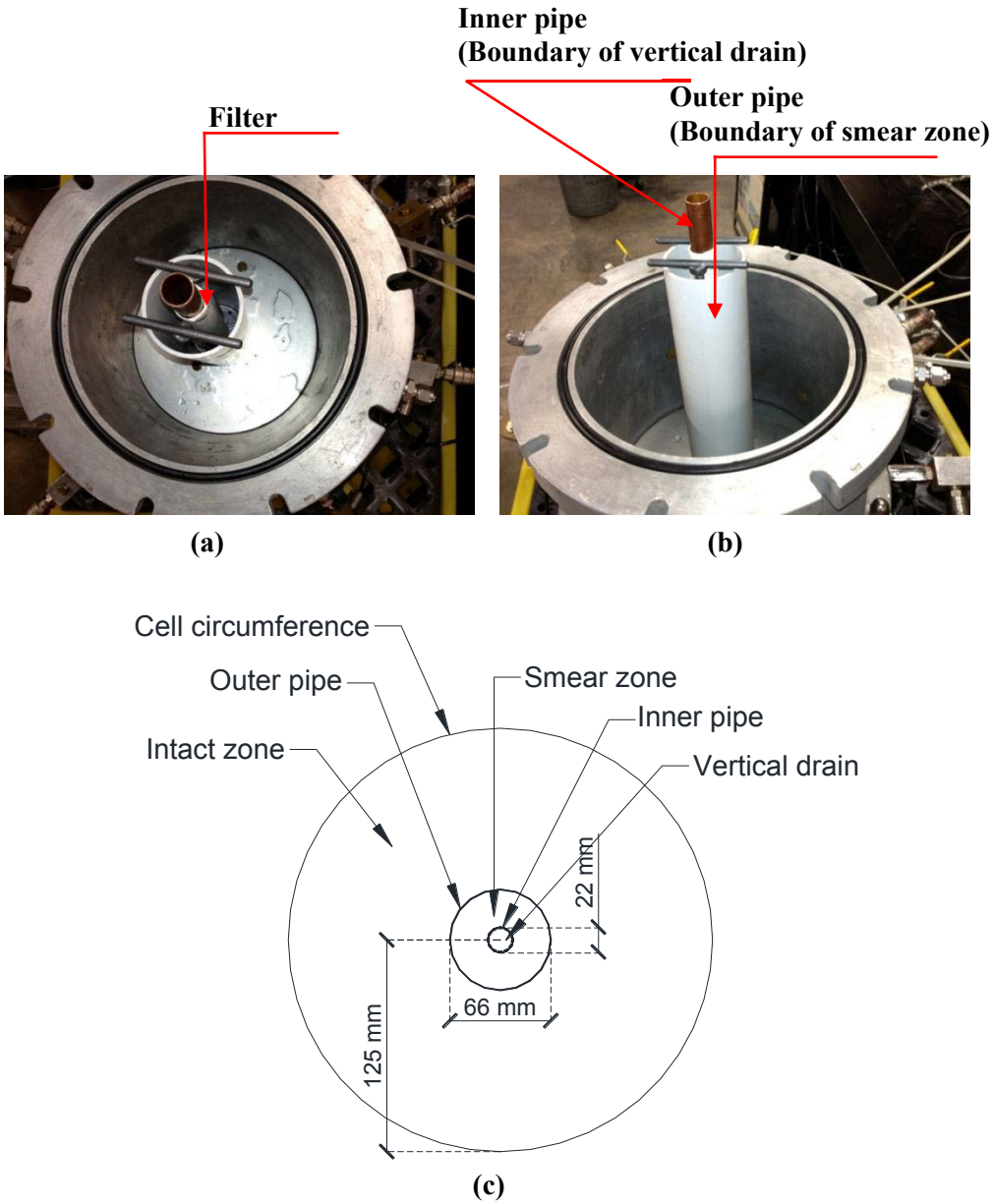

Figure 4.14 Placing PVC and brass pipes as the smear zone boundary and the vertical drain border, (a) top view, (b) side view and (c) a typical cross section of the Rowe cell

The area between the circumference of the cell and the boundary of the smear zone was filled with slurry that was prepared previously, based on the mixture and design of the sample S1 from Table 4.3. The area between the two pipes (the smear zone) was filled with a mixture of 65% kaolinite, 20% bentonite and 15% sand, and a water content of 120% (sample S3 from Table 4.3). The top surfaces of the both areas were levelled and covered with geotextiles. Extra blocks were placed on top of the pipes to stabilise them and minimise any chance of sliding, and then a steel ring was placed

on the intact zone and the surfaces of the smear zone. The sample then was left in this condition for 24 hours to stabilise (Figure 4.15).

(a) **(b)**

Figure 4.15 Sample placement, (a) filling the undisturbed area (intact zone) with the prepared soil and (b) the setup after placing PVC and Brass pipes as the smear zone boundary and vertical drain border

4.2.4 The pre-consolidation process and preparation of the final sample

An initial pre-consolidation pressure of 20 kPa was applied before installing the drain to stabilise the sample in the intact and smear zones. A number of 20mm thick steel rings were manufactured and then placed on top of each zone for pre-consolidation. One (1.8 kPa) ring was added each day to obtain the required pre-consolidation load. The first ring of each set was designed to allow water to drain from the top surface during pre-consolidation. The level of water was checked continuously to keep the sample saturated. The pre-consolidation process is shown in Figure 4.16.

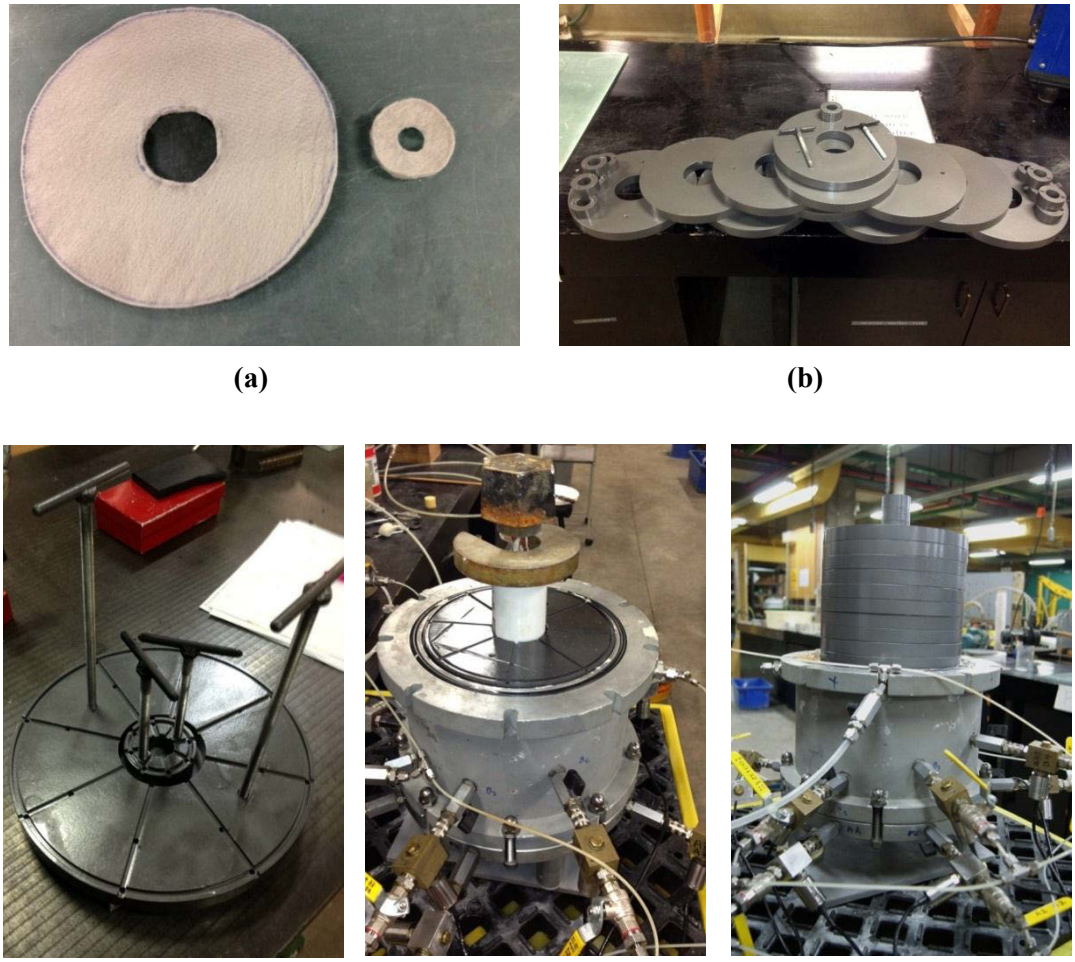

(a) **(b)**

(c) **(d)** **(e)**

Figure 4.16 Rig set up, (a) geotextile filters, (b) pre-consolidation loading rings, (c) the first two loading rings with drainage grooves and holes, (d) placing of the first loading ring and (e) full loading condition

After completing the pre-consolidation process the following steps were carried out to prepare the sample for the main consolidation test:

- All but the last loading ring was removed.
- Sand was poured into the inner pipe to act as a vertical drain and to compact the sand (Figure 4.17a),
- The outer pipe was removed (Figure 4.17b),
- The inner pipe was removed and an extra part of the filter paper was cut (Figures 4.14a and 4.18b),
- The top surface was levelled (Figure 4.19a),
- A geotextile filter and a porous metal plate were placed on the top surface (Figure 4.19b),

- The cell was filled with water (Figure 4.20a),
- A porous stone was placed at the centre of the cell to allow water to drain through the settlement rod,
- The top of the cell, and the diaphragm and settlement rod were placed in position (Figure 4.20b), and
- The top part of the cell was bolted to the body.

(a) **(b)**

Figure 4.17 Testing procedures, (a) Pouring the vertical drain material and (b) Pulling out the outer pipe

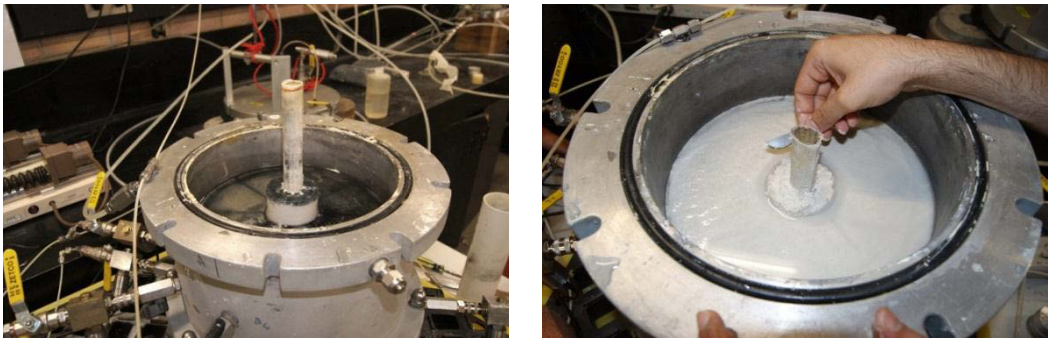

(a) **(b)**

Figure 4.18 Testing procedures, (a) pulling out the inner pipe and (b) cutting the extra part of the filter paper

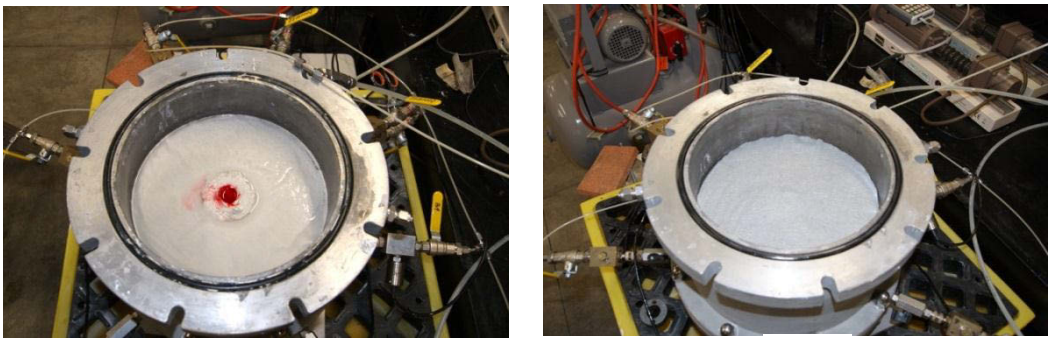

(a) **(b)**

Figure 4.19 Testing procedures, (a) leveling the top surface and (b) placing the geotextile on top surface

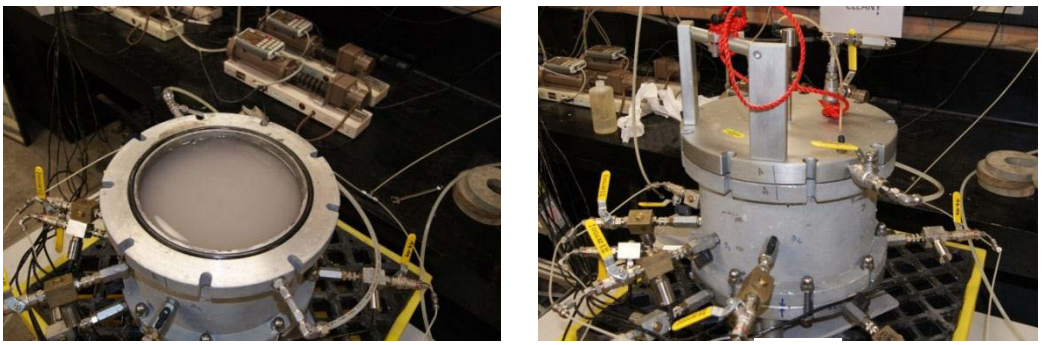

(a) **(b)**

Figure 4.20 Testing procedures, (a) filling the cell with water and (b) placing the cell top

4.2.5 Initial drainage and de-airing of the Rowe cell system

The cell and back pressures were set at 110 kPa and 100 kPa, respectively, to fill the geomembrane diaphragm with de-aired water and carry out a de-airing process based on the diagram shown in Figure 4.21. Water was pumped into the geo-membrane diaphragm through the valve V1 which increased the volume of the diaphragm by the application of 110kPa of pressure. At the same time, the de-airing screw on top of the cell was opened to allow the air trapped in the diaphragm to escape, after which the bolts were tightened again.

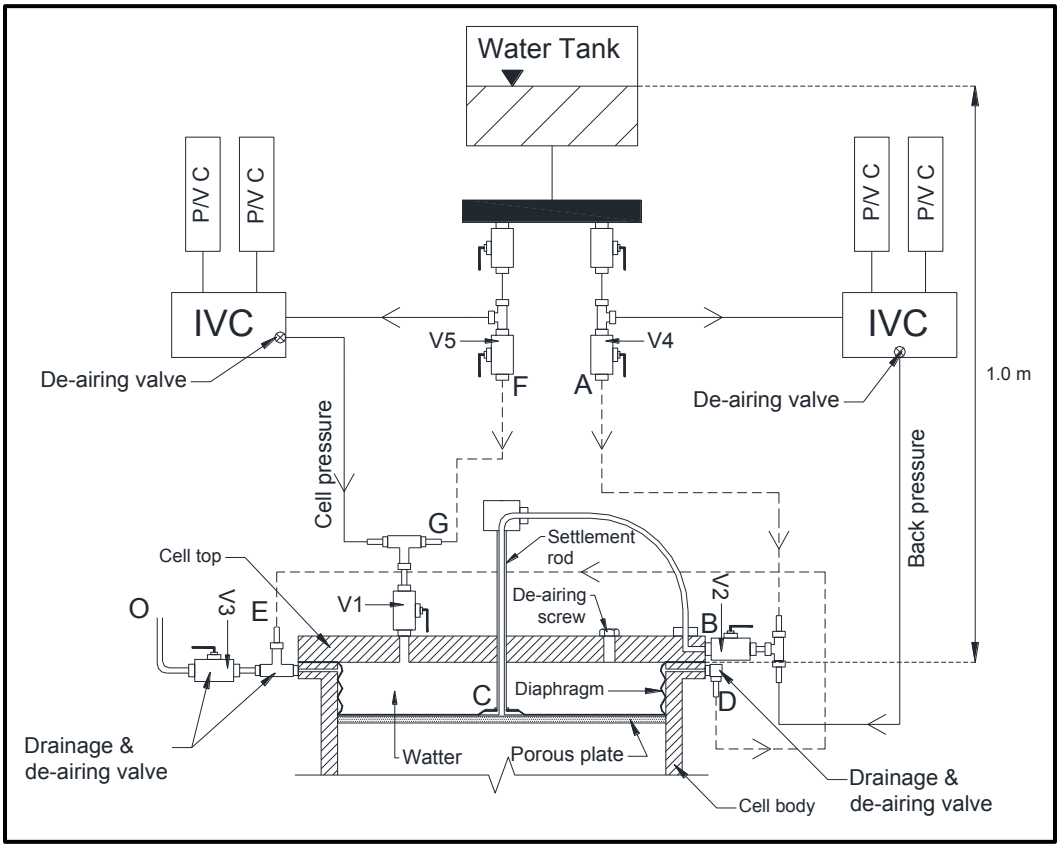

Figure 4.21 Schematic diagram of the de-airing process

The air trapped between the diaphragm, the body of the cell, and the porous plate was drained out due to a sudden increase in the volume of the diaphragm. By closing valve V2 and opening valves V1 and V3, the trapped air escaped through the outlet point O, passing the path DEO (i.e. connecting points D, E, and O). By opening valve V4, water in the tank was discharged through the connecting points A, B, C, D, E, and O. In this way, the air trapped in the pipe between points B and C was drained from the outlet point O. Valves V3 and V4 were closed after this stage was completed.

The air trapped in the pressure lines and controller devices was drained through the de-airing valves installed on the infinite volume controller (IVC). To do this, valves V1 and V2 were closed and valves V4 and V5 were opened; this allowed the water to flow from the tank to the path and push the trapped air through the de-airing valves. This process was repeated several times to ensure that the system was completely de-aired. It should be noted that if the air is not completely removed, the

resulting change in volume, and the settlement and pore water pressure measurements may not be accurate.

4.2.6 Vertical drain assisted consolidation test procedure

Although it was presumed that the soil sample was fully saturated as slurry with a moisture content well above the liquid limit, a pressure of 110 kPa and a back pressure of 100 kPa were applied for 24 hours to ensure full saturation. The criterion for a fully saturated condition and obtaining a pore pressure coefficient ($\beta = \frac{\Delta U}{\Delta \sigma}$) of more than 95%, was reached.

In this study, four loading stages (20 kPa, 50 kPa, 100 kPa, and 200 kPa) were applied to conduct the vertical drain assisted consolidation tests. The cell and back pressures applied in each stage of loading are summarised in Table 4.8. The large Rowe cell with all its connections is shown in Figure 4.5.

Table 4.8 Details of consolidation loading stages

Loading stage	Applied effective pressure (kPa)	Cell pressure (kPa)	Back pressure (kPa)	Loading duration (day)
1	20	120	100	5
2	50	250	200	14
3	100	300	200	28
4	200	400	200	28

The loads mentioned above were applied instantaneously and then maintained for the duration mentioned in Table 4.8, before moving on to the next stage.

4.3 TEST RESULTS

As mentioned earlier, the Rowe cell was filled with the reconstituted soil samples (Table 4.3) to evaluate the undisturbed region and the smear zone with a circular sand drain at the centre. A consolidation test was conducted after the pre-consolidation process (i.e. 20 kPa) was completed. A consolidation surcharge was applied by adjusting the water pressure inside the membrane diaphragm that had been placed on top of the pre-consolidated sample. The time dependent vertical displacements of the sample were recorded using GDSLab software, with an LVDT (Linear Variable Differential Transformer) transducer. Several pore pressure

transducers were used to monitor the dissipation of excess pore water pressure during consolidation. The next stage of loading commenced when the excess pore water pressure from the previous stage had been totally dissipated (i.e. it reached less than 1 kPa). Figure 4.22 illustrates the instrumentation plan for the 250mm Rowe cell.

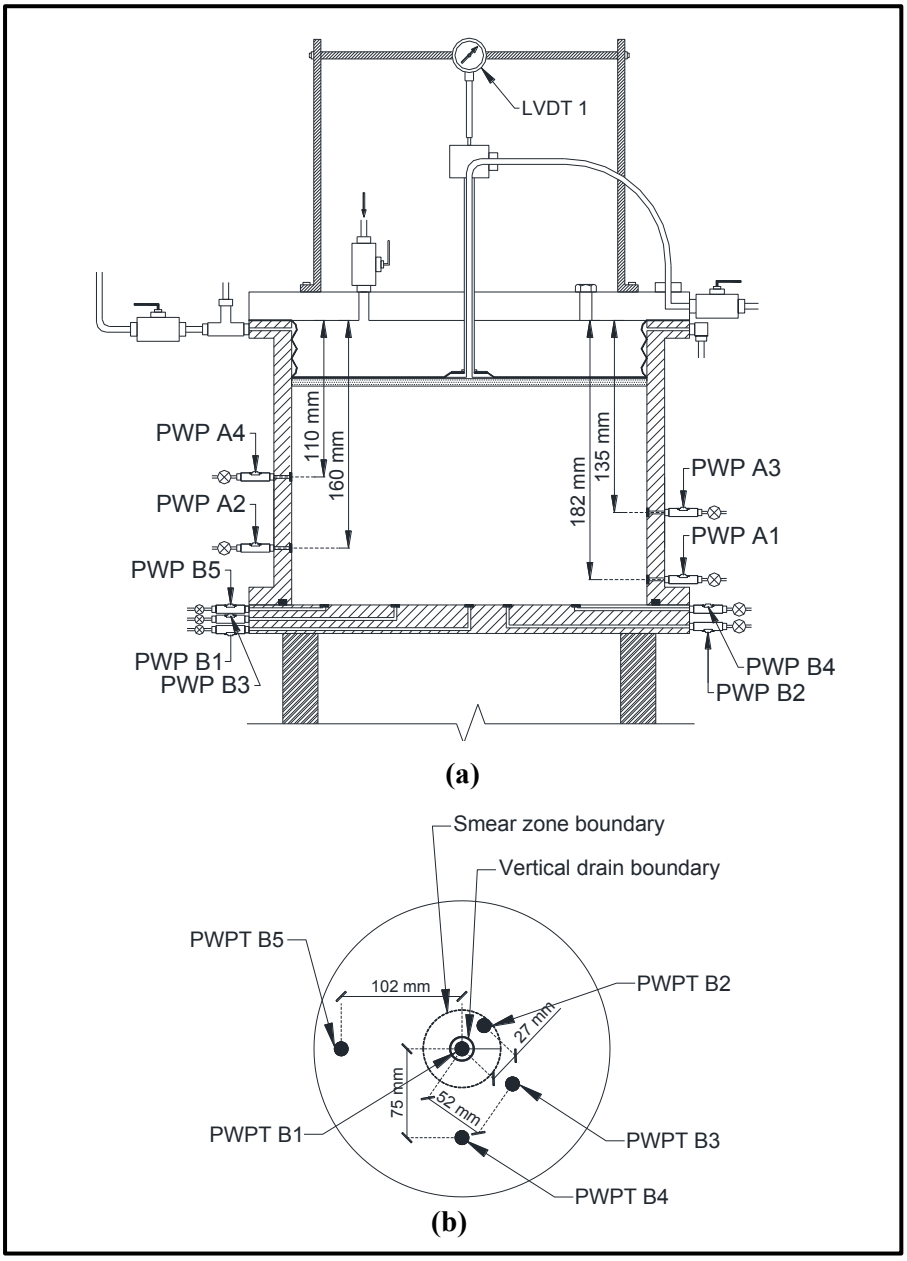

Figure 4.22 Schematic diagram of the instrumentation plan, (a) plan view of the body of Rowe cell and (b) the cross section of bottom of the Rowe cell

Figure 4.23 shows the settlement-time curve along with the loading history. It could be seen that the primary settlement of the sample was about 48 mm after a load of

200 kPa was applied. The total settlement at the end of each loading stage is presented in Table 4.9.

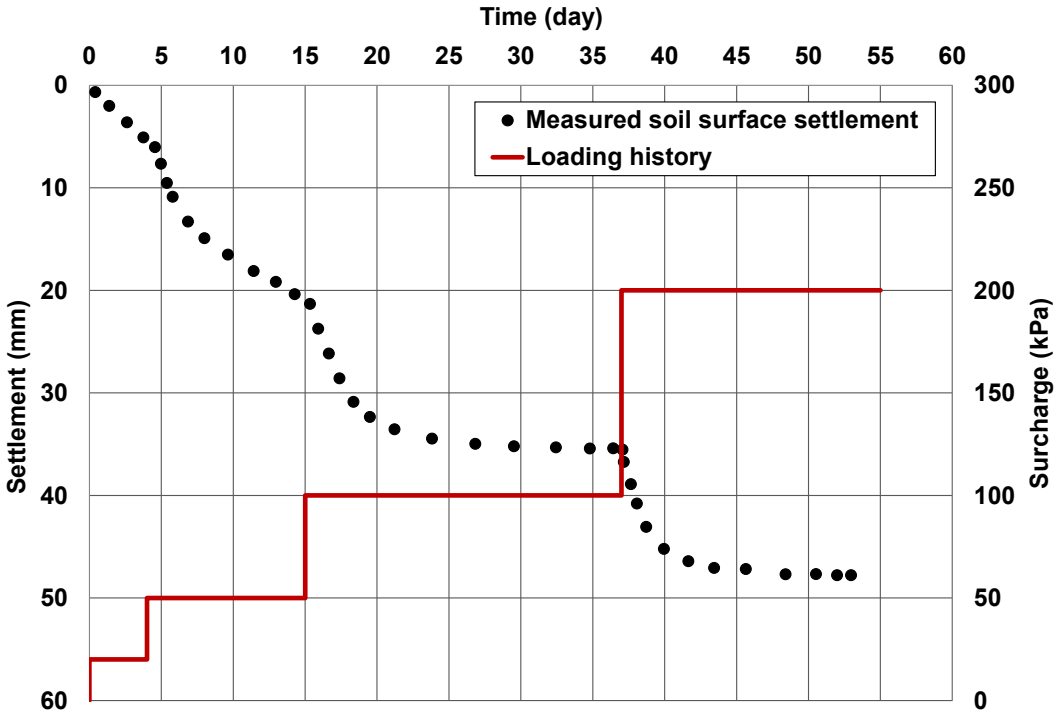

Figure 4.23 Settlement and corresponding surcharge versus consolidation time

Table 4.9 Surface settlement at the end of each loading stage

Applied stress (kPa)	Total settlement (mm)
20	6
50	21
100	35.5
200	48

Note: S_s is the surface settlement; and h is the initial height of the sample

Readings of pore water pressure transducers were used to monitor the dissipation of excess pore water pressure and evaluate the rate of consolidation. The location of the selected pore water pressure transducers are shown in Figure 4.22. The plotted graphs in Figures 4.24 and 4.25 indicate the variation of excess pore water pressure versus consolidation time at different loading stages.

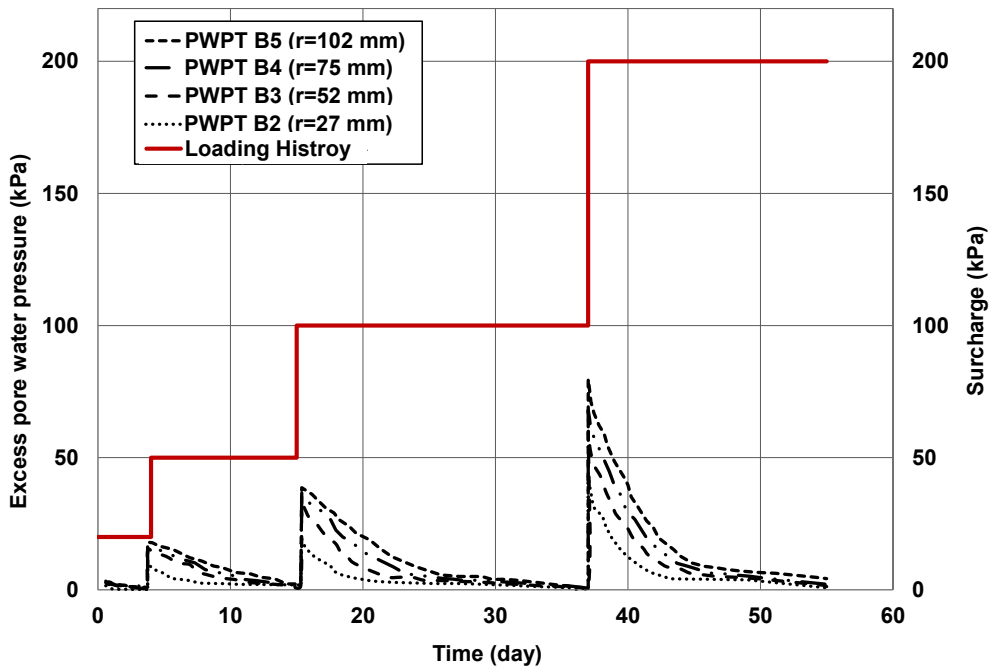

Figure 4.24 Measured excess pore water pressure at transducers located on the bottom of the cell (r is measured from the centre of the drain)

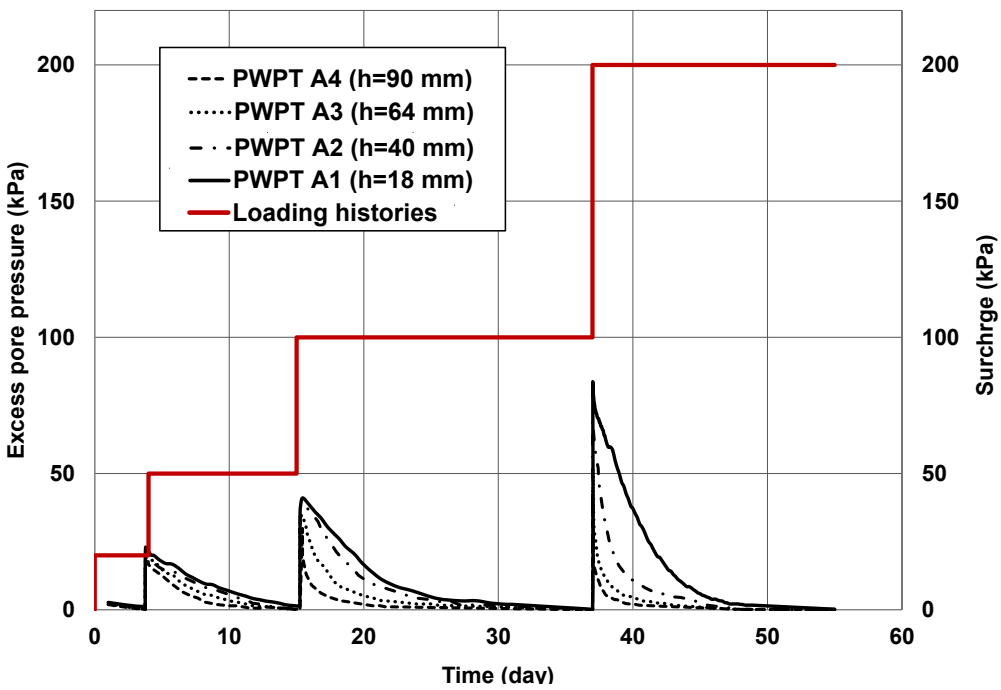

Figure 4.25 Measured excess pore water pressures from transducers located on the sides of the cell (h is measured from the bottom of the impervious boundary of the cell)

It was observed that the pore water pressure transducer B1 (PWPT B1), located inside the vertical drain area (at the centre of the Rowe cell), recorded insignificant excess pore water pressure during consolidation.

According to Figures 4.24 and 4.25, the excess pore water pressure was fully dissipated when all the loading stages had ended, which confirmed reaching the end of primary consolidation. That was the criterion used to commence the next stage of loading. It was noticed that the excess pore water pressure had increased almost immediately after increasing the surcharge, but this rise in pore water pressure was slightly less than the increase in the applied pressure, which could be related to air trapped in the system. According to Figures 4.23-4.25, the settlement has been slightly increased after complete dissipation of pore water pressure in each stage of loading, which can be related to the creep phenomenon (Le et al., 2012; Fatahi et al., 2013).

The variations of normalised excess pore water pressure with vertical and radial distances at certain consolidation times are shown in Figures 4.26 and 4.27, respectively. The readings from the pore water pressure transducers located on the outer impervious wall and the base of the cell have been normalised dividing by surcharge of 200 kPa.

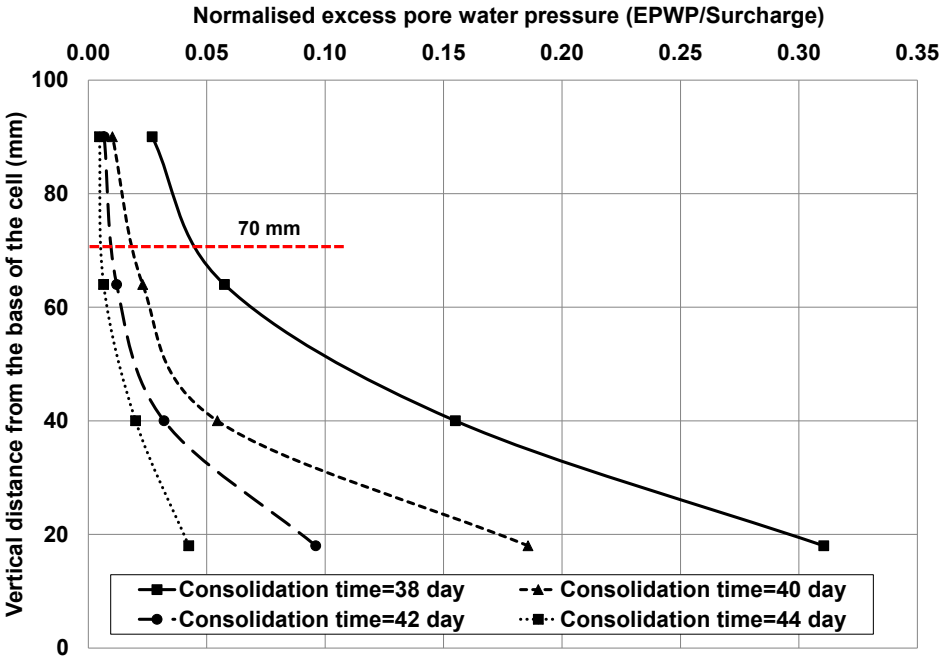

Figure 4.26 Variation of excess pore water pressures with the vertical distance from the base of the cell

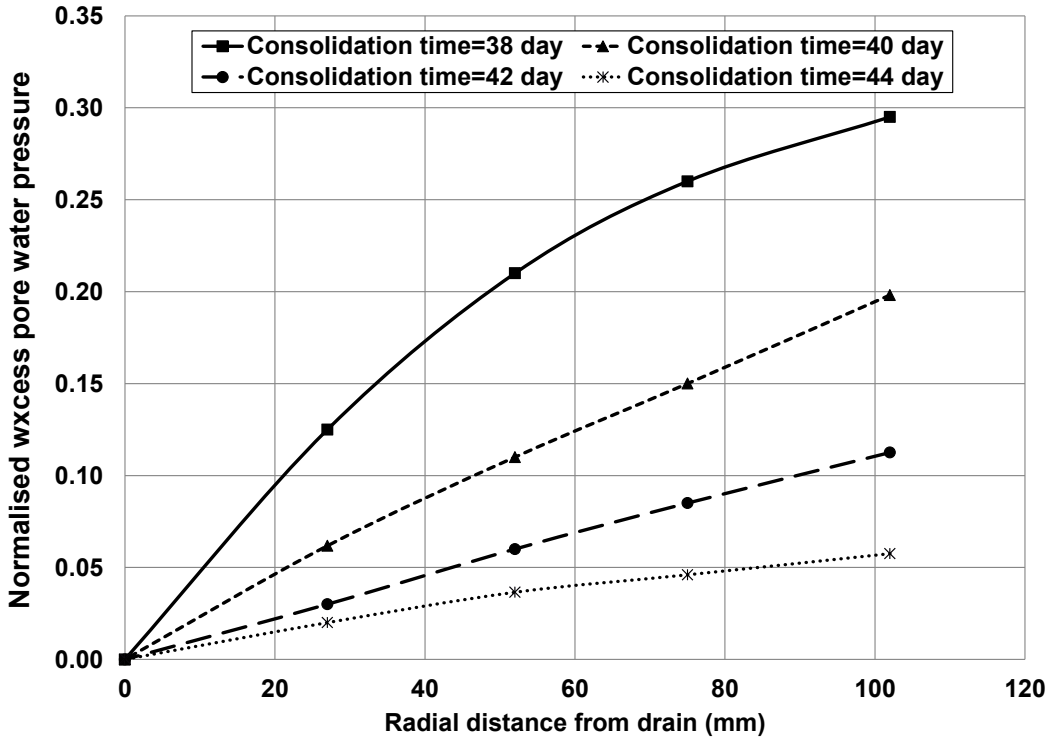

Figure 4.27 Variation of excess pore water pressures with the radial distance from the centre of the drain

Figure 4.26 shows that the excess pore water pressure changed inversely with the vertical distance from the impermeable base, i.e., the excess pore water pressure increased when the distance from the impervious bottom boundary decreased. In the other words the longer vertical distance from the top drainage boundary resulted in a higher remaining excess pore water pressure. For example, the excess pore water pressure at PWPT A1 (h=18 mm) was 62 kPa after 38 days of consolidation, but this was reduced by 70% to 18 kPa at PWPT A2 (h= 40 mm). Furthermore, it was noted that the changes in excess pore water pressure were insignificant in one third of the soil sample (70 mm from the top pervious boundary), indicating that vertical consolidation dominated in this zone and thus the excess pore water pressure dissipated faster.

Figure 4.27 shows that the excess pore water pressure followed an incremental trend when the radial distance from the drain increased, for example, increasing the radial distance from 40 mm to 100 mm resulted in a 70% rise in the excess pore water pressure and a change from 35 kPa to 60 kPa. Moreover, it can be

observed that the excess pore water pressure increased at a sharper rate inside the smear zone in the initial loading stages. Table 4.10 compares the increased rate of excess pore water pressure (kPa/m) with the radial distance, inside and outside the smear zone at different consolidation times.

Table 4.10 The EPWP increase rate from the centre of the drain to the boundary of smear zone for selected consolidation times

Consolidation time (day)	38	40	42	44
EPWP increase rate inside the smear zone (kPa/m)	1.00	0.45	0.22	0.14
EPWP increase rate outside the smear zone (kPa/m)	0.44	0.38	0.21	0.12

4.4 VERIFICATION OF THE NUMERICAL CODE

The laboratory measurements were used to validate the developed numerical code, and an axisymmetric finite difference model was used to simulate the Rowe cell. The hydrostatic water pressure was fixed along the centre line of the cell to model the vertical drain boundary. The loading stages were simulated by applying a uniformly distributed load on top of the cell. The radii of the smear zone and undisturbed area were defined as 33 mm and 125 mm, respectively. It should be mentioned that the initial height of the pre-consolidated sample was 121 mm. The modified Cam-Clay (MCC) constitutive model was used to analyse the consolidation of the reconstituted sample using the soil properties listed in Table 4.7. Figure 4.28 demonstrates the Rowe cell mesh grid that was generated using the numerical code.

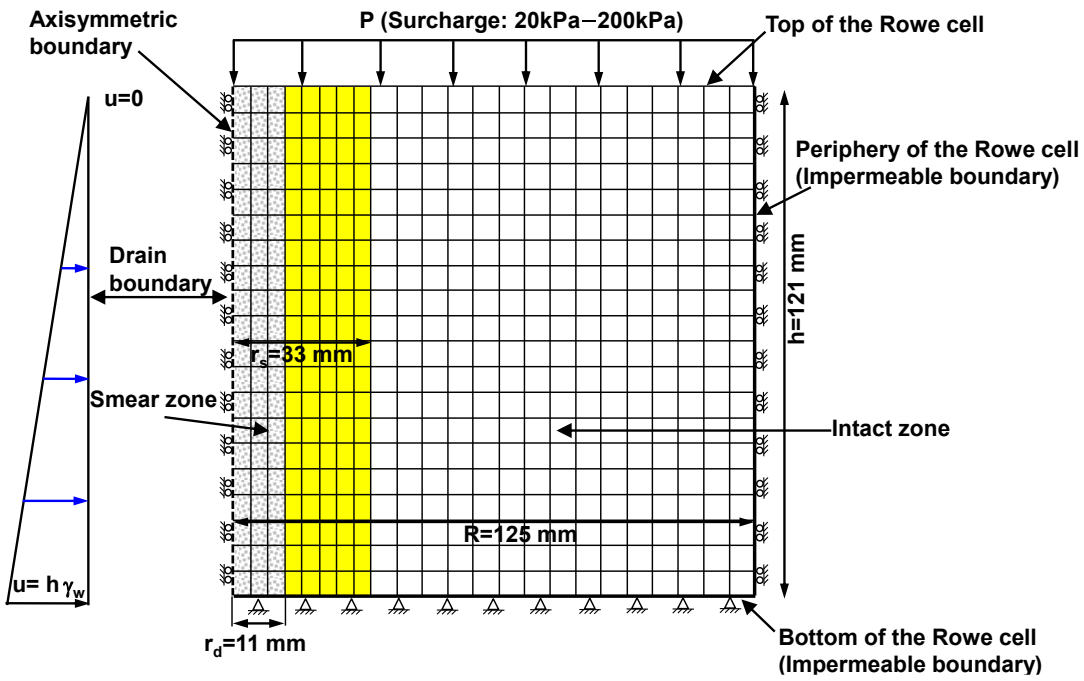

Figure 4.28 Sample of the grid pattern for the simulated Rowe cell using the developed code (r_s= smear zone extent, and R= width of the cell), and the condition of the pore water pressure distribution boundary along the vertical drain.

The discretised finite difference mesh consisted of quadrilateral elements, where only half of the Rowe cell was used by exploiting symmetry. FLAC was used to sub-divide each quadrilateral element into triangular elements, and the pore water pressures were assumed to vary linearly in a triangular element.

The hydrostatic pore water pressure along the vertical drains was used to model the PVD. Zero excess pore water pressure was assumed at the ground surface to model the drainage boundary. The number of fluid and mechanical sub-cycles needed to keep the maximum unbalanced force ratio (or unbalanced force) below a predefined value using "SOLVE auto on age=consolidation time" command was adjusted automatically. The developed numerical code and related sub-routines to simulate the Rowe cell are presented in Appendix B.

A parametric study was carried out by applying the proposed back calculation procedure integrated with the developed numerical code to accurately determine the properties of the smear zone. A number of cases with a constant extent ratio (r_s/r_w) and different permeability ratios (k_h/k_s) were used to conduct the

parametric study, and they are summarised in Table 4.11. The numerical settlement predictions were compared with the laboratory measurements and are shown in Figure 4.29.

Table 4.11 Applied combinations of smear zone permeability and extent in numerical analyses

Case	Permeability ratio (k_h/k_s)	Extent ratio (r_s/r_w)
1	2	3
2	3	3
3	4	3
5	5	3

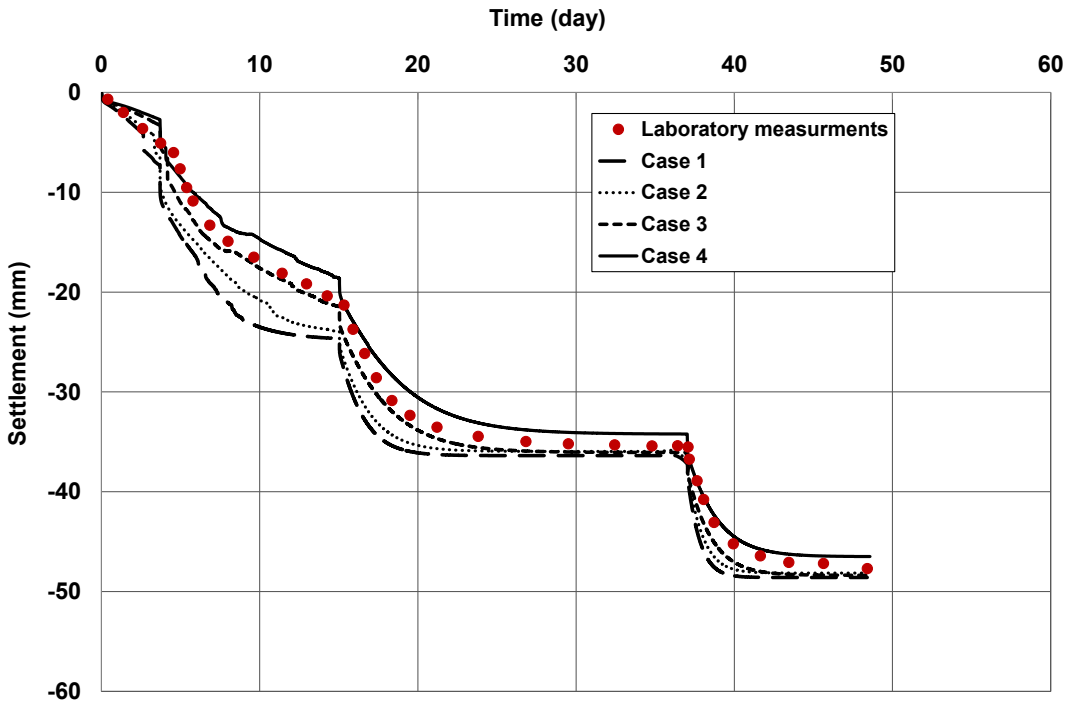

Figure 4.29 Comparison between predicted numerical settlements and laboratory measurements

Figure 4.29 shows that the numerical settlement curves corresponding to Case 3 (r_s/r_w=3 & k_h/k_s=4) and Case 4 (r_s/r_w=3 & k_h/k_s=5) can predict the consolidation of the sample more accurately than the other cases. It should be noted that selecting the optimum case based on observation is a challenging task, so a back calculation procedure was proposed to rectify this problem. Figure 4.30 illustrates the calculated

final cumulative errors (Equation 3.51) for the selected cases using the proposed back calculation procedure (Figure 3.13).

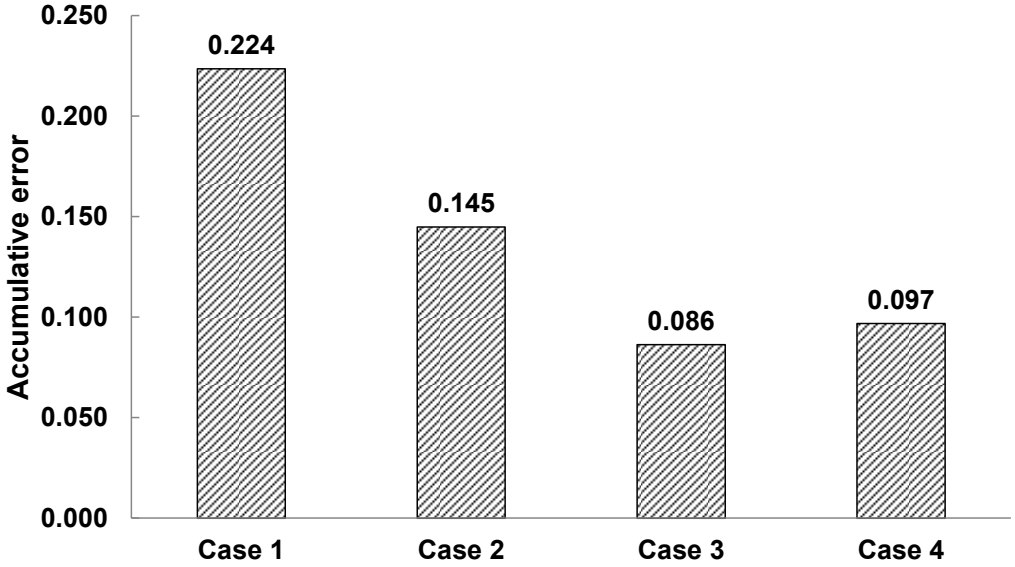

Figure 4.30 Calculated final cumulative error for the selected cases by using the proposed back calculation procedure

The back calculation results indicate that in Case 1 where r_s/r_w=3 and k_h/k_s=2 had the maximum cumulative error, while the minimum error belonged to Case 3 with smear zone properties of r_s/r_w=3 and k_h/k_s=4. Therefore, Case 3 indicated the best agreement with the laboratory measurements, which matched the smear zone properties of the sample used in the test. The results of the parametric study confirmed that the designed back calculation procedure integrated with the developed numerical code can be used to predict the smear zone properties more accurately and reliably.

The numerical predictions for the variations of excess pore water pressure at transducers A1 and B3 were compared with the laboratory measurements that are shown in Figures 4.31 and 4.32.

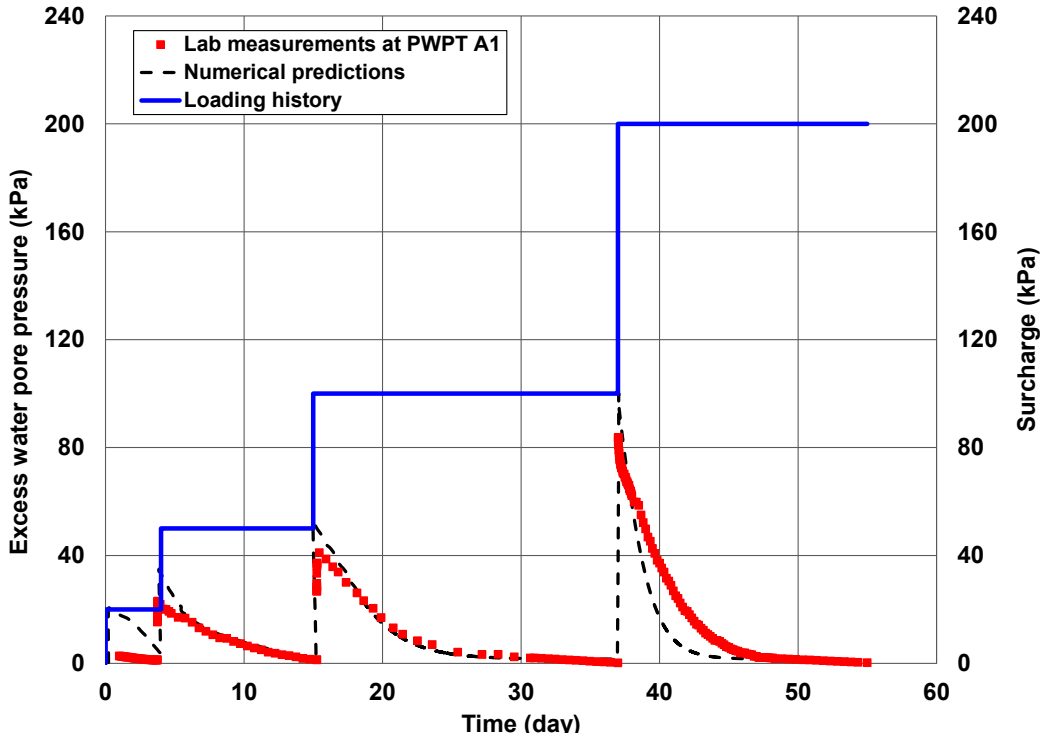

Figure 4.31 Variation of excess pore water pressures at PWPT A1 versus consolidation time

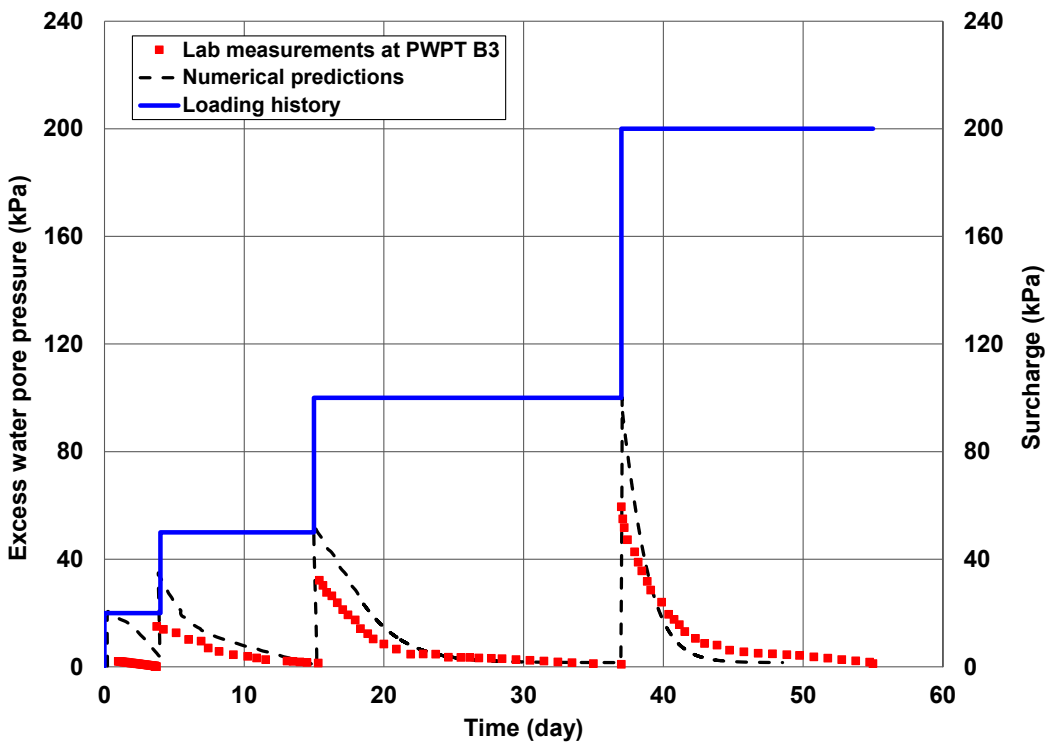

Figure 4.32 Variation of excess pore water pressures at PWPT B3 versus consolidation time

Figures 4.31 and 4.32 show that the excess pore water pressure curves for the numerical predictions and laboratory measurements followed a similar pattern, where the pore water pressures increased at each loading stage and then dissipated with time. Figures 4.31 and 4.32 show that the numerical predictions at PWPT A1 and PWPT B3 agreed with the consolidation test data, although there are some discrepancies.

The graphs in Figures 4.31 and 4.32 indicate that the increase in excess pore water pressures at the commencement of each loading stage that were predicted numerically, was equal to the change in the applied load, but the measured excess pore water pressures were slightly less than the predictions. According to Robinson (1999), the maximum value of the excess pore water pressure is usually less than the pressure increment applied, an effect that may be related to the relationship between the volumetric compliance of the pore water pressure measuring system and the volume compressibility of the soil skeleton (Whitman et al., 1961; Gibson, 1963; Perlof et al., 1965; Sonpal & Katti, 1973).

The overall trends in Figures 4.31 and 4.32 confirmed the validity of the developed FLAC code in modelling the preloading process with prefabricated vertical drains to back calculate the smear zone properties.

4.5 EVALUATION OF AXISYMMETRIC TO PLANE-STRAIN CONVERSION METHODS

As explained earlier in Chapter 2, converting the coefficient of permeability from an axisymmetric to a plane-strain condition is essential to conduct two dimensional (2D) numerical analyses. According to the available literature, different conversion methods have been proposed by researchers (e.g. Hird et al., 1995; Indraratna and Redana, 1997; Lin et al, 2000; Chai et al, 2001; Tuan and Toshiyuki, 2008). In this study, the accuracy of different conversion methods was evaluated by comparing the 2D numerical predictions with the results of the axisymmetric analysis. According to the laboratory measurements, the smear zone permeability ratio (k_h/k_s) and an extent ratio (r_s/r_w) of 4 and 3 should be adopted in the axisymmetric analysis. The adopted conversion methods are summarised in Table 4.12.

Table 4.12 Adopted equations for converting permeability from axisymmetric to plane-strain condition

Method	Intact zone permeability	Smear zone permeability	Reference
1	$k_{ep} = \frac{2k_h}{3\left[ln\left(\frac{R}{r_s}\right) + \left(\frac{k_h}{k_s}\right) ln(s) - \frac{3}{4}\right]}$		Hird et al. (1992)
2	$k_{ep} = \frac{\pi k_h}{6\left[ln\left(\frac{n}{s}\right) + \left(\frac{k_h}{k_s}\right) ln(s) - \frac{3}{4}\right]}$		Lin et al. (2000)
3	$k_{hp} = \frac{0.67k_h}{[ln(n) - 0.75]}$ (ignoring the smear effect)	$k_{sp} = \frac{k_{hp}\beta}{\frac{k_{hp}}{k_h}\left[ln\left(\frac{n}{s}\right) + \left(\frac{k_h}{k_s}\right) ln(s) - 0.75\right] - \alpha}$ $\alpha = \frac{2}{3}\frac{(n-s)^3}{(n-1)n^2}$ $\beta = \frac{2}{3}\frac{(s-1)}{(n-1)n^2}[3n(n-s-1) + (s^2+s+1)]$	Hird et al. (1992) combined with Indraratna et al. (2005a)
4	$k_{hp} = \frac{\pi k_h}{6[ln(n) - 0.75]}$ (ignoring the smear effect)	$k_{sp} = \frac{k_{hp}\beta}{\frac{k_{hp}}{k_h}\left[ln\left(\frac{n}{s}\right) + \left(\frac{k_h}{k_s}\right) ln(s) - 0.75\right] - \alpha}$ $\alpha = \frac{2}{3}\frac{(n-s)^3}{(n-1)n^2}$ $\beta = \frac{2}{3}\frac{(s-1)}{(n-1)n^2}[3n(n-s-1) + (s^2+s+1)]$	Lin et al. (2000) combined with Indraratna et al. (2005a)

Note: where B is the half-width of unit cell, k_h and k_{hp} are axisymmetric and plane-strain horizontal permeability values of the intact zone respectively, k_s and k_{sp} are the axisymmetric and plane-strain horizontal permeability values of the smear zone respectively, k_{ep} is the plane-strain equivalent horizontal permeability of the drain's surrounding soil, n is the spacing ratio equal to $R/r_w=B/b_w$, $s=r_s/r_w$, α, and β are geometric coefficients.

The radial consolidation equation proposed by Hansbo (1981) was applied by Hird et al. (1992) to develop the axisymmetric to plane-strain permeability conversion equation (Method 1). This equation was then used to match the rate of consolidation in a plane-strain and axisymmetric unit cell by incorporating the equality of the average degree of consolidation at every time and every level in the cell. The thickness of the drain and smear zone for matching purposes was omitted by Hird et al. (1992). Lin et al. (2000) assumed an equivalent discharge rate under confined flow to develop the axisymmetric to plane-strain conversion equation (Method 2).

Indraratna et al. (2005a) derived the average excess pore water pressure between the smeared and intact zones by using Darcy's law in the axisymmetric to plane-strain matching process (Methods 3 and 4). Here, the vertical drain system was converted to equivalent parallel drain walls and the total capacity of the drain was assumed to be the same in both systems to determine the equivalent width of the drain and drain spacing. The radial consolidation solution proposed by Hansbo (1981) was equated with the derived radial consolidation equation based on the average excess pore water pressure in order to develop an equation for converting the axisymmetric to plane-strain permeability (Indraratna et al., 2005a).

The plane-strain permeability coefficients of the intact and smear zones were determined using the equations proposed in Table 4.8 to conduct 2D analyses, and which are summarised in Table 4.13. It should be mentioned that methods 1 and 2 used the conversion equations to calculate an equivalent coefficient of permeability to replace the combined smear and intact zones.

Table 4.13 Adopted permeability coefficients for 2D analyses

Method	k_{hp} (m/s)	k_{sp} (m/s)
1	1.47×10^{-9} (combined)	
2	1.16×10^{-9} (combined)	
3	4.38×10^{-9}	6.81×10^{-9}
4	3.42×10^{-9}	7.16×10^{-9}

The permeability coefficients listed in Table 4.10 were used to conduct the plane-strain analyses. The corresponding numerical settlement predictions are compared to the results of the axisymmetric analyses and laboratory measurements in Figure 4.33.

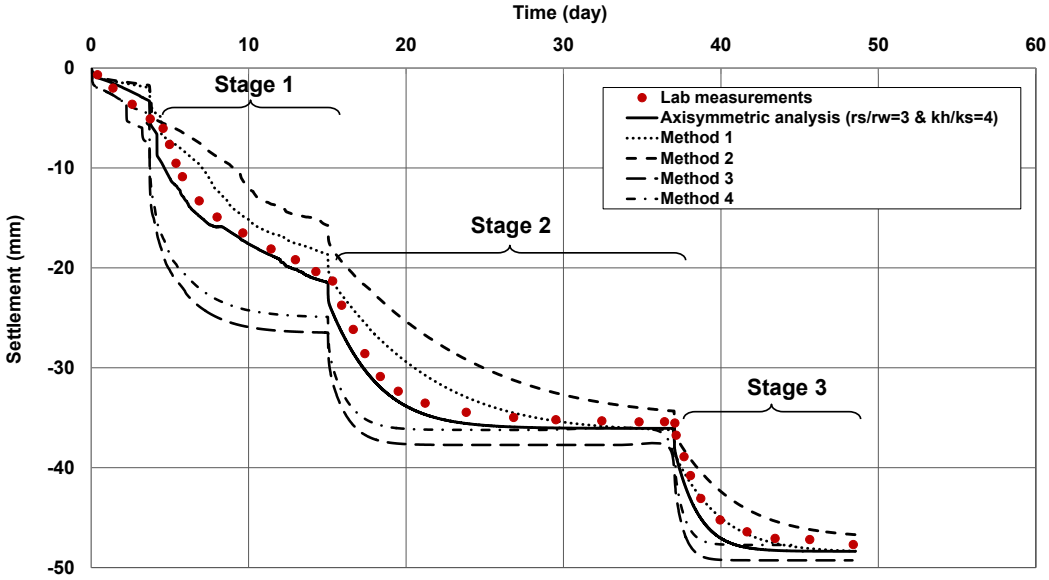

Figure 4.33 Variation of settlement versus consolidation time for different equations used to convert permeability from an axisymmetric to a plane-strain condition

Figure 4.34 illustrates cumulative errors between the plane-strain and axisymmetric settlement values calculated for each stage of loading, in order to systematically evaluate the efficiency of the applied conversion methods.

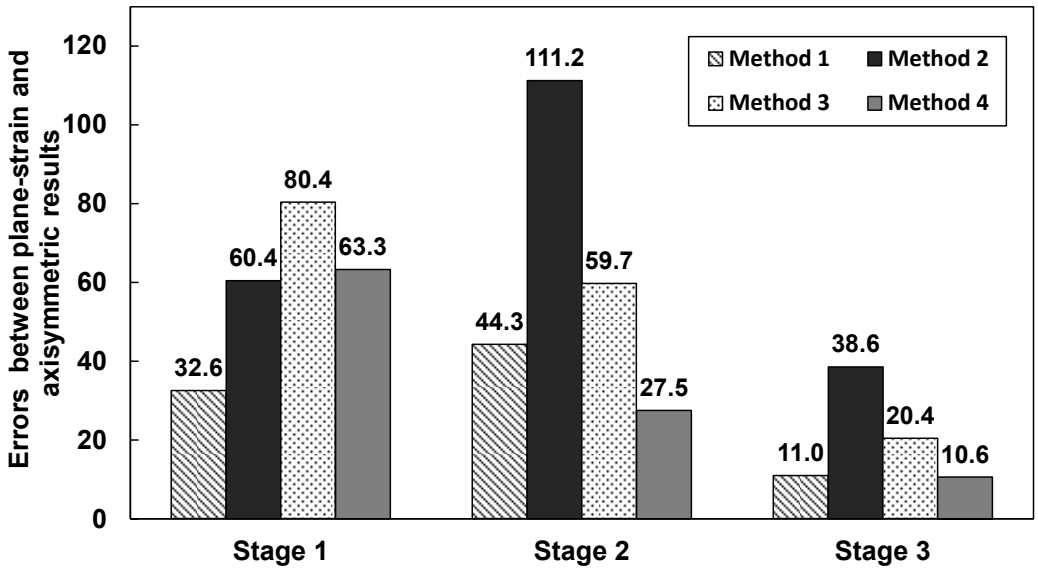

Figure 4.34 Cumulative error between plane-strain and axisymmetric results in each loading stage

Figure 4.34 shows that using conversion method 1 (Hird et al., 1992) resulted in the best fit between the plane-strain and axisymmetric results in the early stages of consolidation (Stage 1), when there were significant changes in the void ratio and permeability. The plotted charts in Figure 4.34 indicate that the accuracy of Methods 3 and 4 increased by a gradual growth in the surcharge pressure and reduction of the void ratio variation rate. It can be seen that in the last two loading stages (Stage 2 and 3) a minimum error occurred when the equation proposed by Lin et al. (2000) was combined with Indraratna et al. (2005a) approach to conversion (Method 4) to determine the permeability of the intact and smear zones for a plane-strain condition.

The variations of excess pore water pressure predicted at the location PWPT A1 for the permeability conversion equations are plotted and compared with the laboratory measurements in Figure 4.35.

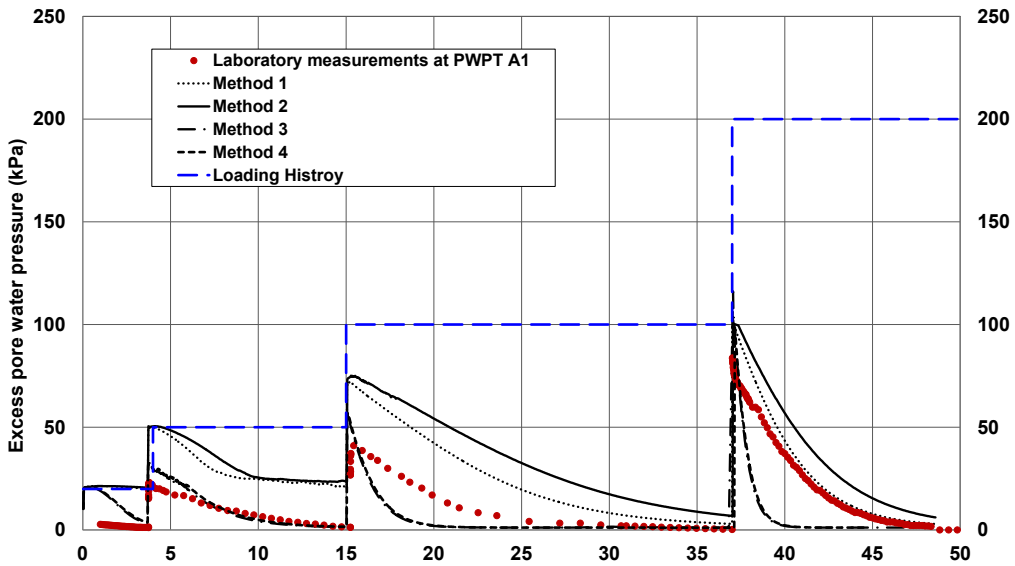

Figure 4.35 Variation of predicted excess pore water pressure versus consolidation time for the adopted equations for permeability conversion from axisymmetric to plane-strain condition

Figure 4.35 shows that the excess pore water pressure graphs obtained from conversion Methods 3 and 4 agreed with the laboratory measurements in the first loading stage, but these methods resulted in an accelerated dissipation of pore water pressure in the initial period of loading Stage 2 compared to the laboratory measurements. In the last stage of loading (Stage 3), the results obtained from Method 1 (Hird et al., 1992) had the best agreement with the test measurements. The

graphs shown in Figure 4.35 confirmed the settlement-time curves shown in Figure 4.33.

4.6 SUMMARY

In this chapter, a fully instrumented large scale Rowe cell apparatus was used to investigate the effect of the smear zone on consolidation and to verify the numerical procedure developed to back calculate the smear zone properties. Staged uniform loads were applied to the sample by water pressure acting on a convoluted rubber jack. An LVDT (Linear Variable Differential Transformer) and pore pressure transducers were used to monitor the variations of settlement and excess pore pressure dissipation respectively, during consolidation.

A number of samples were prepared by mixing different percentages of Q38 kaolinite, ActiveBond23 bentonite, and uniformly graded sand (SP) to conduct an oedometer test and select proper mixtures for the PVD assisted consolidation test using the Rowe cell. Based on the results of the odometer tests, two samples were selected as the intact and smear zones materials that meet the criteria of k_h/k_s=4.

After preparing the Rowe cell, two 66mm diameter and 22mm diameter pipes (r_s/r_w=3) were placed in the centre of the cell at the base, as the smear zone and vertical drain boundaries, respectively. The area between the circumference of the cell and the boundary of the smear zone was filled with slurry that was prepared on the selected mix-design. The reconstituted sample was then pre-consolidated under a 20 kPa load by placing a number of 20mm thick steel rings on top of each other.

A vertical drain was installed by pouring fine sand inside the central pipe after pre-consolidation was complete, and then both pipes were pulled out. A geotextile filter and porous metal plate were placed on the top surface to provide a one way drainage condition. The whole system was de-aired as the final stage of the sample preparation process. Four loading stages (20 kPa, 50 kPa, 100 kPa, and 200 kPa) were applied to conduct the PVD assisted consolidation tests.

The developed numerical code was used to simulate the consolidation test. Laboratory measurements were used to evaluate the validity of the numerical analyses and the proposed back calculation procedure. The results indicated that the back calculation procedure integrated with the developed numerical simulation can reliably predict the smear zone properties.

In addition, further numerical analyses were conducted to evaluate the accuracy of the equations proposed by Hird et al. (1992), Lin et al. (2000), and Indraratna et al. (2005a) for converting the coefficient of permeability from an axisymmetric to a plane-strain condition, and also comparing the results of a 2D plane-strain and axisymmetric numerical analysis. According to these results, using conversion method proposed by Hird et al. (1992) resulted in more accurate predictions in the early stages of consolidation while better predictions were obtained in later stages of consolidation by applying the conversion equations proposed by Indraratna et al. (2005a), combined with Lin et al. (2000) and Hird et al. (1992) methods.

CHAPTER FIVE

5 CASE STUDIES AND FURTHER VALIDATION EXERCISES

5.1 GENERAL

According to the Australian Bureau of Statistics (2008), the population of Australia would experience a growth of 60%, from 22 million to 35 million by 2056, and the population of Queensland and New South Wales would expand by about 110% and 50% by 2056, respectively. This rapid growth in population and urbanisation has increased the need to build and expand infrastructure such as highways, railways and ports. In Australia, the major cities lie along coastlines, consisting of deposits of deep soft clay, especially in Northern Queensland and New South Wales. These deposits can be categorised as problematic soils due to their characteristic low bearing capacity and high compressibility.

Finding efficient ground improvement techniques to modify the properties of soft soil, while considering the project time limitation and construction cost, has been a continuous challenge for construction companies. Various ground improvement methods have been proposed to improve the strength of the soft soil. Over the pasts two decades prefabricated vertical drain (PVD) assisted preloading has been used in Australia as a very efficient method of ground improvement for sites with deposits of deep soft soil.

In this chapter, five case studies of PVD assisted preloading (mainly focusing on projects in Australia that have already been completed) were numerically simulated. For all case studies, the properties of the smear zone accurately estimated, using the proposed back calculation procedure to validate the applied method. The developed FLAC code was used to conduct the numerical simulations. The PVD assisted preloading projects used in this study are summarised in Table 5.1.

Table 5.1 Summary of simulated case studies

Case Study	Location	Preloading Method	Embankment Height (m)	PVD Length (m)	Drain Spacing (m)	Soil Profile
Cumbalum TE	AU	PVD assisted	5.0	22	1.35	DSS
Ballina Bypass TE	AU	PVD/Vacuum assisted	8.5	24	1.0	DSS
Sunshine TE	AU	PVD assisted	2.8	11	2.0	SSS
Chittagong Sea Port TE	BA	PVD assisted	3.0	9	1.0	SSS
Large-scale Consolidometer	UOW	PVD assisted	0.95	0.95	0.225	SS

Note: AU: Australia, UOW: University of Wollongong (Australia), BA: Bangladesh, TE: Trial embankment, DSS: Deep soft soil, SSS: Shallow soft soil, SS: Soft soil

It can be noted that these case histories were selected to cover different possible preloading conditions and evaluate the validity of the back calculation approach in each case. For example, the application of vacuum pressure was modelled to simulate the Ballina Bypass trial embankment. The back calculation procedure was verified for those cases with a shallow soft soil profile by modelling the Sunshine and Chittagong trial embankments, while the deep soft soil profile was considered in the Cumbalum and Ballina Bypass trial embankments. Furthermore, different drain spaces (between 0.5 m to 2.0 m) were applied in these numerical analyses. A large scale consolidometer test was numerically modelled to validate the use of the back calculation method for laboratory investigations.

5.2 CUMBALUM TRIAL EMBANKMENT

5.2.1 Introduction

Expanding populations in the coastal regions of Eastern Australia are gradually outgrowing the existing transport infrastructure. The North-South link connecting Brisbane and Sydney is one of the most important routes and the volume of traffic is growing exponentially. A large proportion of this coastal highway is currently being upgraded, with much of the new construction confined to marginal land corridors that had previously been avoided. The eastern seaboard of Australia is dominated by a succession of easterly flowing rivers that drain the adjacent ranges into the Pacific Ocean. In the lower reaches of these river valleys are extensive estuarine deposits

with complex geological structures (Bishop 2004). The site of the Ballina Bypass was constructed over the floodplain and underlying estuarine deposits near the mouth of the Richmond river in Northern NSW, as shown in Figure 5.1.

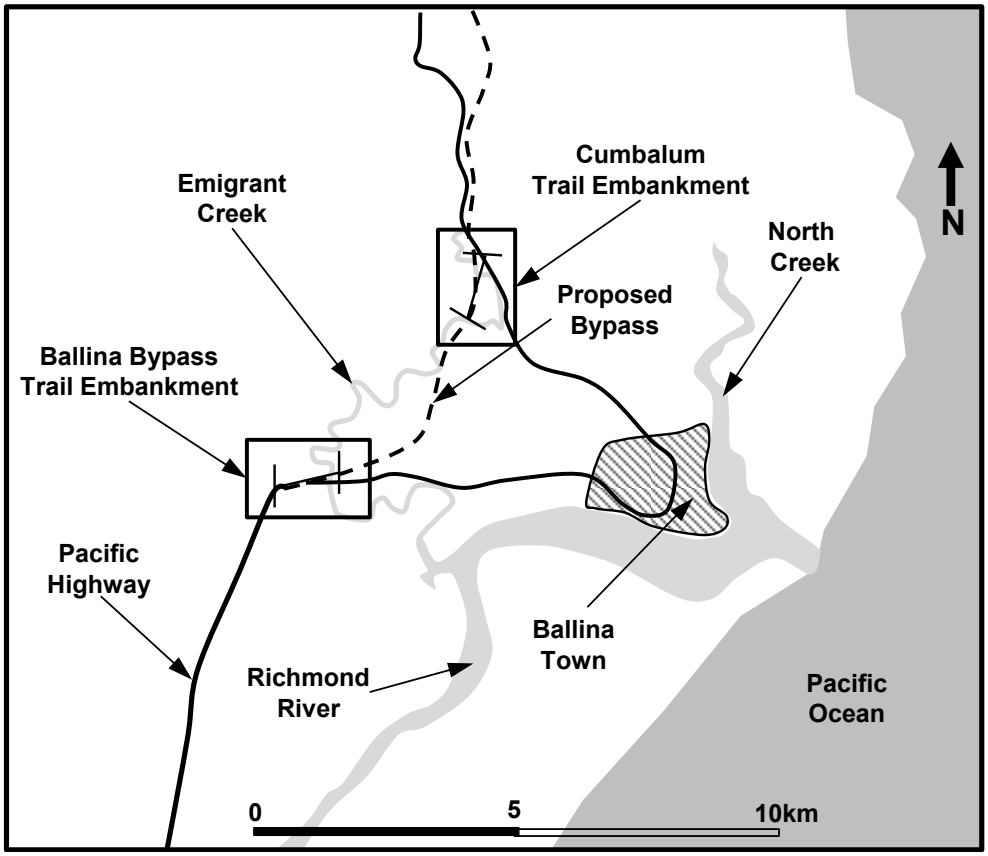

Figure 5.1 A map of the Ballina Bypass upgrade route and surrounding surface features (modified after Bishop, 2004)

The Cumbalum trial embankment was constructed near Cumbalum on the Pacific Highway, 6.3 km north of Ballina, to provide field data to be used in the design of the Ballina Bypass section of the Pacific Highway upgrade in New South Wales (Figure 5.2). The embankment was constructed in 1998 by the Roads and Traffic Authority (RTA), Northern Road Services. This trial embankment also formed part of the northern abutment of a bridge over Emigrant Creek.

The Ballina Bypass traverses a flood plain associated with the Richmond River and its tributary creeks (Bishop, 2004). Soft soil deposits within the flood plain can be up to 25m thick. An embankment constructed on these soils may undergo a considerable amount of settlement during construction, and the settlement process

may take a long time and post construction settlements may be large. PVD assisted preloading can be used as a ground improvement method to accelerate the settlement process.

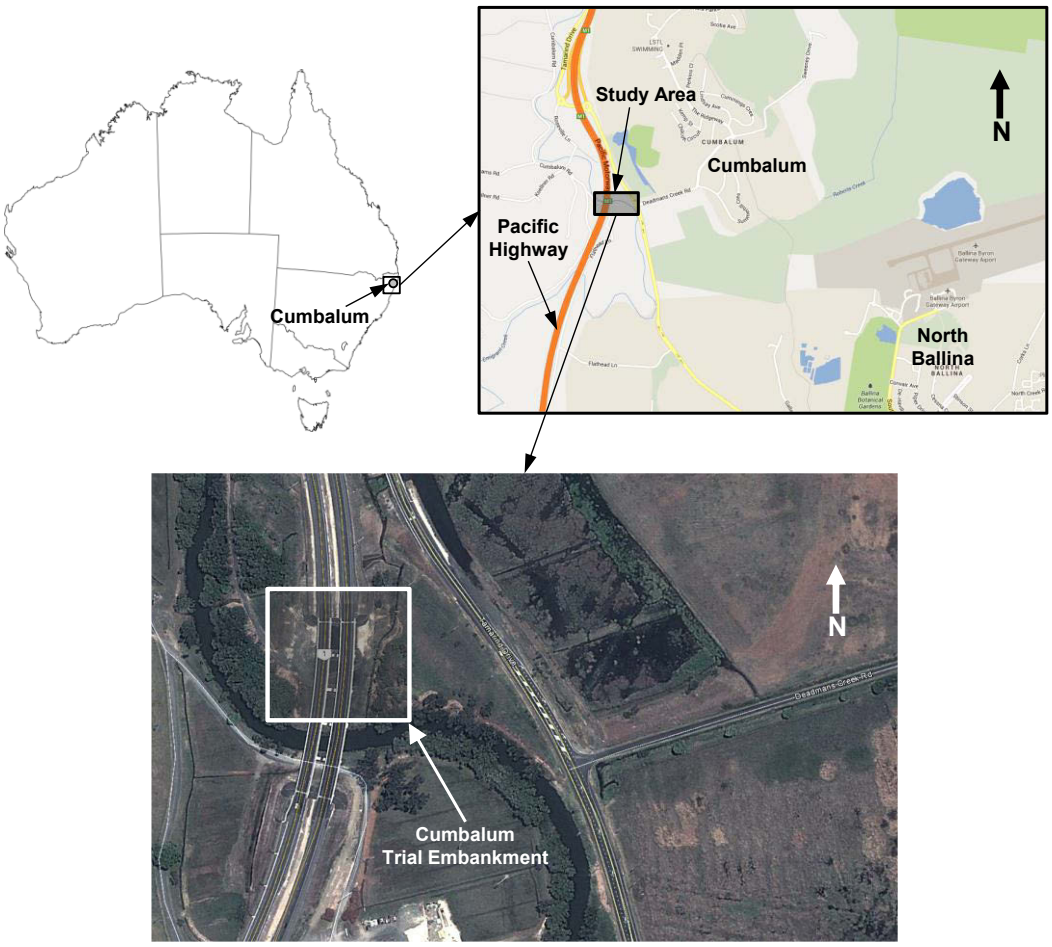

Figure 5.2 Location of the Cumbalum trial embankment (courtesy of Google Maps)

5.2.2 Geological Model and Subsoil Condition

Bishop (2004) developed a geological model for the Richmond River floodplain that includes Quaternary marine and estuarine deposits overlying Tertiary volcanic and Palaeozoic deformed and folded meta-sediments. Three distinct stages of Quaternary deposition have been identified in the geological model proposed by Bishop (2004) as follows:

- Stage 1: 1m to 2m thick deposits of fluvial sandy gravels overlayed by very stiff oxidised clays. These deposits have been eroded and exist in isolated mounds from depth to RL -15m AHD. A highly oxidised and indurated alteration horizon overlies the Stage 1 deposits.

- Stage 2 and 3: deposits graded from gravels and sandy clays at lower levels to dark grey shelly muds in the upper levels. Stage 3 deposits are Holocene in age, and uncomfortably overlay the Stage 2 deposits that mainly comprise clays above RL -10m AHD. The Stage 3 deposit is known as Pimlico Clay.

Within the Pimlico Clay deposit, Bishop (2004) infers that the presence of inter-bedded estuarine sands and muds below RL -10m AHD indicates deposition under high-energy conditions. The absence of sands above RL -10m AHD was interpreted to correspond with the formation of a coastal barrier that created a low energy estuarine deposition environment behind it. The interpreted section derived from borehole logs under the Cumbalum study area (see Figure 5.1) is shown in Figure 5.3. MZ1 and MZ2 are highly oxidised and indurated horizons, which separate the stages.

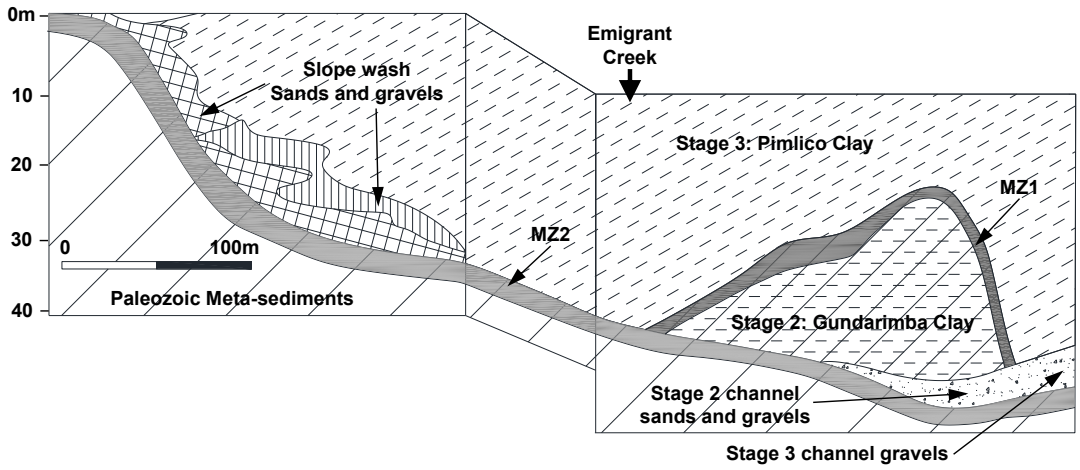

Figure 5.3 Interpreted section for Cumbalum trial embankment study area (after Bishop, 2004)

Site investigations for the Cumbalum trial embankment were conducted by Robert Carr & Associates (RTA, 2000), and then developed further by Coffey International Limited (2007).

The moisture content and Atterberg limits along the soil profile were determined by conducting site investigations and laboratory testing (Figure 5.4). According to Kelly (2008) the subsoil profile consists of lightly consolidated soft clay deposits from the ground surface level to a depth of 10 m. A 2-m thick layer of soft clay is located at the depth of 12 m and is surrounded by two silty sand lenses. The soil deposit between the depth of 15 m and 22 m is categorised as firm clay.

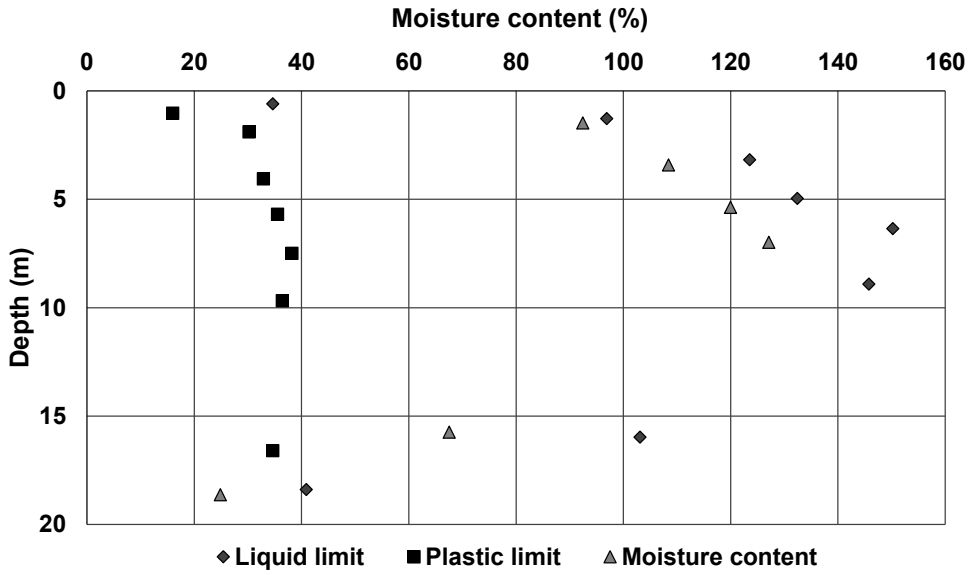

Figure 5.4 Moisture content, liquid limit and plastic limit (after RTA, 2000)

5.2.3 Installation of Vertical Drains and Embankment Construction

Once the drainage blanket (crusher and aggregate) had been completed at the Cumbalum trial embankment, a series of vertical wick drains were installed. The wick drains were designed to facilitate the flow of water from the soil to allow the embankment to achieve its final settlement in a shorter period of time. Vertical drains were installed at a 1.35-m triangular spacing over the entire area of the embankment to a depth of approximately 22 m. The total number of drains installed was 2772, with a total length of 61890 m.

The embankment was constructed between 1998 and 1999 to a nominal fill thickness of 4.5 m. Subsequent site investigations through the trial embankment showed that approximately 5 m of fill had actually been placed on site. The embankment was then allowed to consolidate for about 4.5 years (Kelly, 2008). The

embankment material was compacted with an 18t pad foot roller and a 14t self-propelled smooth drum roller. The material was spread out by a D3-Dozer (RTA, 2000). The construction history of the embankment is shown in Figure 5.5.

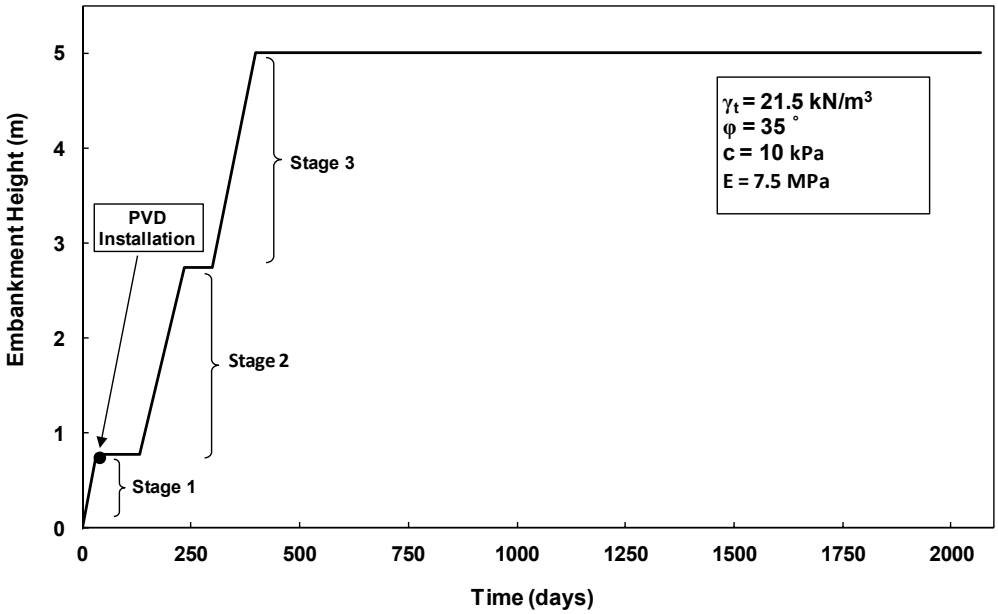

Figure 5.5 Construction history of Cumbalum trial embankment (after Kelly 2008)

The layout of the instrumentation in the embankment is shown in Figure 5.6. Measurements at the settlement plate 9 (SP9) were used for the numerical verification and parametric study. Figure 5.7 presents a cross section of the embankment and subsoil profile at SP9.

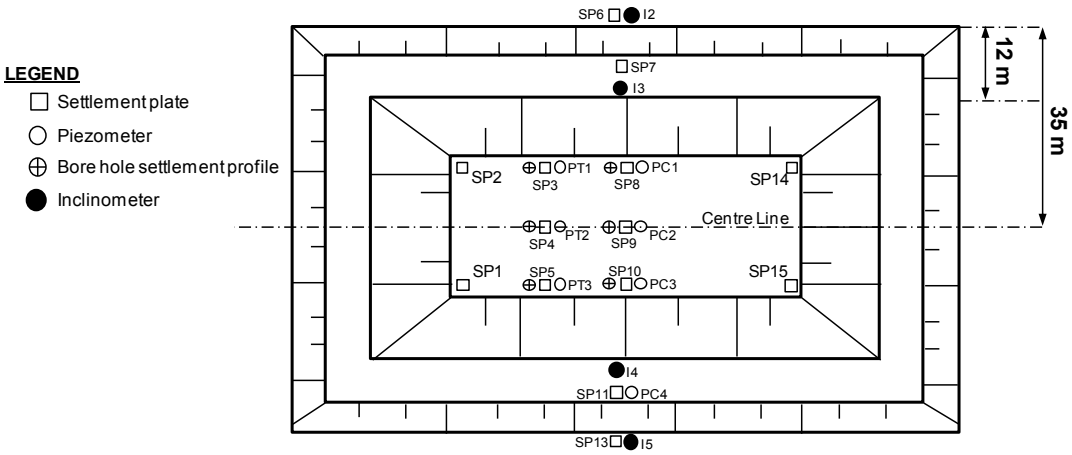

Figure 5.6 Layout of the Cumbalum trial embankment (after RTA, 2000)

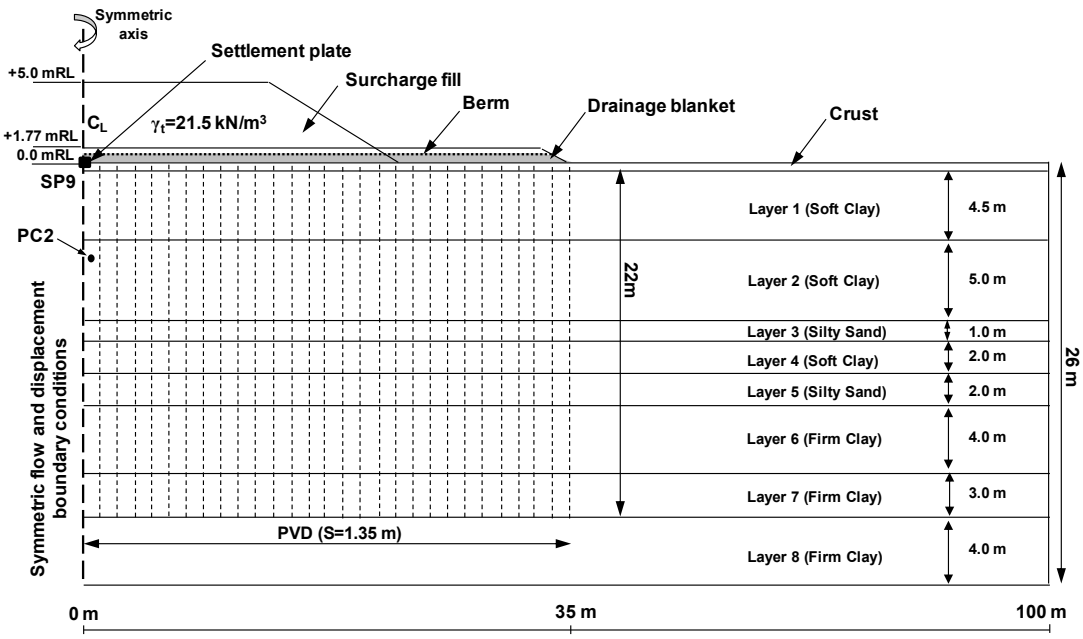

Figure 5.7 Cross section of the Cumbalum trial embankment and subsoil profile

5.2.4 Numerical Simulation

The developed numerical code was used to simulate the Cumbalum trial embankment. The finite difference mesh used for the 2D plane-strain numerical simulation is shown in Figure 5.8. The vertical drains were modelled by fixing the pore pressure to the hydrostatic pressure from the top to the bottom of the drain. A constant reduced permeability was assigned to the area surrounding the vertical drain in each layer to simulate the smear zone as shown in Figure 5.8. The modified Cam-Clay model was used to simulate the behaviour of the soil in the intact region and the smear zone, while the Mohr-Coulomb criteria elastic-perfectly plastic model was used to simulate the embankment. The properties adopted for subsoil layers are summarised in Table 5.2. The vertical drain system was converted into an equivalent parallel drain wall by adopting Equations 2.30 to 2.32.

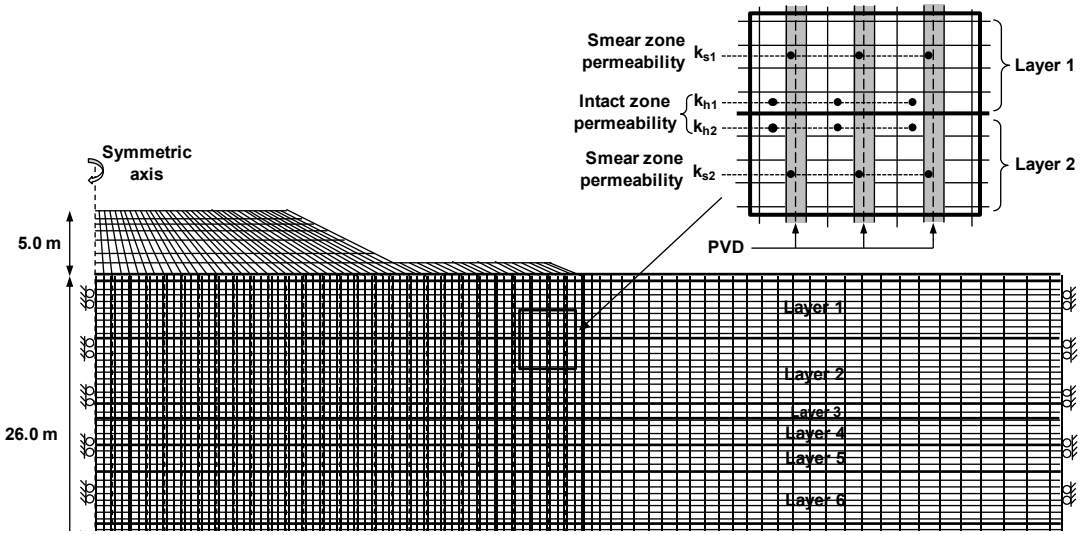

Figure 5.8 Finite-difference meshes for the plane-strain analysis of Cumbalum trial embankment

Table 5.2 Adopted properties for subsoil layers for Cumbalum trial embankment near SP9

Depth: m	λ	κ	$e_\circ$	γ_s (kN/m^3)	k_h (10^{-10} m/s)	k_v (10^{-10} m/s)	OCR
0.0-0.5	0.7	0.042	2.2	17.5	2.04	1.02	3.0
0.5-5.0	0.84	0.118	2.87	15.0	1.71	0.85	2.0
5.0-10.0	0.95	0.134	3.4	14.0	1.71	0.85	1.5
10.0-11.0	0.125	0.031	2.61	18.0	1260	630	3.0
11.0-13.0	0.61	0.087	3.0	15.0	1.74	0.87	1.3
13.0-15.0	0.125	0.031	2.61	18.0	1740	870	3.0
15.0-19.0	0.47	0.067	2.08	17.0	2.94	1.5	1.3
19.0-22.0	0.335	0.047	2.08	20.0	2.94	1.5	3.5
22.0-26.0	0.335	0.047	2.08	20.0	2.94	1.5	2.5

Note: λ and κ are slopes of the specific volume versus *ln(p')* curves for compression and swelling, respectively, where *p'* is the mean effective stress; $e_\circ$ is the initial void ratio; γ_s is the unit weight; k_h is the horizontal permeability of intact zone; k_v is the vertical permeability of intact zone; and *OCR* is the over consolidated ratio

The FLAC code was applied to calculate the properties of the smear zone by adopting the proposed back calculation procedure. The variation of settlement with time is plotted in Figure 5.9. It should be noted that the settlement curve corresponding to the case with smear zone characteristics of $n=k_h/k_s=5$ and

$s=r_s/r_m=5$ agrees with the field measurements, which shows the developed back calculation procedure was validated in predicting the properties of the smear zone.

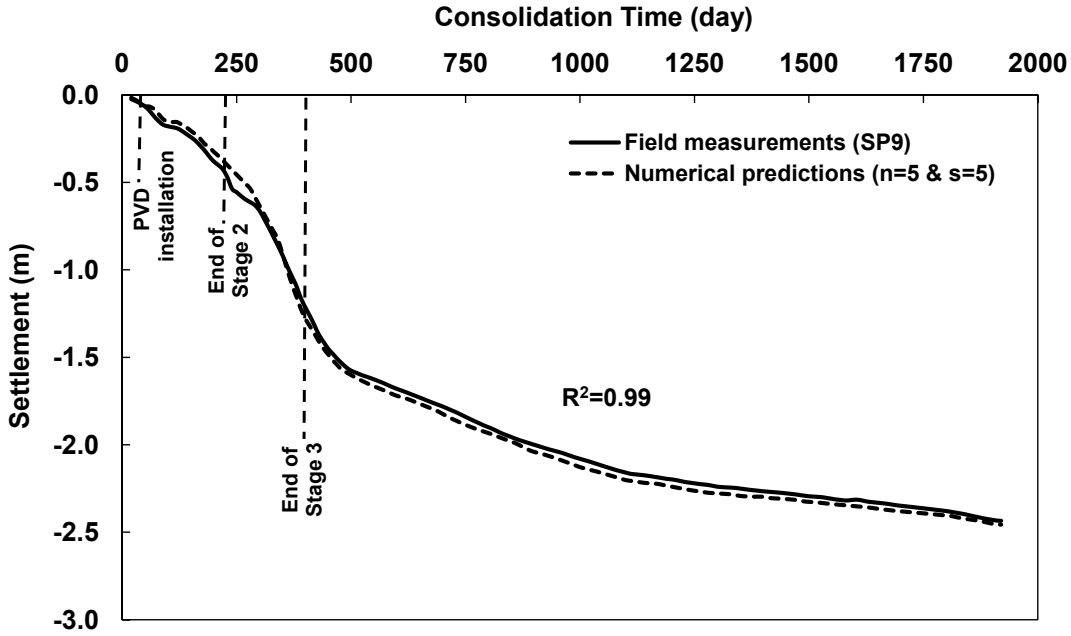

Figure 5.9 Numerical parametric study results; Cumbalum trial embankment at SP9

The predicted and measured values of excess pore water pressure at PC2, at the depth of 5.8 m, for the optimum combination of smear zone properties ($n=k_h/k_s=5$ and $s=r_s/r_m=5$) are shown in Figure 5.10. The overall numerical and measured variations in excess pore water pressure follow a similar trend in Figure 5.10, which agrees with the settlement curves obtained in Figure 5.9, although some discrepancies can be observed.

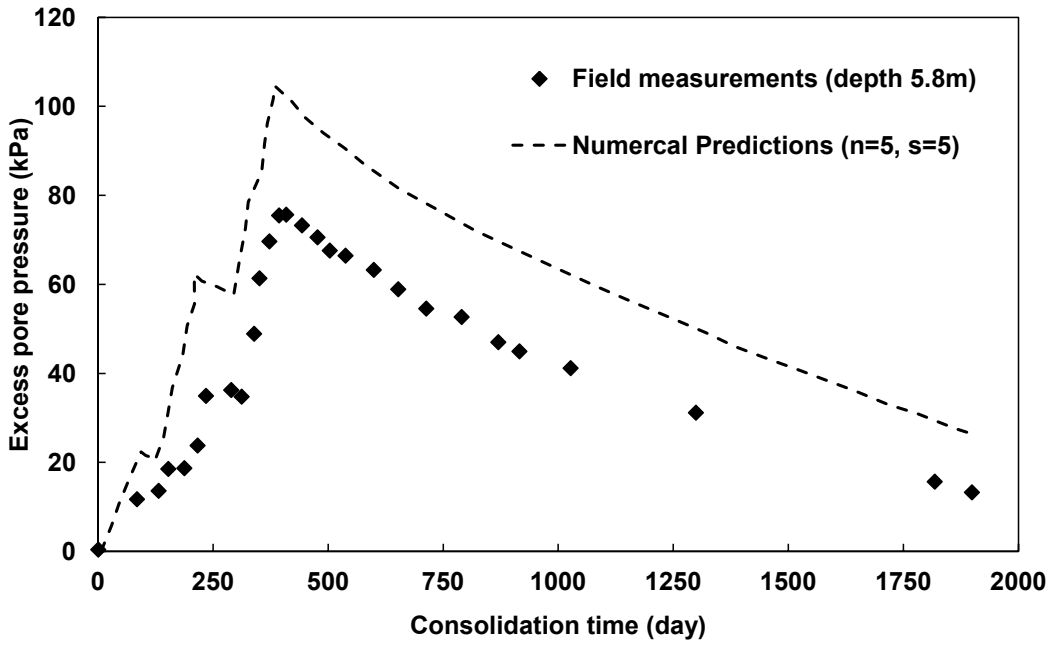

Figure 5.10 Variation of excess pore pressure over time for PC2 at a depth 5.8m

According to Figure 5.10 the excess pore water pressure curves experienced a growth during each stage of embankment construction, followed by a minor dissipation. The field observations by Kabbaj et al. (1988) and Leroueil (1997) showed that the maximum excess pore water pressure in the embankment occurred at the end of the construction process, which is confirmed in Figure 5.9, for both field measurements and numerical predictions. According to Figure 5.10 the maximum predicted excess pore water pressure of 100 kPa occurred at the end of the construction process, while this value for the field measurements was 80 kPa. This discrepancy can be attributed to numerous factors such as the uncertainty of the soil properties, the effect of the smear characteristics, inaccurate assumptions of soil behaviour, and an improper conversion of axisymmetric conditions to plane-strain (2D) analysis of multiple drains. The graphs in Figure 5.10 show that the predicted and measured excess pore water pressures gradually dissipated after the trail embankment had been constructed.

5.3 CASE STUDY 2: BALLINA BYPASS TRIAL EMBANKMENT

5.3.1 Introduction

The Ballina Bypass is part of the Pacific Highway upgrade in New South Wales, Australia. The NSW Minister for Planning approved the Ballina bypass project on 22 May 2003. The project provides 12 kilometres of dual carriageway, extending from south of Ballina at the intersection of the Bruxner and Pacific highway to north of Ballina at the intersection of Ross Lane at Tintenbar. According to Kelly and Wong (2009) the soft soil deposits within the flood plain can be up to 25 m thick, which may cause considerable settlement due to construction of the embankment. The deepest soft soil deposit (25 m) belongs to the section located beneath the southern abutment of a bridge crossing Emigrant Creek, near Cumbalum, as shown in Figure 5.11.

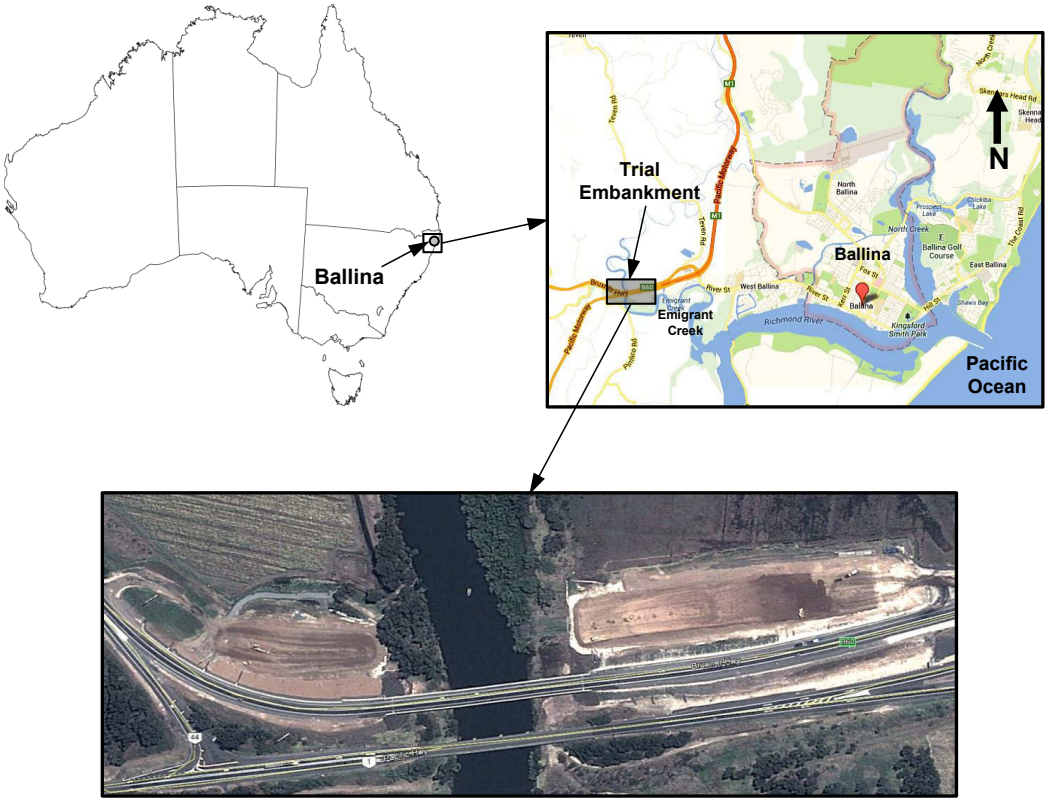

Figure 5.11 Location of the critical section and trial embankment of the Ballina Bypass (courtesy of Google Maps)

Conventional staged construction using surcharge and wick drains was assessed to take many years to complete due to the long consolidation periods required to maintain stability between fill lifts, and this time was not predicted within the timeframe for this project. The other ground improvement techniques such as soil mixing, stone columns, and piled embankments were considered to be too costly for such deep soft soil deposits. The membrane type of vacuum consolidation was considered to be the best ground improvement technique for more rapid construction than PVD assisted preloading, as well as being potentially more cost effective than ground inclusions (Kelly and Wong, 2009). This was the first application of the vacuum consolidation technique in Australia. A trial embankment north-west of Ballina was constructed to investigate the performance of this approach. Figure 5.11 shows the location of the trial embankment.

5.3.2 Geological Model and Subsoil Condition

The geology at the site of the vacuum consolidation trial consists of a uniform deposit of soft to firm silty clay overlying residual soil and bedrock. The silty clay is thickest at 25m, at the northern end of the site, adjacent to Emigrant Creek. The geological section for the Ballina Bypass trial embankment was interpreted by Bishop (2004), and is shown in Figure 5.12. A highly oxidised and indurated alteration horizon called MZ2 was identified, which affects the surface of the basement rocks and the full thickness of the overlying Stage 1 channel gravels and clays. Stage 3 overlies Stage 2, but it does not conform exactly, and it is separated by a second oxidation horizon called MZ1.

Kelly et al. (2008) reported that the geology at the site of the vacuum consolidation trial consists of a uniform deposit of soft to firm silty clay overlying residual soil and bedrock.

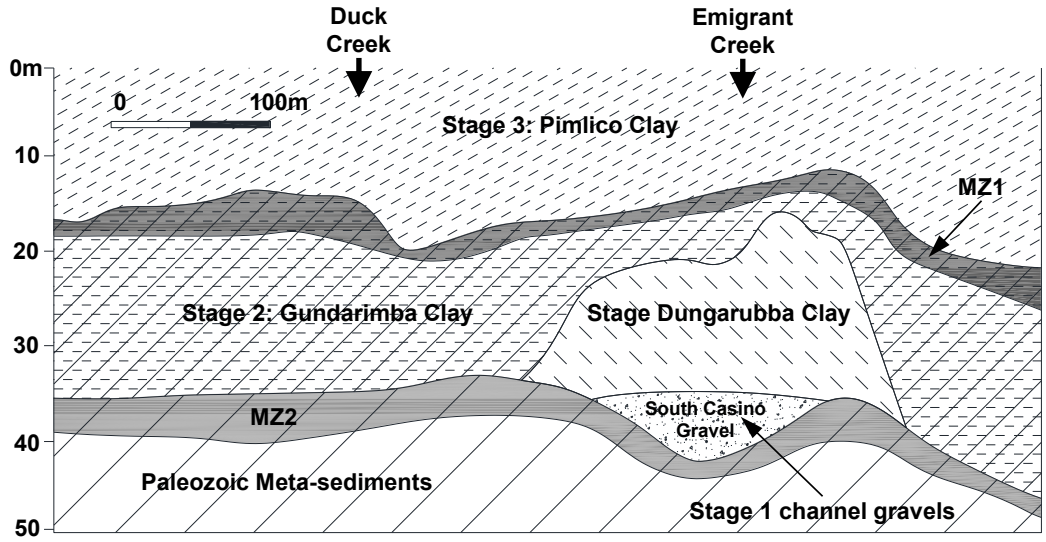

Figure 5.12 Interpreted section for Ballina Bypass trial embankment study area (after Bishop 2004)

5.3.3 Vacuum Consolidation and Embankment Construction

The vacuum consolidation system includes disconnected horizontal and vertical drains where hydraulic connectivity occurs through the sand blanket. The system was sealed by a 1mm thick membrane. Construction of the trial embankment began with the placement of a 1.5 m thick layer of sand with a unit weight of 21.5 kN/m^3 to act as a working platform for plants and the drainage layer. Then 34mm diameter circular vertical drains were installed, 1.0 m apart in a square pattern, and were then connected to 50mm diameter horizontal drains. The vertical drains were installed by a wick drain rig with a 110mm square base plate.

After instrumentation, a layer of fine grained sand was placed on top of the granular material to protect the membrane. The membrane was installed and a layer of fine grain sand was placed on top to protect it from punctures, and then general fill was placed on top of the sand. The embankment was separated into two sections, called Section A, the non-vacuum area, and Section B, the vacuum area. Figure 5.13 shows the location of the field instrumentation, including the surface settlement plates and piezometers.

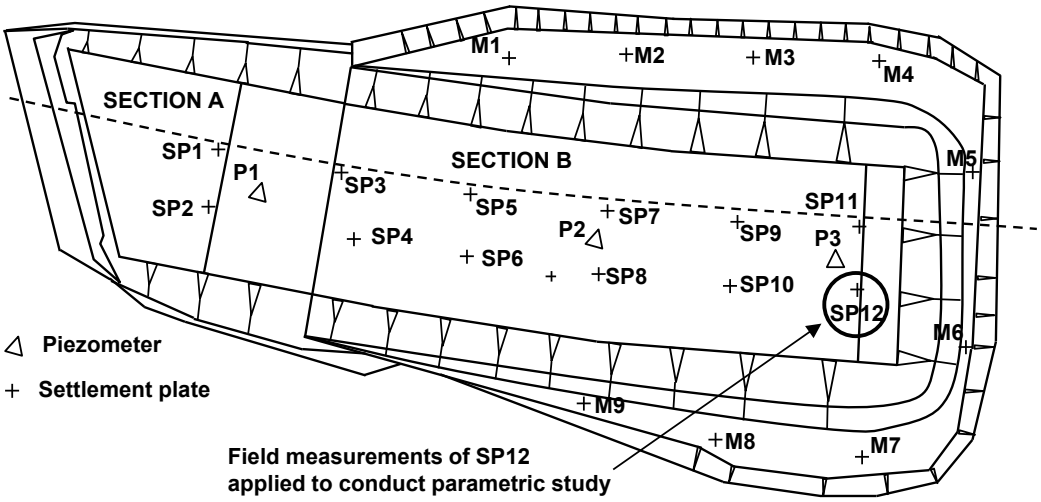

Figure 5.13 Layout of instrumentation for the trial embankment at Ballina Bypass (modified after Kelly and Wong 2009)

The embankment was constructed in stages using a granular material ($\gamma_s = 20$ kN/m^3) up to a height of 8.5 m. A detailed cross section of the embankment and subsoil profile (at the location SP12) is shown in Figure 5.14, and was used for numerical modelling. A vacuum pressure of -70 kPa was applied for a period of 400 days and then removed. The construction history of the trial embankment is shown in Figure 5.15.

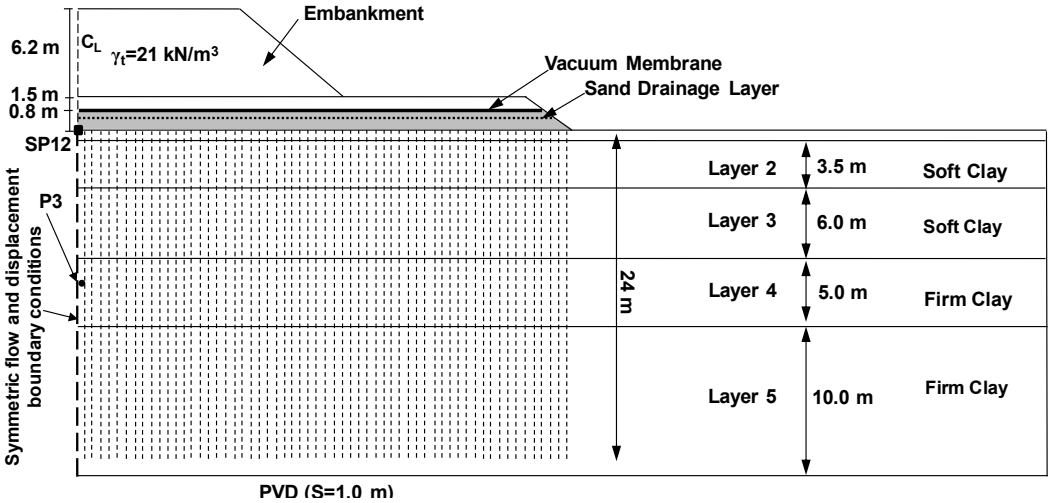

Figure 5.14 Cross section of the Ballina Bypass trial embankment and subsoil profile

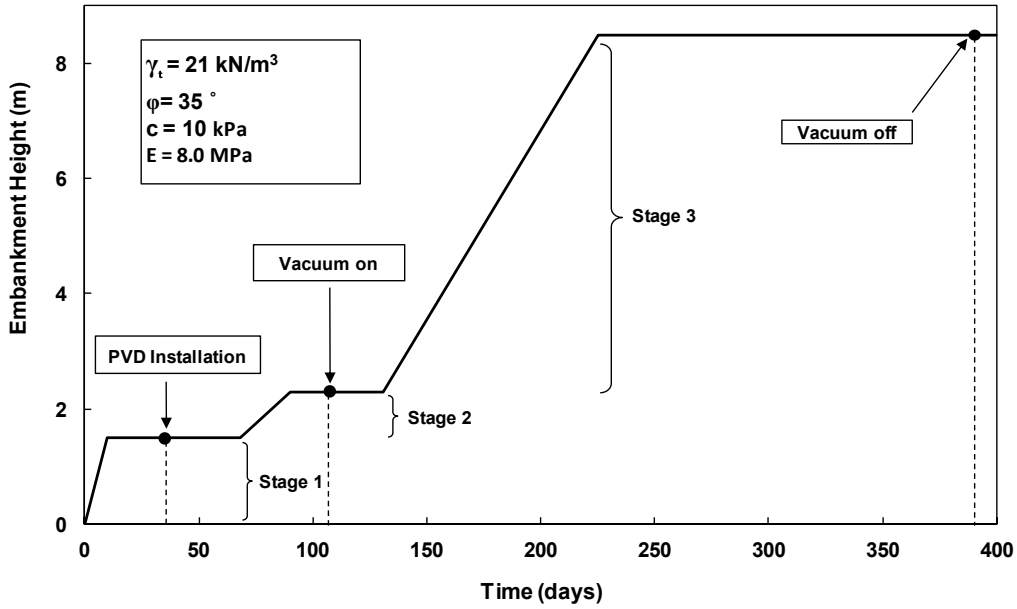

Figure 5.15 Construction history of Ballina Bypass trial embankment

5.3.4 Numerical Simulation

The consolidation behaviour of soft clay beneath the Ballina Bypass trial embankment was simulated using the developed FLAC code, incorporating the modified Cam-Clay model. A fully saturated and coupled flow-deformation simulation was carried out to model the dissipation of pore water pressures. The discretised plane-strain finite difference mesh, composed of quadrilateral elements, is shown in Figure 5.16(a), where only half of the trial embankment was considered by exploiting its symmetry. FLAC sub-divided each quadrilateral element into triangular elements, as shown in Figure 5.16(d). The pore pressures were assumed to vary linearly in a triangular element.

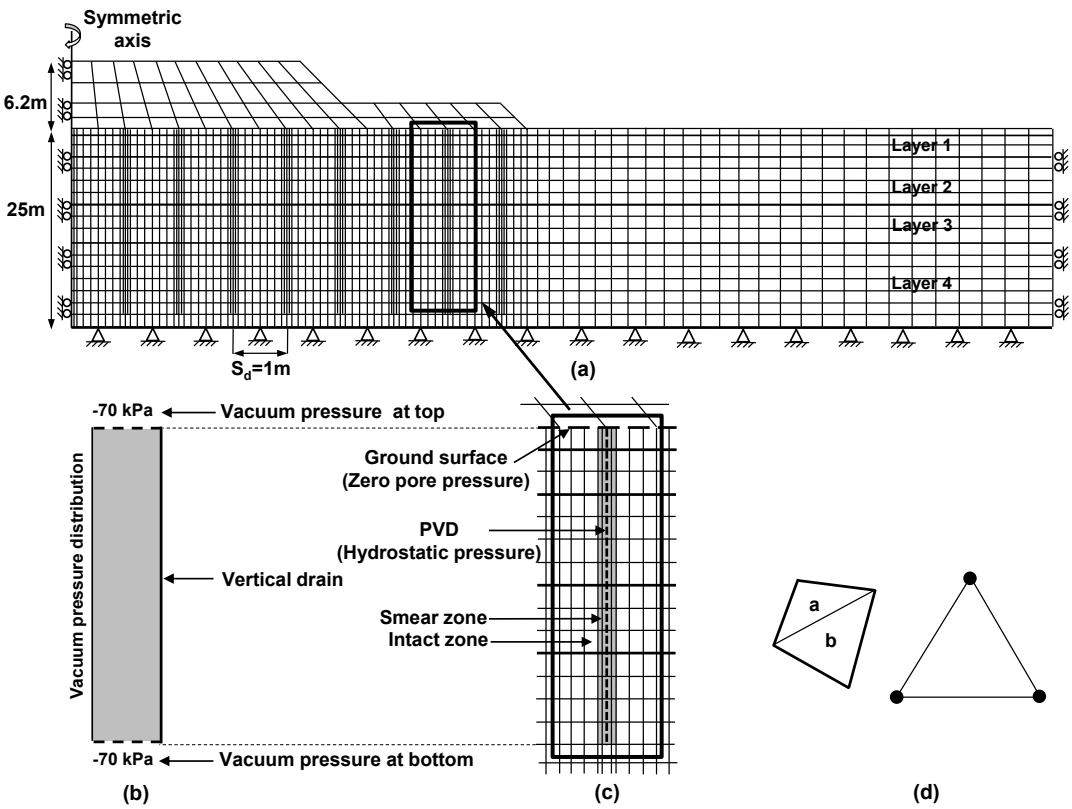

Figure 5.16 (a) Discretised finite-difference mesh of Ballina Bypass trial embankment, (b) Variation of vacuum pressure along the vertical drain, (c) The pattern of meshes in the smear zone and undisturbed region, (d) FLAC zone composed of overlaid triangular elements

To model the PVD, illustrated in Figure 15.16(c), the hydrostatic pore water pressure was considered to be along the vertical drains (before applying the vacuum pressure), and to model the drainage boundary the excess pore pressure at the ground surface was assumed to be zero. According to the field measurements, uniform distribution of vacuum pressure was considered and a constant negative pore pressure of -70 kPa was applied along the vertical drain, as shown in Figure 15.16(b). The parameters adopted for the layers of subsoil, based on the results of the site investigation and laboratory tests used in the numerical analysis, are summarised in Table 5.3.

Table 5.3 adopted for the layers of subsoil for Ballina Bypass trial embankment near SP12

Depth: m	λ	κ	$e_\circ$	γ_s (kN/m^3)	k_h (10^{-10} m/s)	k_v (10^{-10} m/s)	OCR
0.0 - 0.5	0.57	0.057	2.75	14.5	3.0	1.5	2.5
0.5 - 4.0	0.57	0.057	2.75	14.5	6.0	3.0	1.8
4.0 - 10.0	0.67	0.067	2.87	14.5	6.0	3.0	1.7
10.0 -15.0	0.47	0.047	2.61	15.0	15	7.5	1.3
15.0 - 25.0	0.40	0.040	2.09	15.0	15	7.5	1.2

Note: λ and κ are slopes of the specific volume versus $ln(p')$ curves for compression and swelling, respectively, where p' is the mean effective stress; $e_\circ$ is the initial void ratio; γ_s is the unit weight; k_h is the horizontal permeability of intact zone; k_v is the vertical permeability of intact zone; and *OCR* is the over consolidated ratio

Field measurements at settlement plate No.12 (SP12) and piezometer P3 (Figure 5.14) in Section B, in conjunction with the soil profile data, were used with the FLAC code to validate the developed back calculation procedure. The numerical results and field measurements are compared in 5.17. Both the measured and predicted vertical displacements indicated that the consolidation rate had accelerated due to the installation of vertical drains and applying the vacuum pressure.

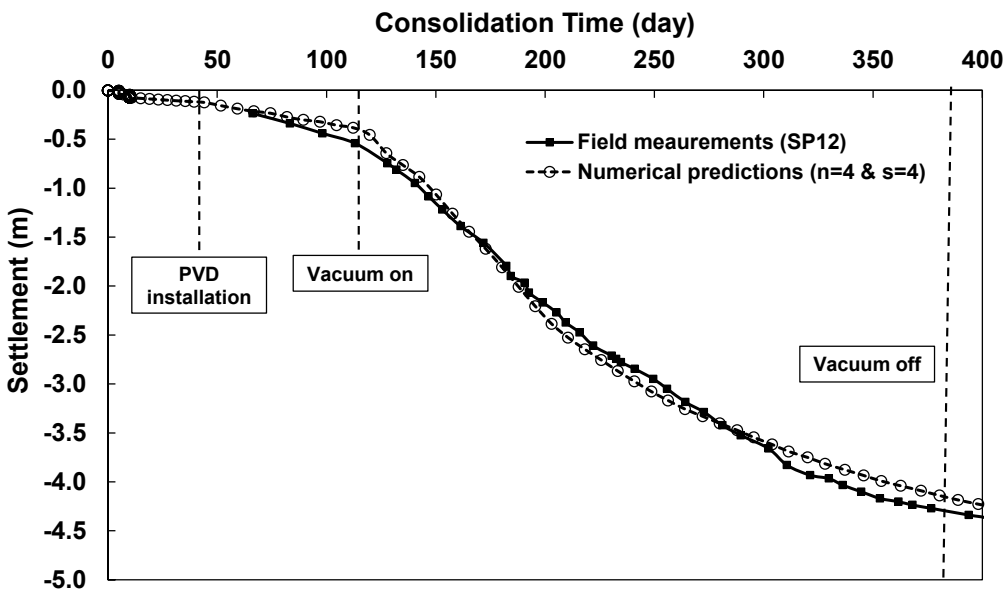

Figure 5.17 Results of numerical parametric study; Ballina Bypass trial embankment at SP12

According to the numerical results, the case with smear zone properties of $s=r_s/r_w=4$ and $n=k_h/k_s=4$ had the best fit with the field measurements, which verified the

validity of the back calculation procedure, when it was integrated with the developed numerical code and then used for a reliable estimation of the properties of the smear zone.

The comparison between the predicted and measured variations of excess pore water pressure over time for the transducer P3 located 11.8 m deep, and 0. 5 m away from the centreline of the embankment for the case with back calculated smear zone properties of *n=4* and *s=4* are shown in Figure 5.18.

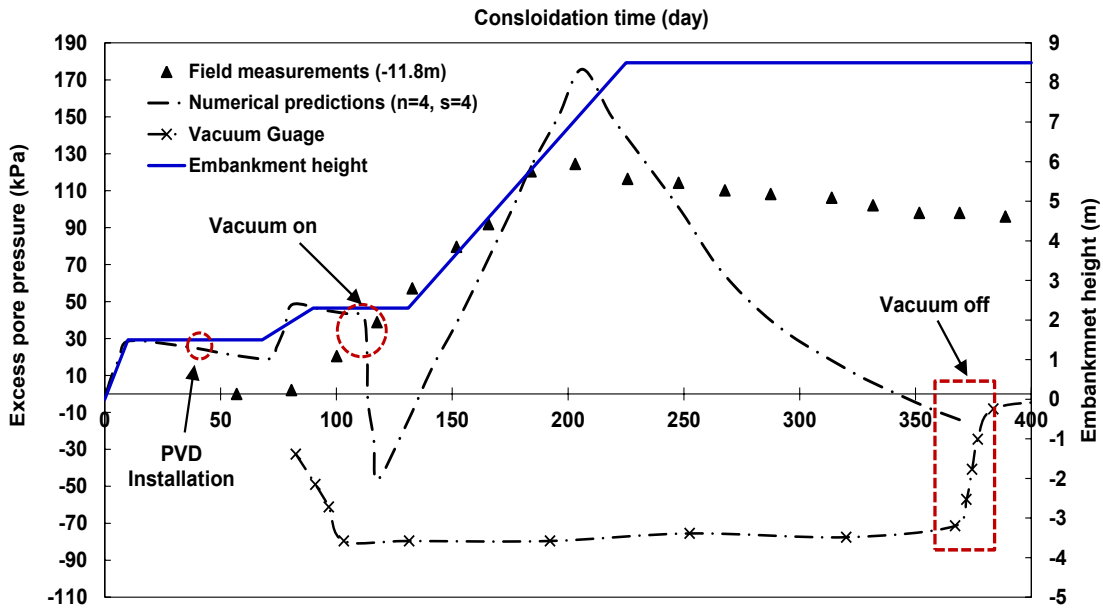

Figure 5.18 Variation of excess pore pressure over time for P3 at a depth 11.8m

Figure 5.18 shows that the calculared excess pore water pressure increases due to the construction of each segment of the trial embankment and then gradually dissipates. A sudden reduction of -70 kPa occurred in the numerical excess pore pressure curve immediately after the vacuum pressure was applied, followed by an incremental trend due to the embankment being constructed. In Figure 5.18, the measured excess pore water pressures due to the staged construction of the trial embankment and the application of negative vacuum pressure are plotted separately, while the numerical predictions are plotted as a combined graph.

Some discrepancies can be observed between the measured and predicted excess pore water pressures in Figure 5.18. It can be noted that the maximum predicted excess pore water pressure occurred at the end of trial embankment construction and were equal to the surcharge applied due to this construction, while

the value for the field measurements were slightly less than the applied pressure. Robinson (1999) reported that the maximum value of excess pore water pressure is usually less than the applied pressure increment, which can be related to the relationship between volumetric compliance of the pore water pressure measuring system and the volume compressibility of the soil skeleton.

Furthermore, field measurements showed that the excess pore pressure values did not dissipate immediately at the end of loading or construction, but in fact increased or stabilised for a period before decreasing. The abnormal behaviour of excess pore water pressure has been reported in many field studies (Conlin and Maddox, 1985; Kabbaj et al., 1988; Rowe and Li, 2002). Two main reasons have recently been proposed to explain that anomalous behaviour; the Mandel-Cryer effect and volumetric strain softening. Schiffman et al. (1969) reported that the Mandel-Cryer effect is due to the increase in total stress caused by the volumetric strain compatibility. The Mandel-Cryer effect is called after Mandel (1953) and Cryer (1963), based on their observations related to the abnormal generation of excess pore water pressure. Cryer (1963) analysed the process of consolidation by applying pressure all around a saturated porous sphere. Since the surface of the sphere is free to drain, the total stress at the centre of the sphere increased temporarily under the applied pressure, because the dissipation of excess pore water pressure at the centre was delayed. This results in an increasing excess pore water pressure for some time before dissipation begins. In addition, the increase or delay in the dissipation of excess pore water pressure may be the result of volumetric strain softening due to unstable behaviour during consolidation when the stress paths depart from the failure line. The constitutive model developed by Kimoto and Oka (2005) can capture the increase in pore water pressure due to stagnation. Moreover, as Asaoka et al. (2000) reported, since the decay of over-consolidation is much faster than degradation of the structure in clay during consolidation, softening becomes possible with volume compression even under a considerably low stress ratio.

5.4 CASE STUDY 3: SUNSHINE MOTORWAY TRAIL EMBANKMENT

5.4.1 Introduction

The Sunshine Coast is one the fastest growing regions in Australia. The continued economic and population growth has increased the pressure on the region's main traffic corridor, the Sunshine Motorway. According to the results of a site investigation, the subsoil at the proposed development route consists of very soft and saturated marine clays, which presented difficulties in developing the new alignment. In order to discover how the foundation would respond under loading, and to evaluate the effectiveness of various ground improvement techniques on these marine clays, a fully instrumented trial embankment was constructed in 1992, located in the Maroochy Shire, Queensland, Australia. This trial embankment was monitored by the Queensland Department of Main Roads (QDMR), Brisbane, Australia. The location of the study area is illustrated in Figure 5.19.

Figure 5.19 Location of the Sunshine Motorway study area, (courtesy of Google Maps)

5.4.2 Subsoil Condition

The subsoil profile consists of sensitive silty clay with an approximate thickness of 11m, overlying a layer of sand with a thickness of about 6m. A thin soft clay layer underlies the sand and extends to a depth of 18m, and another layer of sand is encountered below 18m. The properties of the top sensitive silty clay with depth, including the water content, Atterberg limits, bulk unit weight, undrained shear strength and the compression index ratio are indicated in Figure 5.20.

According to Figure 5.20, the compression index ratio varies from 0.15 to 0.50. The recompression ratio was found to be about 10 times smaller than the compression index ratio (QDMR Report, No.R1765, June 1991). The soft clay was classified as lightly over consolidated soil because the over consolidation ratio (OCR) varied from 1.0 to 1.6.

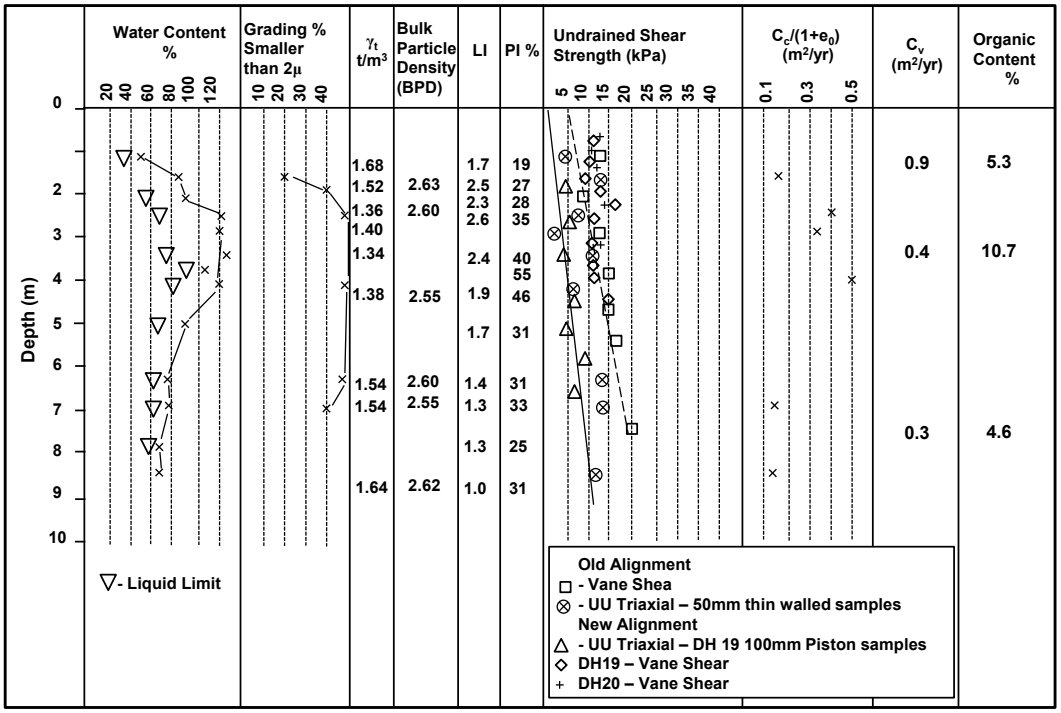

Figure 5.20 Profile of the Geotechnical characteristics (Sunshine Motorway Stage 2 Interim Report, 1992)

5.4.3 Installation of Vertical Drains and Embankment Construction

Figure 5.21 illustrates the base area of the trial embankment with dimensions of approximately 90m by 40m, which was divided into 3 separate sections (Sections A, B, and C). Vertical drains (Nylex Flodrain) were installed in a triangular pattern in sections A and C with the drain spacing of 1m and 2m, respectively. Section B represents the zone without PVDs.

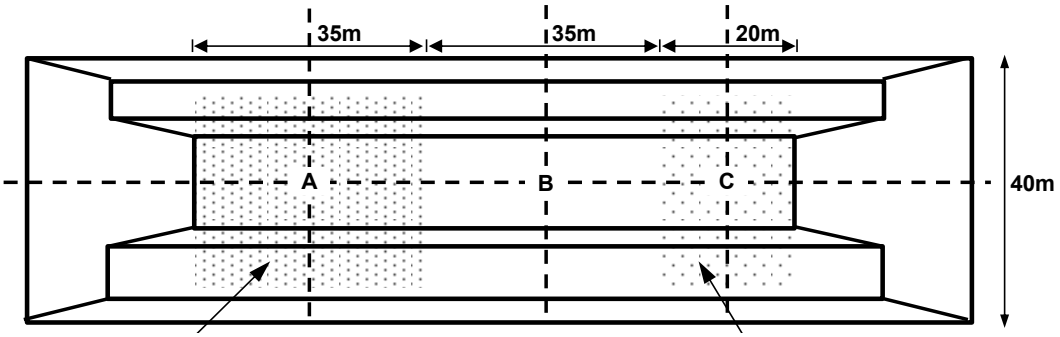

Figure 5.21 Plan view of Sunshine Motorway trial embankment

The subsoil conditions are relatively uniform throughout the site, and consist of silty/sandy clay approximately 11 m thick, overlying a layer of dense sand approximately 6 m thick. Of the sections available in this trial project, the section with vertical drain spacing of 2 m was selected for numerical simulation. Prefabricated vertical drains (Nylex Flodrain, 100×4 mm^2) were installed in a triangular pattern. A working platform 0.65 m thick (500 mm thick drainage layer composed of 7 mm gravel, plus 150 mm of selected fill) was placed on the natural ground surface for access by construction traffic (Sathananthan et al. 2008). PVDs were installed from the working platform to a depth of 11 m. The embankment was constructed in stages using a loosely compacted granular material ($\gamma_t \approx 19$ kN/m^3) up to a height of 2.3 m (Sathananthan et al. 2008).

A schematic cross section of the trial embankment with the selected instrumentation points is shown in Figure 5.22. Two 5m and 8m wide berms were constructed on the sides of the embankment to rectify the problem of stability. The location of the settlement gauges (SC) and piezometers (pneumatic-PP) are illustrated in Figure 5.22.

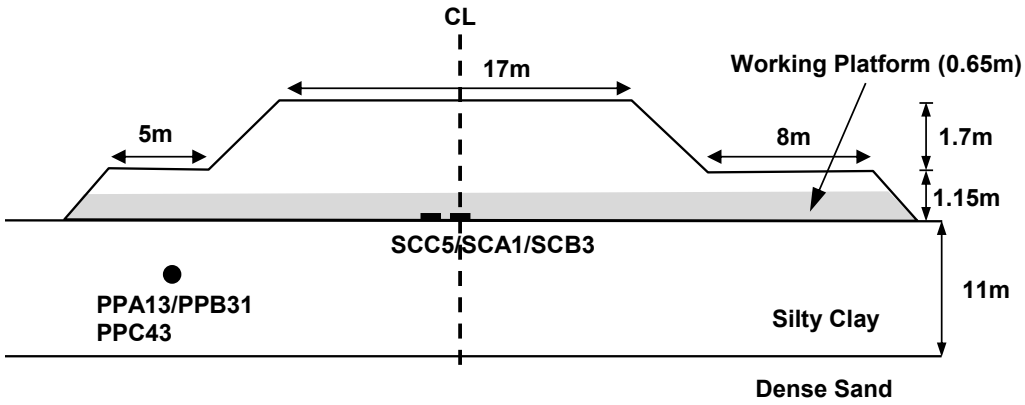

Figure 5.22 Typical cross-section of embankment with selected instrumentation points (after Sathananthan et al. 2008)

5.4.4 Numerical Simulation

The Sunshine trial embankment was modelled numerically to verify the numerical analysis using the developed FLAC code. The equivalent plane-strain model was used to simulate the embankment, and the modified Cam-Clay model was adopted as the soil constitutive model to simulate the behaviour of the soft clay. To model the prefabricated vertical drains, a zero excess pore pressure boundary was considered along the PVD. The smear zone was simulated by applying the mechanical properties of undisturbed soil with a reduced coefficient of permeability. The instrumented side of the trial embankment was simulated due to symmetry and to reduce the time needed for numerical analysis. A detailed cross section of the simulated embankment with the selected instrumentation point is shown in Figure 5.23. A sample of the generated mesh pattern adopting the developed code is shown in Figure 5.24.

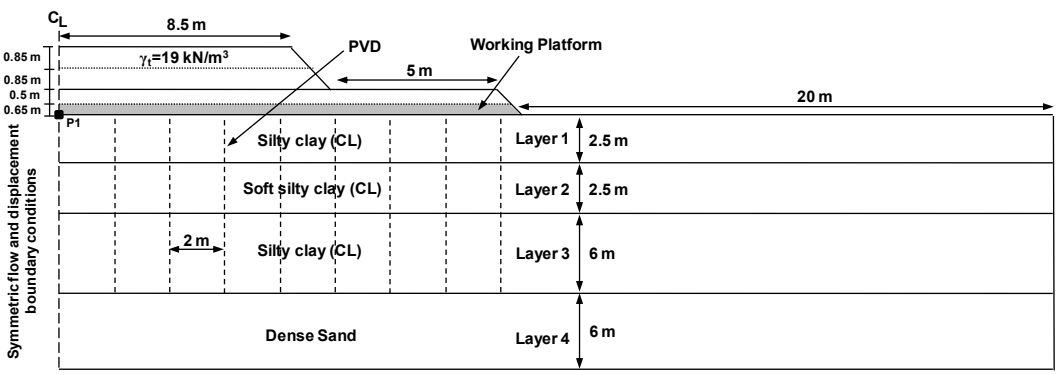

Figure 5.23 Cross section of the Sunshine trial embankment and the subsoil profile

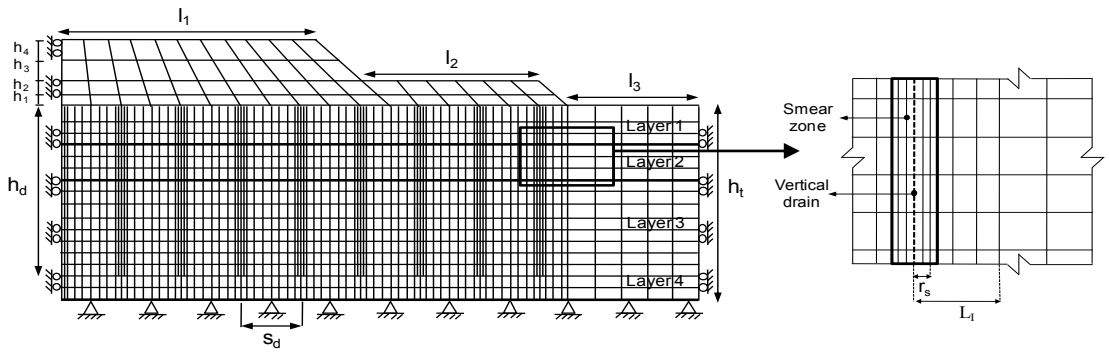

Figure 5.24 Sample of mesh grid pattern for an embankment considering the smear zone and undisturbed region; (r_s= smear zone extent; L_I= intact zone extent; h_t= depth of the soil profile; and h_d= length of the vertical drain, s_d= drain spacing)

It should be noted that the equivalent plane-strain permeability to analyse the PVDs was calculated using Equations 2.30 to 2.32, as proposed by Indraratna et al. (2005b). Figure 5.25 illustrates the construction history of the embankment. The properties of the subsurface ground profile are summarised in Tables 5.4 and 5.5.

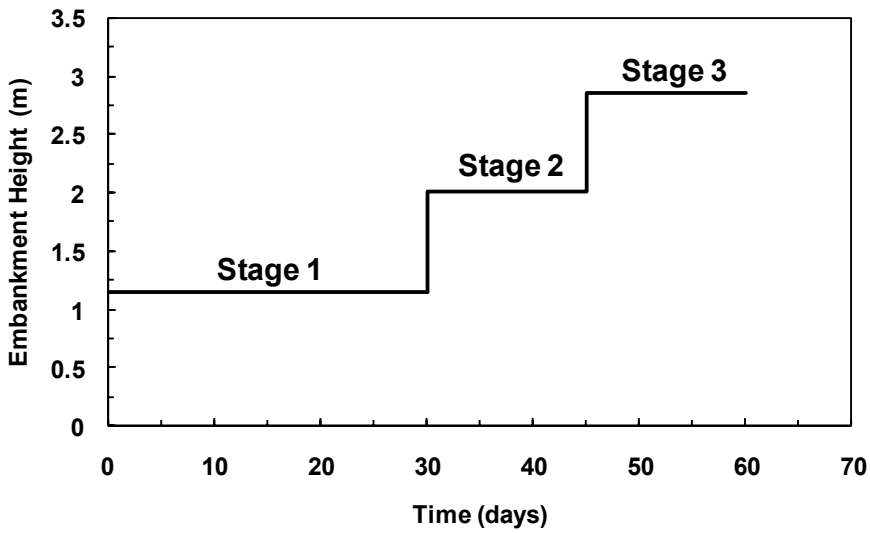

Figure 5.25 Construction history of the trial embankment

Table 5.4 Adopted properties for the numerical simulation (after Sathananthan et al. 2008)

Layer	Soil type	M	λ	κ	μ	$e_\circ$	γ_s (kN/m^3)	k_{hp} (10^{-9} m/s)	k_h/ k_v
1	Silty clay	1.20	0.494	0.0494	0.3	1.6	16.4	9.72	2
2	Soft Silty clay	1.20	2.016	0.2016	0.3	2.2	13.7	0.34	2
3	Silty clay	1.18	0.532	0.0532	0.3	1.8	15.9	0.42	2

Note: M is the slope of the critical state line; λ and κ are slopes of the specific volume versus ln(p′) curves for compression and swelling, respectively, where p′ is the mean effective stress; μ is the Poisson's ratio; $e_\circ$ is the initial void ratio; and k_{hp} is the permeability of intact zone in the plane-strain condition.

Table 5.5 Applied Properties for Sand Layer (after Sathananthan et al. 2008)

Layer	Soil type	c′(kPa)	φ′ (deg)	E (MPa)	μ
4	Dense Sand	13.5	35	7.5	0.3

The settlement gauge P1 (located on the centreline at the interface of the embankment and the ground) was used to verify the numerical predictions against the field measurements, and the results are illustrated in Figure 2.26. It can be noted that the FLAC results are in the best agreement with the field data assuming k_h/k_s=4 (the permeability ratio) and r_s/r_m=3 (the extent ratio), which confirms the validity of the developed FLAC code in a numerical simulation of PVD assisted preloading projects.

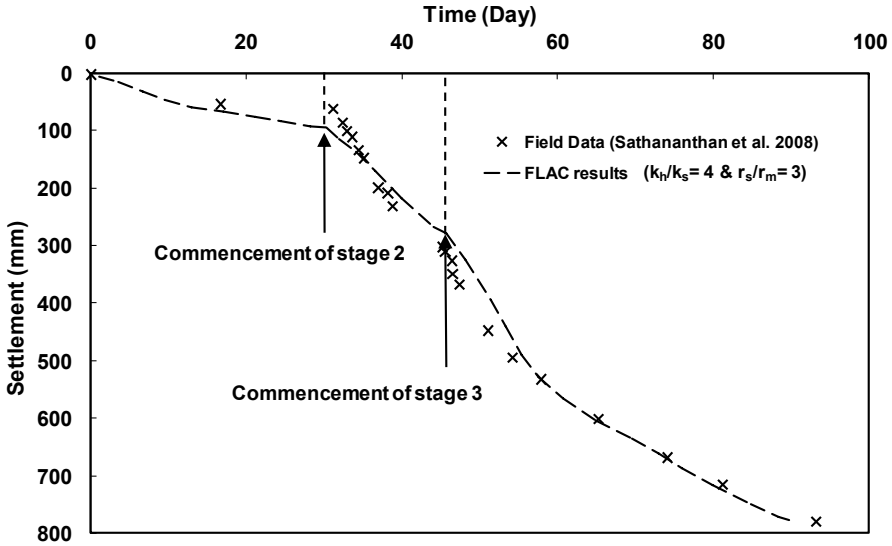

Figure 5.26 Comparison of numerical results with filed data (for settlement plate P1)

Figure 5.26 shows there are more disparities between the numerical predictions and the field measurements in the initial stages of loading, which can be the result of surcharge placement. For example, the settlement predicted at the commencement of stage 2 was 95 mm, which is 60% greater than the field measurement of 60 mm, whereas the difference was about 10% at the commencement of stage 3.

5.5 CHITTAGONG AIRPORT TRIAL EMBANKMENT

5.5.1 Introduction

Chittagong Port is the largest sea port in Bangladesh. A container yard was constructed which covered an area of 60700 m^2 and was designed to support a container load producing a contact pressure of approximately 56 kPa (Dhar et al. 2011). The site is located on the banks of the Karnafully River beside the Bay of Bengal in the Indian Ocean, as shown in Figure 5.27. According to the site investigations, the soil profile contains soft to very soft clayey silt/silty clay layer at depths of 0 to 3.5m below the ground surface with a thickness of 3.0m to 7.0m. A ground improvement work was designed and carried out to pre-consolidate the soft subsoil before the yard was constructed.

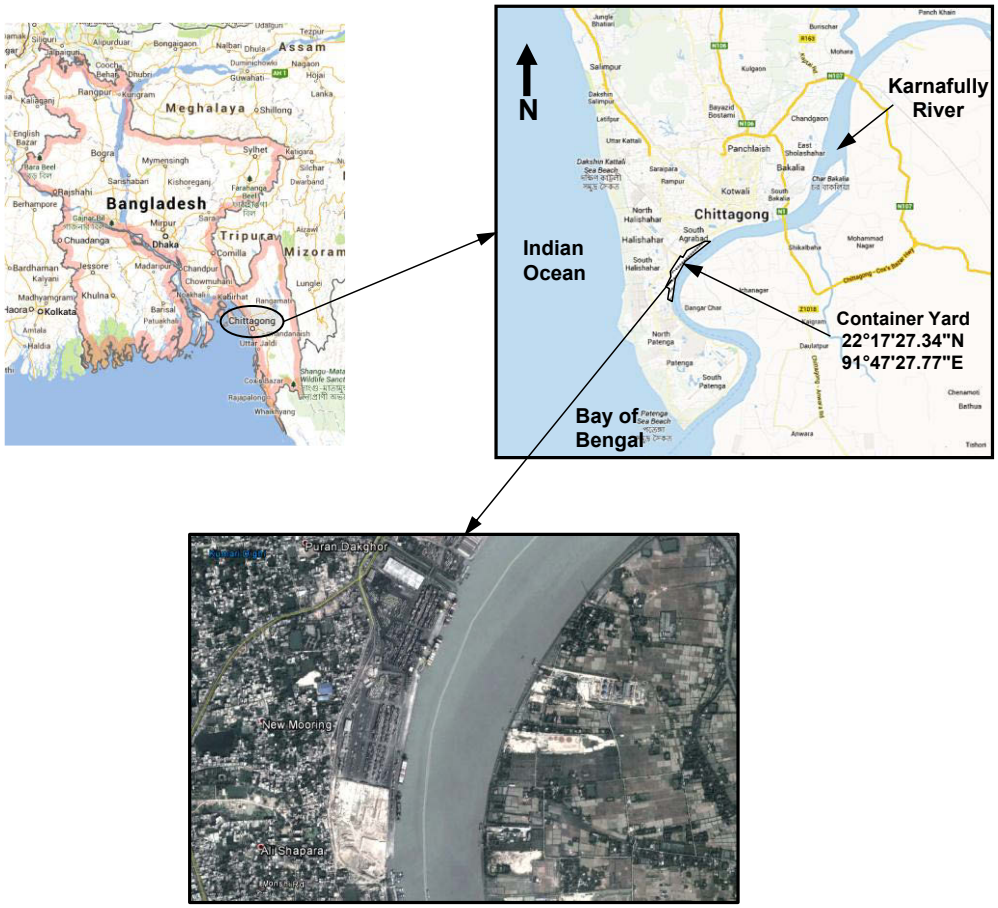

Figure 5.27 Location of the container yard at Chittagong Port (courtesy of Google Maps)

5.5.2 Subsurface Conditions

The site is a tidal plain on a narrow strip between the hilly Chittagong uplands and the Bay of Bengal. The surface geology is mainly governed by shallow sea water and flood plain activities of the Karnafully River and its tributaries. Fifteen boreholes were drilled to collect samples of the subsoil. The distribution of these boreholes over this area is shown in Figure 5.28.

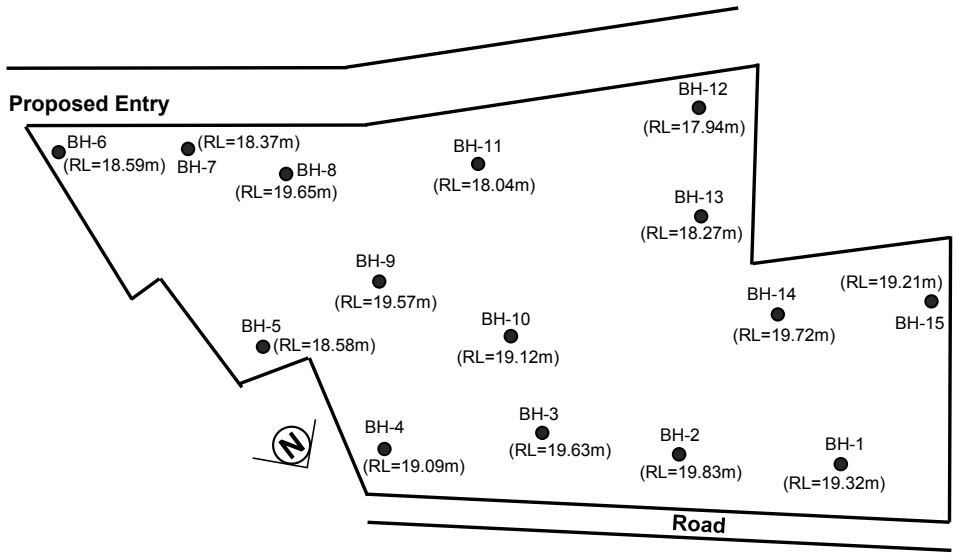

Figure 5.28 Approximate locations of the boreholes, Chittagong Airport trial embankmnet (after Dhar et al., 2011)

125 mm diameter boreholes were drilled to depths ranging from 14m to 24.5m below the ground surface to collect disturbed and undisturbed samples of soil. The results of this site investigation show that the subsoil profile includes very soft to firm silty clay, or clayey silt and fine grained silty sand, with some decomposed materials near the ground surface. The general subsurface condition is illustrated in Figure 5.29.

The condition of the ground at this site varied from borehole to borehole. At the ground surface the soil was generally fill materials consisting of light brown clayey silt or brown silty sand/sandy silt. The clayey silt was firm to stiff and the silty sand or sandy silt was medium dense. The fill materials extended from the ground surface and continued down to depths of 0 to 3.5 m below the existing grade.

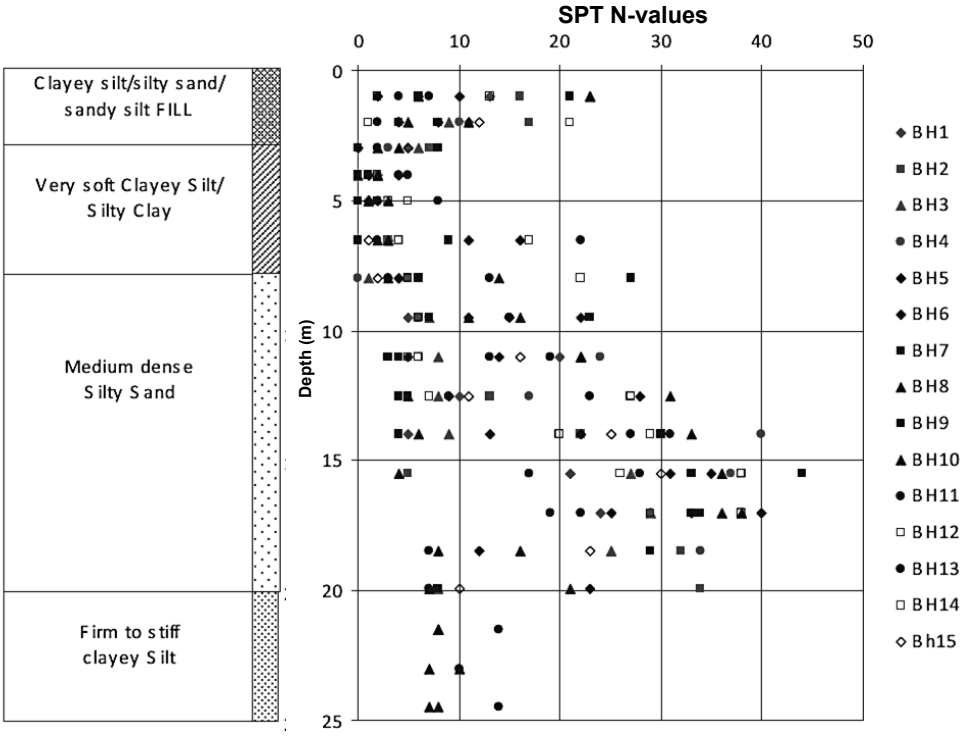

Figure 5.29 General ground profile along with SPT N-values (after Dhar et al., 2011)

5.2.3 Soil Properties

An extensive laboratory investigation was carried out by Dhar et al. (2001) to identify the soil and determine the geotechnical design parameters. The soil samples were classified conducting the Unified Soil Classification System (USCS). Unconsolidated undrained and consolidated undrained triaxial tests were performed to determine the strengths of the cohesive soil. An analysis of the grain size and consolidated drained direct shear tests were conducted for the non-cohesive soil. Table 5.6 indicates the Atterbeg limits, moisture content, and specific gravity of the samples. The bulk unit weight of the soil varied from 20 kN/m^3 to 23 kN/m^3.

Table 5.6 Properties of the cohesive soil samples (Dhar et al., 2011)

Borehole No.	Depth (m)	Natural Water Content (%)	G_s	LL	PL	PI
BH-1	3.1 – 3.55	33.7	2.75	45	26	19
BH-3	34.10 – 4.55	41.15	-	47	28	19
BH-4	6.80 – 7.25	37.55	2.71	32	23	9
BH-5	1.10 – 1.55	35.8	-	56	31	25
BH-5	4.10 – 4.55	51	2.74	43	27	16
BH-7	3.10 – 3.55	50.8	2.75	43	28	15
BH-8	3.10 – 3.55	39.15	-	48	29	19
BH-9	4.10 – 4.55	48.25	2.74	47	27	20
BH-12	2.10 – 2.55	50.8	2.77	51	30	21
BH-13	2.10 – 2.55	36.5	-	41	25	16
BH-14	4.10 – 4.55	45.25	2.76	44	27	17
BH-15	4.10 – 4.55	38.35	-	42	27	15

Nine Shelby tube samples collected from the silty clay or clayey silt layer were used to determine the compressibility and permeability properties using one-dimensional consolidation tests. According to Dhar et al. (2011), the values of C_c from twelve tests were between 0.17 and 0.45 with the average value being equal to 0.3. The recompression index, C_r, was calculated to be between 0.05 and 0.07. The initial void ratios (e_0) of these samples varied from 1.04 to 1.62, with an average of 1.28. Pre-consolidation pressures calculated using the Cassagrande method were found to range between 30 kPa and 50 kPa, which were less than the ground stresses expected under a container load of 56 kPa. The coefficient of vertical permeability and the coefficient of horizontal permeability were found to range from 0.032 m/year to 0.063 m/year and from 0.047 m/year to 0.095 m/year, respectively, within the range of design stress (i.e. 60 to 100 kPa).

5.5.4 Installation of Vertical Drain and Embankment Construction

The results from the laboratory tests and site investigation were used to design soil improvement works for the Chittagong Port, as indicated in Figure 5.27. The thickness of the soft soil and the length of prefabricated vertical drains (PVDs) were 7 m and 9 m long respectively. PVDs with the dimensions of 100mm × 4mm were

installed in a square pattern at a spacing of 1.0 m (centre to centre) to accelerate consolidation. The properties of the applied PVDs are summarised in Table 5.7.

Table 5.7 Properties of the applied PVD (Dhar et al., 2011)

Properties	Specified value
Drains	
Weight per unit length	70 gm/m
Width	100 mm
Thickness	4 mm
Water discharge capacity	2840 m^3/year
Core	
Tensile strength	750 N
Filter Jacket	
Apparent opening size (AOS)	90 µm
Grab tensile strength	400 N
Elongation at break	50 %
Puncture resistance	130 N
Burst strength	800 kPa
Permeability	6310 m/year

According to the designs, a surcharge pressure of 56 kPa was needed for the preloading process, which is equivalent to a 3.0 high embankment and a unit weight of 18 kN/m^3 for the sand.

According to Dhar et al. (2011), the following sequences were conducted to construct the embankment on top of the soft soil:

- Preparation of the existing ground
- Placement of local sand to raise the ground level where required
- Placement of a drainage blanket of coarse sand
- Installation of Prefabricated Vertical Drains (PVDs)
- Pre-loading

An approximately 150 mm thick layer of sand was placed on top of the levelled ground. A drainage blanket of coarse sand was then placed over the sand to facilitate the drainage of water through the vertical drains. The expected consolidation was expected to be compensated for by the 450mm thick layer drainage blanket. The drainage blanket was constructed in two stages, (i) the lower 250 mm thick layer was

placed before the PVDs were installed to provide a working platform for their installation, and (ii) the remainder of the drainage layer was placed after the PVDs were installed to allow the drains to discharge into the sand layer. The PVDs were installed using a mandrel combined with an anchor having a maximum cross sectional area of 7000 mm^2. The PVDs were installed to a depth of 9 m below ground level to cover the full depth of the soft soil. The remaining 200 mm thick layer of coarse sand was placed on top of the final surface after the PVDs installation, and then compacted and levelled to place the settlement measuring gauges.

Thirty settlement measuring gauges were used to measure the rate of vertical displacement. A schematic plan of the approximate locations of settlement gauges is shown in Figure 5.30. A settlement gauge is illustrated in Figure 5.30(a), and it includes a base plate and a stand pipe. The base plate for the gauge was placed on top of the levelled granular layer, while the elevation of the top of the stand pipe was monitored to obtain the ground settlement.

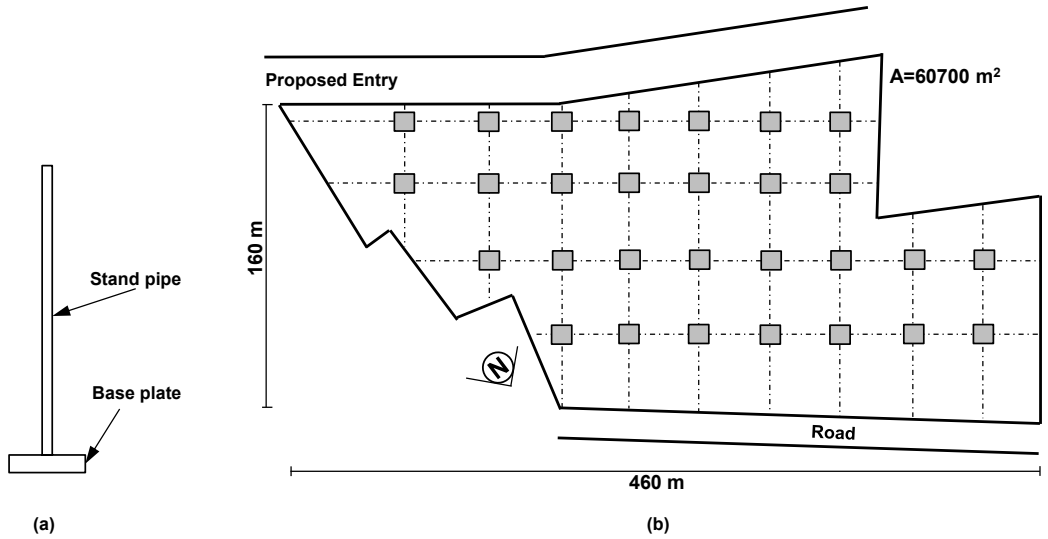

Figure 5.30 Settlement monitoring program, (a) Settlement gauge and (b) Points of settlement measurement (schematic plan) (after Dhar et al. 2011)

The pre-loading process was conducted by constructing a 3.0m high embankment over the drainage. The surcharge material was placed in two layers of approximately equal thickness. The sand bags or brick stacks were used to contain the sides of the

surcharge load vertically along the boundary of the area. Details of the ground improvement work are shown in Figure 5.31.

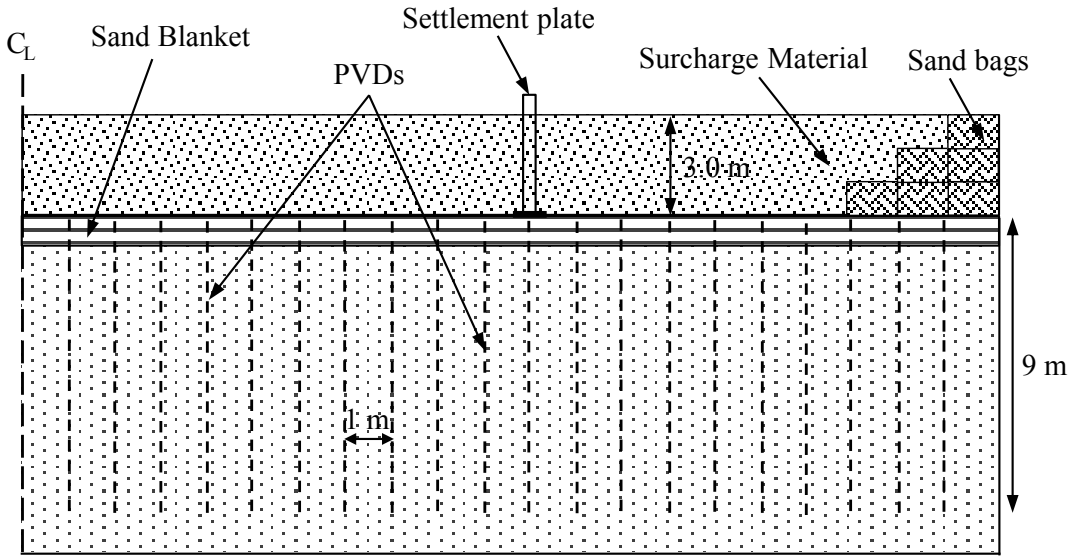

Figure 5.31 Schematic details of the ground improvement works (after Dhar et al., 2011).

5.5.4.1 Monitoring of Settlement

The settlement rates were monitored immediately after the embankment was constructed and continued until consolidation was completed. Immediately after placing the surcharge to its full height (in 10 - 12 days), the ground settlements were measured using the settlement gauges. The first measured settlement for each gauge was called the "initial settlement".

The settlement rates at different locations are plotted in Figure 5.32. These measurements began with an initial settlement of 80-300 mm due to the placement of the 3.0 m high surcharge. The maximum settlements measured during the monitoring period varied from 220 mm to 415 mm. Figure 5.32 reveals that the settlements were almost completed after 30 to 52 days of preloading.

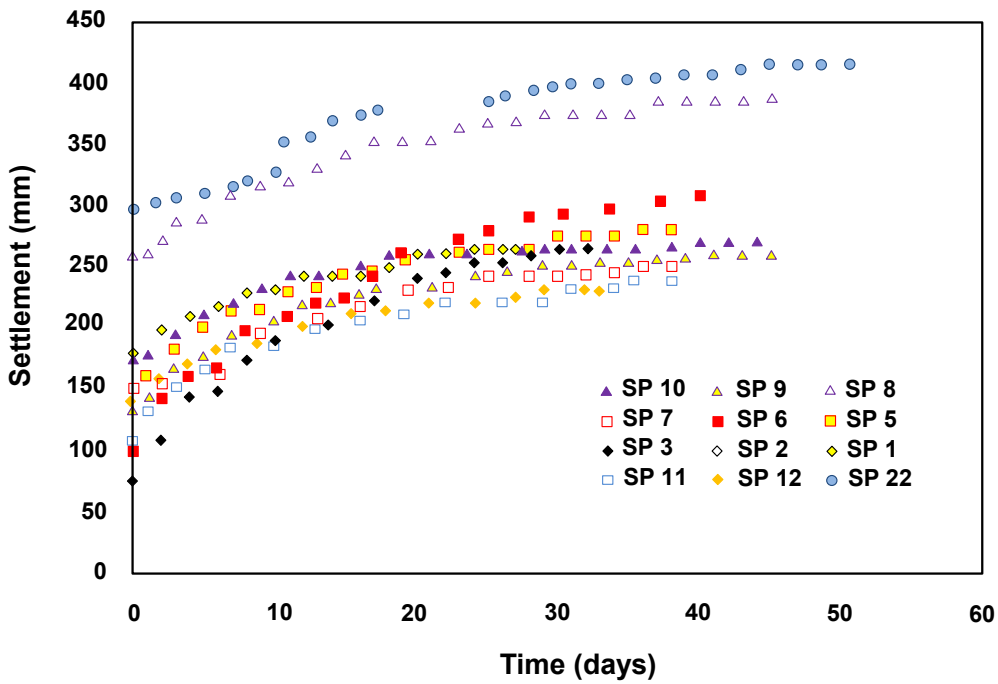

Figure 5.32 Variation of ground settlement with time

5.5.5 Numerical Simulation

A soft to very soft clayey silt/silty clay deposit with a thickness of approximately 7 m was used to conduct the numerical simulation. Details of the simulated model are shown in Figure 5.33.

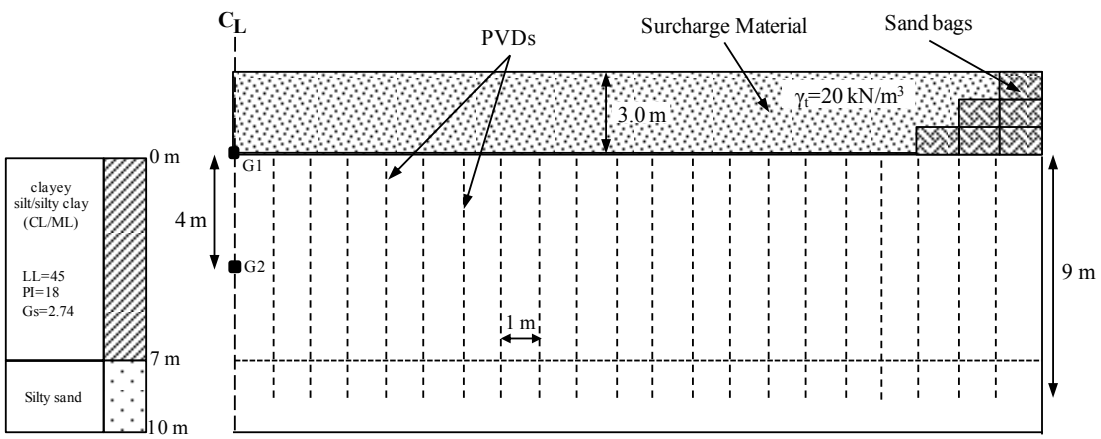

Figure 5.33 Cross section of constructed embankment at Chittagong Port site

Points G1 and G2 were selected to monitor the settlement and changes in pore pressure respectively. Figure 5.34 shows the construction history of the embankment.

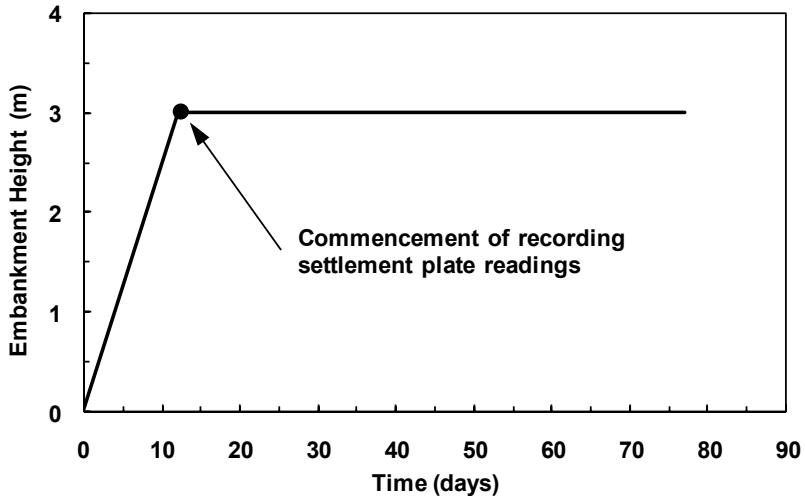

\ Figure 5.34 Construction history (Chittagong Port embankment)

FLAC 2D numerical code incorporating the modified Cam-Clay constitutive soil model was used to simulate the Chittagong Port preloading process by applying plane-strain conditions. The simulated discretised finite-difference mesh is illustrated in Figure 5.35. To model the PVD and surface drainage, a zero excess pore water pressure was assumed along the vertical drains and ground surface boundary, respectively. Equations 2.30 to 2.32 were used to calculate the equivalent plane-strain permeability needed in this analysis. The soil properties used in the numerical analysis are summarised in Table 5.8.

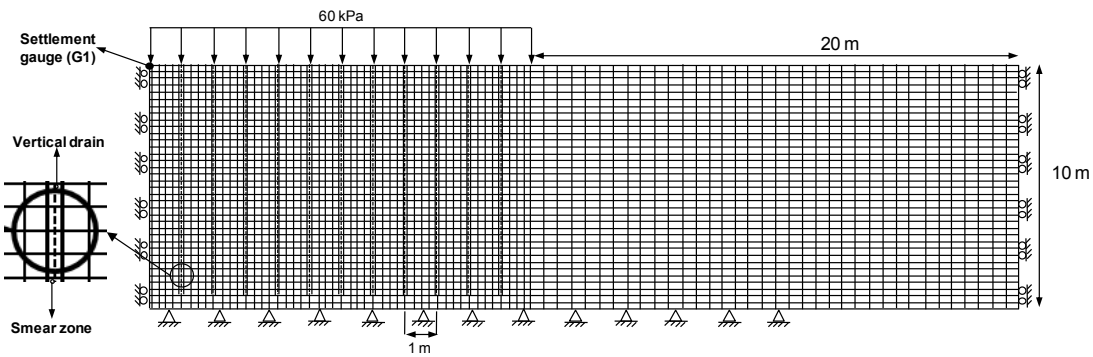

Figure 5.35 Sample of mesh grid pattern for Chittagong Port embankment considering the smear

Table 5.8 Adopted soil properties in FLAC simulation (after Dhar et al. 2011)

Layer	Soil type	M	λ	κ	ν	e_o	γ_s (kN/m^3)	k_h (10^{-9} m/s)	k_h/ k_v
Clayey Silt	Soft soil	0.94	0.13	0.026	0.3	1.28	14.0	2.31	1.5

The numerical results are compared with the field measurements in Figure 5.36. The average field settlement was calculated by averaging the results of 16 variable settlement plates (SP1-10 and SP16-20) close to the centre of the embankment on the ground surface.

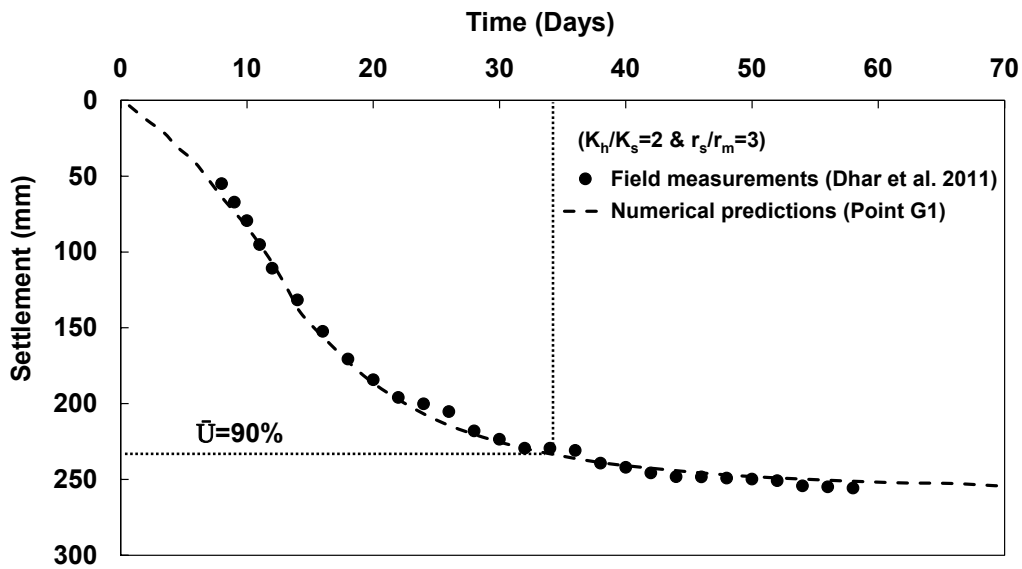

Figure 5.36 Comparison of numerical results with filed data at Chittagong Port site

According to Figure 5.36, the FLAC predictions are in a very good agreement with the field measurements where k_h/k_s=2 and r_s/r_m=3. As illustrated in Figure 5.36, field settlements were measured immediately after placing the surcharge to the full height of 3 m (12 days). Primary consolidation settlement was predicted to be approximately 258 mm, which was confirmed by the settlement measured in the field. It can be noted that 90% degree of consolidation was obtained after 34 days.

Figure 5.37 illustrates the numerical variation of excess pore water pressure for the case where the smear zone properties were k_h/k_s=2 and r_s/r_m=3. It can be noted that the predicted dissipation of excess pore water pressure commenced after reaching a peak value of 60 kPa at the end of embankment construction process.

According to Figure 5.37, the excess pore water pressure was completely dissipated after about 70 days, which shows the end of the primary consolidation process and confirmed the settlement graph shown in Figure 5.36.

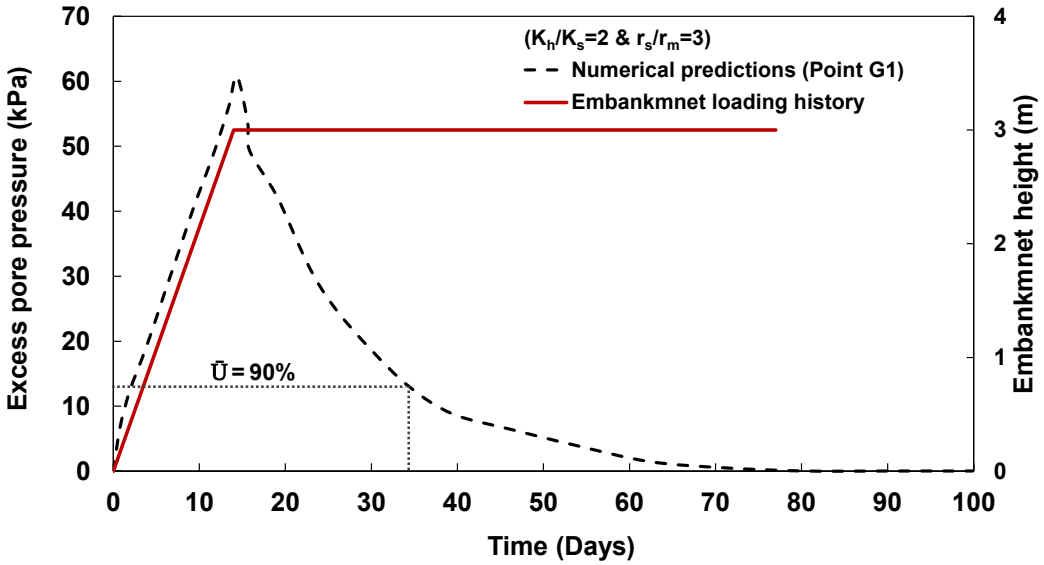

Figure 5.37 Numerical variation of excess pore water pressure against consolidation time

The plotted graphs shown in Figures 5.36 and 5.37 indicate that the proposed back calculation procedure in conjunction with the developed numerical code can be used as a reliable tool to accurately predict the properties of the smear zone.

5.6 CASE STUDY 5: LARGE-SCALE CONSOLIDOMETER

5.6.1 Test Apparatus

Bamunawita (2004) used a large consolidometer designed and built at the University of Wollongong, Australia by Indraratna and Redana (1998) to investigate the effectiveness of vacuum preloading (Figure 5.38). For this purpose, a central vertical drain was installed in the soil specimen placed in a large stainless steel cell (450 mm in diameter by 950 mm high) using a specially designed mandrel, and then the surcharge load was applied under two different conditions, (I) without vacuum pressure, and (II) with vacuum pressure. In this study, the condition without a vacuum pressure was used validates the developed numerical code.

Figure 5.38 Large scale consolidometer (after Bamunawita, 2004)

A 1.5 mm thick sheet of Teflon was wrapped around the internal circumference of the cell, and at the bottom, to reduce friction on the boundary of the cell. The surcharge loading system was applied with an air jack compressor system via a rigid piston, while an LVDT was placed at the top to measure vertical displacement. Strain gauge type pore pressure transducers were installed to measure the excess pore water pressures at various locations. Figure 5.39 illustrates the large consolidometer schematically.

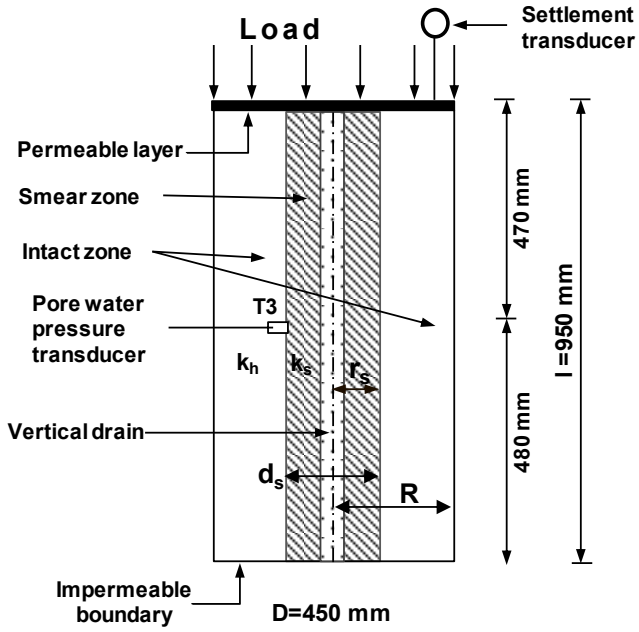

Figure 5.39 Cross section of the large consolidometer (modified after Indraratna et al. 2004a)

5.6.2 Test Sample

The size of each soil sample meant that the large scale consolidometer was approximately 0.15m^3. Reconstituted alluvial clay from Moruya, NSW, was used to make the large samples because obtaining an undisturbed sample of this size was not feasible. The properties of the reconstituted alluvial clay are listed in Table 5.9. Particles of clay (<2μm) and particles smaller than silt size (<6μm) accounted for about 40%-50% and 90%, of the sample, respectively. The reconstituted clay was categorised as CH (high plasticity clay), based on the Casagranade Plasticity Chart.

Table 5.9 Soil properties of the reconstituted sample of Moruya clay (after Bamunawita 2004)

Properties	Specified values
Clay Content (%)	40-50
Silt Content (%)	45-60
Water content, w (%)	40
Liquid Limit, w_L (%)	70
Plastic Limit, w_P (%)	30
Plasticity Index, PI (%)	40
Unit Weight, (t/m^3)	1.81
Specific Gravity, G_s	2.63

5.6.3 Test Procedure

The saturated clay was placed in the cell and compacted in layers, and then the final surface of the compacted clay was covered by the filter material to facilitate water drainage. After filling the chamber with the soft saturated clay (γ_t=18.1 kN/m^3), an initial consolidation pressure of 20 kPa was applied via a rigid piston. When the pre-consolidation phase was completed, a PVD 100mm × 3mm was installed with a rectangular mandrel. The end of the drain was attached to a shoe (anchor) to ensure that the drain remained in position when the mandrel was withdrawn. Then a surcharge load without vacuum pressure was applied in two stages, (i) 50 kPa for 17 days, and (ii) 100 kPa for 14 days. The loading increments were equivalent to an earth fill (γ_t=18.1 kN/m^3) with the heights of about 2.5m and 6m, respectively. The loading history of the test is presented in Figure 5.40.

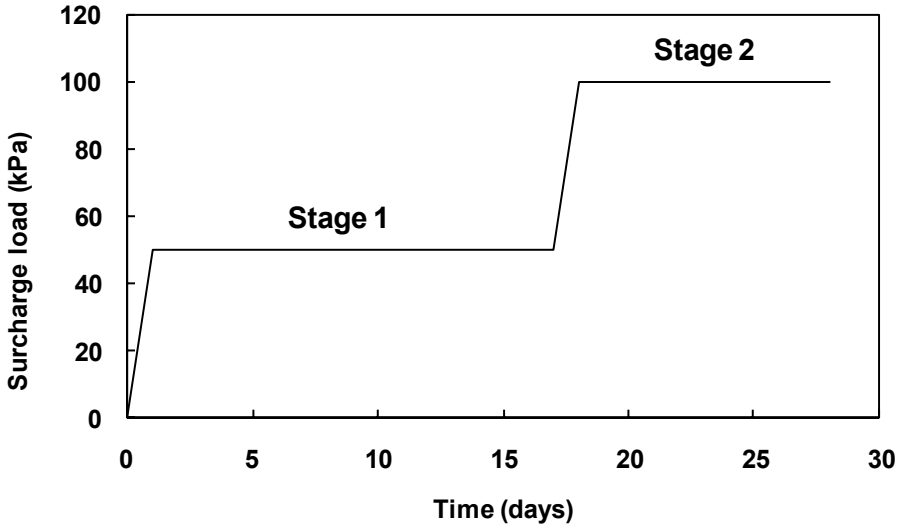

Figure 5.40 Loading history for the large scale consolidometer

5.6.4 Verification of the Developed Numerical Code

The axisymmetric finite difference model was used to simulate the large consolidometer. As Figure 5.41 shows, the zero excess pore water pressure with the hydrostatic water pressure was assumed on the boundary of the drain, and then a uniformly distributed load was assumed on top of the cell to simulate the surcharge pressure. Figures 5.41(a) and 5.41(b) show the large-cell mesh grid, which was generated using the numerical code, and the pore pressure boundary condition (hydrostatic with zero excess pore water pressure) along the vertical drain, respectively. The properties of the soil adopted in this study are summarised in Table 5.10.

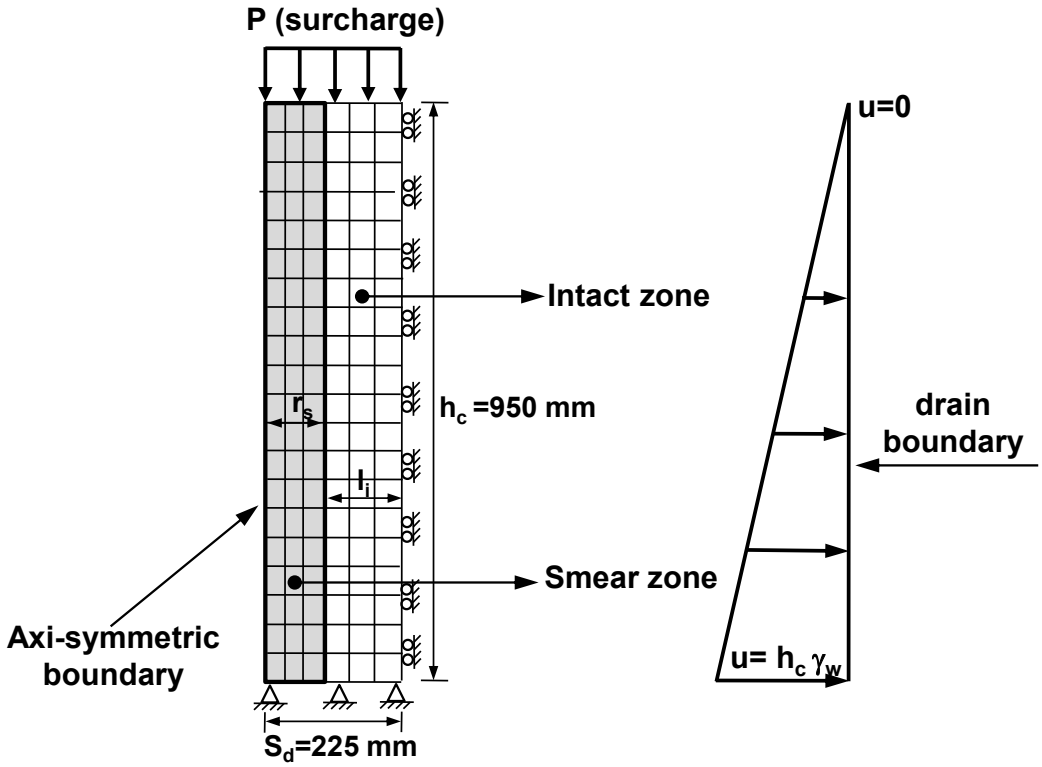

Figure 5.41 Sample of grid pattern for the large consolidometer applying developed code (r_s= smear zone extent; li= intact zone extent; s_d= drain space, h_c= length of the cell, w= width of the cell), (a) boundary conditions applied to simulated cell and (b) pore pressure distribution boundary condition along the vertical drain

Table 5.10 Soil properties for Modified Cam-Clay (after Indraratna et al. 2004a)

Property	M	λ	κ	μ	e_{cs}	k_{hp} (10^{-11} m/s)	LL	PI	G_s
Moruya clay	1.1	0.15	0.05	0.25	1.55	9.1	70	40	2.63

Note: e_{cs} is the void ratio at the critical state

The top vertical displacement gauge and pore water pressure transducer T3 (Figure 5.39) were selected to verify the numerical predictions with the test measurements. The numerical results were compared with the laboratory measurements in Figures 5.42 and 5.43, and indicate that the developed numerical code can predict the behaviour of PDV improved soft soil under a surcharge pressure quite well. According to the back calculation analyses and the proposed procedure, the smear zone characteristics of k_h/k_s=1.7 (permeability ratio) and r_s/r_m=3 (extent ratio) obtained a settlement curve having minimum error with the test measurements.

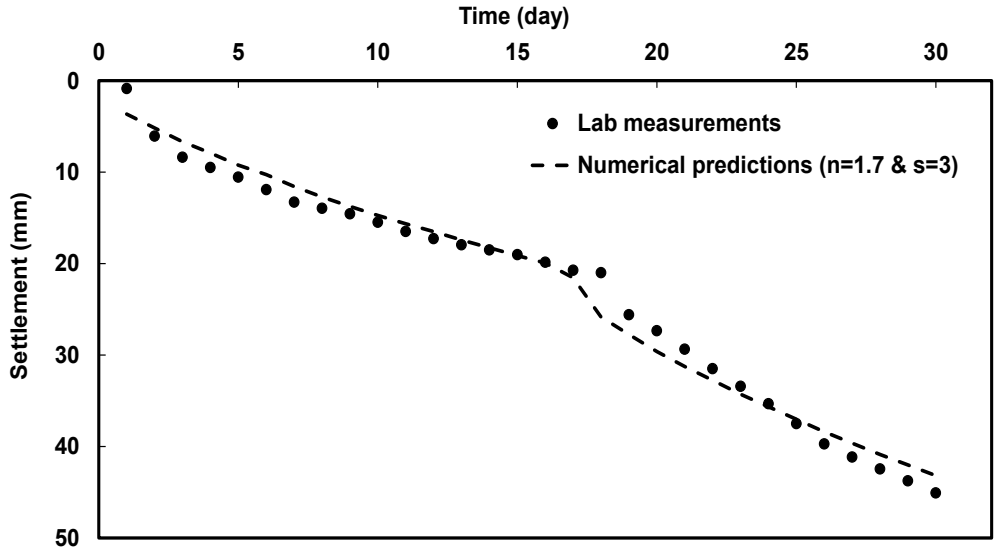

Figure 5.42 Results of large consolidometer cell: Settlement versus consolidation time

As Figure 5.42 shows, the disparities between the numerical predictions and experimental measurements increased overtime, which can be associated with the viscous behaviour of the soil. The current numerical method uses constant compressibility parameters (λ, κ) and ignores the viscous deformation of the soil during consolidation. According to Yin and Graham (1989) soil creep occurs on pore water pressure during dissipation, which contributes to larger deformations.

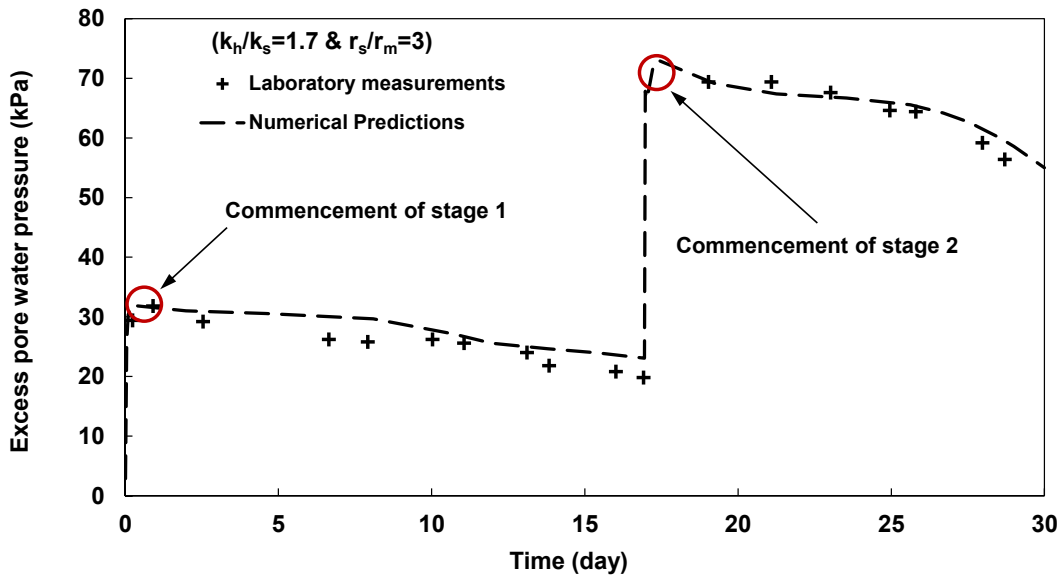

Figure 5.43 Results of large consolidometer cell: Excess pore pressure versus consolidation time

It can be noted that the overall trends for variations in the numerical and experimental excess pore water pressure were similar, which shows the accuracy of the back calculated smear zone properties, even though there were still some disparities.

Figure 5.43 shows that the predicted excess pore water pressure curve experienced sudden changes after each stage of loading that were equal to the extra pressure applied, although this increase occurred over a period of time for the laboratory measured values. There were two main reasons for this abnormal excess pore water pressure behaviour, the Mandel-Cryer effect and volumetric strain softening, both of which were explained previously. Both curves of the experimental and variation in the numerical excess pore water pressure shown in Figure 5.43 indicate that primary consolidation was not obtained at the end of consolidation time, which is in agreement with the plotted settlement graphs in Figure 5.42.

5.7 SUMMARY

In this chapter five PVD assisted preloading case studies, including four trial embankments and a large-scale consolidometer, were explained in detail. The selected case studies were simulated numerically using the developed numerical code that incorporated the back calculation procedure for predicting the properties of the smear zone.

The Cumbalum trial embankment constructed near Cumbalum (New South Wales, Australia) in 1998 with a fill thickness of 5.0 m, was as the first case study to be simulated. Vertical drains were installed at 1.35 m apart in a triangular pattern, to a depth of approximately 22 m, and the embankment was allowed to consolidate for about 4.5 years. The second simulated case study was the Ballina Bypass trial embankment, which was constructed north west of Ballina (New South Wales, Australia) to a height of 8.5 m on 25 m thick soft soil deposits, to investigate the performance of the vacuum preloading ground improvement technique. 34-mm diameter vertical drains were installed 1.0 m apart in a square pattern, and were then connected to horizontal drains. A vacuum pressure of 70 kPa was applied for a period of 400 days and then removed. The Sunshine trial embankment was the third case history, and it was constructed in 1992 in Maroochy Shire, Queensland, Australia. The the soft soil was 11 m thick and was overlying a layer of dense sand.

Vertical drains were installed in a triangular pattern 2 m apart. The trial embankment had a final height of 2.85 m. The fourth case study was the Chittagong Port embankment that was constructed on top of a 7m thick deposit of soft clay on the banks of the Karnafully River beside the Bay of Bengal. The site was designed to support a container load producing a contact pressure of approximately 56 kPa. Vertical drains were installed in a square pattern to a depth 9 m to cover the full depth of the soft clay. The final height of the embankment was 3.0. A fully instrumented large consolidometer built at the University of Wollongong, Australia was simulated as the last case study. The height of the cell was 950 mm and the diameter was 450 mm. The saturated clay was placed in the cell and a central vertical drain was installed with a mandrel, after the pre-consolidation process was completed. A surcharge pressure of 100 kPa was applied in two stages.

In the numerical analyses, the modified Cam-Clay model was used to simulate the behaviour of soft soil in the intact zone and the smear zones, while the Mohr-Coulomb model was used to simulate the embankment. The hydrostatic pressure was fixed along the drain boundary to simulate the PVDs and a constant negative pore pressure was used to simulate the uniform distribution of vacuum pressure. A zero excess pore pressure was assumed at the ground surface to model the drainage boundaries. The smear zone was modelled by assigning a constant reduced permeability to the area surrounding the vertical drain and simulated fully saturated coupled flow-deformation was carried out to model the dissipation of pore water pressure.

The numerical results indicated that the settlement curves obtained by adopting the properties of the back calculated smear zone were in good agreement with the field and laboratory measurements. These results confirmed the validity of using the back calculation procedure combined with the numerical code to accurately predict the smear zone properties, even though there were some disparities between the variations in the numerical and field pore pressure. According to these variations in pore pressure, the maximum predicted excess pore water pressure occurred immediately after completion of the trial embankment and it was equal to the applied surcharge. However, this value was slightly less than the applied pressure for the field measurements; this can be related to the relationship between the volumetric compliance of the pore water pressure measuring system and the compressibility of

the soil skeleton. Furthermore, the field measurements showed that the excess pore pressures did not dissipate immediately at the end of loading or construction, but either increased or stabilised for a period before decreasing; this can be explained by the Mandel-Cryer effect and volumetric strain softening.

CHAPTER SIX

6 DETERMINING THE MINIMUM PERIOD OF MONITORING FOR PREDICTING SMEAR ZONE PROPERTIES OF A TRIAL EMBANKMENT

6.1 GENERAL

The construction of a fully instrumented trial embankment has been extensively used as a reliable method to determine the feasibility of preloading with vertical drains and to estimate the properties of the smear zone by applying a back calculation procedure (Kelly, 2008). The long time required to construct the trial embankment has bee a major challenge in using this method to conduct the back calculation analysis and estimate the extent and permeability of the smear zone. Hence, in many cases it may cause a considerable delay in constructing the actual embankment and impose a significant increase in the project cost. Estimating the extent and permeability of the smear zone in the early stages of constructing a trial embankment can convert this method into a very practical, accurate, and cost effective approach.

This chapter is allocated to establishing the minimum degree of consolidation (i.e. the minimum waiting time after constructing a trial embankment) that results in accurate prediction of smear zone properties. For this purpose, a systematic procedure, illustrated in Figure 6.1 has been used in conjunction with the developed numerical code. As Figure 6.1 shows, the approach starts with collecting the input data, including the soil properties, PVD assisted preloading specifications (PVD pattern and loading history) and the results of field monitoring (i.e. variations in settlements and excess pore pressures). The first stage is then completed by defining the initial values, the maximum and minimum values, and the incremental rates for the ratios of extent and permeability. In the second stage, a well-designed parametric study is conducted to predict the behaviour of the ground, determine the corresponding settlement curves for different combinations of smear zone characteristics, and calculate cumulative error between the numerical results and field measurements at every degree of consolidation. Stage two stops as soon as the

extent ratio is out of the input range. The minimum required degree of consolidation is determined in the last stage and results in appropriate smear zone characteristics.

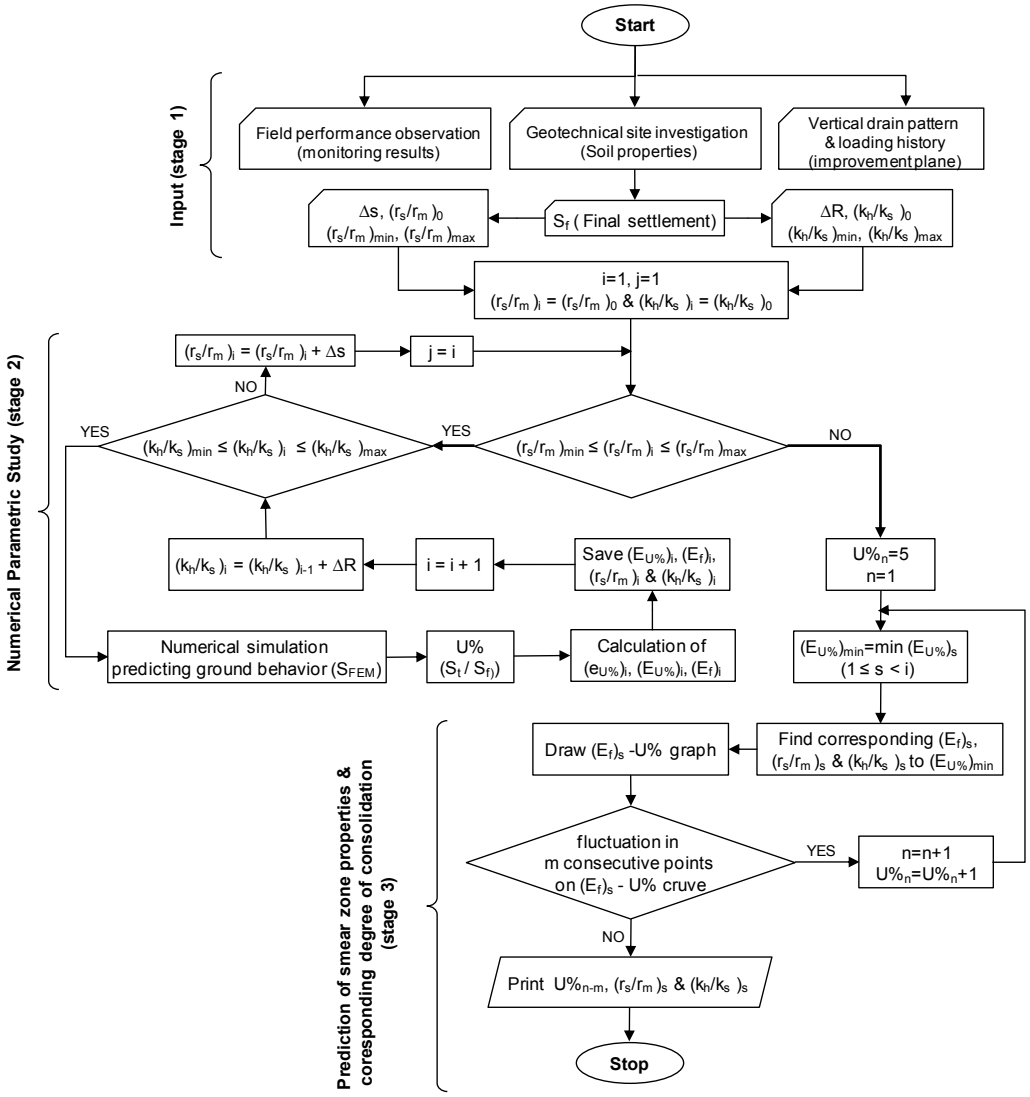

Figure 6.1 Flowchart of the systematic procedure to determine the minimum degree of consolidation resulting in an accurate estimation of smear zone characteristics

A four-step solution has been suggested to apply the procedure proposed in Figure 6.1, which computes the minimum degree of consolidation (minimum preloading time), using the simulated case studies, explained in Chapter 5. The four-step solution includes: (i) estimating the primary consolidation settlement, (ii) conducting the parametric study, (iii) determining the error, and (iv) establishing the minimum

waiting time required. A detailed explanation of the solution procedure is provided in the following sections.

6.2 STEP I: ESTIMATING THE PRIMARY CONSOLIDATION SETTLEMENT

The final settlement for each case study under the embankment surcharge was predicted by applying the developed numerical code. This final settlement can then be used to determine the degree of consolidation at any time during or after construction of the trial embankment, using Equation (6.1).

$$U\% = \frac{s_t}{s_f} \times 100 \tag{6.1}$$

where, $U\%$ is the degree of consolidation at time t, s_t is the field settlement at time t, and s_f denotes the predicted final primary consolidation settlement. Table 6.1 shows the primary consolidation settlement and the corresponding degree of consolidation for the simulated case studies.

Table 6.1 Primary consolidation settlements and the corresponding degree of consolidations

Case Study	Chittagong Sea Port trial embankment	Cumbalum at SP9	Ballina Bypass at SP12	Sunshine at P1	Large-scale consolidometer
S_f (m)	0.258	3.3	5.2	1.75	0.086
S_{pr} (m)	0.258	2.45	4.4	0.75	0.045
t_{pr} (day)	55	2000	400	90	30
U_{pr} (%)	100%	75%	85%	40%	52%

Note: S_f is the predicted final primary consolidation settlement; S_{pr} is the field settlement at the end of preloading time; t_{pr} is the preloading time; U_{pr} is the degree of consolidation at the end of preloading

6.3 STEP II: CONDUCTING PARAMETRIC STUDIES

A parametric study was conducted for each case study to obtain the time-settlement curves for different combinations of the extent and permeability of the smear zone used to determine the error between the field measurements and numerical predictions. The numerical analyses were performed by adopting different combinations of the extent and permeability of the smear zone, and in each case the results were then compared with the field measurements. Furthermore, the effects of the smear zone properties on the preloading process were also investigated.

6.3.1 Chittagong Sea Port Trial Embankment

A comprehensive parametric study was conducted for the Chittagong Sea Port trial embankment to obtain the variations in settlement against the consolidation time, and also to investigate the influence that different combinations of the smear zone characteristics have on the preloading design. For this purpose k_h/k_s (permeability ratio) and r_s/r_m (extent ratio) were changed from 2 to 5. It should be noted that the developed numerical code, including the supplementary FISH sub-routines were used, which allowed for an automatic parametric study in the required range of parameters, while the characteristics of the smear zone, drain spacing, and adjusted finite difference mesh and grids changed simultaneously, which is a unique feature facilitating the parametric study. Details of the geotechnical model and numerical verification exercise for this case study has been explained in Section 5.5 in Chapter 5. Figure 6.2 illustrates the results of the parametric study in the form of settlement-time curves.

According to Figure 6.2, the settlement curves are converged to a unique value of approximately 258 mm, which is the primary consolidation settlement. The time required to obtain 90% of primary consolidation settlement (232 mm) was used to investigate the effect of the properties of the smear zone in the consolidation process. The 90% degree of consolidation has been adopted by researchers as an acceptable value for near completion of consolidation resulting in accurate settlement predictions (Basu et al. 2006, Indraratna 2009, Saowapakpiboon et al. 2011). It should be noted that 90% degree of consolidation is also often used by practising geotechnical engineers as the indication of the time for the removal of the surcharge.

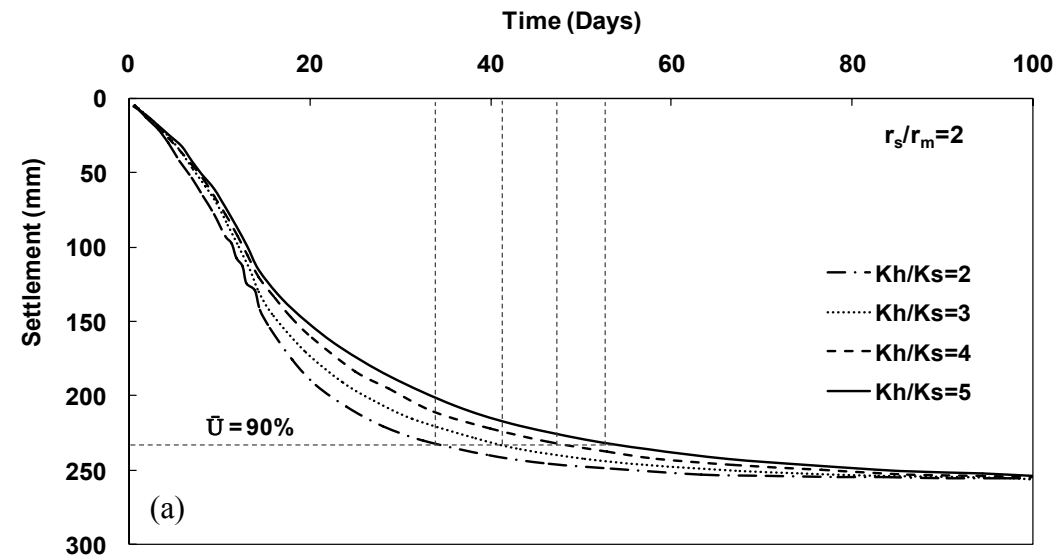
Time (Days)
0
20
40
60
80
100
Settlement (mm)
0
50
100
150
200
250
300
r_s/r_m=2
Kh/Ks=2
Kh/Ks=3
Kh/Ks=4
Kh/Ks=5
Ū = 90%
(a)

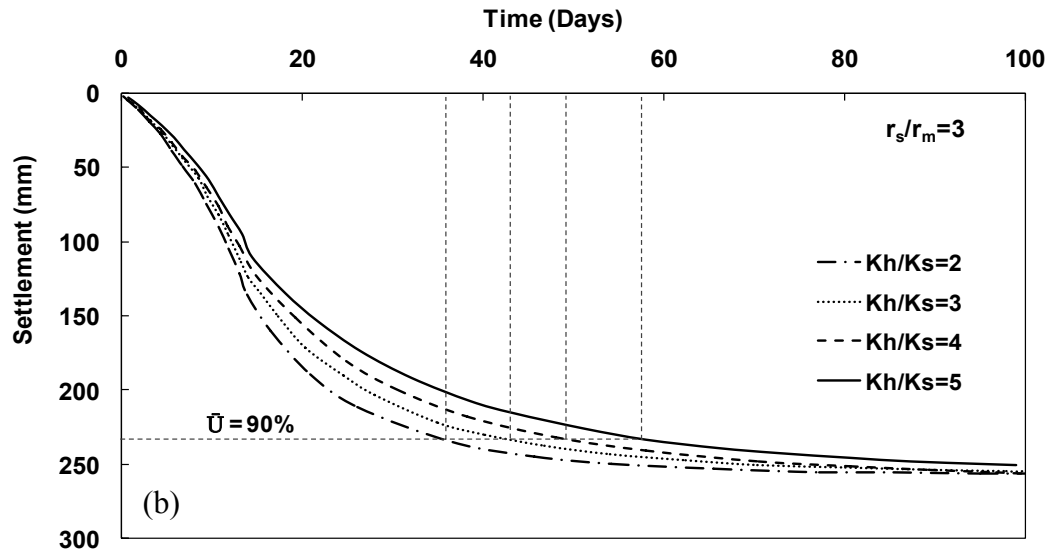
Time (Days)
0
20
40
60
80
100
Settlement (mm)
0
50
100
150
200
250
300
r_s/r_m=3
Kh/Ks=2
Kh/Ks=3
Kh/Ks=4
Kh/Ks=5
Ū = 90%
(b)

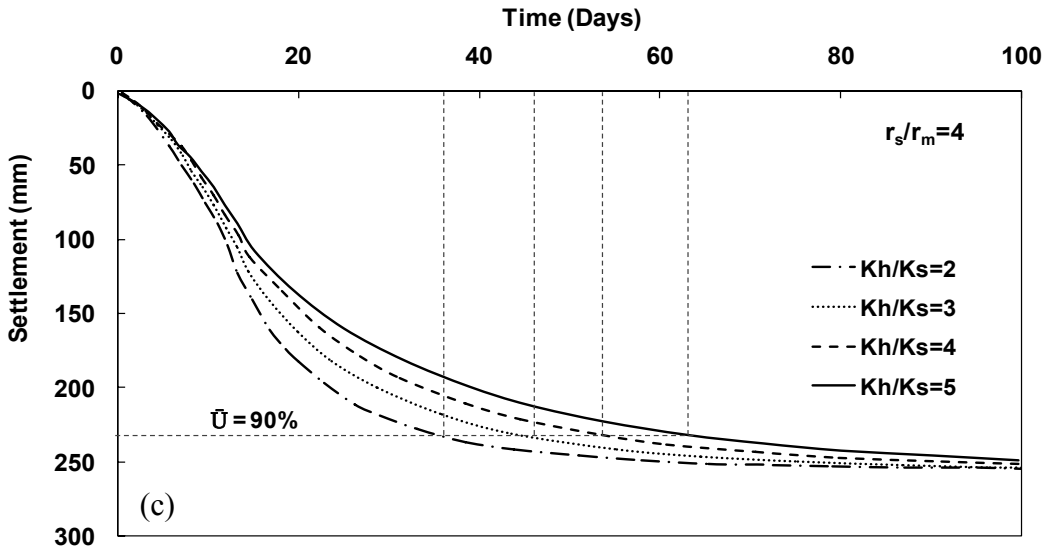
Time (Days)
0
20
40
60
80
100
Settlement (mm)
0
50
100
150
200
250
300
r_s/r_m=4
Kh/Ks=2
Kh/Ks=3
Kh/Ks=4
Kh/Ks=5
Ū = 90%
(c)

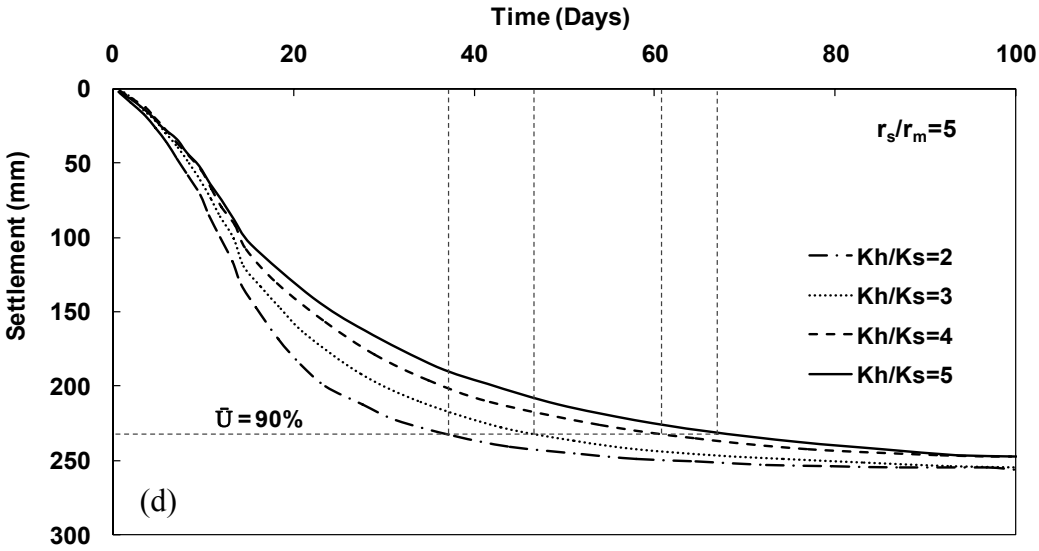

Figure 6.2 Parametric study results for Chittagong port case history at point G1, (a) r_s/r_m=2, (b) r_s/r_m =3, (c) r_s/r_m =4, and (d) r_s/r_m =5

Figure 6.2(a) shows that a minimum of 33 days was required to achieve 90% degree of consolidation, while considering k_h/k_s=2 and r_s/r_m=2. When the properties of the smear zone were k_h/k_s=5 and r_s/r_m=5, the time required was the highest and equal to 67 days, which is approximately two times longer than the minimum duration. According to the plotted curves in Figure 6.2, the influence of the variations in the permeability of the smear zone was more critical when the ratio of the extent of the smear zone was larger. For instance, the time required to obtain 90% degree of consolidation was increased by 60% (from 33 days to 53 days) by changing the permeability ratio from 2 to 5 and making the extent ratio equal to 2, whereas this increase was 80% (from 37 days to 67 days) for an extent ratio of 5.

The general trend in Figures 6.2(a)-6.2(d) shows that changing the permeability ratio in a smaller range resulted in larger variations of the time required to obtain 90% degree of consolidation with a constant extent ratio. According to Figure 6.2(a), the consolidation time increased by 23% by varying the permeability ratio from 2 to 3, while this change was 17% and 12% when the permeability ratio was changed from 3 to 4 and 4 to 5, respectively.

Figure 6.3 illustrates the results of the numerical parametric study investigating the influence that the smear zone properties had on the dissipation of excess pore water pressure (EPWP). Graphs were plotted for point G2, located at a

depth of 4m (see Figure 5.34). Figure 6.3 confirms that increasing the permeability and extent ratios prolongs the dissipation of excess pore water pressure (EPWP) quite considerably. According to Figures 6.3(a)-6.3(d), the permeability ratio was a more critical parameter than the extent ratio, although the influence that the variations of the extent ratio had on consolidation time cannot be neglected. For example, according to Figure 6.3(b), there was a 160% difference between the predicted excess pore pressure after 34 days (90% field degree of consolidation) for k_h/k_s=2 (EPWP=13 kPa) and k_h/k_s=5 (EPWP=34 kPa), while keeping r_s/r_m=3 (Figure 6.3(b)).

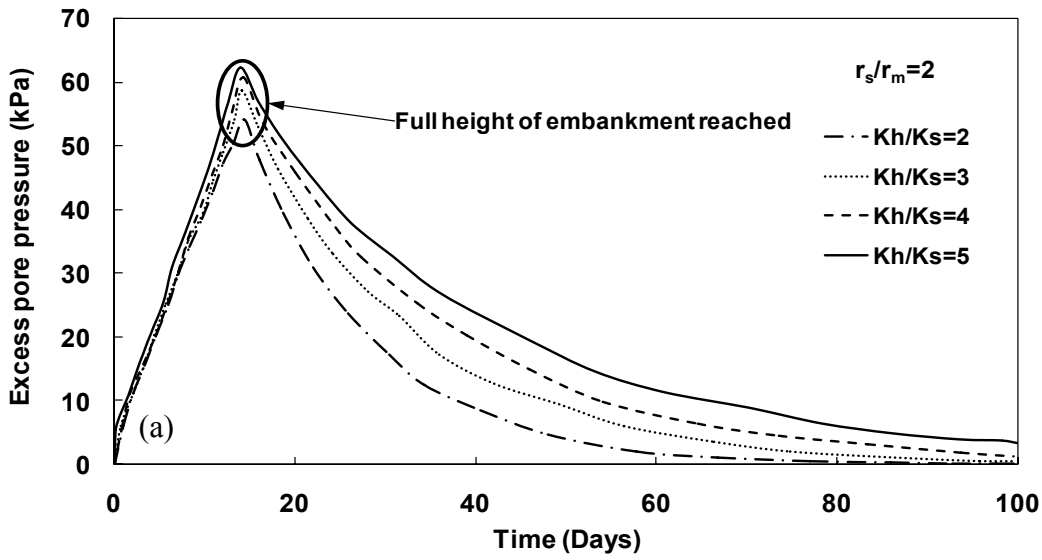

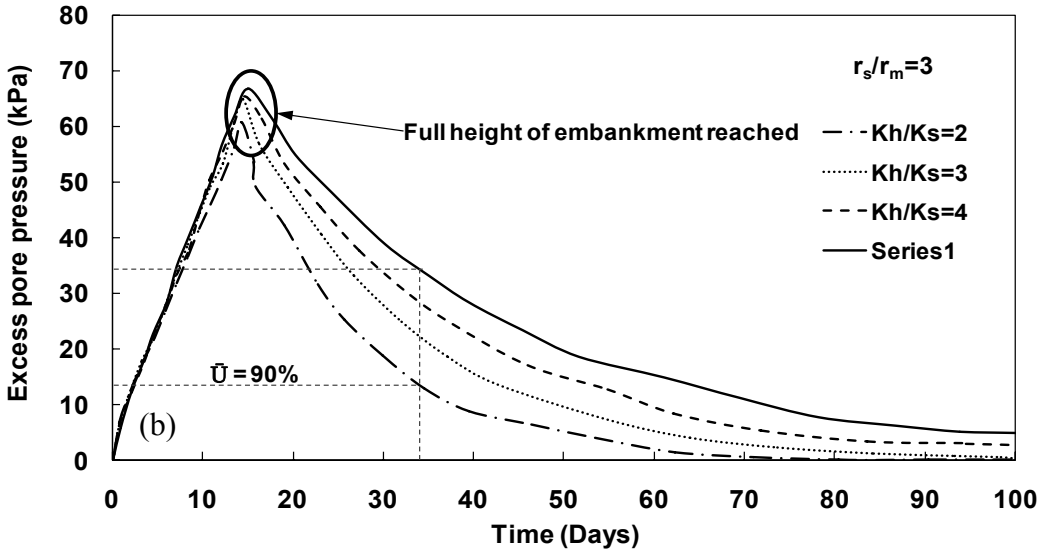

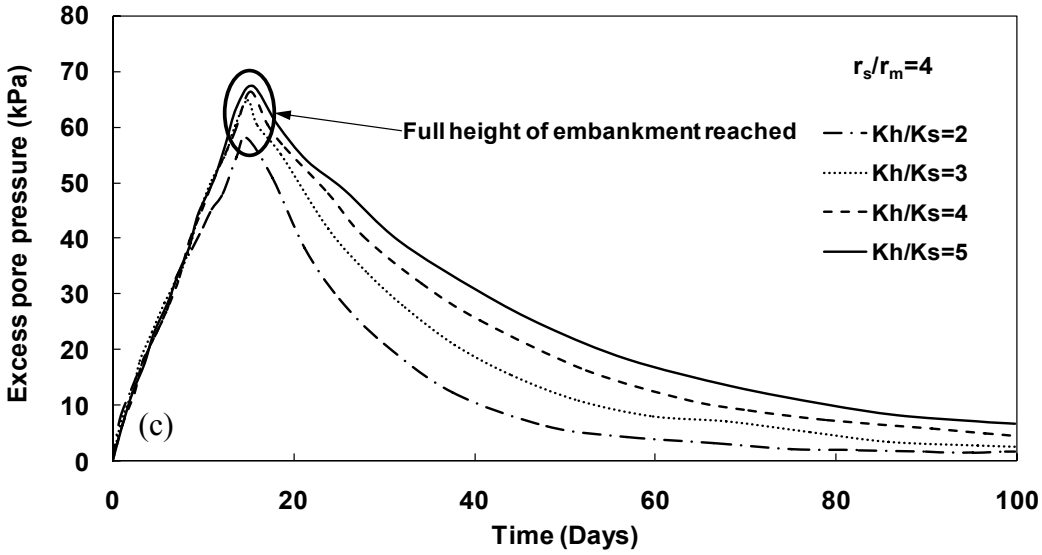

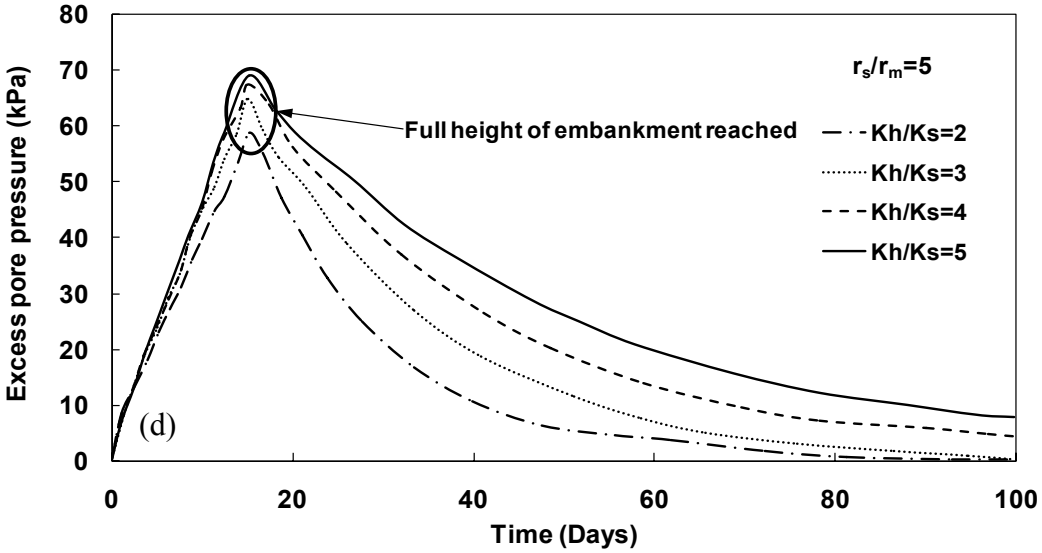

Figure 6.3 Results of parametric study using the FLAC code developed to investigate the influence of the smear zone properties on the dissipation of excess pore water pressure for Chittagong port case history at point G2, (a) r_s/r_m=2, (b) r_s/r_m=3, (c) r_s/r_m=4, and (d) r_s/r_m=5

The time required to obtain 90% degree of consolidation for the different smear zones is illustrated in Figure 6.4 using the results of the parametric study, which interprets the effects the smear zone properties on consolidation time better.

According to Figure 6.4, the consolidation time depends on the extent and permeability of the smear zone, for example, assuming that r_s/r_m=2 for the cases where k_h/k_s=2 and k_h/k_s=5, the time needed to obtain 90% degree of consolidation is

approximately 33 days and 53 days, respectively, indicating a 60% difference. This difference is more significant for larger values of r_s/r_m.

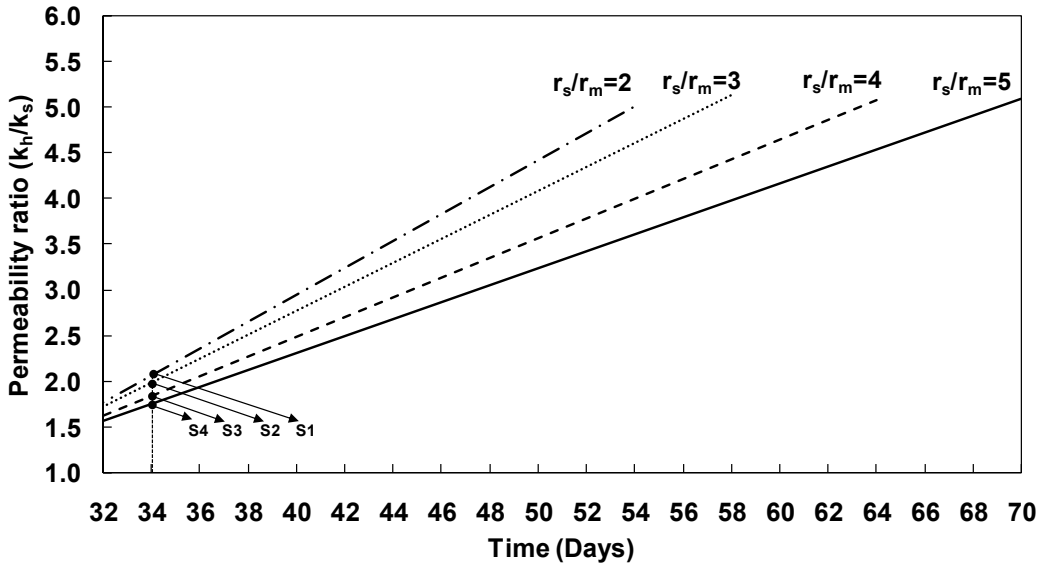

Figure 6.4 Predicted time to obtain 90% degree of consolidation (Chittagong trial embankment)

Figure 6.4 clearly indicates that the extent ratio (r_s/r_m) of the smear zone is an important parameter influencing the consolidation time and cannot be neglected. By varying r_s/r_m from 2 to 5 and assuming k_h/k_s as a constant parameter can influence the consolidation time needed by more than 25%. A combination of the variables in the extent and permeability in the smear zone will result in large changes in the consolidation time. The results presented in Figure 6.4 clearly indicate that the influence of variables in r_s/r_m becomes more important when the permeability of the smear zone decreases.

According to the numerical results presented in Figure 5.37, the predicted settlement curve is in the best agreement with the field measurements when the properties of the smear zone are k_h/k_s=2 and r_s/r_m=3. The time required to obtain 90% degree of consolidation for this condition is equal to 34 days, which is highlighted as point S2 in Figure 6.4. A vertical line is plotted from $t_{90\%}$= 34 days, which intersects the set of lines at points S1, S2, S3, and S4. The properties of the smear zone at these points are summarised in Table 6.2.

Table 6.2 Back calculated smear zone properties to achieve $t_{90\%}$= 34 days (Chittagong trial embankment)

Point	S1	S2	S3	S4
k_h/k_s	2.10	2.0	1.85	1.75
r_s/r_m	2	3	4	5

Different combinations of the extent and permeability of the smear zone (Table 6.2) that result in the same $t_{90\%}$= 34 days were used to compare the variations in settlement and excess pore water pressure with the consolidation time by applying the developed FLAC code; the results are presented in Figure 6.5.

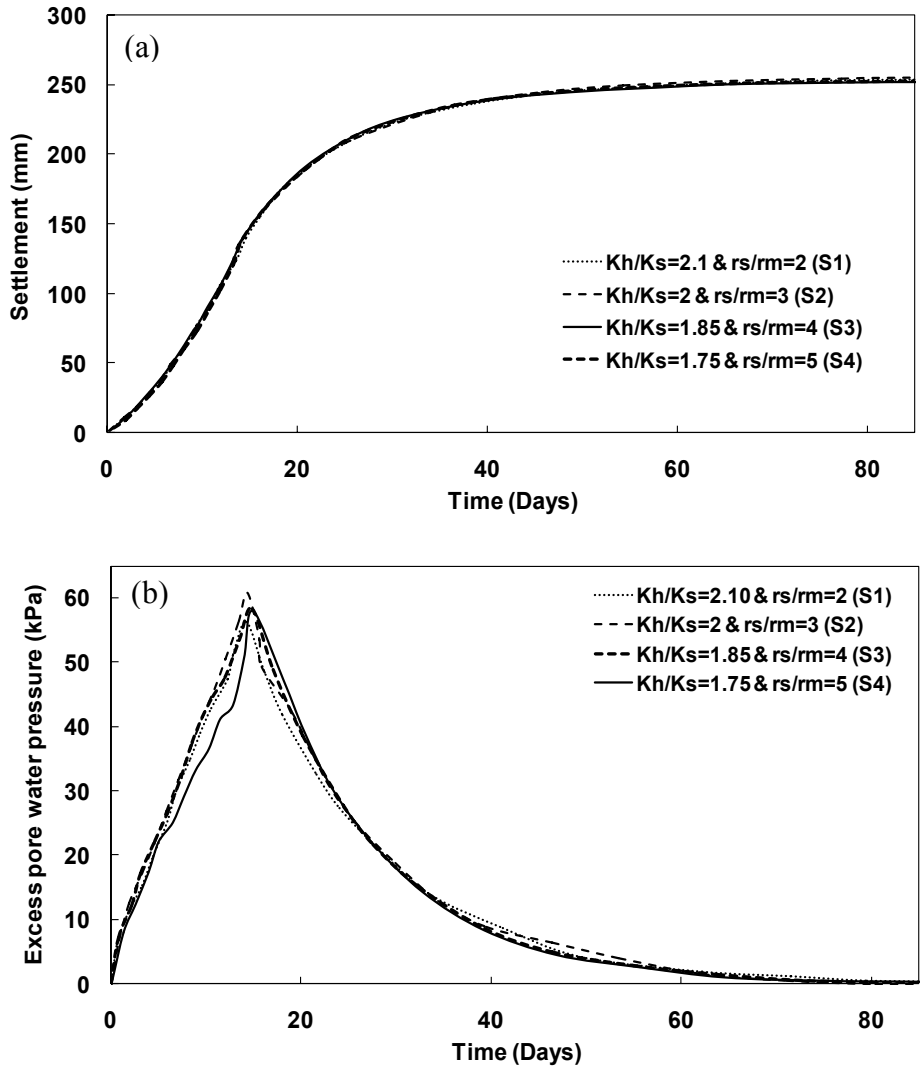

Figure 6.5 Results of FLAC analysis for points in Table 7, using the Chittagong port case history, (a) Settlement variation, and (b) dissipation of excess pore water pressure

Figure 6.5 shows that the curves for the variations in settlement and dissipation of excess pore water pressure over time follow the same trend for points S1, S2, S3, and S4. Therefore, the properties of the smear zone of any of these points can be used for practical design purposes to reduce inaccuracies. In other words, the extent ratio (r_s/r_m) can assumed to be a constant value and the permeability ratio (k_h/k_s) can be changed to conduct the parametric study and determine the optimum combination.

The numerical results (settlement variation versus consolidation time) were compared with the field measurements in Figure 6.6 by varying the permeability ratio ($n=k_h/k_s$) from 2 to 5, while the extent ratio ($s=r_s/r_m$) was kept at a constant value of 3.

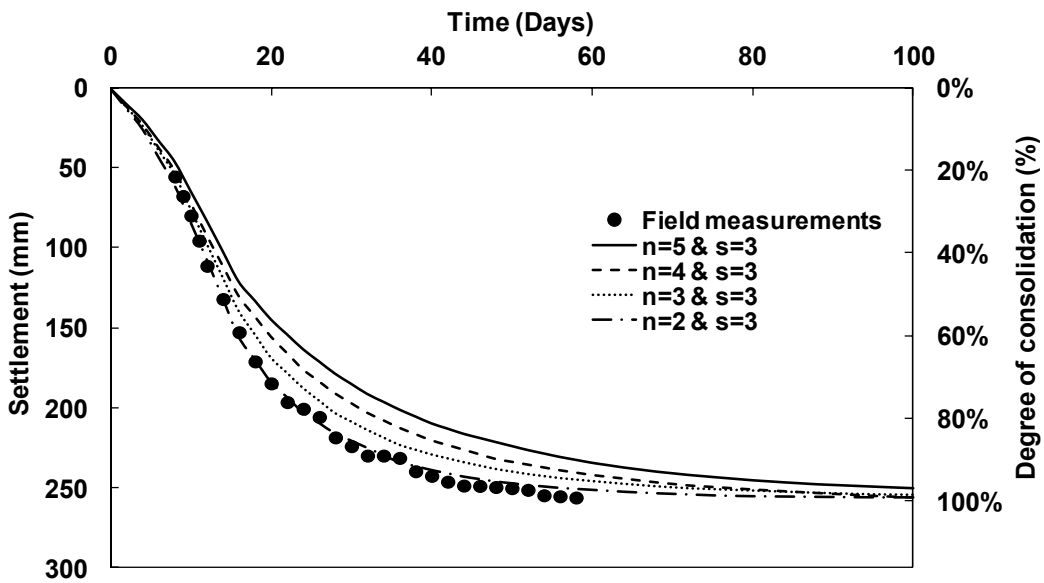

Figure 6.6 Settlement variations against consolidation time for the Chittagong trial embankment

The overall trend in Figure 6.6 indicates that the case with the permeability ratio of 2 and smear extent of 3 had the best fit with the field measurements, but this was impossible to clarify in the early stages of the preloading process by observation.

6.3.2 Cumbalum Trial Embankment

The Cumbalum trial embankment was simulated using the developed FLAC code and the systematic analysis procedure (Figure 6.1) was used to conduct a parametric

study by varying the k_h/k_s and r_s/r_m from 2 to 6. The geotechnical model developed for the site and the numerical modelling procedure for this case study have been explained in detail in Chapter 5, Section 5.2. The numerical predictions are plotted in Figure 6.7 and compared with the field measurements by adopting the selected combinations of k_h/k_s and r_s/r_m. It can be observed that the variation of the extent and permeability of the smear zone had a substantial influence on the settlement rate.

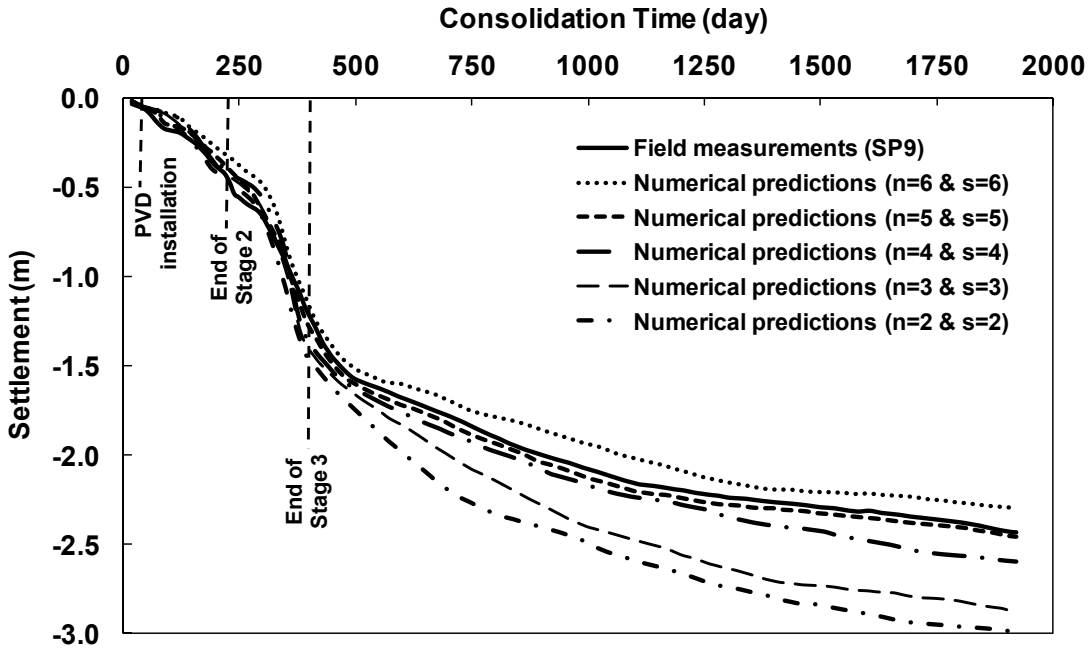

Figure 6.7 Results of numerical parametric study: Cumbalum trial embankment at SP9

Figure 6.7 shows that the settlement has increased from 2.3 m to 3.0 m by varying k_h/k_s and r_s/r_m from 6 to 2 after 1900 days of consolidation. According to the graphs plotted in Figure 6.7, the settlement curve corresponding to the case with smear zone characteristics of k_h/k_s=5 and r_s/r_m=5 agrees well with the field measurement. However, it was not possible to verify this agreement by observation at the initial stages of construction, thus a rigours analytical procedure was required.

Figure 6.8 illustrates the predicted and measured values of excess pore water pressures at the location of PC2, at a depth of 5.8m (see also Figures 5.7 and 5.8 for more details). It can be observed that the excess pore water pressure curves for the numerical predictions and the field measurements followed a similar pattern. Pore water pressures increased during the fill placement at each stage of construction

and then gradually dissipated. The maximum excess pore water pressure for each case occurred at the end of the construction process, which was similar to the field observations reported by Kabbaj et al. (1988) and Leroueil (1997). Figure 6.8 shows that the maximum excess pore water pressure of 120 kPa occurred at the end of the construction process by adopting k_h/k_s=6 and r_s/r_m=6. It can be noted that lower k_h/k_s and r_s/r_m values caused a faster dissipation of excess pore water pressure. For example, 90% of the excess pore water pressure had been dissipated after 1900 days by adopting k_h/k_s=2 and r_s/r_m=2, while this dissipation was 70% when k_h/k_s=6 and r_s/r_m=6.

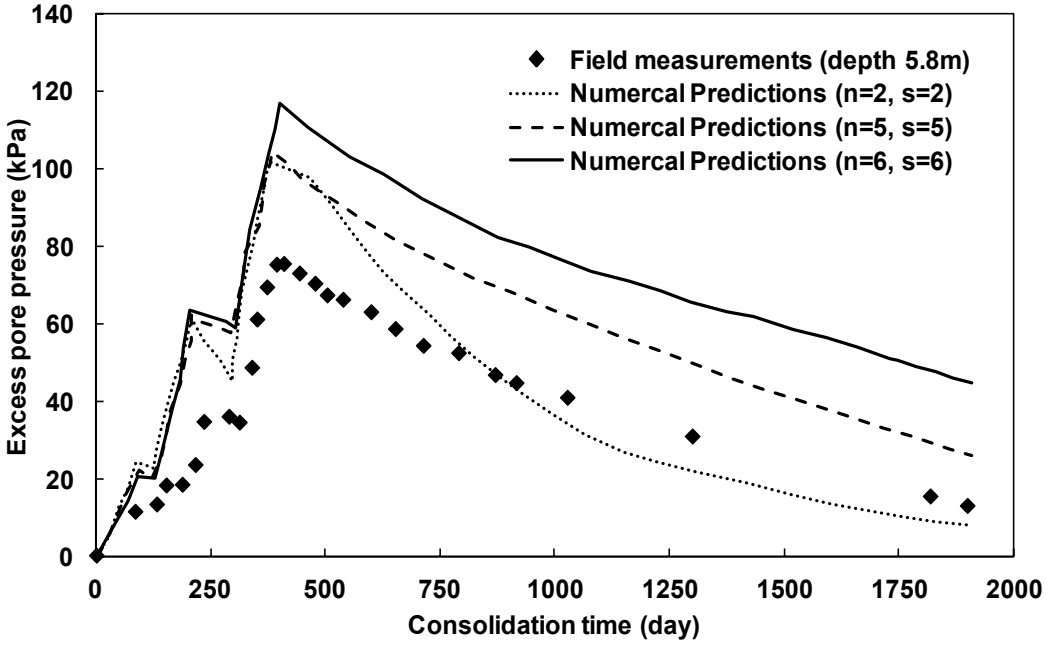

Figure 6.8 Variation of excess pore pressure with time for the Cumbalum trial embankment at PC2 (depth 5.8m)

Figure 6.8 shows that there are some discrepancies between the measured and the predicted excess pore water pressures. Compared to the field values, the predicted excess pore pressures were larger at the end of the construction process, and in better agreement when the degree of consolidation increased. This discrepancy can be attributed to numerous factors such as uncertainties in the soil properties, the effect of smear zone characteristics, and the simplified improper conversion of the axisymmetric condition to the plane-strain (2D) condition to analyse the multiple drains.

6.3.3 Ballina Bypass trial Embankment

The developed FLAC code was applied to the Ballina Bypass trial embankment using the second stage of the proposed procedure shown in Figure 6.1 to conduct the parametric studies. The geotechnical model adopted and the details of this case study, as well as the results from the numerical modelling verified against the field measurements, have been reported earlier in Chapter 5, Section 5.3. Different combinations of the permeability ratio ($n=k_h/k_s$) and extent ratio ($s=r_s/r_m$) were used to investigate how variations in the properties of the smear zone could affect the consolidation settlement and to compare the numerical results with the field measurements. The results of the selected numerical parametric study are compared with the field measurements in Figure 6.9.

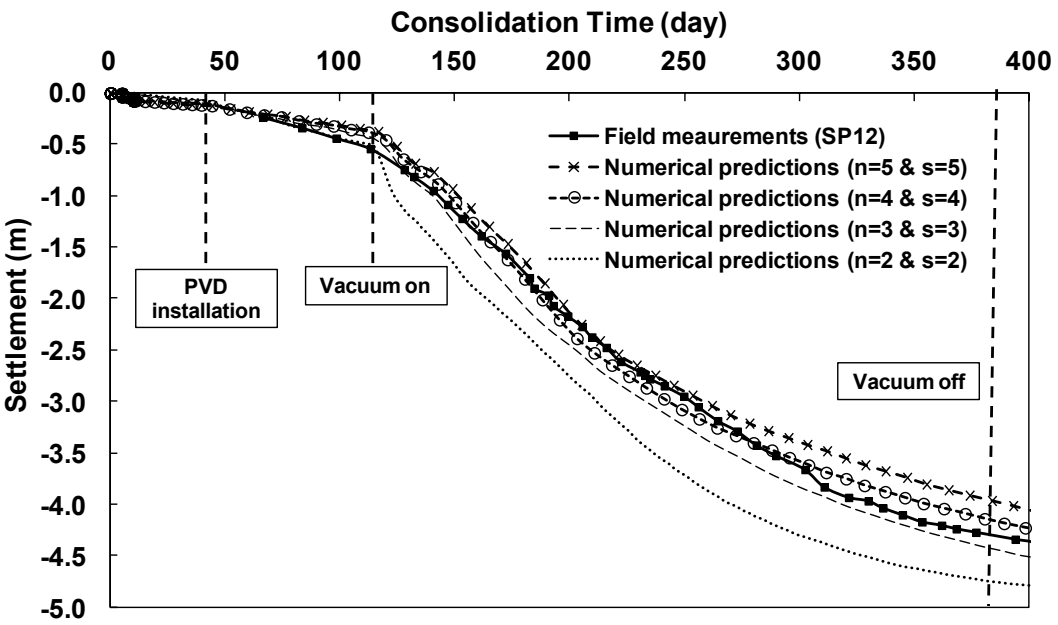

Figure 6.9 Results of numerical parametric study: Ballina Bypass trial embankment at SP12

According to the numerical results in Figure 6.9, using $r_s/r_w=2$ and $k_h/k_s=2$ causes a settlement of 4.8 m at the end of the vacuum process while the settlement is 4.0 m when $r_s/r_w=5$ and $k_h/k_s=5$ are used. This indicates that by varying r_s/r_w and k_h/k_s between 2 to 5 a considerable reduction is caused in the degree of consolidation.

Figure 6.9 shows that the smearing effect on the consolidation process is much more in low ranges of r_s/r_w and k_h/k_s.

A comparison of the predicted and measured variations of excess pore water pressure with time for the transducer P3 located 11.8 m deep and 0. 5 m away from the centreline of the embankment (refer to Figures 5.15 and 5.16) is shown in Figure 6.10. According to the numerical predictions, the rate of consolidation accelerated, due to installation of vertical drains. It can be observed that the numerical excess pore pressure curve has experienced a sudden change to -70 kPa when the vacuum pressure was applied, followed by an incremental trend due to the embankment construction.

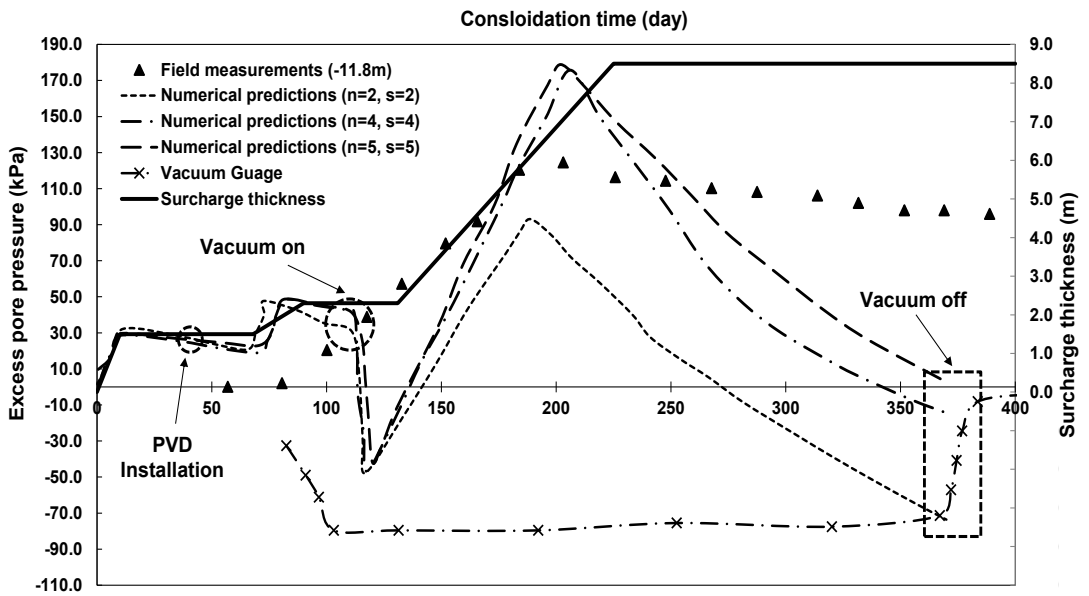

Figure 6.10 Variation of excess pore pressure variation with time for Ballina Bypass trial embankment at P3 (depth 11.8m)

The numerical results in Figure 6.10 clearly indicate that the variations in the properties of the smear zone affected the dissipation of excess pore water pressure quite considerably, and as expected, the higher smear zone permeability accelerated this dissipation. Figure 6.10 also shows that the excess pore water pressures were fully dissipated at the end of vacuum process, where $r_s/r_w=2$ and $k_h/k_s=2$, confirming the numerically predicted settlement results in Figure 6.9. Using $r_s/r_w=5$ and $k_h/k_s=5$ prolonged the dissipation of excess pore water pressure with the minimum settlement at the end of the vacuum process. It can be noted that the variation of r_s/r_w and k_h/k_s

in the low ranges (2 to 3) was more critical and influenced the dissipation of excess pore water pressure quite considerably, which is in agreement with the settlement predictions given in Figure 6.9. In Figure 6.10, the measured excess pore water pressures due to the staged construction of trial embankment and the application of a negative vacuum pressure were plotted separately, while the numerical predictions were plotted as a combined graph.

Figure 6.10 shows the disparities in the predicted excess pore water pressures and field measurements. The field measurements showed that the excess pore pressure did not dissipate immediately after loading or construction was completed, but actually increased or stabilised for a period before decreasing. The abnormal behaviour of excess pore water pressure has been reported in many field studies (Conlin and Maddox, 1985; Kabbaj et al., 1988; Rowe and Li, 2002), and two reasons have already been proposed to explain this anomalous behaviour; the Mandel-Cryer effect and volumetric strain softening. Schiffman et al. (1969) reported that the Mandel-Cryer effect is due to the increase in total stress caused by the volumetric strain compatibility. The Mandel-Cryer effect called after Mandel (1953) and Cryer (1963), based on their observations related to the abnormal generation of excess pore water pressure. Cryer (1963) analysed the process of consolidation by applying pressure around a saturated porous sphere whose surface is free to drain under the pressure applied. Here the total stress at the centre of the sphere increased temporarily because the dissipation of excess pore water pressure at the centre was delayed, which increases the excess pore water pressure for some time before dissipation begins. In addition, this increase or delay in the dissipation of excess pore water pressure may be the result of volumetric strain softening due to unstable behaviour during consolidation when the stress paths depart from the failure line. The constitutive model developed by Kimoto and Oka (2005) can capture the increase in pore water pressure due to stagnation. Moreover, Asaoka et al. (2000) reported that as the decay of over consolidation is much faster than the degradation of the structure in clay during consolidation, softening becomes possible as the volume is compressed, even under a considerably low stress ratio.

6.3.4 Sunshine Trial Embankment

The proposed back calculation scheme was used while adopting different combinations of smear zone properties to conduct a systematic parametric study simulating the Sunshine trial embankment, the results of which are reported in Figure 6.11. For this purpose the extent ratio ($s=r_s/r_w$) was a constant value of 3, while the permeability ratio ($n=k_h/k_s$) varied from 2 to 6. Details of the geotechnical properties of the site, construction sequence, and the numerical simulation using FLAC have been explained in Chapter 5, Section 5.4.

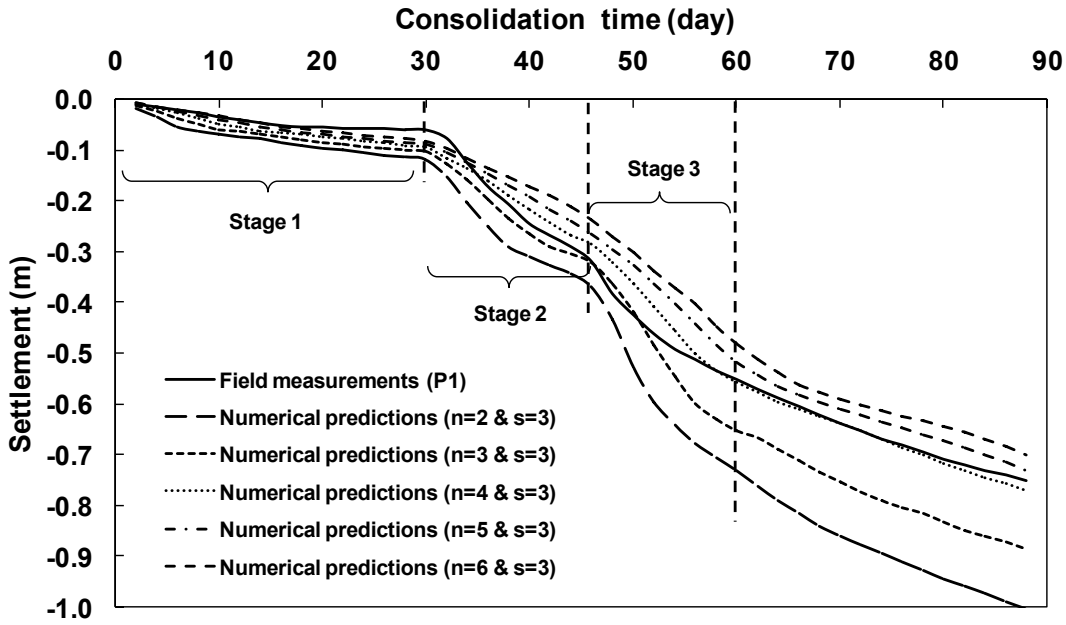

Figure 6.11 Results of numerical parametric study: Sunshine trial embankment at P1

Figure 6.11 shows that there was 1.0 m of settlement after 90 days of consolidation, where k_h/k_s=2 and r_s/r_m=3, while using k_h/k_s=6 and r_s/r_m=3 could reduce consolidation by 0.3 m after the same elapsed time. This result shows that the variation of smear zone properties can affect the rate of consolidation rate quite considerably. Figure 6.11 indicates that k_h/k_s=4 and r_s/r_m=3 provides the best fit with the field measurements. However, according to the plotted settlement graphs in Figure 6.11, the observational approach cannot be used to predict the optimum smear zone properties in the early stages of constructing the trial embankment and a systematic procedure for this calculation is needed to determine the case having minimum errors with the field measurements.

It can be noted that the permeability ratio of the smear zone is not a key factor in the first stage of constructing the embankment, which lasted 30 days. However, when the height was increased from 1.15 m to 2.85 m, the variations in the permeability ratio (k_h/k_s) played a more significant role in the predicted settlement curve. It is clearly observed that the smear zone uncertainties can significantly affect the consolidation time, particularly in the higher degrees of consolidation.

6.3.5 Large Scale Consolidometer

The large scale consolidometer test was simulated using the FLAC code (see Chapter 5, Section 5.6 for details) and the back analysis procedure was applied to perform the parametric study with a constant extent ratio ($s=r_s/r_w$) of 3 and a smear zone permeability ratio ($n=k_h/k_s$) between 1.5 and 3.0. The results of the numerical parametric study are shown in Figure 6.12.

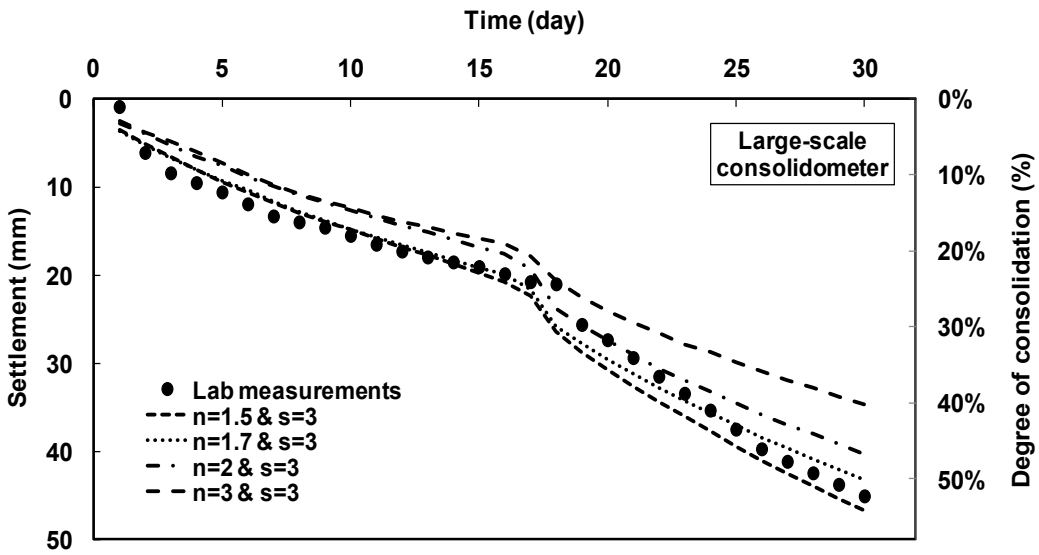

Figure 6.12 Results of numerical parametric study: Large scale consolidometer test

According to the graphs illustrated in Figure 6.12, the predicted settlement at the end of the consolidation test increased by 30% (from 35mm to 46mm) by varying the permeability ratio ($n=k_h/k_s$) from 3 to 1.5. This confirmed the substantial effect that the smear zone properties had on the PVD assisted preloading design. Figure 6.12 indicates that where $k_h/k_s = 1.5$ and $k_h/k_s = 1.7$ they were in good agreement with the test measurements, but selecting the optimum ratios by observation is not feasible.

The predicted settlements for different combinations of the extent and permeability of the smear zone were located in a narrow band in the early stages of applying the surcharge, while the settlement-time curves diverged due to the increase in consolidation time. The tight settlement graphs caused problems in determining the best fitted curve to the test measurements and corresponding smear zone characteristics by observation in the early stages of preloading, which reconfirmed the importance of using the proposed procedure shown in Figure 6.1.

6.4 STEP III: DETERMINING THE ERROR

The conducted parametric studies revealed that the observational technique cannot be used to predict the smear zone properties precisely in the early stages of constructing the trial embankment, which resulted in the settlement curves having the best agreement with the measurements. Therefore the existing error between the field measurements and numerical predictions for the smear zone properties applied must be determined at every time step (corresponding to the degree of consolidation) in order to find the optimum combination of r_s/r_w and k_h/k_s. For this reason, the normalised cumulative error at each time step during the consolidation process was calculated using Equation (6.2).

$$(E_t)_n = \sum_{i=1}^{n} \frac{(S_t)_i - (S_{tp})_i}{N \times S_f} \tag{6.2}$$

where, E_t is the normalised cumulative error at time t, n is the observation point number, N is the total number of observation points, S_t is the field settlement at time t, S_{tp} is the predicted settlement at time t, and S_f is the final primary consolidation settlement.

The curves in Figure 6.13 show the changes of normalised cumulative error with the degree of consolidation for all the simulated case studies where selected combinations of smear zone properties were used. The degree of consolidation was determined for each case by dividing the predicted settlement at every numerical step with the final calculated settlement.

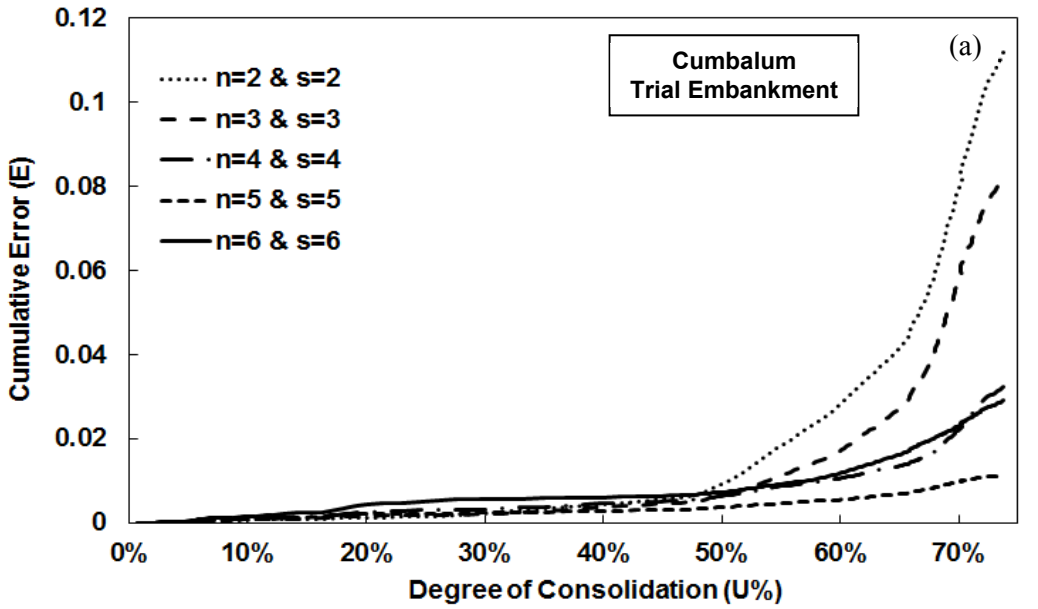
Cumbalum
Trial Embankment
(a)
n=2 & s=2
n=3 & s=3
n=4 & s=4
n=5 & s=5
n=6 & s=6
Cumulative Error (E)
0.12
0.1
0.08
0.06
0.04
0.02
0
0%
10%
20%
30%
40%
50%
60%
70%
Degree of Consolidation (U%)

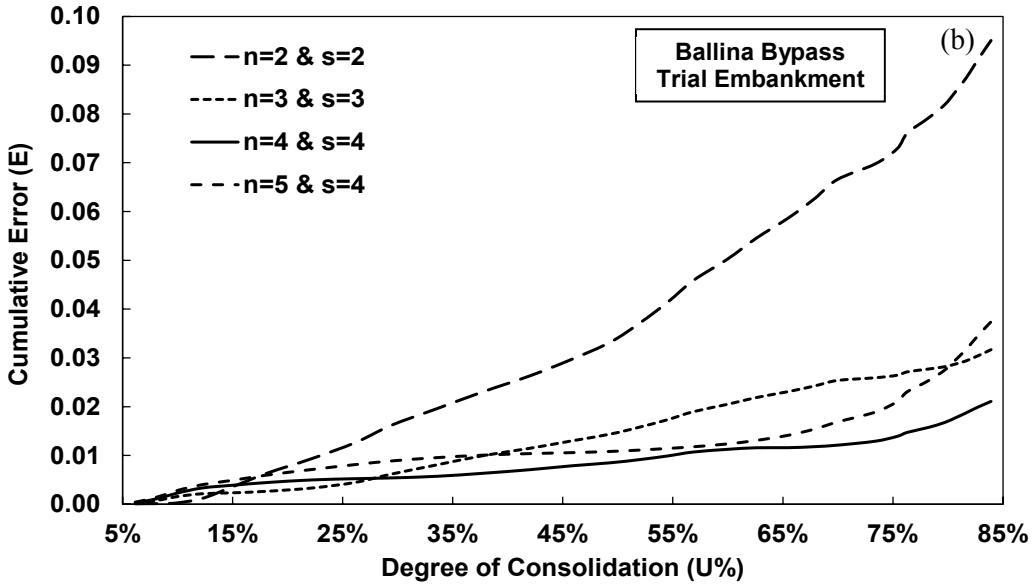
Ballina Bypass
Trial Embankment
(b)
n=2 & s=2
n=3 & s=3
n=4 & s=4
n=5 & s=4
Cumulative Error (E)
0.10
0.09
0.08
0.07
0.06
0.05
0.04
0.03
0.02
0.01
0.00
5%
15%
25%
35%
45%
55%
65%
75%
85%
Degree of Consolidation (U%)

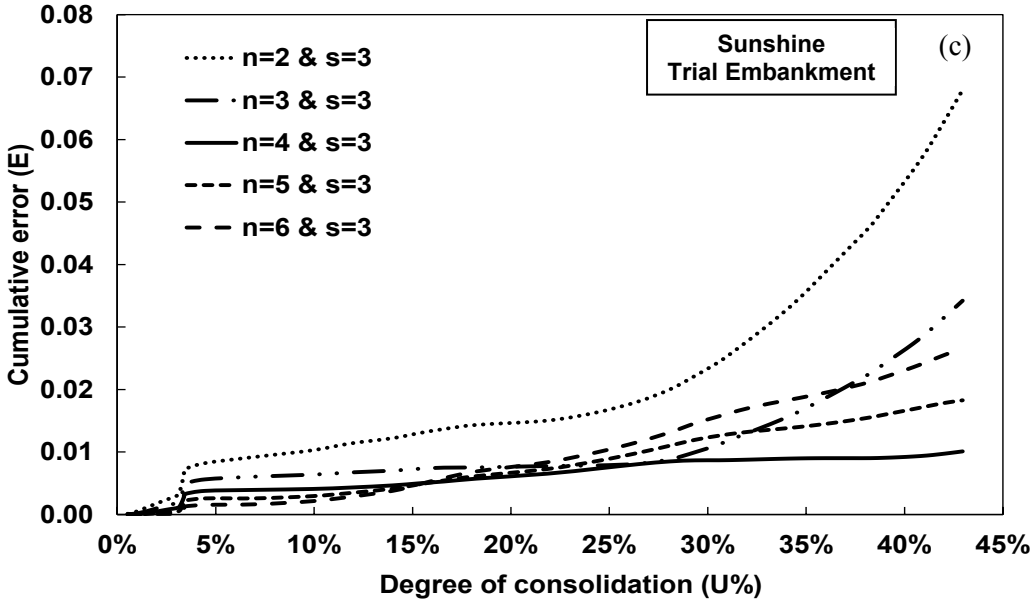
Sunshine
Trial Embankment
(c)
n=2 & s=3
n=3 & s=3
n=4 & s=3
n=5 & s=3
n=6 & s=3
Cumulative error (E)
0.08
0.07
0.06
0.05
0.04
0.03
0.02
0.01
0.00
0%
5%
10%
15%
20%
25%
30%
35%
40%
45%
Degree of consolidation (U%)

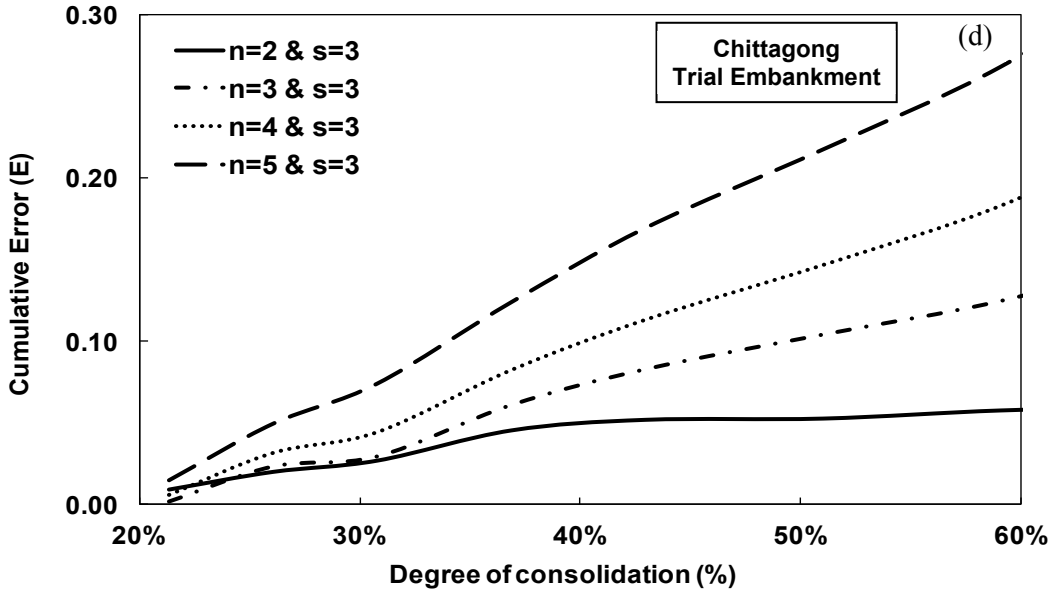

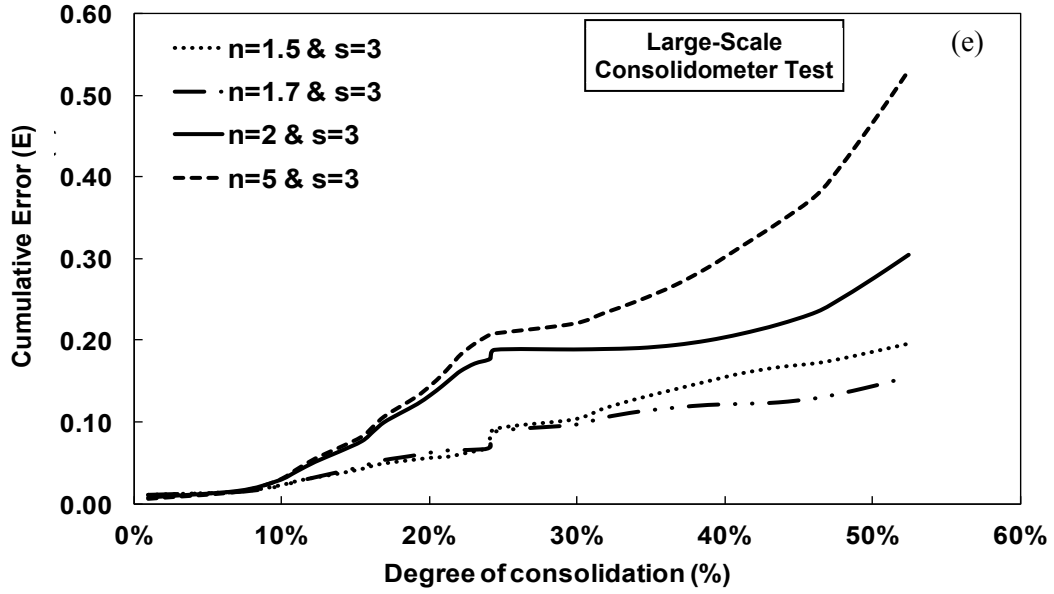

Figure 6.13 Normalised cumulative error versus degree of consolidation for different smear zone properties, (a) Cumbalum trial embankment at SP9, (b) Ballina Bypass trial embankment at SP12, (c) Sunshine trial embankment at P1, (d) Chittagong Port trial embankment, and (e) large-scale consolidometer

In each case study the best smear zone properties ($s=r_s/r_w$ and $n=k_h/k_s$) predicted belonged to the case with the minimum final cumulative error. The final cumulative errors for different combinations of n and s are shown in Table 6.3. The highlighted cells are the smear zone properties that resulted in the minimum final cumulative

error and where the corresponding curve had the best fit with the field measurements. These can be reported as the best smear zone characteristics predicted.

Table 6.3 The final cumulative errors for different combinations of smear zone properties

Cumbalum Trial Embankment					
n (k_h/k_s)	2	3	4	5	6
s (r_s/r_m)	2	3	4	5	6
E_f	0.113	0.083	0.032	0.011	0.029
Ballina Bypass Trial Embankment					
n (k_h/k_s)	2	3	4	5	
s (r_s/r_m)	2	3	4	5	
E_f	0.095	0.032	0.021	0.037	
Sunshine Trial Embankment					
n (k_h/k_s)	2	3	4	5	6
s (r_s/r_m)	3	3	3	3	3
E_f	0.068	0.034	0.010	0.018	0.027
Chittagong Sea Port Trial Embankment					
n (k_h/k_s)	2	3	4	5	
s (r_s/r_m)	3	3	3	3	
E_f	0.22	0.34	0.67	1.03	
Large Consolidometer Test					
n (k_h/k_s)	1.5	1.7	2	3	
s (r_s/r_m)	3	3	3	3	
E_f	0.2	0.15	0.3	0.53	

Note: E_f denotes the final cumulative error

6.5 STEP IV: DETERMINING THE MINIMUM REQUIRED MONITORING TIME

Figures 6.13 indicates that estimating the smear zone characteristics at the early stages after applying the surcharge is a challenging task and accurate values may not readily be obtained. To determine the minimum degree of consolidation (minimum waiting time after applying the surcharge) that results in predicting the most accurate r_s/r_w and k_h/k_s values, the final cumulative error corresponding to the case with the minimum cumulative error at every degree of consolidation was determined and the results are plotted in Figures 6.14(a) to 6.14(e). The minimum degree of consolidation required and the corresponding time belong to the first point with the minimum final cumulative error. The predicted smear zone properties (r_s/r_m and k_h/k_s) at that point can be reported as reliable values for practical design purposes.

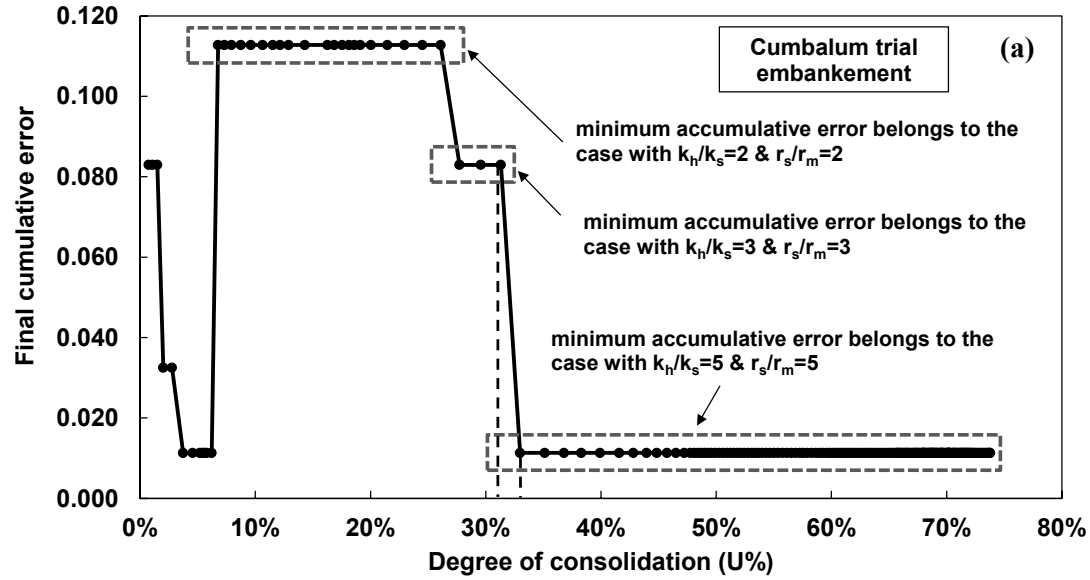
Cumbalum trial embankement
(a)
minimum accumulative error belongs to the case with k_h/k_s=2 & r_s/r_m=2
minimum accumulative error belongs to the case with k_h/k_s=3 & r_s/r_m=3
minimum accumulative error belongs to the case with k_h/k_s=5 & r_s/r_m=5
Final cumulative error
Degree of consolidation (U%)
0.120
0.100
0.080
0.060
0.040
0.020
0.000
0%
10%
20%
30%
40%
50%
60%
70%
80%

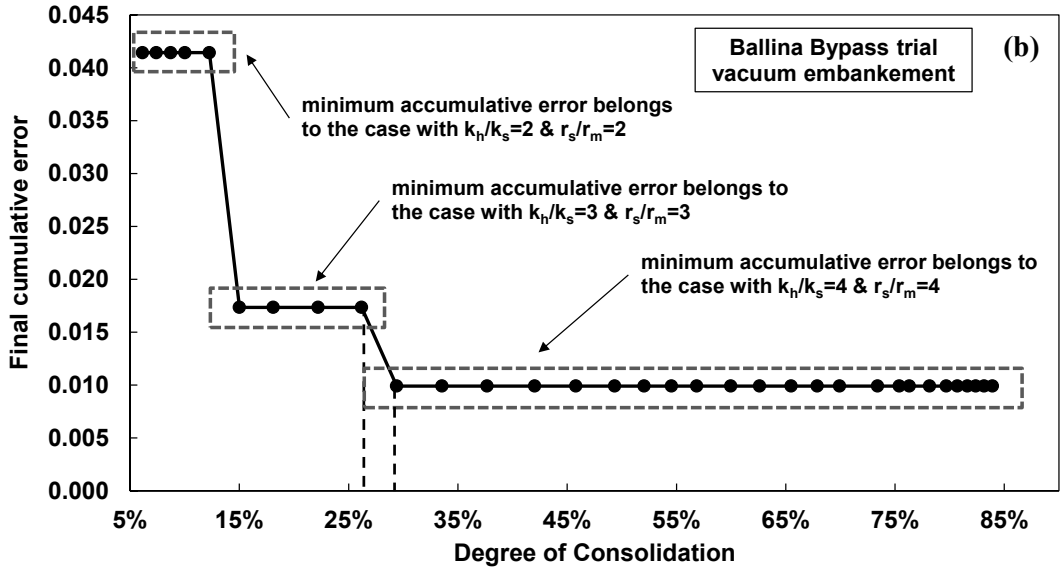
Ballina Bypass trial vacuum embankement
(b)
minimum accumulative error belongs to the case with k_h/k_s=2 & r_s/r_m=2
minimum accumulative error belongs to the case with k_h/k_s=3 & r_s/r_m=3
minimum accumulative error belongs to the case with k_h/k_s=4 & r_s/r_m=4
Final cumulative error
Degree of Consolidation
0.045
0.040
0.035
0.030
0.025
0.020
0.015
0.010
0.005
0.000
5%
15%
25%
35%
45%
55%
65%
75%
85%

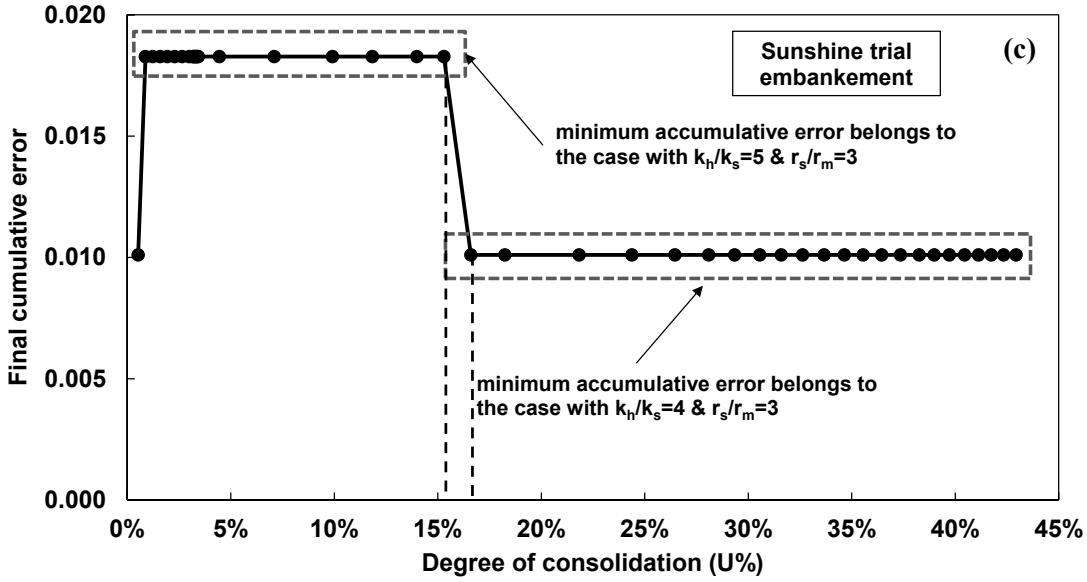
Sunshine trial embankement
(c)
minimum accumulative error belongs to the case with k_h/k_s=5 & r_s/r_m=3
minimum accumulative error belongs to the case with k_h/k_s=4 & r_s/r_m=3
Final cumulative error
Degree of consolidation (U%)
0.020
0.015
0.010
0.005
0.000
0%
5%
10%
15%
20%
25%
30%
35%
40%
45%

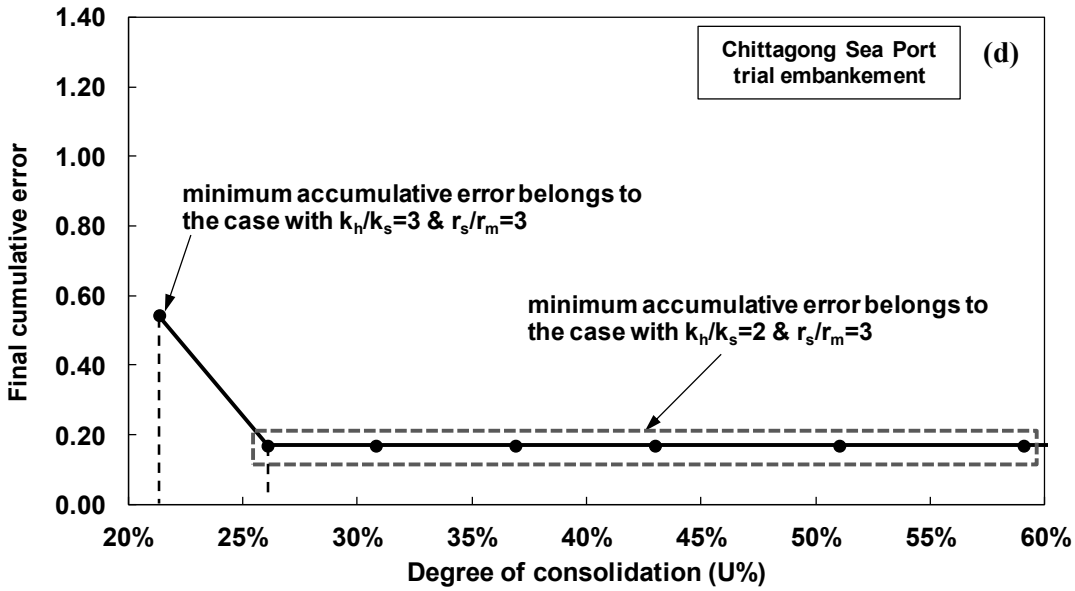

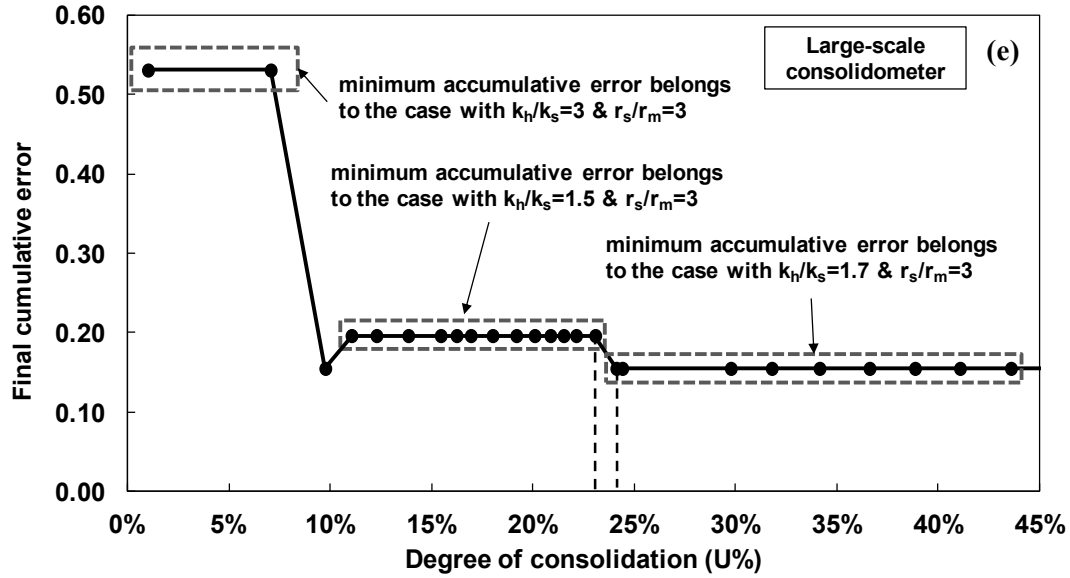

Figure 6.14 Total cumulative error (for the smear zone properties resulting in minimum cumulative error) versus degree of consolidation, (a) Cumbalum trial embankment at SP9, (b) Ballina Bypass trial embankment at SP12, (c) Sunshine trial embankment at P1, (d) Chittagong Port trial embankment at G1, and (e) Large-scale consolidometer test

According to the graph plotted for the Cumbalum trial embankment in Figure 6.14(a), 33% degree of consolidation was the minimum period that must be considered to estimate the smear zone characteristics accurately. Figure 6.14(b) shows there was no change in the value of the final cumulative error after 26% degree of consolidation for the Ballina Bypass trial embankment that corresponds to

a case with smear zone properties of $r_s/r_w=4$ and $k_h/k_s=4$, and therefore reliable predictions for the smear zone properties predictions can be obtained after 26% degree of consolidation. Figure 6.14(c) shows that the smear zone properties for the Sunshine trial embankment can be predicted quite well when at least 16% degree of consolidation has been obtained. Referring to Figure 6.14(c), the final cumulative error for Sunshine trial embankment has a constant and minimum value of 0.01 after 16% degree of consolidation, which belongs to the case with $k_h/k_s=4$ and $r_s/r_m=3$.

Figure 6.14(d) shows a minimum final cumulative error of 0.17 after the Chittagong trial embankment had reached 25% degree of consolidation; this belongs to the case with smear zone properties of $r_s/r_w=2$ and $k_h/k_s=3$. According to Figure 6.14(e), the permeability ratio is 1.5 ($r_s/r_m=3$) with a final cumulative error of 0.20 between 10% and 24% degree of consolidation for the large consolidometer test. The minimum final cumulative error has a constant value of 0.15 after 24% degree of consolidation, which corresponds to the case with smear zone properties of $r_s/r_w=1.7$ and $k_h/k_s=3$. This variation in the smear zone properties that resulted in a minimum final cumulative error was insignificant after 10% degree of consolidation, which can be reported as the minimum degree of consolidation needed for acquiring reliable smear zone properties. The minimum required degree of consolidation and corresponding time resulting in predictable smear zone properties for each case study is summarised in Table 6.4.

Table 6.4 Minimum required degree of consolidation and corresponding time resulting in predicting reliable smear zone properties

Case Study	Cumbalum TR	Ballina Bypass TR	Sunshine TR	Chittagong Sea Port	Large Consolidometer
$U\%_{min}$	33%	26%	16%	25%	10%
t_{min} (day)	600	104	15	14	3
$(k_h/k_s)_{opt}$	5	4	4	2	1.5-1.7
$(r_s/r_m)_{opt}$	5	4	3	3	3

Note: TR is trial embankment; $U\%_{min}$ is the minimum required degree of consolidation; t_{min} is the corresponding consolidation time to the $U\%_{min}$; $(k_h/k_s)_{opt}$ is the predicted permeability ratio at $U\%_{min}$; $(r_s/r_m)_{opt}$ is the predicted extent ratio at $U\%_{min}$

The results summarised in Table 6.4 indicate that the designed systematic procedure (Figure 6.1) can be used to accurately estimate the smear zone properties in the early stages of constructing a trial embankment. Therefore, constructing a trial embankment with field measurements, in conjunction with the proposed systematic procedure (Figure 6.1), is a very practical solution for accurately estimating the smear zone properties and significantly reducing the time and cost of construction. According to Table 6.4, the minimum required degree of consolidation needed to predict reliable smear zone characteristics varied between 10% and 33% for the large scale consolidometer test and the Cumbalum trial embankment, respectively. This showed that a shorter waiting time was needed to accurately predict the smear zone properties in the laboratory PVD assisted consolidation test compared to the time needed to construct the trial embankment.

According to the back calculation results, 33% can be the minimum required degree of consolidation needed to reliably estimate the extent and permeability of the smear zone during the trial embankment construction process.

6.6 SUMMARY

In this chapter, a systematic procedure (explained in Chapter 3) was used to determine the minimum degree of consolidation needed to predict reliable smear zone properties. For this purpose a four-step solution combined with the developed numerical code (Figure 6.1) was proposed, that includes: (i) an estimation of primary consolidation settlement, (ii) a parametric study to estimate various extent and permeability of the smear zone, (iii) calculating the settlement prediction error, and (iv) determination of the minimum time needed for back calculating reliable smear zone properties. The PVD assisted preloading case studies, including four trial embankments (i.e. Chittagong Sea Port, Cumbalum, Ballina Bypass, and Sunshine) and one large scale laboratory consolidometer test (described in Chapter 5) were used in this investigation.

The first three steps of the developed back calculation procedure, in conjunction with the FLAC code, were used to calculate the normalised cumulative error at each stage of consolidation in order to determine the error existing between the field measurements and the numerical predictions for the applied smear zone properties at every degree of consolidation, and find the optimum combination of

r_s/r_w and k_h/k_s. The smear zone properties that resulted in the minimum final cumulative error were presumed to be the best predicted smear zone characteristics. The results of this stage indicated that estimating the smear zone characteristics at the early stages of constructing the trial embankment was a challenging task and accurate values may not be obtained straightaway.

The parametric studies indicated that although both the extent and permeability of the smear zone affected the consolidation process quite substantially, the permeability ratio was more critical. Moreover, the influence of the variability in r_s/r_m became important when the permeability of the smear zone decreased. According to the numerical results, several combinations of smear zone properties can be used for practical design purposes.

In the last stage of the proposed solution (Figure 6.1), the minimum degree of consolidation needed to predict the most accurate r_s/r_w and k_h/k_s values were determined using the outcomes of the previous stages. For this reason, the final cumulative error corresponding to the minimum error accumulated at every degree of consolidation was determined, and the results for all case studies were plotted. The minimum required degree of consolidation belongs to the first point with the minimum final cumulative error. The smear zone properties (r_s/r_m and k_h/k_s) predicted at that point can be reported as reliable values for practical design purposes.

The minimum required degree of consolidation for the Cumbalum, Ballina, Sunshine, and Chittagong trial embankments were determined as 33%, 26%, 16%, and 25%, respectively. This minimum value was determined as low as 10% for a large consolidometer test, indicating that reliable smear zone properties can be predicted much faster in PVD assisted laboratory tests than field trial embankment. According to the analyses presented in this chapter, the extent and permeability of the smear zone can be predicted using the proposed calculation procedure during construction of a trial embankment, when at least 33% of the predicted final settlement has been reached (i.e. after achieving 33% degree of consolidation).

CHAPTER SEVEN

7 CONCLUSIONS AND RECOMMENDATIONS

7.1 SUMMARY

A comprehensive introduction and literature review of prefabricated vertical drains (PVDs) assisted preloading were presented in Chapters 1 and 2 with a focus on the effects of smearing. Chapter 2 reviewed the factors affecting the consolidation of clay deposits improved with PVDs, the concepts of the smear zone generation, the advancements in determining the properties of the smear zone, the developments in radial consolidation theory by considering the characteristics of the smear zone, and the methods available for converting permeability from an axisymmetric to a plane-strain condition. In Chapter 3 the explicit finite difference program FLAC 2D was introduced and used to develop a numerical code to simulate ground improvement using PVD combined with surcharge and vacuum preloading. Furthermore, a systematic back calculation procedure was proposed to determine the properties of the smear zone using the data consolidated from laboratory or field preloading projects. Chapter 4 presented an experimental procedure where a large Rowe cell was used to simulate the combined vertical and radial consolidation process with vertical drain by considering artificially introduced smear zone properties. The laboratory results were used to validate the proposed back calculation procedure to obtain the properties of the smear zone by adopting the developed numerical code. In Chapter 5 the properties of the smear zone for five case histories of PVD assisted preloading were back calculated by using the proposed systematic back calculation procedure to examine the validity of the method developed for different conditions. Chapter 6 presented an expanded back analysis procedure to determine the minimum required degree of consolidation and corresponding time resulting in predictable smear zone properties.

7.2 CONCLUSIONS

Preloading with prefabricated vertical drains is highly recommended as an effective ground improvement technique in deposits of soft soil. Installation of vertical drains accelerates the rate of settlement quite significantly by reducing the drainage path. Prefabricated vertical drains were installed using a mandrel, but the mandrel disturbs the soil around the drain to a certain extent and reduces the permeability of the soil in this region, which is called the smear zone, and affects the consolidation rate quite considerably. Generally, two major parameters were proposed to characterise the smear zone; the permeability (k_s), and the extent (r_s) of the smear zone. Determination of the smear zone properties is a challenging task and as such, has been the subject of intense discussion in the literature. Despite several investigations that were conducted by researchers, no comprehensive approach for predicting the properties of the smear zone precisely, has been recommended. Thus, developing a reliable method for estimating the properties of the smear zone can assist practising engineers increase the accuracy of practical designs and predictions.

According to the current literature, the extent of the smear zone (r_s) may vary from 1.6 to 7 times of the radius of the drain (r_w), or 1 to 6 times of the equivalent diameter of the mandrel (r_m) where the proposed range for the permeability ratio (k_h/k_s) is 1.03 to 10. It can be noted that wide ranges were proposed for k_h/k_s and r_s/r_m. The assumptive properties for the characteristics of the smear zone may result in inaccurate predictions of ground behaviour. This can lead to an early removal of the surcharge during construction resulting in excessive post construction settlement or excessive construction time that increases the project cost.

In this study, the FLAC program was used to investigate how the properties of the smear zone affect the consolidation process. According to the results of the numerical parametric study, the combined effects of the variability in the extent and permeability of the smear zone may increase the time required to obtain 90% degree of consolidation with a factor of two. Furthermore, the numerical analyses revealed that different combinations of the extent and permeability of the smear zone can be reported as acceptable values, which results in similar predictions of settlement and excess pore water pressure. Thus, any of the reported combinations can be adopted for practical design purposes to predict the settlement and excess pore water

pressure. This outcome can be used to conduct the parametric study and determine the optimum combination by assuming the extent ratio (r_s/r_m) as a constant value and by changing the permeability ratio (k_h/k_s).

A fully instrumented large Rowe cell (Figure 4.1a) was used in this study to conduct the PVD assisted consolidation tests. The intact and smear zones were formed by the clay with different permeability coefficients, and a vertical sand drain was placed at the centre of the cell. Readings from the pore water pressure transducers were used to investigate the influence of the radial and vertical distances on the excess pore water pressure. According to the laboratory measurements, the excess pore water pressure reduced as the vertical distance increased from the impervious boundary (cell base). The excess pore water pressures were dissipated much faster in the top half of the soil layer indicating that the vertical consolidation was dominant in the top part of the sample. The laboratory measurements indicated that the incremental variation of excess pore water with radial distance was sharper within the smear zone, especially during the initial stages of loading.

In order to facilitate and accelerate the numerical simulation process, a 2D model can be applied instead of a 3D model, by adopting the equivalent plane-strain permeability for the intact region and the smear zone. In this study, the equations available for converting permeability from an axisymmetric state to a plane-strain condition were evaluated by comparing the plane-strain analysis with the axisymmetric results and laboratory measurements. Numerical analyses indicated that adopting the method of conversion proposed by Hird et al. (1992) may result in better agreement between the plane-strain and axisymmetrically predicted settlement curves, in the early stages of consolidation. It was noted that adopting the method for converting axisymmetric to plane-strain proposed by Indraratna et al. (2005a) combined with Lin et al. (2000) and Hird et al. (1992) resulted in better predictions in the later stages of consolidation by increasing the surcharge and decreasing the void ratio.

In this research, a systematic back calculation procedure combined with the developed numerical code has been proposed to estimate the predicted the properties of the smear zone precisely using laboratory or field measurements (Figure 3.13). A numerical code was developed with various capabilities of simulating PVD assisted preloading with or without vacuum pressures. The code developed was also used to

conduct parametric studies. The proposed back calculation procedure can record the existing error between the numerical results and field measurements in every computational step. The final output of the back calculation procedure is a prediction of the extent and permeability of the smear zone that results in the minimum cumulative error between the numerical results and field measurements. The Rowe cell test measurements (settlement and pore water pressure) were compared with the numerical predictions to validate the proposed back calculation procedure. The results confirmed that the designed back calculation procedure integrated with the developed numerical code can be used as a reliable tool for accurately predicting the properties of the smear zone.

Five case studies of PVD assisted preloading, including four trial embankments and a large scale consolidometer, were numerically simulated and then parametric studies were conducted for each case to determine the properties of the smear zone using the proposed back calculation procedure. In each case study, a specific aspect of the PVD assisted preloading process was included and simulations were conducted to verify how well the proposed back calculation procedure could predict the properties of the smear zone under different conditions. The results validated the capability of this back calculation procedure, in conjunction with the developed numerical code, to reliably estimate the properties of the smear zone in PVD assisted preloading combined with vacuum pressure and embankment loading.

The parametric studies conducted on simulated case studies indicated that the higher smear zone permeability (k_h/k_s) accelerates the dissipation of excess pore water pressure. According to the results, the permeability ratio was more a critical parameter than the ratio of the extent of the smear zone, although the influence of variation in the extent ratio on the consolidation time cannot be neglected, because it can affect the consolidation time by more than 25%. Furthermore, the variation of the extent ratio (r_s/r_m) and the permeability ratio (k_h/k_s) in the low ranges (i.e. 2 to 3) was more critical and substantially influenced the consolidation time and dissipation of excess pore water pressure. According to the numerical analyses, it can be concluded that the variability in r_s/r_m becomes more important when the permeability of smear zone decreases.

The long time required to construct a trial embankment was a major challenge in using this method to conduct the back calculation analysis for estimating

the characteristics of the smear zone and in many cases may cause considerable delay in constructing the actual embankment and a significant increase in the project cost. Estimating the extent and permeability of the smear zone in the early stages of constructing the trial embankment can convert this method into a very practical, accurate, and cost effective approach. In this study, and to rectify this problem, an expanded back calculation procedure was proposed to determine the minimum required degree of consolidation that would result in predictable smear zone properties. The expanded back calculation procedure was designed in four steps, including (i) estimating the primary consolidation settlement, (ii) conducting the parametric study, (iii) determining he normalised error, and (iv) determining the minimum waiting time (Figure 6.1). The PVD assisted preloading case studies including four trial embankments (Chittagong Sea Port, Cumbalum, Ballina Bypass, and Sunshine) and one large-scale consolidometer test was used to conduct the analyses. According to the results, the extent and permeability of the smear zone can be predicted quite well by using the proposed systematic back calculation procedure, when at least 33% of the final settlement predicted, has been obtained (i.e. after achieving 33% degree of consolidation).

According to the results of the parametric study, the back calculated smear zone permeability ratio for the laboratory study on PVD assisted preloading test case was less than the value obtained for the real trial embankments. Furthermore, the results of the back calculation showed that the minimum time needed to reliably predict the properties of the smear zone for the laboratory PVD assisted preloading tests can be determined after obtaining 10% degree of consolidation, and was approximately 65% faster than the value determined for the real embankment.

It is recommended that engineers use the construction of a trial embankment in combination with the proposed systematic back calculation procedure in order to determine the properties of the smear zone with 33% degree of consolidation as the minimum waiting time needed to obtain reliable values. The back calculation procedure can be conducted by assuming a constant extent ratio (e.g. $r_s/r_m=3$ or $r_s/r_m=4$) and change the permeability ratio to obtain the optimum combination that results in the minimum amount of cumulative error between the numerical results and field measurements.

7.3 RECOMMENDATIONS FOR FUTURE RESEARCH

This area of research can be further expanded by conducting the following studies:

- In this study, a two-zone hypothesis was used to describe the disturbed area near the drain. The three-zone hypothesis, which divides the soil surrounding the drain into the inner smear zone, the outer smear zone (the transition zone), and the undisturbed zone, can be applied in future research and the results can be compared to the outcomes of this study.

- The test procedure can be conducted using a larger cell combined with vacuum pressure to determine the minimum degree of consolidation needed to obtain reliable smear zone properties. Furthermore, the accuracy of axisymmetric to plane-strain permeability conversion methods can be evaluated while a vacuum is being applied.

- The proposed minimum waiting time was obtained through the simulation of five case studies. Further verifications, using more data from other case studies, would strengthen this conclusion.

- The proposed back calculation procedure can be combined with the 3D numerical modelling to predict the properties of the smear zone, and then the results can be compared to the 2D analyses. Furthermore, the 3D simulation can be used to evaluate the efficiency of the available axisymmetric to plane-strain permeability conversion equations.

- The variations in the over consolidation ratio (OCR) inside the smear zone can be captured to investigate the influence of OCR on mandrel driven PVD consolidation process, particularly when determining the rates of settlement and distribution of excess pore water pressure.

- Predicting soft soil creep is generally a challenging research because creep can play a significant role in the long-term deformation of soil stabilised with PVD assisted preloading. A large amount of deformation may take place even after the excess pore pressure has dissipated. The effect of creep on an elasto visco-plastic constitutive model, which influences the dissipation of excess pore

water pressure and settlement rates, can be included in the numerical analysis to obtain more reliable results.

REFERENCES

AS: 1289.3.5.2, 2002, 'Methods of testing soils for engineering purposes - Soil classification tests - Determination of the soil particle density of combined soil fractions - Vacuum pycnometer method', Standards Association of Australia.

Aboshi, H. 1992, 'Applied ground improvement techniques, workshop', *Southeast Asian Geotechnical Society (SEAGS), Asian Institute of Technology*, Bangkok, Thailand, p 40.

Abuel-Naga, H. and Bouazza, A. 2009, 'Equivalent diameter of a prefabricated vertical drain', *Geotextiles and Geomembranes*, 27(3), pp. 227-231.

Akagi, T. 1976, 'Effect of displacement type sand drains on strength and compressibility of soft clays', *Doctor of Philosophy. thesis,* University of Tokyo, Japan.

Almedia, M. S. S., Danzigner, F. A. B., F., Almedia M. C., L., Carvalho S. R. and M, Martins I. S. 1993, 'Performance of an embankment built on a soft disturbed clay', *In Proceedings of the 3rd International Conf. Case Histories in Geotechnical Engineering*, Missouri, pp. 351-356.

Almeida, S. S., Marques, M. E. S. and Spotti, A. P. 2005, 'Two case histories of vertical drain in very soft clays', *Ground improvement case histories*, Elsevier, 3, 145-157.

Arulrajah, A., Nikraz, H. and Bo, M. W. 2005, 'Finite element modelling of marine clay deformation under reclamation fills', *Ground Improvement*, 9(3), pp. 105-118.

Asaoka, A., Nakano, M., Noda, T. and Kaneda, K. 2000, 'Delayed compression/consolidation of natural clay due to degradation of soil structure', *Soils and Foundations*, 40(3), pp. 75-85.

Atkinson, K. and Han, W. 2005, 'Finite difference method', *Theoretical Numerical Analysis*, Springer New York, 39**:** 249-271.

Atkinson, M. S. and Eldred, P. J. L. 1981, 'Consolidation of soil using vertical drains', *Geotechnique*, 31(1), pp. 33-43.

Australian Bureau of Statistics 2008. 'Population projections, Australia, 2006 to 2101', Available from http://www.abs.gov.au/Ausstats/abs@.nsf/mf/3222.0.

Balasubramaniam, A. S., Huang, M., Bolton, M., Oh, E. Y. N., Bergado, D. T. and Phienwe, N. j. 2007, 'Interpretation and analysis of test embankments in soft clays with and without ground improvement', *Sixteenth southeast Asian geotechnical conference*, Southeast Asian geotechnical society.

Bamunawita, C. 2004, 'Soft clay foundation improvement via prefabricated vertical drains and vacuum preloading', *Doctor of Philosophy. thesis*, School of Civil, Mining and Environmental Engineering, Faculty of Engineering, The University of Wollongong, Australia.

Barron, R. A. 1948, 'Consolidation of fine-grained soils by drain wells', *Transactions of the American Society of Civli Engineering*, 113(1), pp. 718-742.

Basu, D., Basu, P. and Prezzi, M. 2006, 'Analytical solutions for consolidation aided by vertical drains', *Geomechanics and Geoengineering*, 1(1), pp. 63-71.

Basu, D. and Prezzi, M. 2007, 'Effect of the smear and transition zones around prefabricated vertical drains installed in a triangular pattern on the rate of soil consolidation', *International Journal of Geomechanics*, 7(1), pp. 34-43.

Basu, D., Prezzi, M. and Madhav, M. R. 2010, 'Effect of soil disturbance on consolidation By prefabricated vertical drains installed in a rectangular pattern', *Geotech. and Geolog. Eng.*, 28(1), pp. 61-77.

Bellezza, I. and Fentini, R. 2008, 'Prefabricated vertical drains: a simplified design procedure', *In Proceedings of the the ICE - Ground Improvement*, 161(4), pp. 173-178.

Bergado, D. T., Asakami, H., Alfaro, M. C. and Balasubramaniam, A. S. 1991, 'Smear effects of vertical drains on soft bangkok clay', *Journal of Geotechnical Engineering*, 117(10), pp. 1509-1530.

Bergado, D. T., Manivannan, R. and Balasubramaniam, A. S. 1996, 'Proposed criteria for discharge capacity of prefabricated vertical drains', *Geotextiles and Geomembranes*, 14(9), pp. 481-505.

Bergado, D. T., Mukherjeea, K., Alfaroa, M. C. and Balasubramaniama, A.S. 1993, 'Prediction of vertical-band-drain performance by the finite-element method', *Geotextiles and Geomembranes*, 12(6), pp. 567-586.

Bergadoa, D.T., Singha, N., Sima, S.H., Panichayatuma, B., Sampacoa, C.L. and Balasubramaniama, A.S. 1990, 'Improvement of soft Bangkok clay using vertical geotextile band drains compared with granular piles', *Geotextiles and Geomembranes*, 9(3), pp. 203-231.

Bhosle, P., Vaishampayan, V.V. 2009, 'Case study for ground improvement using PVD with preloading for coal and iron ore stack yard', *Annual Conference of the Indian Geotechnical Society (IGC)*, Guntur, India, pp. 504-510.

Biot, M. A. 1941, 'General theory of three-dimensional consolidation', *Applied Physics*, 12, pp. 155-164.

Bishop, D. 2004, 'A proposed geological model and geotechnical properties of a NSW estuarine valley: A case study', *In Proceedings of the 9th ANZ Conference on Geomechanics*, Auckland NZ, pp. 261-267.

Bo, M. W. 2004, 'Discharge capacity of prefabricated vertical drain and their field measurements', *Geotextiles and Geomembranes*, 22(12), pp. 37-48.

Bo, M. W., Arulrajah, A. and Nikraz, H. 2007, 'Preloading and prefabricated vertical drains design for foreshore land reclamation projects: a case study', *Ground Improvement*, 11(2), pp. 67-76.

Bo, M.W., Chu, J. and Choa, V. 2003, 'Soil improvement: prefabricated vertical drain techniques', Thompson, Singapore.

Britto, A. M. and Gunn, M. J. 1987, 'Critical state soil mechanics via finite elements', *Chichester:: Ellis Horwood Limited*, p 486.

Budhi, M. 2010, 'Soil Mechanics and Foundations', Wiley.

Burns, S. E. and Mayne, P. W. 1998, 'Monotonic and dilatory pore pressure decay during piezocone tests in clay', *Canadian Geotechnical Journal*, 35(6), pp. 1063–1073.

Cao, L. F., Chang, M. F., Teh, C. I. and Na, Y. M. 2001, 'Back-calculation of consolidation parameters from field measurements at a reclamation site', *Canadian Geotechnical Journal*, 38(4), pp. 755-769.

Carillo, N. 1942, 'Simple two and three dimensional cases in the theory of consolidation of soils', *J. Math. and Phys*, 21(1), pp. 1-5.

Carroll, R.G., 1983, 'Geotextile filter criteria', *Engineering Fabrics in Transportation Construction, Transportation Research Record 916*, Transportation Research Board, Washington, DC, USA.

Casagrande, L. and Poulos, S. 1969, 'On the effectiveness of sand drains', *Can. Geotech. J.*, 6(3), pp. 287-326.

Chai, J. and Miura, N. 1999, 'Investigation of factors affecting vertical drain behavior', *Journal of Geotechnical and Geoenvironmental Engineering*, 125(3), pp. 216-226.

Chai, J. C. and Bergado, D. T. 1993, 'Performance of reinforced embankment on Muar clay deposit', *Soils and Foundations*, 33(4), pp. 1-17.

Chai, J. C., Bergado, D. T., Miura, N. and Sakajo, S. 1996, 'Back calculated field effect of vertical drain', *In Proceedings of the 2nd Int. Conf. Soft Soil Engrg.*, Hohai University, Nanjing, China, pp. 270–275.

Chai, J. C., Miura, N., Sakajo, S. and Bergado, D. T. 1995, 'Behavior of vertical drain improved subsoil under embankment loading', *Soils and Foundations*, 35(4), pp. 49-61.

Chai, J., Carter, J. P. and Hayashi, S. 2005, 'Ground deformation induced by vacuum consolidation', *Journal of Geotechnical and Geoenvironmental Engineering*, 131(12), pp. 1552-1561.

Chai, J., Carter, J. P. and Hayashi, S. 2006, 'Vacuum consolidation and its combination with embankment loading', *Canadian Geotechnical Journal*, 43(10), pp. 985-996.

Chai, J., Miura, N. and Bergado, D. T. 2008, 'Preloading clayey deposit by vacuum pressure with cap-drain: Analyses versus performance', *Geotextiles and Geomembranes*, 26(3), pp. 220-230.

Chai, J. and Shen, S. L. 2001, 'Simple method of modeling PVD-improved subsoil', *Journal of Geotechnical and Geoenvironmental Engineering*, 27(11), pp. 965-972.

Christopher, B. R. and Holtz, R. D. 1985, 'Geotextile engineering manual', FHWA-TS-86/203, U.S. Federal Highway Administration.

Chu, J., Yan, S. and Indraranata, B. 2008, 'Vacuum preloading techniques - recent developments and applications', *GeoCongress , Geosustainability and Geohazard Mitigation GPS 178*, New Orleans, pp. 586-595.

Chu, J., Yan, S. W. and Yang, H. 2000, 'Soil improvement by the vacuum preloading method for an oil storage station', *Géotechnique*, 50(6), pp. 625-632.

Chung, S. G., Lee, N. K. and Kim, T. H. 2009, 'Hyperbolic method for prediction of prefabricated vertical drains performance', *Journal of Geotechnical and Geoenvironmental Engineering*, 135(10), pp. 1519-1528.

Collins, I. F. and Yu, H. S. 1996, 'Undrained cavity expansion in critical state soils', *International journal for numerical and analytical methods in geomechanics*, 20(7), pp. 489-516.

Conlin, B.H. and Maddox, W.P. 1985, 'An assessment of the behaviour of foundation clay at Tarsiut N-44 Caisson retained island', *In Proceedings of the 17th Offshore Technology Conference*, Houston, Texas, pp. 379-388.

Craig, H. 2000, 'Soil Mechanics', Chapman & Hall, London.

Cryer, C.W. 1963, 'A comparison of the three dimensional consolidation theories of Biot and Terzaghi', *Quartery Journal of Mechanics and Applied Mathematics*, 16(4), pp. 401-412.

Das, B. M. 2008, 'Advanced Soil Mechanics', Taylor & Francis.

Den Hoedt, G., 1981. 'Laboratory testing of vertical drains', *In Proceedings of the 10th International Conference on Soil Mechanics and Foundation Engineering*, Stockholm, 1, pp. 627–630.

Dhar, A. S., Siddique, A. and Ameen, S. F. 2011, 'Ground improvement using pre-loading with prefabricated vertical drains', *International Journal of Geoengineering Case Histories*, 2(2), pp. 86-104.

Eriksson, U., Hansbo, S. and Torstensson, B. A. 2000, 'Soil improvement at Stockholm-Arlanda airport', *Ground Improvement*, 4(2), pp. 73-80.

Fatahi, B., Khabbaz, H. and Indraratna, B. (2009), 'Parametric studies on bioengineering effects of tree root-based suction on ground behaviour', *Ecological Engineering*, 35(10), pp 1415-1426.

Fatahi, B., Khabbaz, H. and Indraratna, B. (2010), 'Bioengineering ground improvement considering root water uptake model', *Ecological Engineering*, 36(2), pp 222-229.

Fatahi, B., Le, T. M., Le, M. Q. and Khabbaz, H. (2012), 'Soil creep effects on ground lateral deformation and pore water pressure under embankments', *Geomechanics and Geoengineering*, 8(2). pp 107-124.

Fellenius, B.H. and Castonguay, N.G, 1985, 'The Efficiency of band shaped drains – a full scale laboratory study', Report to the National Research Council of Canada and the Industrial Research Assistance Programme.

Fox, P. J. and Berles, J. D. 1997, 'CS2: A piecewise-linear model for large strain radial consolidation', *International journal for numerical and analytical methods in geomechanics*, 21(7), pp. 453-475.

Gao, C. 2004, 'Vacuum preloading method for improving soft soils of higher permeability', *Ground Improvement*, 8(3), pp. 101-107.

Geng, Xueyu, Indraratna, Buddhima and Rujikiatkamjorn, Cholachat 2012, 'Analytical solutions for a single vertical drain with vacuum and time-dependent surcharge preloading in membrane and membraneless systems', *International Journal of Geomechanics*, 12(1), pp. 27-42.

Gens, A. and Potts, D. M. 1988, 'Critical state model in computational geomechanics', *Engng Comput.*, 5, pp. 178–197.

Ghandeharioon, A., Indraratna, B. and Rujikiatkamjorn, C. 2010, 'Analysis of soil disturbance associated with mandrel-driven prefabricated vertical drains using an elliptical cavity expansion theory', *International Journal Geomechanics*, 10(2), pp. 53-64.

Ghandeharioon, Ali, Indraratna, Buddhima and Rujikiatkamjorn, Cholachat 2012, 'Laboratory and finite-element investigation of soil disturbance associated with the installation of mandrel-driven prefabricated vertical drains', *Journal of Geotechnical and Geoenvironmental Engineering*, 138(3), pp. 295-308.

Gibson, R. E. 1963, 'An analysis of system flexibility and its effect on time-lag in pore-water pressure measurements', *Géotechnique*, 13(1), pp. 1-11.

Graham, B. 2010, 'Soil mechanics, principles and practice', Palgrave.

Hansbo, S 1997, 'Practical aspects of vertical drain design', *In Proceedings of the 14th International Conference on Soil Mechanics and Foundation Engineering*, Hamburg, pp. 1749-1752.

Hansbo, S. 1960, 'Consolidation of clay: With special reference to influence of vertical sand drains', *In Proceedings of the Swedish Geotechnical Institute*, Stockholm, Sweden, Swedish Geotechnical Institute.

Hansbo, S. 1979, 'Consolidation of clay by band-shaped prefabricated drains', *Ground Engineering*, 12(5).

Hansbo, S. 1981, 'Consolidation of fine-grained soils by prefabricated drains', *In Proceedings of the 10th International Conference on Soil Mechanics and Foundation Engineering*, Stockholm, Sweden, Balkema, Rotterdam, the Netherlands, pp. 677-682.

Hansbo, S. 1987, 'Design aspects of vertical drains and lime-column installations', *In Proceedings of the 9th Southeast Asian Geotech. Conf.*, Bangkok, Thailand, pp. 8-12.

Hansbo, S. 1994, 'Foundation Engineering', Elsevier Sience B. V., Amsterdam.

Hansbo, S., Jamiolkowski, M. and Kok, L. 1981, 'Consolidation by vertical drains', *Geotechnique*, 31, pp. 45-66.

Hawlader, B. C. and Muhunthan, B. 2002, 'Numerical study of the factors affecting the consolidation of clay with vertical drains', *Geotextiles and Geomembranes*, 20(4), pp. 213-239.

Hird, C. C. and Moseley, V. J. 2000, 'Model study of seepage in smear zones around vertical drains in layered soil', *Géotechnique*, 50(1), pp. 89-97.

Hird, C. C. and Sangtian, N. 2002, 'Model study of seepage in smear zones around vertical drains in layered soil: further results ', *Géotechnique*, 52(5), pp. 375-378.

Hird, C.C., Pyrah, I.C. and Russell, D. 1992, 'Finite element modelling of vertical drains beneath embankments on soft ground', *Géotechnique*, 42(3), pp. 499-511.

Holtz, R.D. 1987, 'Preloading with prefabricated vertical strip drains', *Geotextiles and Geomembranes*, 6(1-3), pp. 109-131.

Holtz, R.D. and Holm, B.G. 1973, 'Excavation and sampling around some sand drains at Ska°-Edeby, Sweden', *In Proceedings of the Sixth Scandinavian Geotechnical Meeting, Trondheim*, Oslo, Sweden, Norwegian Geotechnical Institute, pp. 79-85.

Holtz, R.D., Jamiolkowski, M.B., Lancellotta, R. and Pedroni, R. 1991, 'Prefabricated vertical drains: design and performance', CIRIA, Butterworth-Heinemann, London.

Huang, W., Fityus, S., Bishop, D., Smith, D. and Sheng, D. 2006, 'Finite-element parametric study of the consolidation behavior of a trial embankment on soft clay', *International Journal of Geomechanics*, 6(5), pp. 328-341.

Indraratna, B. 2009, 'Recent Advances in the Application of Vertical Drains and Vacuum Preloading in Soft Soil Stabilisation', *E.H. Davis Memorial Lecture*, Australian Geomechanics Society.

Indraratna, B. 2002, 'Book chapter: Soft ground improvement by vertical drains', *In-situ Characetrisation of Soft Soil*. O. I. P. Saxena, India and Swets & Zeitlinger Publishers, The Netherlands.

Indraratna, B., Aljorany, A. and Rujikiatkamjorn, C. 2008, 'Analytical and numerical modeling of consolidation by vertical drain beneath a circular embankment', *International Journal of Geomechanics*, 8(3), pp. 199-206.

Indraratna, B. and Bamunawita, C. I. 2002, 'Soft clay stabilisation by mandrel driven geosynthetic vertical drains', *Australian Geomechanics Journal*, 37(5), pp. 57-86.

Indraratna, B., Bamunawita, C. and Khabbaz, H. 2004a, 'Numerical modeling of vacuum preloading and field applications', *Canadian Geotechnical Journal*, 41(6), pp. 1098-1110.

Indraratna, B. and Redana, I. W. 1997, 'Plane-strain modeling of smear effects associated with vertical drains', *Journal of Geotechnical and Geoenvironmental Engineering*, 123(5), pp. 474-478.

Indraratna, B. and Redana, I. W. 1998, 'Laboratory determination of smear zone due to vertical drain installation', *Journal of Geotechnical and Geoenvironmental Engineering*, 124(2), pp. 180-184.

Indraratna, B. and Redana, I. W. 2000, 'Numerical modeling of vertical drains with smear and well resistance installed in soft clay', *Canadian Geotechnical Journal*, 37(1), pp. 132-145.

Indraratna, B. and Rujikiatkamjorn, C. 2004b, 'Mathematical modeling and field evaluation of embankment stabilized with vertical drains incorporating vacuum preloading', *The Fifth International Conference on Case Histories in Geotechnical Engineering*, New York, pp. 201-208.

Indraratna, B., Rujikiatkamjorn, C. and Chu, J. 2007a, 'Soft clay stabilization with geosynthetic vertical drains beneath road and railway embankments: A Critical Review of Analytical Solutions and Numerical Analysis', *New Peaks in Geotechnics*, Denver, ASCE, pp. 1-20.

Indraratna, B., Rujikiatkamjorn, C., Kelly , R. and Buys, H. 2010, 'Sustainable soil improvement via vacuum preloading', *Proc. of the ICE - Ground Improvement*, 163(1), pp. 31-42.

Indraratna, B., Rujikiatkamjorn, C. and Sathananthan, I. 2005a, 'Analytical and numerical solutions for a single vertical drain including the effects of vacuum preloading', *Canadian Geotechnical Journal*, 42(4), pp. 994-1014.

Indraratna, B., Rujikiatkamjorn, C., Sathananthan, I., Shahin, M. and Khabbaz, H. 2005c, 'Analytical and numerical solutions for soft clay consolidation using geosynthetic vertical drains with special reference to embankments', *The Fifth International Geotechnical Engineering Conference*, Cairo, Egypt, pp. 55-86.

Indraratna, B., Sathananthan, I. , Rujikiatkamjorn, C. and Balasubramaniam, A. S. 2005b, 'Analytical and numerical modeling of soft soil stabilized by prefabricated vertical drains incorporating vacuum preloading', *International Journal of Geomechanics*, 5(2), pp. 114-124.

Indraratna, B., Rujikiatkamjorn, C., Ameratunga, J. and Boyle, P. 2011, 'Performance and prediction of vacuum combined surcharge consolidation at Port of Brisbane', *Geotechnical and Geoenvironmental Engineering*, 137(11), pp. 1009-1018.

Indraratna, B., Rujikiatkamjorn, C., Balasubramaniam, C., Wijeyakulasuriya, V. 2005d, 'Predictions and observations of soft clay foundations stabilized with

geosynthetic drains and vacuum surcharge', *Ground Improvement: Case Histories*, Elsevier, 3(Chapter 7), 199-230.

Itasca Consulting Group, Inc. 2008, 'FLAC – Fast lagrangian analysis of continua', Version 6.0 User's Manual, Itasca, Minneapolis.

Jacob, C.E. 1940, 'On the flow of water in an elastic artesian aquifer', *Transactions of the American Geophysical Union 21*, Part II, pp. 574–586.

Jamiolkowski, M., Lancellotta, R. and Wolski, W. 1983, 'Precompression and speeding up consolidation', *In Proceedings of the 8th European Conference on Soil Mechanics and Foundation Engineering*, Helsinki, 23-26 May 1983, Balkema, Rotterdam, the Netherlands, pp. 1201-1226.

Johnson, S. J. 1970, 'Foundation precompression with vertical sand drains', *Journal of Soil Mechanics & Foundations Division*, 96(1), pp. 145–175.

Kabbaj, M., Tavenas, F. and Leroueil, S. 1988, 'In situ and laboratory stress-strain relationships', *Geotechnique*, 38(1), pp. 83-100.

Kamon, M. and Bergado, D. T. 1992, 'Ground improvement techniques', *9th Asian regional conf. on Soil Mech. and Found. Eng'g*, Bangkok, pp. 526-546.

Kawaida, M., Kosaka, T., Yamada, K. and Nakakuma, K. 2012, 'Vacuum consolidation for construction of expressway embankment on extremely soft ground', *Journal of the Society of Materials Science, Japan*, 61(1), pp. 46-51.

Kelly, R. B. 2008, 'Back analysis of the Cumbalum trial embankment', *Australian Geomechanics*, 43(1), pp. 47-54.

Kelly, R. B. and Wong, P. K. 2009, 'An embankment constructed using vacuum consolidation', *Australian Geomechanics*, 44(2), pp. 55-64.

Kelly, R., Small, J. and Wong, P. 2008, 'Construction of an embankment using vacuum consolidation and surcharge fill', *In Proceedings of the GeoCongress 2008: Geosustainability and Geohazard Mitigation (GSP 178)*, Orleans, Louisiana, 9–12 March 2008, American Society of Civil Engineers, New York.

Kianfar, K., Indraratna, B. and Rujikiatkamjorn, C. 2013, 'Radial consolidation model incorporating the effects of vacuum preloading and non-Darcian flow', *Geotechnique*, 63(12), pp. 1060-1073.

Kim, R., Choi, Y., Lee, J. and Lee, W. 2010, 'Evaluation of the PVD smear zone using micro penetrometer', *In Proceedings of the GeoFlorida 2010: Advances in Analysis, Modeling & Design (GSP 199)*, 20-24 Feb 2010, American Society of Civil Engineers, New York, pp. 998-1007.

Kim, T., Kim, N., Tumay, M. and Lee, W. 2007, 'Spatial distribution of excess pore-water pressure due to piezocone penetration in overconsolidated clay', *Journal of Geotechnical and Geoenvironmental Engineering*, 133(6), pp. 674–683.

Kimoto, S. and Oka, F. 2005, 'An elasto-viscoplastic model for clay considering destructuralisation and consolidation analysis of unstable behaviour', *Soils and Foundations*, 45(2), pp. 29-42.

Kjellman, W. 1952, 'Consolidation of clayey soils by atmospheric pressure', *In Proceedings of the Conference on Soil Stabilization*, Massachusetts Institute of Technology, Boston, pp. 258-263.

Koda, E., Szymanski, A. and Wolski, W. 1984, 'Laboratory tests on geodrains durability in organic soils', *Seminar on Laboratory Testing of Prefabricated Band-Shaped Drains*, Milan, Italy.

Koerner, R. M. 1987, 'Soft soil stabilization using geosynthetics', Elsevier, Applied Science, London.

Koerner, R. M. and Ko, F. K. 1992, 'Laboratory studies on long-term drainage capability of geotextiles', *In Proceedings of the 2nd Int. Conf. on Geotextiles*, Las Vegas, pp. 91-95.

Kremer, R., De Japer, W., Maagdenberg, A., Megrogel, I. and Oostveen, J. 1982, 'Quality standards for vertical drains', *In Proceedings of the Second International Conference on Geotextiles*, Las Vegas, Nevada, pp. 319–324.

Kremer, R. R. H. J., Oostven, J. P., Van Weele, A. F., Dejager, W. F. J. and Meyvogel, I. J. 1983, 'The quality of vertical drainage', *In Proceedings of the Eighth European Conference on Soil Mechanics and Foundation Engineering*, Helsinki, pp. 721–726.

Le, T. M., Fatahi, B. and Khabbaz, H. (2012), 'Viscous Behaviour of Soft Clay and Inducing Factors', *Geotechnical and Geological Engineering*, 30(5), pp 1069-1083.

Leo, C. J. 2004, 'Equal strain consolidation by vertical drains', *Journal of Geotechnical and Geoenvironmental Engineering*, 130(3), pp. 316-327.

Leroueil, S. 1997, 'Closure to 'Compressibility of clays: Fundamental and practical aspects', *J. Geotech. and Geoenvir. Engrg.*, 123(9), 895p.

Lin, D. G., Kim, H. K. and Balasubramaniam, A. S. 2000, 'Numerical modelling of prefabricated vertical drain', *Geotechnical Engineering Journal of the Southeast Asian Geotechnical Society*, 31(2), pp. 190-125.

Lin, D.G. and Chang, K.T. 2009, 'Three-dimensional numerical modelling of soft ground improved by prefabricated vertical drains', *Geosynthetics International*, 16(5), pp. 339-353.

Liu, C. and Evett, J 2013, 'Soils and foundations', Pearson.

Liu, H. l. and Chu, J. 2009, 'A new type of prefabricated vertical drain with improved properties', *Geotextiles and Geomembranes*, 27(2), pp. 152-155.

Liu, H. L., Chu, J. and Ren, Z. 2009, 'New methods for measuring the installation depth of prefabricated vertical drains', *Geotextiles and Geomembranes*, 27(6), pp. 493-496.

Lo, D. O. K. 1991, 'Soil improvement by vertical drains', *Doctor of Philosophy. thesis*, The University of Illinois at Urbana.

Logan, D. L. 2007, 'A First course in the finite element method', Thompson, Tampa, USA.

Long, R. and Covo, A. 1994, 'Equivalent diameter of vertical drains with an pblong cross section', *Journal of Geotechnical Engineering*, 120(9), pp. 1625-1630.

Madhav, M. R., Park, Y. M. and Miura, N. 1993, 'Modelling and study of smear zones around band shaped drins', *Soils and Foundations*, 33(4), pp. 135-147.

Mandel, J 1953, 'Consolidation des sols (Etude Mathematique)', *Geotechnique*, 3(7), pp. 287-299.

Masse, F., Yee, K. and Varaksin, S. 2002, 'Successful application of Vacuum Consolidation method to Nakdong River soft clay in Kimhae, South Korea', *4the Conference on Ground Ipmrovement Techniques*, Kuala Lumpur, Malaysia.

Mesri, G., Kelly, W. E., Vallee, R. P. and Andersland, O. B. 1973, 'Coefficient of secondary compression (discussion)', *Journal of Soil Mechanics & Foundations*, Div 99, no. Proc Paper.

Mesri, G. & Lo, D.O.K. 1991, 'Field Performance of Prefabricated Vertical Drains', *In Proceedings of the International Conference on Geotechnical Engineering for Coastal Development-Theory to Practice*, Yokohama, Japan, 1, pp 231–236.

Mesri, G., Lo, D.O.K. and Feng, T-W. 1994, 'Settlement of embankments on soft clays', *In Vertical and Horizontal Deformations of Foundations and Embankments*, *Proceedings* of Settlement 94, GSP 40, ASCE, New York, pp. 8-56.

Mohamedelhassan, E. and Shang, J. Q. 2002, 'Vacuum and surcharge combined one-dimensional consolidation of clay soils', *Canadian Geotechnical Journal*, 39(5), pp. 1126-1138.

Morris, P. H. 2005, 'Analytical solutions of linear finite- and small-strain one-dimensional consolidation', *International journal for numerical and analytical methods in geomechanics*, 29(2), pp. 127-140.

Murray, H. H. 1999, 'Applied clay mineralogy today and tomorrow', *Clay Minerals*

34(1), pp. 39–49.

Nagtegaal, J. C., Parks, D. M. and Rice, J. R. 1974, 'On numerically accurate finite element solutions in the fully plastic range', *Comp. Meth. in Appl. Mech. and Eng.*, 4, pp. 153-177.

Nelson, J.D. and Miller, D.G. 1997, 'Expansive soil: problems and practice in foundation and pavement engineering', John Wiley & Sons, New York.

Onoue, A. 1988, 'Consolidation by vertical drains taking well resistance and smear into consideration', *Soils and Foundations*, 28(4), pp. 165-174.

Onoue, A., Ting, N. H., Germaine, J. T. and Whitman, R. V. 1991, 'Permeability of disturbed zone around vertical drains', *In Proceedings of the Geotechnical Engineering Congress (GSP 27)*, American Society of Civil Engineers, New York, pp. 879-890.

Oostveen, J. P. 1986, 'Research acticities on vertical drainahe in the Netherland', *Seminar on vertical drainage*, Delf University of Technology, pp. 8-9.

Perlof, W. H., Nair, K. and Smith, J. G. 1965, 'Effect of measuring system on pore water pressures in the consolidation test', *In Proceedings of the 6th ICSMFE*, Montreal, pp. 338-341.

Pradhan, T. B. S., Imai, G., Murata, T., Kamon, M. and Suwa, S. 1993, 'Experiment study on the equivalent diameter of a prefabricated band-shaped drain', *In Proceedings of the Proc. 11th Southeast Asian Geotech. Conf.*, 1.

Qian, J. H., Zhao, W. B., Cheung, Y. K. and Lee, P. K. K. 2003, 'The theory and practice of vacuum preloading', *Computers and Geotechnics*, 13(2), pp. 103-118.

Queensland Department of Transport, Sunshine Motorway Stage 2, 1992, 'Performance of the trial embankment area 2A (Ch 28490-28640)', *Report R1802*, Materials and Geotechnical Services Branch.

Rixner, J. J., Kraemer, S. R. and Smith, A. D., 1986, 'Prefabrieated vertical drains', *Engineering Guideline, FHWA/RD-86/168*, Federal Highway Administration, Virginia.

Robinson, R. G. 1999, 'Consolidation analysis with pore water pressure measurements', *Géotechnique*, 49(1), pp. 127-132.

Roscoe, K. H. and Burland, J. B. 1968, 'On the generalised stress-strain behaviour of 'wet clay', Engineering Plasticity', *Heyman and Leckie (ed)*, pp. 535-609.

Rowe, R. K. and Li, A. K. 2002, 'Behaviour of reinforced embankments on soft rate sensitive soils', *Geotechnique*, 52(1), pp. 859-869.

RTA, 2000, 'Trial embnakment construction report', *Roads and Traffic Authorithy of NSW*, Pacific highway office, Grafton.

Rujikiatkamjorn, C., Ghandeharioon, A. and Indraratna, B. 2009, 'Finite element simulation of mandrel penetration in a normally consolidated soil', *Geotechnics of Soft Soils – Focus on Ground Improvement –*, Leoni, K., Taylor & Francis Group, London**,** 287-292.

Rujikiatkamjorn, C. and Indraratna, B. 2009, 'Design procedure for vertical drains considering a linear variation of lateral permeability within the smear zone', *Canadian Geotechnical Journal*, 46(3), pp. 270-280.

Rujikiatkamjorn, C. and Indraratna, B. 2010, 'Radial consolidation modelling incorporating the effect of a smear zone for a multilayer soil with downdrag caused by mandrel action', *Canadian Geotechnical Journal*, 47(9), pp. 1024-1035.

Rujikiatkamjorn, C., Indraratna, B. and Chu, J. 2008, '2D and 3D numerical modeling of combined surcharge and vacuum preloading with vertical drains', *International Journal of Geomechanics*, 8(2), pp. 144-156.

Saowapakpiboon, J., Bergado, D. T., Voottipruex, P., Lam, L. G. and Nakakuma, K. 2011, 'PVD improvement combined with surcharge and vacuum preloading including simulations', *Geotextiles and Geomembranes*, 29(1), pp. 74-82.

Saowapakpiboon, J., Bergado, D. T., Youwai, S. J., Chai, C., Wanthong, P. and Voottipruexe, P. 2009, 'Measured and predicted performance of prefabricated vertical drains (PVDs) with and without vacuum preloading', *Geotextiles and Geomembranes*, 28(1), pp. 1-11.

Saowapakpiboon, J., Bergado, D. T., Youwai, S., Chai, J. C., Wanthong, P. and Voottipruex, P. 2010, 'Measured and predicted performance of prefabricated vertical drains (PVDs) with and without vacuum preloading', *Geotextiles and Geomembranes*, 28(1), pp. 1-11.

Sathananthan, I. 2005, 'Modelling of vertical drains with smear installed in soft clay', *Doctor of Philosophy. thesis*, School of Civil, Mining and Environmental Engineering, The University of Wollongong, Wollongong, NSW.

Sathananthan, I. and Indraratna, B. 2006, 'Laboratory evaluation of smear zone and correlation between permeability and moisture content', *Journal of Geotechnical and Geoenvironmental Engineering*, 132(7), pp. 942-945.

Sathananthan, I., Indraratna, B. and Rujikiatkamjorn, C. 2008, 'Evaluation of smear zone extent surrounding mandrel driven vertical drains using the cavity expansion theory', *International Journal of Geomechanics*, 8(6), pp. 355-365.

Schiffman, R. L., Chen, A. T.-F. and Jordan, J. C. 1969, 'An analysis of consolidation theories', *Journal of the soil mechincs and fondation division*, 95(SM1), pp. 285-312.

Scott, R. F. 1963, 'Principles of soil mechanics', Addison-Wesley, Massachusetts.

Seah, T. H. 2006, 'Design and construction of ground improvement works at Suvarnabhumi Airport', *Geot. Eng, J. of Southeast Asian Geot. Society*, 37, pp. 171-188.

Sharma, J. and Xiao, D. 2000, 'Determination of smear zone around vertical Drains', *Proceedings of the Soft Ground Technology* Noordwijkerhout, the Netherlands, GSP, pp. 270-279.

Sheng, D., Eigenbrod, K. D. and Wriggers, P. 2005, 'Finite element analysis of pile installation using large-slip frictional contact', *Computers and Geotechnics*, 32(1), pp. 17-26.

Shin, D. H., Lee, C., Lee, J. S. and Lee, W. 2009, 'Detection of smear zone using micro-cone and electrical resistance probe', *Canadian Geotechnical Journal*, 46(6), pp. 719-726.

Sivaram, B. and Swamee, P. 1977, 'A computational method for consolidation coefficient', *Soils and Foundations*, 17(2), pp. 48-52.

Skempton, A. W. 1954, 'The pore-pressure coefficients A and B', *Géotechnique*, 4(4), pp. 143-147.

Small, J.C., Booker, J. R. and Davis, E. H. 1976, 'Elasto-Platic consolidation of soil', *International Journal of Solids and Strucrures*, 12, pp. 431-448.

Songa, Y.S. and Kim, T. H. 2004, 'Improvement of estuarine marine clays for coastal reclamation using vacuum-applied consolidation method', *Ocean Engineering*, 31(16), pp. 1999-2010.

Sonpal, R. C. and Katti, R. K. 1973, 'Consolidation analysis with pore pressure measurements', *8th Int. Conf. on Soil Mechanics and Foundation Eng.*, Moscow, pp. 385-388.

Spaulding and Porbaha, A. 2004, 'Embankment construction on marshland using vacuum consolidation technology', *Geotechnical Engineering for Transportation Projects (GSP 126)*, ASCE, Los Angeles, CA, pp. 1943-1950.

Stapelfeldt, T., Vepsäläinen, P. and Yin, Z. Y. 2008, 'Numerical modelling of a test embankment on soft clay improved with vertical drains', *In Proceedings of the Second International Workshop on Geotechnics of Soft Soils*, Glasgow, Scotland, 3-5 September 2008, Taylor & Francis Group, London, pp. 173-179.

Tang, X. W. and Onitsuka, K. 2000, 'Consolidation by vertical drains under time-dependent loading', *International journal for numerical and analytical methods in geomechanics*, 24(9), pp. 739-751.

Tavenas, F., Tremblay, M., Larouche, G. and Leroueil, S. 1986, 'In situ measurement of permeability in soft clays', *ASCE Spec. Conf. on Use of in Situ Tests in Geotech. Engrg.*, ASCE, New York, pp. 1034–1048.

Teparaksa, W. and Trung Ngo, D. 2012, 'Performance of vacuum consolidation on very soft clay at Nakorn Sri Thammarat Airport', *International Conference on Ground Improvement*, Wollongong, Australia.

Terzaghi, K. 1925, 'Erdbaumechanik auf bodenphysikalischer Grundlage', Deuticke, Vienna, Austria.

Terzaghi, K. T. and Frohlich, O. K. 1936, 'Theorie der Setzung von Tonschichten', Leipzig, pp. 166.

Tran-Nguyen, H.H. and Edil, T.B. 2011, 'The characteristics of PVD smear zone', *In Proceedings of the Geo-Frontiers 2011: Advances in Geotechnical Engineering*, 13–16 March 2011, ASCE, New York, pp. 748-757.

Tran, T. A. and Mitachi, T. 2008, 'Equivalent plane strain modeling of vertical drains in soft ground under embankment combined with vacuum preloading', *Computers and Geotechnics*, 35(5), pp. 655-672.

Vaziri, H. H. and Christian, H. A. 1994, 'Application of Terzaghi's consolidation theory to nearly saturated soils', *Canadian Geotechnical Journal*, 31(2), pp. 311-317.

Walker, J. and Yu, H. S. 2006, 'Adaptive finite element analysis of cone penetration in clay', *Acta Geotechnica*, 1, pp. 43-57.

Walker, R. and Indraratna, B. 2006, 'Vertical drain consolidation with parabolic distribution of permeability in smear zone', *Journal of Geotechnical and Geoenvironmental Engineering*, 132(7), pp. 937-941.

Walker, R. and Indraratna, B. 2007, 'Vertical drain consolidation with overlapping smear zones', *Géotechnique*, 57(5), pp. 463-467.

Walker, R. and Indraratna, B. 2009a, 'Consolidation analysis of a stratified soil with vertical and horizontal drainage using the spectral method', *Géotechnique*, 59(5), pp. 439-449.

Walker, R., Indraratna, B. and Sivakugan, N. 2009b, 'Vertical and radial consolidation analysis of multilayered soil using the spectral method', *Journal of Geotechnical and Geoenvironmental Engineering*, 135(5), pp. 657-663.

Wang, T. R. and Chen, W. H. 1996, 'Development in application of prefabricated drains in treatment of soft soils', *In Proceedings of the Third Symposium on Weak Ground Improvement using PVD*, China, pp. 13–40.

Wang, X. S. and Jiao, J. J. 2004, 'Analysis of soil consolidation by vertical drains with double porosity model', *Int. J. Numer. Anal. Meth. Geomech.*, 28, pp. 1385–1400.

Welker, A. L., and K. M. Herdin. 2003, 'Evaluation of Four Equivalent Diameter Formulations for Prefabricated Vertical Drains Using Flow Rates', *Geosynthetics International*, 10(3), pp. 103-109.

Whitman, R. V., Richardson, A. M. and Healy, K. A. 1961, 'Time-lags in pore pressure measurements', *In Proceedings of the 5th ICSMFE.*

Wood, D. M. 1990, 'Soil behaviour and critical state soil mechanics', Cambridge University Press, Cambridge, UK.

Xie, K. H. 1987, 'Consolidation theories and optimisation design for vertical drains', *Doctor of Philosophy. thesis*, The Zhejiang University, China.

Xie, K. H., Xie, X. Y. and Gao, X. 1999, 'Theory of one dimensional consolidation of two-layered soil with partially drained boundaries', *Computers and Geotechnics*, 24(4), pp. 265-278.

Xie, K. H., Xie, X. Y. and Jiang, W. 2002, 'A study on one-dimensional nonlinear consolidation of double-layered soil', *Computers and Geotechnics*, 29(2), pp. 151-168.

Xie, K.H. and Leo, C.J. 2004, 'Analytical solutions of one-dimensional large strain consolidation of saturated and homogeneous clays', *Computers and Geotechnics*, 31(4), pp. 301-314.

Yan, H.S. and Cao, D.Z. 2005, 'Application of low-level vacuum preloading technique in offshore projects', *Ocean and River Hydraulics*, 3, pp. 41-43.

Yan, S.-W. and Chu, J. 2005, 'Soil improvement for a storage yard using the combined vacuum and fill preloading method', *Can. Geotec. J.*, 42(4), pp. 1094-1104.

Yildiz, A. and Karstunen, M. 2009, 'Numerical modeling of vertical drains with advanced constitutive models', *Computers and Geotechnics*, 36(6), pp. 1072-1083.

Yildiz, A., M., Karstunen and H., Krenn 2006, 'Numerical modelling of vertical drains with advanced constitutive models', *In Proceedings of the The sixth European Conf. on Num. Meth. in Geotech. Engng.*, Graz, Austria.

Yildiz, Abdulazim 2009, 'Numerical analyses of embankments on PVD improved soft clays', *Advances in Engineering Software*, 40(10), pp. 1047-1055.

Yin, J.-H. and Graham, J. 1989, 'Viscous-elastic-plastic modelling of one-dimensional time-dependent behaviour', *Canadian Geotechinical Journal*, 26(2), pp. 199-209.

Yoshikuni, H. and Nakanodo, H. 1974, 'Consolidation of fine-grained soils by drain wells with finite permeability', *Soils and Foundations*, 14(2), pp. 35-46.

Yu, H. 2000, 'Cavity expansion methods in geomechanics', Kluwer academic Publishers.

Zeng, G. X. and Xie, K. h. 1989, 'New development of the vertical drain theories', *In Proceedings of the 12th International Conference on Soil Mechanics and Foundation Engineering*, Rio de Janeiro, Brazil, pp. 1435-1438.

Zhu, G. and Yin, J. H. 1998, 'Consolidation of soil under depth-dependent ramp load', *Canadian Geotechnical Journal*, 35(2), pp. 344-350.

Zhu, G. and Yin, J. H. 2001, 'Consolidation of soil with vertil and horizontal drainage under ramp load', *Géotechnique*, 51(4), pp. 361-367.

Zhu, X. R., Xie, K. H., Pan, Q.Y. 1993, 'Soft clay ground improvement of Ningbo international airport', *Third international conference on case histories in geotechnical engineering*, St. Louis, Missouri, pp. 983-987.

Zienkiewicz, O. C., Taylor, R. L. and Nithiarasu, P. 2005, 'The Finite element method for fluid dynamics', Elsevier.

Appendix A

DEVELOPED FLAC CODE TO SIMULATE TRIAL EMBANKMENT

A-1 Geometry and Materials properties

```
;***Function to Enter Input Data***
;***Geometries, PVD properties, and required ratios***
def input1

  ;***Embankment & PVD dimension***
      h0=25.0; depth of the soil profile
      h1=24.0; length of the PVD
      h2=h0-h1
      a1=60; the total length of the trial embankment
      a2=60.0; length of the ground at sides of the embankment
      a0=a1+a2
      rm=0.045; radius of mandrel or drain
      smr=3.0; extend ratio (rs/rm)
      sdrain=1.0; drain spacing
      krat=3.0; permeability ratio (kh/ks)
      khv=1.0 the ratio of the horizontal permeability over the vertical one (kh/kv)
      gn1=1.0; the number of mesh zones inside the smear zone
      glrat1=3; length of the mesh outside the smear zone over the inside one
      glrat2=3; ratio for generating meshes and grids
      gnv1=(h1/0.5); the length of the mesh zones in the vertical direction
      glratv=1.0; ratio for generating meshes and grids

  ;***Depths of soil layer interfaces***
      ly1=0.5; depth of layer 1 from the ground surface
      ly2=4.0
      ly3=10.0
      ly4=15.0
      ly5=24.0
      ly6=25.0

  ;***Embank construction history***
      stno=12; number of construction stages

  ;***SOIL PROPERTIES Layer 01***
      kix01=1.0e-131.0e-13; horizontal mobility coefficient of the intact zone (kh)
      kiy01=kix01/khv; vertical mobility coefficient of the intact zone (kv)
      sden01=698; dray density of the soil (ρd)
      spois01=0.27; Poisson's ratio (μ)
      sbulk01=5.0e7;5.0e6; soil bulk modulus (K)
      smm01=1.2; frictional constant (M)
      slanda01=0.569; slope of the normal consolidation line (λ)
      skapa01=0.057; slope of the swelling line (κ)
      smpc01=5.51e3; tpreconsolidation pressure (pc)
      smp101=1e2;1.76e4; reference pressure (p1)
      smv101=5.93;2.55; specific volume at reference pressure (vλ)
      sshear01=1.2e6; shear modulus
```

```
    spor01=0.73 porosity of soil (n)
;***SOIL PROPERTIES Layer 02***
    kix02=6.0e-14
    kiy02=kix02/khv
    sden02=698
    spois02=0.27
    sbulk02=5.0e7;5.0e6
    smm02=1.2
    slanda02=0.569
    skapa02=0.057
    smpc02=3.33e4
    smp102=1e2;1.76e4
    smv102=6.97;2.55
    ;smv002=2.8
    sshear02=1.2e6
    spor02=0.73
;***SOIL PROPERTIES Layer 03***
    kix03=3.0e-14
    kiy03=kix02/khv
    sden03=674
    spois03=0.27
    sbulk03=5.0e7;5.0e6
    smm03=1.2
    slanda03=0.672
    skapa03=0.0672
    smpc03=7.83e4
    smp103=1e2;1.76e4
    smv103=8.29;2.55
    ;smv003=2.8
    sshear03=1.2e6
    spor03=0.74
;***SOIL PROPERTIES Layer 04***
    kix04=5.00e-15
    kiy04=kix04/khv
    sden04=720
    spois04=0.3
    sbulk04=5.0e7;5.0e6
    smm04=1.18
    slanda04=0.47
    skapa04=0.047
    smpc04=1.1e5
    smp104=1e2;1.76e4
    smv104=6.87;2.55
    ;smv004=2.8
    sshear04=7.8e6
    spor04=0.72
;***SOIL PROPERTIES Layer 05***
    kix05=2.00e-15
    kiy05=kix05/khv
```

```
    sden05=845
    spois05=0.3
    sbulk05=5.0e7;5.0e6
    smm05=1.18
    slanda05=0.40
    skapa05=0.040
    smpc05=1.59e5
    smp105=1e2;1.63e5
    smv105=6.04;2.55
    ;smv005=2.8
    sshear05=7.8e6
    spor05=0.68
;***SOIL PROPERTIES Layer 06***
    kix06=1.00e-15
    kiy06=kix06/khv
    sden06=923
    spois06=0.3
    sbulk06=5.0e7;5.0e6
    smm06=1.18
    slanda06=0.368
    skapa06=0.0368
    smpc06=1.69e5
    smp106=1e2;1.76e4
    smv106=5.54;2.55
    ;smv006=2.8
    sshear06=7.8e6
    spor06=0.65
;***PERMEABILITY (SMEAR & INTACT ZONES)***
    ks01=kix01/krat; smear zone permeability of the layer1 (ks1)
    ks02=kix02/krat
    ks03=kix03/krat
    ks04=kix04/krat
    ks05=kix05/krat
    ks06=kix06/krat
;***WATER PROPERTIES***
    wden=1000.0; density of water (ρw)
    wbu=8.5e7;2.0e8; bulk modulus of water (Kw)
```

A-2 GRIDS AND MESH GENERATION

```
;***Horizontal Griding Calculations***
        ls=rm*smr
        li=(sdrain/2)-ls
        ndrain0=a1/sdrain
        delt=ndrain0-int(ndrain0)
           if delt<0.5
                ndrain=int(ndrain0)
           else
                ndrain=int(ndrain0)+1
           end_if
        a4=ndrain*sdrain
        gl1=ls/gn1
        gl20=glrat1*gl1
        gn20=li/gl20
        df1=gn20-int(gn20)
           if df1<0.5
                gn2=int(gn20)
           else
                gn2=int(gn20)+1
           end_if
        gl2=li/gn2
        a5=sdrain/2
        a6=a0-(ndrain+0.5)*sdrain
        gl30=glrat2*gl2
        gn30=a6/gl30
        df2=gn30-int(gn30)
           if df2<0.5
                gn3=int(gn30)
           else
                gn3=int(gn30)+1
           end_if
        gl3=a6/gn3
        gnt=(2*ndrain+1)*(gn1+gn2)
        gnemb=gnt+1
        znh=gn3+gnt;+gn4

;***Vertical Griding Calculations***
        glv1=h1/gnv1
        glv20=glratv*glv1
        gnv20=h2/glv20
        dfv1=gnv20-int(gnv20)
           if dfv1<=0.5
                gnv2=int(gnv20)
           else
                gnv2=1+int(gnv20)
           end_if
```

```
            if gnv20=0
                gnv2=0
                glv2=0
            else
            if gnv20<1
                gnv2=1
                glv2=h2/gnv2
            else
                glv2=h2/gnv2
            end_if
            end_if
        h00=glv1*gnv1+glv2*gnv2
         znv=gnv1+gnv2

;*****embankment grids******
        meshx1=znh+2
        meshx2=znh+2*ndrain+2
        meshy1=znv+2
        meshy01=meshy1+1
        meshy2=znv+stno+1
        meshy02=meshy2-1
        iembmax=meshx2+1
        iemb01=imax+1
        jmeshmax=meshy2+1
        meshnullx1=znh+1
        meshnullx2=meshx2-5
        meshnullx3=meshx2-5-1
        meshnully1=znv+1
        meshnully2=meshy2-5
        jemb01=meshy1+1
        jemb02=jemb01+1
        emb03=jemb02+1
        jemb04=jemb03+1
        jemb05=jemb04+1
        jemb06=jemb05+1
        jemb07=jemb06+1
        jemb08=jemb07+1
        jemb09=jemb08+1
        jemb10=jemb09+1
        jemb11=jemb10+1
        jemb12=jemb11+1
        jemb13=jemb12+1

 ;***Required Gird Lines***
        i1=1.0
        i2=i1+gn1+gn2
        idrain=gnt+1
        imax=znh+1
        j1=1.0
```

```
        j2=gnv2+1
        jmax=znv+1
end
;*** End of "input1" Function
input1
;***Mesh Generation Process***
        config gw extra 3
        grid meshx2 meshy2
        mod cam i 1 znh j 1 znv
        mod elas i meshx1 meshx2 j meshy1 meshy2
        ;mod null i meshnullx1
        ;mod null i meshnully1
        ;mod null i meshx1 meshx2 j 1 jmax
        ini x=0.0 i=1
        ini y=0.0 j=1
;***FUNCTION "hzone": Mesh Generating in Horizontal Direction***
def hzone
        k1=2
        xi=0.0
        is1=1+gn1
           loop while k1<=i2
           loop while k1<=is1
                xi=xi+gl1
                command
                ini x=xi i=k1
                endcommand
                k1=k1+1
           endloop
                xi=xi+gl2
                command
                ini x=xi i=k1
                endcommand
                k1=k1+1
           endloop
                k2=i2+gn2
        step1=1
           loop while step1<=ndrain
           loop while k1<=k2
                xi=xi+gl2
                command
                ini x=xi i=k1
                endcommand
                k1=k1+1
           if xi<=hisxpp1
                ipp1=k1
                xpp1=xi+gl1
           endif
           if xi<=a1
                iload=k1
```

```
        xload=xi+gl1
endif
endloop
        k3=k2+gn1
loop while k1<=k3
        xi=xi+gl1
        command
        ini x=xi i=k1
        endcommand
        k1=k1+1
if xi<=hisxpp1
        ipp1=k1
        xpp1=xi+gl1
endif
if xi<=a1
        iload=k1
        xload=xi+gl1
endif
endloop
        k4=k3+gn1
loop while k1<=k4
        xi=xi+gl1
        command
        ini x=xi i=k1
        endcommand
        k1=k1+1
if xi<=hisxpp1
        ipp1=k1
        xpp1=xi+gl1
endif
if xi<=a1
        iload=k1
        xload=xi+gl2
endif
endloop
        k5=k4+gn2
loop while k1<=k5
        xi=xi+gl2
        command
        ini x=xi i=k1
        endcommand
        k1=k1+1
if xi<=hisxpp1
        ipp1=k1
        xpp1=xi+gl1
endif
if xi<=a1
        iload=k1
        xload=xi+gl2
```

```
            endif
            endloop
                k2=k5+gn2
                step1=step1+1
            endloop
                k6=imax
                loop while k1<=k6
                xi=xi+gl3
                command
                ini x=xi i=k1
                endcommand
                k1=k1+1
            endloop
        xmax=xi
        end
;***End of "hzone" Function***
Hzone

;***FUNCTION "vzone": Mesh Generating in Vertical Direction***
def vzone
        s1=2.0
            loop while s1<=j2
                y1=y1+glv2
                command
                ini y=y1 j=s1
                endcommand
                s1=s1+1
            endloop
            loop while s1<=jmax
                y1=y1+glv1
                command
                ini y=y1 j=s1
                endcommand
                s1=s1+1
            endloop
        ymax=y1
end
;*** End of "vzone" Function***
vzone
;***Embankment Mesh Generating***
def embankmesh
        iem2=imax+2
        iemax=meshx2+1
        lem1=sdrain/2
        lem2=lem1-1
        command
        ini x add lem2 i iem2 iemax
        endcommand
        xmeshno=(26/(sdrain/2))
```

```
        ixnull=iemax-xmeshno
        ixgroup=ixnull-1
        iemb01=imax+1
        iemb02=iemax-6;meshnullx2
        iembmax=meshx2+1
        jemb0=jemb01-1
        meshnullx4=iemb02-1;meshx2-7
        embankl=sdrain*(ndrain+0.5)
        embank2=embankl-8.5
        command
        gen 0,25 0,33.5 embankl,33.5 embankl,25 i iemb01 iemax j jemb0 jemb12
        gen same 0,27.3 55.4,27.3 same i iemb01 iemax j jemb0 jemb05
        gen same 0,33.5 20,33.5 same i iemb01 ixnull j jemb05 jemb12
        mod null i ixnull iemax j jemb05 jemb12
        ini y add 0.1 j=jemb01
        ini y add 0.1 j=jemb02
        ini y add 0.2 j=jemb03
        ini y add 0.2 j=jemb04
        endcommand
end
;*** End of  Function***
Embankmesh
```

A-3 LAYERING AND ASSIGNING SOIL PROPERTIES

```
; ***Required Grid Points for Layering Process***
def gridpoints
;*******  group i & j*****
        yg1=0
        yg2=0
        nn2=0
          loop while yg1<ly1
                yg1=glv1*nn2
                nn2=nn2+1
          endloop
        yg2=glv1*(nn2-2)
        delta01=yg1-ly1
        delta02=ly1-yg2
          if delta01>delta02
                jg1=jmax-nn2+2
          else
                jg1=jmax-nn2+1
          endif
        yg1=0
        yg2=0
        nn2=0
          loop while yg1<ly2
                yg1=glv1*nn2
                nn2=nn2+1
          endloop
        yg2=glv1*(nn2-2)
        delta01=yg1-ly2
        delta02=ly2-yg2
          if delta01>delta02
                jg2=jmax-nn2+2
          else
                jg2=jmax-nn2+1
          endif
        yg1=0
        yg2=0
        nn2=0
          loop while yg1<ly3
                yg1=glv1*nn2
                nn2=nn2+1
          endloop
        yg2=glv1*(nn2-2)
        delta01=yg1-ly3
        delta02=ly3-yg2
          if delta01>delta02
                jg3=jmax-nn2+2
          else
```

```
        jg3=jmax-nn2+1
    endif
yg1=0
yg2=0
nn2=0
    loop while yg1<ly4
        yg1=glv1*nn2
        nn2=nn2+1
    endloop
yg2=glv1*(nn2-2)
delta01=yg1-ly4
delta02=ly4-yg2
    if delta01>delta02
        jg4=jmax-nn2+2
    else
        jg4=jmax-nn2+1
    endif
yg1=0
yg2=0
nn2=0
    loop while yg1<ly5
        yg1=glv1*nn2
        nn2=nn2+1
    endloop
yg2=glv1*(nn2-2)
delta01=yg1-ly5
delta02=ly5-yg2
    if delta01>delta02
        jg5=jmax-nn2+2
    else
        jg5=jmax-nn2+1
    endif
yg1=0
yg2=0
nn2=0
    loop while yg1<ly6
        yg1=glv1*nn2
        nn2=nn2+1
    endloop
yg2=glv1*(nn2-2)
delta01=yg1-ly6
delta02=ly6-yg2
    if delta01>delta02
        jg6=jmax-nn2+2
    else
        jg6=jmax-nn2+1
    endif
ly1check=(jmax-jg1)*glv1
ly2check=(jmax-jg2)*glv1;h0-(gnv2*glv2)-(grj2-gnv2-1)*glv1
```

```
        ly3check=(jmax-jg3)*glv1;h0-(gnv2*glv2)-(grj3-gnv2-1)*glv1
        gri1=1
        gri2=imax-1
        grj0=jmax-1
        grj1=jg1-1
        grj2=jg2-1
        grj3=jg3-1
        grj4=jg4-1
        grj5=jg5-1
        grj6=1
        gri3=gnt+1
end
; ***End of "Grid point for history" Function***
gridpoints
; ***Layering Process***
        group 'layer01' i 1 znh j grj1 grj0
        group 'layer02' i 1 znh j grj2 grj1
        group 'layer03' i 1 znh j grj3 grj2
        group 'layer04' i 1 znh j grj4 grj3
        group 'layer05' i 1 znh j grj5 grj4
        group 'layer06' i 1 znh j grj6 grj5
        group 'stage01' i meshx1 meshx2 j meshy1
        group 'stage02' i meshx1 meshx2 j jemb01
        group 'stage03' i meshx1 meshx2 j jemb02
        group 'stage04' i meshx1 meshx2 j jemb03
        group 'stage05' i meshx1 meshx2 j jemb04
        group 'stage06' i meshx1 ixgroup j jemb05
        group 'stage07' i meshx1 ixgroup j jemb06
        group 'stage08' i meshx1 ixgroup j jemb07
        group 'stage09' i meshx1 ixgroup j jemb08
        group 'stage10' i meshx1 ixgroup j jemb09
        group 'stage11' i meshx1 ixgroup j jemb10
        group 'stage12' i meshx1 ixgroup j jemb11
        attach aside from 1,jmax to idrain,jmax bside from iemb01,jemb0 to
        iemax,jemb0
        mod null group 'stage01'
        mod null group 'stage02'
        mod null group 'stage03'
        mod null group 'stage04'
        mod null group 'stage05'
        mod null group 'stage06'
        mod null group 'stage07'
        mod null group 'stage08'
        mod null group 'stage09'
        mod null group 'stage10'
        mod null group 'stage11'
        mod null group 'stage12'
        prop dens sden01 poiss spois01 bu sbulk01 mm smm01 lambda slanda01
        kappa skapa01 group 'layer01'
```

```
prop shear_mod sshear01 mpc smpc01 mp1 smp101 mv_l smv101 group 'layer01'
prop k11 kix01 k22 kiy01 por spor01 group 'layer01'
prop dens sden02 poiss spois02 bu sbulk02 mm smm02 lambda slanda02 kappa skapa02 group 'layer02'
prop shear_mod sshear02 mpc smpc02 mp1 smp102 mv_l smv102 group 'layer02'
prop k11 kix02 k22 kiy02 por spor02 group 'layer02'
prop dens sden03 poiss spois03 bu sbulk03 mm smm03 lambda slanda03 kappa skapa03 group 'layer03'
prop shear_mod sshear03 mpc smpc03 mp1 smp103 mv_l smv103 group 'layer03'
prop k11 kix03 k22 kiy03 por spor03 group 'layer03'
prop dens sden04 poiss spois04 bu sbulk04 mm smm04 lambda slanda04 kappa skapa04 group 'layer04'
prop shear_mod sshear04 mpc smpc04 mp1 smp104 mv_l smv104 group 'layer04'
prop k11 kix04 k22 kiy04 por spor04 group 'layer04'
prop dens sden05 poiss spois05 bu sbulk05 mm smm05 lambda slanda05 kappa skapa05 group 'layer05'
prop shear_mod sshear05 mpc smpc05 mp1 smp105 mv_l smv105 group 'layer05'
prop k11 kix05 k22 kiy05 por spor05 group 'layer05'
prop dens sden06 poiss spois06 bu sbulk06 mm smm06 lambda slanda06 kappa skapa06 group 'layer06'
prop shear_mod sshear06 mpc smpc06 mp1 smp105 mv_l smv106 group 'layer06'
prop k11 kix06 k22 kiy06 por spor06 group 'layer06'
water bulk wbu tens wt den wden
```

A-4 Defining the location of instrumentations and transducers

history 1 gwtime
history 2 unbalanced
history 3 sratio
history 4 ydisp i=1, j=51; “ydisp” stands for vertical displacement
history 5 ydisp i=1, j=49
history 6 ydisp i=1, j=47
history 7 ydisp i=1, j=45
history 8 ydisp i=3, j=51
history 9 ydisp i=3, j=49
history 10 ydisp i=3, j=47
history 11 ydisp i=3, j=45
history 12 gpp i=3, j=50; “gpp” stands for pore pressure at gridpoint
history 13 gpp i=3, j=49
history 14 gpp i=3, j=48
history 15 gpp i=3, j=47
history 16 gpp i=3, j=46
history 17 gpp i=7, j=50
history 18 gpp i=7, j=49
history 19 gpp i=7, j=48
history 20 gpp i=7, j=47
history 21 gpp i=7, j=46

A-5 BOUNDARY CONDITIONS, INITIAL STRESSES, and UNDRAINED ANALYSIS

```
;***Boundary Conditions***
        fix x i=1
        fix x i=imax
        fix y j=1
        initial pp 0 j jmax
        initial sat 1 j jmax
        initial pp 0 j jemb0
        initial sat 1 j jemb0
        fix pp j jmax
        fix s j jmax
        fix pp j jemb0
        fix s j jemb0
;***Initial Conditions***
call ininv.fis
        set grav 9.8; earth gravity
        set wth=25 k0x=0.66 k0z=0.66; the water depth and the coefficients of lateral
        pressure
ininv
;***Settings***
        set flow off
;***undrained response***
        solve sratio 1e-3
```

A-6 SIMULATION OF PRECONSOLIDATION STAGE

```
;***Simulation of Preconsolidation Process – without PVD***
;***Settings***
        set sratio 1.0
        set step 2000000
        set nmech 1
;***Stage01***
        model mohr group 'stage01'
        prop sh 1.e8 bu 2.e8 coh 1.e3 fri 35 dens 2100 group 'stage01'
        fix x i=meshx1
        set flow off
        solve
        set flow on
        set nmech 20
        solve auto on age 4.32e5
;***Stage02***
        model mohr group 'stage02'
        prop sh 1.e8 bu 2.e8 coh 1.e3 fri 35 dens 2100 group 'stage02'
        set flow off
        set nmech 1
        solve
        set flow on
        set nmech 20
        solve auto on age 8.64e5
;***Stage03***
        model mohr group 'stage03'
        prop sh 1.e8 bu 2.e8 coh 1.e3 fri 35 dens 2100 group 'stage03'
        set flow off
        set nmech 1
        solve
        set flow on
        set nmech 20
        solve auto on age 3.71e6
```

A-7 SIMULATION OF PVDs SMEAR ZONE

```
;***FUNCTION "pdrain": Simulation of PVDs and Smear Zone***
def pdrain01
        is01=1+gn1
        ppd1=h1*9800
        ppd2=(-1)*ppd1
        command
        initial pp ppd1 var 0 ppd2 i=1 j=j2,jmax
        initial s=1 from 1,j2 to 1,jmax
        fix pp i=1 j=j2,jmax
        fix sat i=1 j=j2,jmax
        prop perm ks01 i=1,is01 j=grj1,grj0;group 'layer01'
        prop perm ks02 i=1,is01 j=grj2,grj1;group 'layer02'
        prop perm ks03 i=1,is01 j=grj3,grj2;group 'layer03'
        prop perm ks04 i=1,is01 j=grj4,grj3 group 'layer04'
        prop perm ks05 i=1,is01 j=grj5,grj4 group 'layer05'
        mark i 1 j j2,jmax
        endcommand
        end
def pdrain
        idr=(gn1+gn2)*2+1
        is1=idr-gn1
        is2=idr+gn1
        step2=1
           loop while step2<=ndrain
                command
                initial pp ppd1 var 0 ppd2 i=idr j=j2,jmax
                initial s=1 i=idr j=j2,jmax
                fix pp i=idr j=j2,jmax
                fix sat i=idr j=j2,jmax
                prop perm ks01 i=is1,is2 j=grj1,grj0;group 'layer01'
                prop perm ks02 i=is1,is2 j=grj2,grj1;group 'layer02'
                prop perm ks03 i=is1,is2 j=grj3,grj2;group 'layer03'
                prop perm ks04 i=is1,is2 j=grj4,grj3;group 'layer04'
                prop perm ks05 i=is1,is2 j=grj5,grj4 group 'layer05'
                mark i idr j j2,jmax
                endcommand
                step2=step2+1
                idr=idr+2*(gn1+gn2)
                is1=idr-gn1
                is2=idr+gn1
           endloop
end
;***End of "pdrain" Function***
pdrain01
pdrain
```

A-8 SIMULATION OF VACUUM PRESSURE

```
;***Function to Simulate Variation of Vacuum Pressure Alomg the Vertical
Drain***
def vacuum01
        is01=1+gn1
        command
        initial pp -70000 i=1 j=j2,jmax
        initial s=1 from 1,j2 to 1,jmax
        fix pp i=1 j=j2,jmax
        fix sat i=1 j=j2,jmax
        mark i 1 j j2,jmax
        endcommand
        end
        def vacuum02
        idr=(gn1+gn2)*2+1
        is1=idr-gn1
        is2=idr+gn1
        step2=1
           loop while step2<=ndrain
                command
                initial pp -70000 i=idr j=j2,jmax
                initial s=1 i=idr j=j2,jmax
                fix pp i=idr j=j2,jmax
                fix sat i=idr j=j2,jmax
                mark i idr j j2,jmax
                endcommand
                step2=step2+1
                idr=idr+2*(gn1+gn2)
                is1=idr-gn1
                is2=idr+gn1
           endloop
end
vacuum01
vacuum02
```

A-9 CONSTRUTION OF TRIAL EMBANKMENT AND CONSOLIDATION PROCESS

```
;***Stage04***
        model mohr group 'stage04'
        prop sh 1.e8 bu 2.e8 coh 1.e3 fri 35 dens 2100 group 'stage04'; tens 1e10
        fix x i=meshx1
        set flow off
        set nmech 1
        solve
        set flow on
        set nmech 20
        solve auto on age 7.77e6
;***Stage05***
        model mohr group 'stage05'
        prop sh 1.e8 bu 2.e8 coh 1.e3 fri 35 dens 2100 group 'stage05'; tens 1e10
        fix x i=meshx1
        set flow off
        set nmech 1
        solve
        set flow on
        set nmech 20
        solve auto on age 9.85e6
;***Stage05***
        set sratio 1.9
        model mohr group 'stage06'
        prop sh 1.e8 bu 2.e8 coh 1.e3 fri 35 dens 2100 group 'stage06'; tens 1e10
        set flow off
        set nmech 1
        solve
        set flow on
        set nmech 20
        initial pp 0 j jemb06
        initial sat 0 j jemb06
        fix pp j jemb06
        fix sat j jemb06
solve auto on age 1.28e7
        model mohr group 'stage07'
        prop sh 1.e8 bu 2.e8 coh 1.e3 fri 35 dens 2100 group 'stage07'; tens 1e10
        set flow off
        set nmech 1
        solve
        set flow on
        set nmech 20
        initial pp 0 j jemb07
        initial sat 0 j jemb07
        fix pp j jemb07
        fix sat j jemb07
```

```
 solve auto on age 1.43e7
        model mohr group 'stage08'
        prop sh 1.e8 bu 2.e8 coh 1.e3 fri 35 dens 2100 group 'stage08'; tens 1e10
        set flow off
        set nmech 1
        solve
        set flow on
        set nmech 20
        initial pp 0 j jemb08
        initial sat 0 j jemb08
        fix pp j jemb08
        fix sat j jemb08
solve auto on age 1.56e7
        model mohr group 'stage09'
        prop sh 1.e8 bu 2.e8 coh 1.e3 fri 35 dens 2100 group 'stage09'; tens 1e10
        set flow off
        set nmech 1
        solve
        set flow on
        set nmech 20
        initial pp 0 j jemb09
        initial sat 0 j jemb09
        fix pp j jemb09
        fix sat j jemb09
solve auto on age 1.68e7;***195days***
        model mohr group 'stage10'
        initial pp 0 j jemb10
        initial sat 0 j jemb10
        fix pp j jemb10
        fix sat j jemb10
        prop sh 1.e8 bu 2.e8 coh 1.e3 fri 35 dens 2100 group 'stage10'; tens 1e10
        set flow off
        set nmech 1
        solve
        set flow on
        set nmech 20
solve auto on age 1.81e7
        model mohr group 'stage11'
        initial pp 0 j jemb11
        initial sat 0 j jemb11
        fix pp j jemb11
        fix sat j jemb11
        prop sh 1.e8 bu 2.e8 coh 1.e3 fri 35 dens 2100 group 'stage11'; tens 1e10
        set flow off
        set nmech 1
        solve
        set flow on
        set nmech 20
solve auto on age 1.94e7
```

```
        model mohr group 'stage12'
        initial pp 0 j jemb12
        initial sat 0 j jemb12
        fix pp j jemb12
        fix sat j jemb12
        prop sh 1.e8 bu 2.e8 coh 1.e3 fri 35 dens 2100 group 'stage12'; tens 1e10
        set flow off
        set nmech 1
        solve
        set flow on
        set nmech 20
solve auto on age 2.07e7
        set nmech 20
solve auto on age 3.37e7
```

Appendix B

DEVELOPED FLAC CODE TO SIMULATE ROWE CELL TEST

```
;***Input Data Function for Cell & PVD Dimensions ***
def indata
        hc=0.1213;h0
        hd=0.1213;h1
        h2=hc-hd
        rc=0.125
        rm=0.011
        smr=3.0
        krat=2.5
        gns=8.0
        lrat=1.5
        gnv1=20.0
        glratv=1.0
;***Permeability (Smear and & Intact Zones)***
        ki=1.0e-12
        ks=ki/krat
;***Soil Properties***
        sden=935.0
        spois=0.3
        sbulk=2.0e7
        smm=1.1
        slanda=0.35
        skapa=0.045
        smpc=2.1e4
        smp1=1.0e1
        smv1=4.78
        spor=0.57
;***Propertied of Water***
        wden=1000.0
        wbu=5.0e6;4.5e7
        wt=1.0e10
;***Lateral Pressure Coefficients***
        kx0=0.7
        kz0=0.7
;***Calculations***
        rs=rm*smr
        li=rc-rs
        gls=rs/gns
        gli0=lrat*gls
        gni0=li/gli0
        df=gni0-int(gni0)
           if df<0.5
                gni=int(gni0)
           else
                gni=int(gni0)+1
           end_if
        gli=li/gni
        gnh=gns+gni
        rcc=gls*gns*gli*gni
```

```
;*** Calculations  for Generating Vertical Grids ***
        glv1=hd/gnv1
        glv20=glratv*glv1
        gnv20=h2/glv20
        dfv1=gnv20-int(gnv20)
           if gnv20=0
                glv2=0
           else
           if dfv1<=0.5
                gnv2=int(gnv20)
                glv2=h2/gnv2
           else
                gnv2=1+int(gnv20)
                glv2=h2/gnv2
           end_if
           end_if
        znv=gnv1+gnv2
;***Required Grid Lines***
        ismear=gns+1
        imax=gnh+1
        jmax=znv+1
        jdrain=gnv2+1
        i1=int((imax-ismear)/2)+ismear
        jmid=int(jmax/2)
        jtop=jmax-1
end
indata
;*** Mesh Generating ***
        config ax gw
        grid gnh znv
        model cam
        gen 0,0 0,hc rs,hc rs,0
        gen rs,0 rs,hc rc,hc rc,0
        ini x=0 i=1
        ini y=0 j=1
;***FUNCTION "vzone": Mesh Generating in Vertical Direction***
def vzone
        s1=2.0
           loop while s1<=jdrain
                y1=y1+glv2
                command
                ini y=y1 j=s1
                endcommand
                s1=s1+1
           endloop
           loop while s1<=jmax
                y1=y1+glv1
                command
                ini y=y1 j=s1
```

```
                endcommand
                s1=s1+1
            endloop
end
vzone
;***End of " vzone" FUNCTION" ***
def szone
        aa=2
        i2=1+gns
            loop while aa<=i2
                x2=x2+gls
                command
                ini x=x2 i=aa
                endcommand
                aa=aa+1
            endloop
end
def izone
        i3=1+gnh
        x3=rs
        loop while aa<=i3
                x3=x3+gli
                command
                ini x=x3 i=aa
                endcommand
                aa=aa+1
        endloop
end
szone
izone
        group 'initial01' notnull
        prop dens sden poiss spois bu sbulk mm smm lambda slanda kappa skapa
        group 'initial01'
        prop mpc smpc mp1 smp1 mv_l smv1 group 'initial01'
        prop perm ki por spor  group 'initial01'
        water bulk wbu tens wt den wden
;*** Boundary Conditions ***
        fix x i=1
        fix x i=imax
        fix x y j=1
;*** Initial Conditions ***
        call ininv.fis
        set grav 9.8
        set wth=hc k0x=kx0 k0z=kz0
        ininv
;*** Recording the PWP and Settlement at the Location of PWPTs and LVDT***
        history 1 gwtime
        history 2 unbalanced
        history 6 ydisp i=1, j=21
```

```
        history 10 ydisp i=3, j=21
        history 11 ydisp i=14, j=21
        history 14 gpp i=24, j=4
        history 15 gpp i=24, j=8
        history 18 gpp i=24, j=12
        history 19 gpp i=24, j=16
        history 20 gpp i=4, j=1
        history 21 gpp i=8, j=1
        history 22 gpp i=12, j=1
        history 23 gpp i=16, j=1
        history 24 gpp i=21, j=1
        history 25 ydisp i=14, j=21
;*** Undrained Analysis***
        set step 2000000
        set flow off
        solve sratio 1e-3
;*** Simulation of Vertical drain & Smear Zone ***
        initial pp 1.96e3 var 0 -1.96e3 i=1 j=jdrain, jmax
        initial s=1 from 1,jdrain to 1,jmax
        fix pp i=1 j=jdrain, jmax
        fix sat i=1 j=jdrain, jmax
def pp1
        zh0=1
        zh1=ismear-1
        zh2=ismear
        zh3=imax-1
        zv0=1
        zv1=jdrain-1
        zv2=jdrain
        zv3=jmax-1
           if gnv20=0
                command
                group 'smear' i=zh0,zh1 j=zv0,zv3
                prop perm ks por spor group 'smear'
                endcommand
                else
                command
                group 'smear' i=zh0,zh1 j=zv2,zv3
                prop perm ks por spor group 'smear'
                endcommand
           end_if
end
pp1
;*** Staged Loading & Consolidation Process***
        apply pres 2e4 hist ramp from 1,jmax to imax,jmax
        set step 3000000
        set flow on srat 1e-3
        set nmech 1
        solve auto on age 3.2e5
```

```
apply pres 5e4 hist ramp from 1,jmax to imax,jmax
solve auto on age 1.3e6
apply pres 1e5 hist ramp from 1,jmax to imax,jmax
solve auto on age 3.2e6
apply pres 2e5 hist ramp from 1,jmax to imax,jmax
solve auto on age 4.2e6
```